Aerodynamics of Track Cycling

By Lindsey Underwood

A thesis presented for the Degree of

Doctor of Philosophy

at

The University of Canterbury

Department of Mechanical Engineering

Christchurch, New Zealand

June 2012

Abstract

The aim of this thesis was to identify ways in which the velocity of a track cyclist could be increased, primarily through the reduction of aerodynamic drag, and to determine which factors had the most significant impact on athlete performance. An appropriate test method was set up in the wind tunnel at the University of Canterbury to measure the aerodynamic drag of different cycling positions and equipment, including helmets, skinsuits, frames and wheels, in order to measure the impact of specific changes on athlete performance. Rather than comparing standard cycling positions, such as the Obree, dropped, upright and aero positions, a number of individual and multiple changes were made to the height, width and length of the handlebars, seat height, head and helmet position, and hand position to provide a rank of importance in terms of which changes had the greatest impact (gain or loss) on the aerodynamic drag.

A mathematical model of the Individual Pursuit (IP) event was also created to calculate the velocity profile and finishing time for athletes competing under different race conditions. The model was created in Microsoft Excel and used first principles to analyse the forces acting on a cyclist, which lead to the development of equations for power supply and demand. The model included the effects of leaning in the bends, and used SRM power data to determine the actual position of the rider on the track. The mathematical model was validated using SRM data for eleven, elite track cyclists, and was found to be accurate to 0.31s (0.16%). An analysis of changes made to the bike, athlete, and environmental conditions using the mathematical model showed that the drag area and air density had the greatest impact on the finishing time. As the air density is fixed for all athletes competing in the same race, these results suggest that athletes should focus on minimising their drag area in order to maximise performance. The model was then used to predict the finishing times for different pacing strategies by generating different power profiles for a given athlete with a fixed stock of energy (the work done remained the same for all generated power profiles) in order to identify the optimal pacing strategy for the IP. A comparison of the predicted finishing times for the different pacing strategies showed that an all-out and even or all-out and variable strategy with an initial acceleration phase of 12s resulted in the fastest finishing time for a male, IP athlete with a fixed stock of energy whose efficiency is not a function of power output or speed. The length of time spent in the initial acceleration phase was found to have a significant impact on the results, although all strategies simulated with an initial acceleration phase resulted in a faster finishing time than all other strategies simulated.

Results from the wind tunnel tests also showed that, in general, changes made to the position of the cyclist had the greatest impact on the aerodynamic drag compared to changes made to the equipment. Multiple changes in position had a greater impact on drag than individual changes in position, but the changes were not additive; the total gain or loss in drag for multiple changes in position was not the sum of individual gains or losses in drag. Actual gains and losses also varied significantly between athletes, primarily due to differences in body size and shape, riding experience, and reference position from which changes were made from. However, certain changes in position or equipment had a significant impact ($>\pm1\%$) on the drag of all athletes tested compared to the reference position. For example, by wearing a shoe cover all athletes showed a reduction in drag of $>1\%$ regardless of shoe, cleat or pedal worn. Changes in position that resulted in a reduction of the frontal area, such as lowering the handlebars and head, were the most successful at reducing the aerodynamic drag, and a change in skinsuit was found to have the greatest impact on drag out of all equipment changes, primarily due to the choice of material and seam placement. The mathematical model was used to quantify the impact of changes in position and equipment made in the wind tunnel on the overall finishing time for a given athlete competing in an IP event. Time savings of up to 8 seconds were seen for

multiple changes in position, and up to 5 seconds for changes to the equipment.

Overall this thesis highlights the significance of aerodynamics on athlete performance in track cycling, suggesting that it is worthwhile spending time and money on research and technology to find new ways to reduce the aerodynamic drag and maximise the speed of cyclists. Although this thesis primarily concentrates on the Individual Pursuit event in track cycling, the same principles can be applied to other cycling disciplines, as well as to other sports.

Acknowledgements

I would like to thank Dr Mark Jermy for giving me the opportunity to carry out this research and providing me with support and encouragement throughout my time at the University of Canterbury. My thanks also extend to the technicians Graeme Harris and Eric Cox for assisting me with all the testing and procedures carried out in the wind tunnel, and also to my co-supervisor Stephanie Gutschmidt for her general support.

Thanh, Laura and Lisa, I could not have got through the past few years without having such great office mates. Those morning chats are invaluable, and you have provided great friendship and support that I hope will continue when we go our separate ways.

Thanks to BikeNZ, SPARC, the REC centre, and all the athletes and coaches who provided data for my thesis, gave me the opportunity to get involved in the High Performance Programme, and helped me attend conferences and competitions to develop my knowledge in sports engineering and track cycling. I must also thank Stuart McIntyre for his outstanding knowledge on apparel design, and for his enthusiam throughout the skinsuit project - you have been a pleasure to work with, and I hope that we can work together again in the future.

I would like to show my appreciation to all the international students who have worked with me in the wind tunnel and on projects related to my thesis. Particular thanks must go to Jana, Julien, and Amaury for their hard work and also the entertainment they provided.

I am grateful to my flatmates, my friends, and of course my boyfriend, who have all made my time in New Zealand so enjoyable. You have provided me with a home away from home, and a friendship and companionship that I am sure will last a lifetime. Finally my thanks must go to my parents and my brother. Without your continuous love and support, even when I am the other side of the world, I would not be where I am today.

List of Publications

1. L. Underwood and M.C. Jermy, Mathematical model of track cycling: the individual pursuit, *The Engineering of Sport 8*, 2 (2): 3217–3222, 2010.

2. L. Underwood and M.C. Jermy, Optimal hand position for individual pursuit athletes, *The Engineering of Sport 8*, 2 (2): 2425–2429, 2010.

3. L. Underwood and M.C. Jermy, Fabric testing for cycling skinsuits, *5th Asia-Pacific Congress on Sports Technology (APCST)*, 13: 350-356, 2011.

4. L. Underwood, J. Schumacher, J. Burette-Pommay and M. Jermy, Aerodynamic drag and biomechanical power of a track cyclist as a function of shoulder and torso angles, *Sports Engineering*, 14 (2-4): 147-154, 2011.

5. L. Underwood and M.C. Jermy, Determining the optimal pacing strategy for the track cycling individual pursuit event with a fixed energy mathematical model, *Submitted to Sports Engineering - in review*, May 2012.

6. L. Underwood and M.C. Jermy, Optimal handlebar position for individual pursuit athletes, *Submitted to Sports Engineering - in review*, May 2012.

Contents

List of Figures

List of Tables

Chapter 1

Introduction

1.1 Motivation for research

The significance of cycling aerodynamics became well known when Graeme Obree broke the hour record and individual pursuit record in the Obree position in 1993, and was the individual pursuit champion in 1995 in the superman position. The aerodynamics of cycling can be controlled, and the performance gains that can be made through research in this area are highly advantageous, leading to a signficant competitive advantage.

Wind tunnel testing of cyclists has become a popular method of measuring the aerodynamic drag of a cyclist, as this is the most realistic way to reproduce actual racing conditions without needing the athlete to perform continually at race pace for the duration of an event. Although wind tunnel testing of athlete position and cycling equipment has been carried out in the past, the testing is very generalised and primarily carried out for road cycling. The reason for concentrating on track cycling is that the aerodynamics of track cyclists is not as well established as road cycling, and track cycling races are won within milliseconds; every small gain that can be made through changes in position and/or equipment is significant. The equipment used for track cycling can be designed and manufactured specifically for the athletes, and the methods applied to other sports and cycling events. However, the main motivation for carrying out this research was to try to answer the question 'How can we maximise the speed of all track cyclists, and which method results in the biggest gain?'

1.2 Aims and Objectives

The aim of this thesis is to identify ways in which the velocity of a track cyclist can be increased, and to determine which of these factors has the greatest impact on the performance of all athletes through gaining a greater understanding of the aerodynamics of cycling and the flow around a cyclist. This thesis will concentrate on those factors which can be modified and controlled for individual athletes, and not factors which are considered 'fixed', such as the track surface and geometry.

The main objectives which will enable the aim to be achieved are:

- To develop appropriate testing methods using the wind tunnel to measure the aerodynamic drag and drag area of a cyclist, so that comparisons can be made between changes in position and equipment;
- To develop a mathematical model for track, pursuit events to calculate the velocity profile and the time savings for changes to the input variables, and to identify the optimal pacing strategy for pursuit cyclists;
- To compare changes made in the wind tunnel to athlete position and equipment to identify those factors with the greatest impact on drag, to provide a rank of importance, and to identify the most significant ways in which the drag can be reduced. Effects of training, nutrition and drugs have been declared out of scope for this thesis, however, biomechanical efficiency is within the scope.

1.3 Thesis Structure

This thesis is divided into ten chapters, starting with some background into track cycling to provide the reader with an understanding of track cycling, aerodynamics, and the factors that affect athlete performance. Chapter 3 consists of a review of the research that has been carried out on mathematical modelling of cycling and cycling aerodynamics, concentrating on those factors which affect the aerodynamic drag the most and the ways in which drag has been reduced successfully. A description of a mathematical model for track cycling is provided in Chapter 4, which can be used to predict the finishing time for pursuit cyclists and to simulate different pacing strategies to determine the optimal strategy for pursuit cyclists. Chapter 5 explains the wind tunnel, cycle rig, and testing procedure for measuring the aerodynamic drag of cyclists, followed by an experiment looking into the boundary layer of a cyclist in Chapter 6 to provide a more detailed analysis of the flow over a cyclist. Chapters 7 and 8 consist of experimental work using the wind tunnel, cycle rig, and testing procedures to compare cycling equipment, athlete attire, and athlete position. Chapter 9 brings together all experimental data and the mathematical model to identify how gains and losses can be made through changes in position and equipment, and to identify which factors have the greatest impact on drag. The mathematical model is used to provide quantitative information on time savings and time losses for each change in position and equipment, specifically for the pursuit event. Finally a summary of the work and final conclusion are provided in Chapter 10, along with recommendations for future work in this area.

Chapter 2

Background

Track cycling has been around since 1870 and is a bicycle racing sport held on either an indoor or outdoor velodrome. A velodrome is a banked, hard surface track made from concrete, wood or grass, and has two straight sections and two bends. An image of a typical indoor velodrome is shown in Figure 2.1.

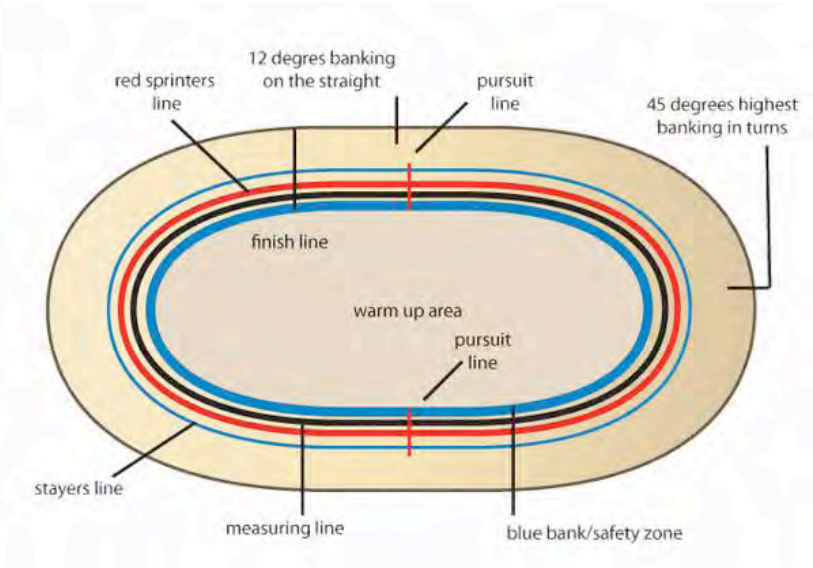

Figure 2.1: Schematic of an indoor veldrome

The length and width of the track, and the radius of the bends vary, although indoor velodromes used for World Championship and Olympic events must lie within the specifications outlined by the International Cycling Union (UCI), shown in Table 2.1, where the length is measured 20cm from the inner edge of the track (the upper edge of the blue band and inner edge of the black band). The three major track cycling competitive events are:

1. Olympic Games, held every four years and in 2012 there will five events for both men and women (team sprint, sprint, team pursuit, keirin and omnium).

2. UCI Track Cycling World Championships, held every year with 10 events for men and 9 events for women.

3. UCI Track Cycling World Cup Classics, held four times a year over a period of three days. Points are scored for winning an event, which count towards qualification places individually and for their nation in the World Championships at the end of the season.

Length (m)	250	285.714	333.33	400
Radius (m)	19-25	22-28	25-35	28-50
Width (m)	7-8	7-8	7-9	7-10

Table 2.1: Specifications for velodromes

The UCI is the regulating body for technical and ethical aspects of cycling on an international level, who set the rules and regulations for all major cycling disciplines around the world [Regulations, 2009]. These rules and regulations limit the influence of technology in sport, and therefore define the limit to which changes can be made to help increase the velocity of a cyclist. A summary of the rules and regulations outlined by the UCI is given in Appendix A. These rules limit the changes in position and equipment that can be made. With a minimum weight of 6.8 kg, most marketed bikes used for competitions are already as light as possible. As many of the components of the bike frame must be constructed in a certain way, and because it is prohibited to add any device to the bike to reduce aerodynamic drag, the shape of the frame and handlebar elements may be the only modification which can be made to the bike. However, the 3:1 ratio restricts the number of possible aerodynamic shapes which could be allowed. The bike itself accounts for only 30% of the overall drag on a cyclist [Oggiano et al., 2008], so the gains which could be made from very small modifications to the frame would be minimal compared to those which could be made through changes in position. The most common cycling positions are the dropped, aero, Obree and Superman positions, as shown in Figure 2.2. However, the rules brought in by the UCI have now banned the Obree and Superman positions, mainly due to their extreme aerodynamic advantage and the issue with safety when riding in such extreme positions. When using handlebar extensions, the forearms must be horizontal. This limits the potential to reduce aerodynamic drag through changes in arm position, as only the effect of tapered bars, the width of the extensions, the hand position, and the extension of the arms may be altered. The extension of the handlebars and movement of the saddle are also limited to +75cm and -5cm from the bottom bracket respectively, to prevent athletes adopting a position similar to the superman position. Although there is no rule for the height of the handlebars, the restrictions on the frame dimensions will limit how low the handlebars can be. Therefore there are only so many modifications which can be made to alter the position of the athlete on the bike in order to reduce their aerodynamic drag. At present, the only limitations to skinsuits for track cyclists are that they must be above the knee and must not be sleeveless. Therefore there is potential for reductions in aerodynamic drag to be made through the choice of material and cut of skinsuits, which would benefit all athletes.

(a) Dropped Position

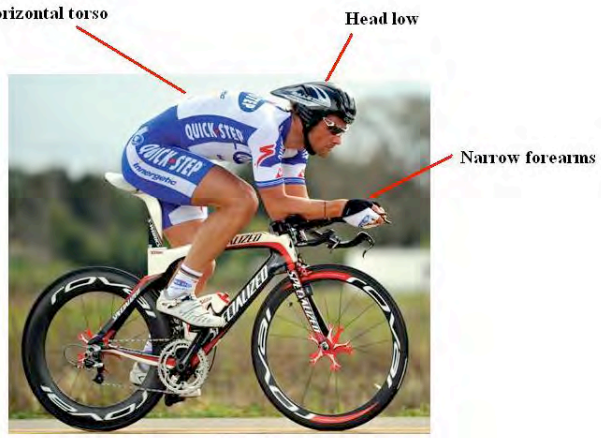

(b) Aero Position

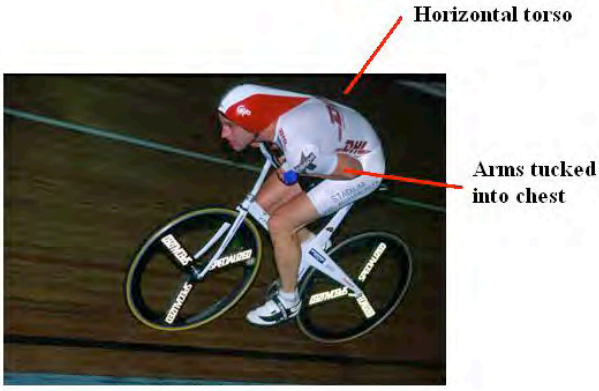

(c) Obree Position

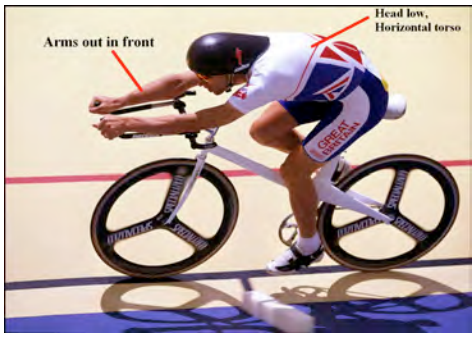

(d) Superman Position

Figure 2.2: Common Cycling Positions

Track bikes are single speed bikes, with no brakes, gears or freewheel. Early bikes were made from wood reinforced with metals, until 1869 when steel became more widely available leading to the production of tension wheels, rubber (solid) tyres, and tubular steel construction [Wilson, 2004]. Continued refinement of materials and improved design has resulted in bikes weighing one third of what they used to, with aluminium, titanium and now resin reinforced carbon fibre being the most popular light-weight materials for frame construction [Wilson, 2004]. Not only have bikes become lighter, but the increased knowledge of the significance of aerodynamics, when Graham Obree broke the hour record in the Obree position and the IP record in the Superman position, has resulted in manufacturers concentrating on making frames and wheels more aerodynamic and athletes focusing on optimising their position in terms of aerodynamics rather than comfort. A more detailed discussion of the aerodynamics of cycling will be given in the Literature Review (Section 3.2).

Track cycling events require the athlete to generate power output both anaerobically and aerobically, and

through effective training elite riders develop key physiological and physical attributes, which match the requirements of the events. Track cycling events are split into two categories: sprint and endurance, the main ones of which are shown in Table 2.2. Professional athletes compete in one or other of these events, as the strategy and power requirements differ between the two categories. However, no significant correlation between the anthropometric characteristics of the athletes and individual performance has been seen [McLean and Parker, 1989]. In general, sprint races consist of two riders competing against each other over a total distance up to 1000m. The small number of laps involved in sprint races means athletes must use both tactics and sprinting power to defeat their opponents. Endurance races last much longer (>1000m) with athletes competing in either one-on-one or group races lasting from 3000m to 4000m for pursuit events, up to 50km for a full length points race. Although endurance races primarily test a rider's endurance ability, the madison, points and scratch races also test the rider's ability to sprint.

Sprint	**Endurance**
Sprint	Individual Pursuit
Team Sprint	Team Pursuit
Keirin	Scratch
Time Trial	Points
	Madison
	Omnium

Table 2.2: Track Cycling Events

Performance in track cycling is dependent only on factors that affect power demand and supply. In general, it is only physiological factors which influence the power supplied, and mechanical and environmental factors which affect power demand, as shown in Table 2.3 [Craig and Norton, 2001, Jeukendrup et al., 2000, Olds, 2001].

Factors Affecting Power Demand	**Factors Affecting Power Supply**
Athlete position	Aerobic energy sources
Mass of rider, bike and components	Anaerobic energy sources
Bike and component geometry	Nutrition
Type of wheels and tyres	Training
Rolling resistance	Pacing strategy
Gradient	Body position
Clothing and helmet	
Air temperature	
Relative humidity	
Barometric air pressure	
Body Shape	
Air resistance	

Table 2.3: Factors affecting power supply and power demand

The overall aim of competitive track cycling is to minimise the demand of power so that less power output is needed to match this demand and as little energy as possible is wasted. The contribution of each factor

of supply and demand to athlete performance varies, and some of these factors cannot be controlled, mainly the atmospheric conditions, track geometry, and athlete body shape. However, it is possible for an athlete to train in specific conditions in order to acclimatise to extreme temperatures and/or altitudes. As the factors affecting power supply are mainly determined by the athlete, these factors will not be analysed in detail in this thesis, but a short summary will be provided. This thesis will concentrate on those factors most influential on power demand.

2.1 Factors Affecting Power Supply

The contribution of anaerobic and aerobic energy systems of athletes varies depending on the event, with endurance riders in general having a higher aerobic contribution than sprint riders [Craig et al., 1993]. A summary of the contribution of energy from power sources, taken from Craig and Norton [2001], is shown in Table 2.4. Specific training can help athletes improve their energy contributions to increase their power supply. According to Craig et al. [1993] a 15% improvement in VO_2max can reduce the finishing time by 15.5s, and a 10% increase in Maximum Accumulated Oxygen Deficit (MAOD) can reduce the finishing time by 1s.

Event	**World Record (min:sec)**	**Contribution from Power Systems (%)**			**Estimated Competition Work Rate (%VO_{2max})**
		Alactic	**Anaerobic glycolytic**	**Aerobic**	
200m Sprint					
male	0:09.865	40	55	5	280
female	0:10.831	40	55	5	235
Olympic Sprint					
1st position	0:44.233	40	55	5	355
2nd position		30	60	10	290
3rd position		20	40	40	245
Time Trial					
male (1000m)	1:00.148	10	40	50	180
female (500m)	0:34.010	20	45	35	245
Individual Pursuit					
male (4000m)	4:11.114	1	14	85	105
female (3000m)	3:30.816	1	24	75	110
Team Pursuit					
male (4000m)	4:00.958	1	24	75	125-135
1-hr Record (km)					
male	56.375	<1	4	>95	85-90
female	48.159	<1	4	>95	85-90

Table 2.4: World Record Times and Estimations of the Contribution of Energy Systems [Craig and Norton, 2001]

Cycling power mainly depends on pedalling rate, muscle size, muscle fibre-type distribution, cycling position, and fatigue [Martin et al., 2007]. The transfer of energy from the rider to the bike is carried out in a complex but coordinated way. Lower extremity muscles provide the force and torque required to rotate the crank and accelerate the bike, while the upper body provides stability during this motion. A muscle can produce its

greatest force at its resting length or at a low shortening velocity [Raasch et al., 1997, Too and Landwer, 2004, Neptune et al., 2009]. According to Too and Landwer [2004] and Neptune et al. [2009], maximal power occurs at 30% of the muscle shortening velocity. It should be noted that there is a delay from when the muscle fiber is excited and when the muscle becomes activated; muscles cannot be turned on and off instantly [Neptune et al., 2009].

The study of the pedal cycle is important from the musculary point of view. Efficiency isn't constant throughout the entire, 360 degree cycle; pedalling efficiency depends on the subject and the ability of the cyclist to synchronise muscle action [Belluye and Cid, 2001]. The muscle recruitment pattern is related to the crank cycle, which can be broken down into the three phases shown in Figure 2.3 of (1) downstroke/propulsive phase, (2) upstroke/recovery phase, and (3) foot pushed forwards at the Top Dead Centre (TDC).

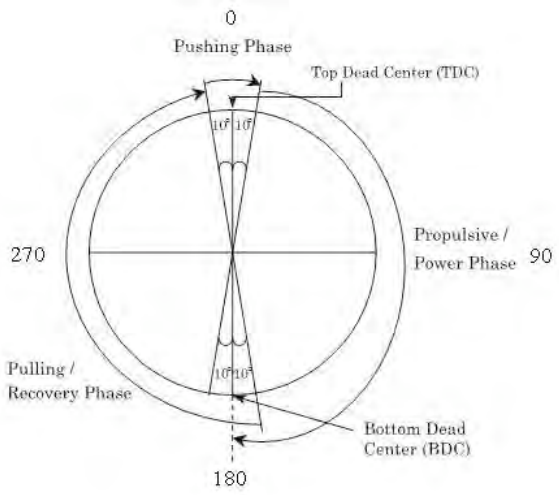

Figure 2.3: Crank Cycle

Belluye and Cid [2001] studied the power transmitted by a cyclist to the pedals throughout the pedal stroke, Figure 2.4, and found that most power was produced between 36^{o} and 162^{o}.

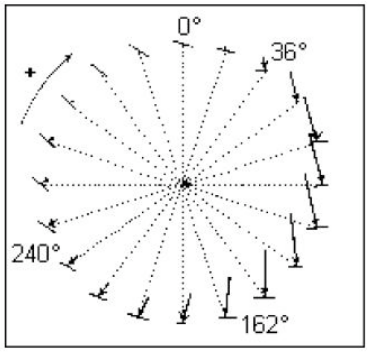

Figure 2.4: Power Transmitted to the Pedals throughout the Pedal Stroke

Cycling power is produced by muscles that span the hip, knee and ankle, all of which simultaneously extend during the downstroke and flex during the upstroke [Martin et al., 2007]. According to Neptune et al. [2009], the hip and knee flexors work to drive the pedal rearward at the 180 degree point in the cycle (Bottom Dead Centre) and lift the pedal during a large proportion of the recovery phase. A summary of the muscle activation pattern during cycling is given in Table 2.5.

Muscles	**Function**	**Approx Range of Action (°)**	**Approx Peak Activity Angle (°)**
Gluteus maximum	Hip extension	340-130	80
Vastus lateralis	Knee extension	300-130	30
Vastus medialis	Knee extension	300-130	30
Rectus femoris	Knee extension/Hip flexion	200-110	20
Soleus	Ankle stabilizer	340-270	90
Gastrocnemius	Ankle stabilizer/Knee flexion	350-270	110
Tibialis anterior	Ankle stabilizer/Ankle flexion	All the range	280
Hamstrings (without biceps femoris)	Knee flexion	10-230	100
Biceps femoris	Knee flexion/Hip extension	350-230	110

Table 2.5: Muscle Activiation Pattern in Cycling [Neptune et al., 2009]

The contribution of the hip, knee and ankle muscles during submaximal and maximal cycling was studied by Martin et al. [2007] and Martin and Brown [2009], who found that although the knee contributes the most to the power delivered to the cranks for both submaximal and maximal cycling, there is some variation between the actual percentage contribution of all muscles involved, as summarised in Table 2.6.

	Submaximal Cycling Martin, Davidson & Pardyjak (2007)	**Maximal Cycling** Martin & Brown (2009)
Knee	49%	71.2%
Hip	32%	8.7%
Ankle	9%	12.3%
Transferred across the hip	9%	-

Table 2.6: Contribution of hip, knee and ankle to power delivered to the cranks during submaximal and maximal cycling at 120rpm

Muscle recruitment pattern changes with fatigue, cadence, posture, seat height, and crank arm length. Fatigue is the failure of muscles to maintain the target force, and an increase in fatigue will slow the speed at which muscle activation occurs and reduce the force output from a particular muscle group [So et al., 2005]. Standing or seating postures use different muscle recruitment patterns, but athletes in similar seated positions will have similar hip, knee and ankle angles, resulting in similar muscle recruitment patterns. Only when one or more of these angles changes will the muscle recruitment pattern change. A change in the seat height will

alter the maximum and minimum angles of the hip and knee, as well as the range of muscle length [So et al., 2005]. Changes in the crank arm length also affect the muscle lengthening and shortening; an increase in the crank arm length results in a greater torque produced at the crank with the same force [Too and Landwer, 2004]. The external mechanical variables, including the crank arm length, seat tube angle, and seat-to-pedal distance, should all be set to correspond to the proportion of the force-length curve closest to the resting length to produce the force that will maximise the torque and power production [Too and Landwer, 2004]. The most important external factor on muscle recruitment pattern appears to be the cadence. Baum and Li [2003] analysed the effect of frequency and inertia on lower extremity muscle activity and found that for more than 45% of the lower extremity muscles tested, the muscle activity pattern changed significantly with pedalling frequency, mainly due to the alteration of the timing of muscular activity with a change in the speed of movement. A cyclist's ability to accelerate the crank with the working muscles decreases at higher pedalling rates due to increased negative muscle work; negative muscle work would need to be overcome by additional positive work to maintain a given power output [Neptune et al., 2009]. There is still some debate as to what the optimal cadence for cycling should be, mainly because the pedalling frequency affects the muscle fibre-type recruitment pattern (type I and type II muscle fibre types), but the percentage of type I muscle fibres is strongly affected by the length of training [Faria et al., 2005]. For professional cyclists the gross efficiency was found to be higher at 100rpm compared to 60rpm (24.2% compared to 22.4% respectively) suggesting that higher cadences are more beneficial for professional cyclists [Faria et al., 2005].

Theoretical models to predict the power or velocity of a cyclist have become a useful alternative to systems that collect power data, and are often used to assist coaches and athletes for analysing different conditions, pacing strategies or even equipment without the need for the athlete to actually perform such scenarios. More detail about mathematical models will be discussed later in the thesis.

The effects of nutrition on athlete performance is another important factor that affects power supply. Athletes need to ensure they select the approriate foods and fluids to maintain their body weight, replenish glycogen stores, and provide adequate protein to build and repair tissue, as well as ensure they are well hydrated before an event and drink enough during and after an event [Rodriguez et al., 2009]. According to Jeukendrup and Martin [2001] water and carbohydrate beverages can improve athlete performance by 2.3% over 40km, and high caffine doses (5mg/L caffine concentration in urine) can increase power output by 5%. It should be noted that caffine concentration is monitored for track cycling events, but not considered prohibited [Regulations, 2009, World Anti Doping Code Jan 2011].

Training is considered one of the main modifiers of athlete performance, with a 5% improvement in VO_{2max} and 8.4% improvement in finishing time for athletes with a relatively low starting level who train 40-55 minutes, 5 times a week for 8 weeks [Jeukendrup and Martin, 2001]. Research into the influence of training on athlete performance suggests that greater gains can be made for untrained individuals and the elderly, as their initial VO_{2max} levels are very low [Jeukendrup and Martin, 2001]. There is limited information about the effect of training on the performance of elite athletes who are already well trained, although Jeukendrup and Martin [2001] suggest elite cyclists will only see a 1 to 3% improvement in performance with training compared to a 5 to 10% improvement in performance for novice cyclists. The different types of training techniques and their effect on performance will not be discussed in this thesis, but it is important to recognise that training can improve athlete performance regardless of athlete position and equipment used.

2.2 Factors Affecting Power Demand

The most significant factor affecting the power demand of cycling at speeds above 15kph on flat terrain is the air resistance, accounting for over 90% of the resistive forces at speeds over 50kph [Grappe et al., 1997, Broker, 2003, Lukes et al., 2005, Oggiano et al., 2008, Zdravkovich et al., 1996]. Drag is affected by athlete position, the shape of the equipment and body of the athlete, and the surface friction of the equipment and clothing. The remaining 10% of resistive forces comes from tyre and bearing rolling resistance, and the efficiency of the drivechain. When cycling on a steep gradient (>10%) the weight resistance of the athlete and equipment becomes increasingly more significant compared to drag, but this only comes into effect on hilly terrain and not in a velodrome. Aerodynamic drag is the focus of this thesis, as it accounts for the highest contribution of resistance in elite, track cycling, and is therefore the most significant factor for increasing the speed of a cyclist. Aerodynamic drag will therefore be discussed in more detail, but a summary of the contribution of all other resistive forces in cycling is given below.

Rolling Resistance

On flat terrain at cycling speeds less than 13kph (8mph) rolling resistance is the dominant resistive force [Kyle, 2003a]. Rolling resistance depends on the surface of the track or ground, tyre pressure, tyre surface, tyre geometry, weight on the tyres, ambient temperature, velocity, and steering angle. According to Kyle [2003a], surface roughness, tyre material and construction, tyre pressure, and total load on the wheel are considered to be the most influencial on rolling resistance. The rolling resistance on the rear wheel is greater than on the front wheel because 60% of the total weight is located on the rear wheel [Kyle, 2003a, Oggiano et al., 2008]. In order to reduce rolling resistance, the weight of the frame, wheels and tyres should be as low as possible, and the tyres should be thin with a thin, smooth tread. The other factors which affect rolling resistance (temperature, steering angle, velocity and track surface) cannot be improved and will vary depending on the athlete, race conditions, and the velodrome used. Technology has enabled bike frames, wheels, and tyres to be extremely light and aerodynamic and it has reached a stage where the development of new equipment, in particular of tyres, has slowed. Time and money is now better spent concentrating on trying to improve athlete position, where gains can be much greater due to the individuality of athlete position. The bike frame and components only account for 30% of the total drag, compared to the athlete's position, which account for 70% of the total resistance to forward motion [Oggiano et al., 2008]. Typical values for the coefficient of rolling resistance have been determined by Grappe et al. [1997] and Groot et al. [1995]. Grappe et al. [1997] calculated the rolling resistance for four different positions (upright, dropped, aero, and Obree) by fitting linear and V^2 functions to the data for a cyclist performing trials on a velodrome. The results showed that the rolling resistance was 2.79N, 1.25N, 2.51N and 1.24N for the upright, dropped, aero and Obree positions respectively, which gave an average coefficient of rolling resistance of $C_{rr} = \frac{R_T}{mg} = 0.003$. Groot et al. [1995] obtained data for seven cyclists in the dropped position using coast down tests on a flat, asphalt surface. The deceleration due to rolling resistance, a_r, was found to be between $0.035 < a_r < 0.040$, and assuming $a_r = C_{rr}g$, the coefficient of rolling resistance found to be between $0.0036 < C_{rr} < 0.0041$.

Drive Chain Efficiency

Drive chain efficiency is the power output at the wheels divided by the power input at the cranks, and is usually 95-98% efficient between 100-400W power inputs [Kyle, 2003a]. The efficiency is dependent on load, gear ratio, chain tension, chain bend, crank rpm, gear combination, chain type, chain position, and lubrication [Kyle, 2003a]. As racing track bikes have no gears, will be well lubricated, will be correctly aligned and the

athletes will pedal fast, the efficiency of these drive chain systems will be as high as possible (around 98% efficient).

Gravity and Weight

Gravity effects only become significant when a cyclist is travelling uphill, slowing the rate of ascent, or downhill, increasing the rate of decent. Accoring to Kyle [2003a] the speed of a cyclist downhill will never compensate for the time lost uphill. Reducing the weight of the bike and/or rider will increase the climbing rate, and therefore reduce the overall finishing time over a hilly course. For velodrome races where the rider does not go up or down the banking, such as the Individual Pursuit (IP), the effects of gravity can be ignored because of the symmetry of the velodrome. An increase in weight of the bike and/or athlete will cause an increase in tyre deformation and load on the bearings, resulting in a higher rolling resistance [Kyle, 2003a]. However, the effects of weight on the overall resistance of a cyclist is minimal compared to aerodynamic effects; a 10g reduction in drag is equivalent to a reduction in weight by 1kg [Kyle, 2003a]. The UCI has actually limited the weight of track bikes and wheels to 6.8kg, excluding any additional accessories such as an SRM Power Meter, to prevent any unfair advantages. Although a decrease in body weight may benefit athletes climbing hills or going up the banking, it has been suggested that oxygen uptake is affected by body mass [Jensen et al., 2001]. However, no significant relationship between body mass and drag area has been found [Garcia-Lopez et al., 2008].

Ambient Conditions, Cross Wind and Altitude

The effect of temperature, pressure, relative humidity and altitude on the aerodynamics of cycling will be discussed in the Literature Review (Section 3.2.2.8). The effect of external wind is significant in road cycling, where it has been suggested that athletes should increase their power in a headwind rather than maintain a constant power output in order to reduce their finishing time [Swain, 1997]. However, in an indoor velodrome external wind effects are negligible due to the controlled conditions and track symmetry, so can be ignored.

Chapter 3

Literature Review

Introduction

This chapter provides a discussion on the previous research carried out on mathematical models for cycling, and of the aerodynamics of cycling. The review of existing mathematical models used for cycling provides a brief discussion of the most common expressions used to calculate the performance variables (speed, time or power) followed by a discussion of each significant resistive factor, highlighting which models include or exclude these factors. A summary of the assumptions used by the most common existing mathematical models for cycling and of their reported accuracy is also provided. This is followed by a review on previous research carried out on team pursuit and drafting mathematical models, and of different pacing strategies used for different cycling events. The discussion on the aerodynamics of cycling includes some background on different types of drag, the boundary layer, and separation, followed by a more detailed discussion on factors that affect the aerodynamic drag of cycling and how the drag can be reduced for each factor involved.

3.1 Literature Review: Mathematical Model

Mathematical models have become popular tools for assisting athletes and coaches with training techniques, racing strategies, and what equipment to use for high performance sports in order to gain a competitive advantage. They are useful for analysing how, and to what extent, different variables influence performance systematically, without the need for athletes to consistently perform at race pace. This enables comparisons to be made between athletes for the same race, and for the same athlete for different race conditions; by modifying the variables in a mathematical model, 'what if?' scenarios can be answered. The use of mathematical models for track cycling has increased over the last fifteen years, primarily due to the introduction of the SRM, which has allowed power, velocity and cadence data to be collected during training and racing. Although accurate models were available before the introduction of the SRM [Olds et al., 1993, 1995] the SRM has made it easier for data to be collected, increasing the accuracy of cycling models and the amount of data that is now available for the power supply, which cannot be modelled to the same accuracy as power demand.

3.1.1 Types of Models

As mentioned in the Chapter 2 (Background) performance in track cycling is effectively only dependent on factors associated with power supply and demand, and according to Olds [2001] mathematical models can be classified as either supply, demand, or supply-demand models, which are then categorised into either goodness of fit or first principle models depending on how supply and demand are connected.

3.1.1.1 Supply, Demand, and Supply-Demand Models

One of the simplist types of high performance models uses chronological year to predict performance; by plotting velocity as a function of year, the improvement in performance can be identified [Olds, 2001]. However, very few models like this exist, as they have a tendancy to combine variables of interest together. This not only makes the accuracy of the models questionable, but makes it almost impossible to assess 'what if?' scenarios. More rational models include those where all factors affecting supply and demand are separated and can be altered individually to analyse 'what if?' scenarios. These include supply side models, demand side models, and supply-demand models.

Supply side models focus on the aerobic and anaerobic energy supply of the athlete, and relate supply side variables to performance. The demand side variables are either not present, or are represented as a constant demand [Olds, 2001]. Such models are also known as physiological models, as they focus on the mechanical, physical and biochemical functions of the body. Examples of models, which use solely supply side variables are those by Olds et al. [1993, 1995] and Di Prampero et al. [1979]. In these models equations are formed for the supply side as a function of velocity and distance to determine the energy which can be produced by the cyclist, and for the demand side as a function of time to determine the energy required during cycling. These equations are then evaluated for a fixed distance by iteratively adjusting time (and hence velocity) until supply is equal to demand. These models are fairly complex as they include all factors associated with energy supply (internal energy, oxygen uptake, rate at which energy can be supplied, inefficiency of the human-machine system) and energy demand (rolling resistance, air resistance, gradient, acceleration) of cycling. Only those models created by Di Prampero et al. [1979] and Olds et al. [1993, 1995] consider factors for the energy available to perform work during cycling, derived from anaerobic and aerobic energy sources. These parameters are difficult and time consuming to measure, and although literature does exist for values associated with anaerobic and aerobic energy expenditure for high performance athletes, Martin et al. [1998] and Bassett Jr et al. [1999] argue that maximal oxygen consumption, VO_{2max}, is not always a good indicator of performance due to the high variability between individuals. Accurate mathematical models have been created without the inclusion of anaerobic and aerobic data (demand side models), so it is a valid assumption that supply side variables can be considered a constant.

Demand side models focus on what effect frictional and inertial resistances have on forward motion of the system and the factors that modify them, and generally assume power supplied is constant or unitary [Olds, 2001]. Such models are also known as biophysical models, as they focus on the application of physics to understand the effect on the biological system. The power produced by an athlete can then be calculated by determining the amount of power required to overcome the resistance to forward motion, assuming the athlete can produce the same power for each scenario.

The most sophisticated and accurate models are those which incorporate both supply and demand side variables by generating a physiological model for the supply side and a biophysical model for the demand

side [Olds, 2001]. However, there are very few models which incorporate all of these factors. Existing models demonstrate that high accuracy can be achieved by considering either the supply side or demand side, and that finishing times can be accurately predicted from measured power if it is assumed that the supply side is constant [Bassett Jr et al., 1999, Candau et al., 1999, Lukes et al., 2006, Martin et al., 1998, 2006].

3.1.1.2 Goodness of Fit and First Principle Models

Goodness of fit models establish correlations between input variables and performance indices [Olds, 2001]. Although useful when linear regression can be applied, such models are of no benefit for modelling track cycling, as aerodynamic drag accounts for the majority of cycling demand and is a function of the third power of velocity. Although goodness of fit models may be beneficial to highlighting trends, using statistical relationships to generate model parameters does not necessarily produce the most accurate results.

On the other hand, first principle models are generated from the ground up, and use accepted descriptions of exercise responses and experimental data rather than statistical methods to create model parameters [Olds, 2001]. The majority of mathematical models created for high performance sports are first principle models, which use physical laws to determine a relationship between the inputs and performance indices [Candau et al., 1999, Di Prampero et al., 1979, Bassett Jr et al., 1999, Lukes et al., 2006, Martin et al., 1998, Olds et al., 1993, 1995, Martin et al., 2006].

3.1.2 Existing Models for Cycling

The majority of literature related to mathematical modelling of cycling focuses on only eight expressions relating supply and demand (see Appendix B for a description of these models). These models either calculate the power output from a known velocity, time and/or distance [Martin et al., 1998, Bassett Jr et al., 1999, Di Prampero, 1999, Candau et al., 1999], or calculate the velocity from a known power output or power profile [Lukes et al., 2006, Olds et al., 1993, 1995, Martin et al., 2006]. All models are formed from first principles and equate supply and demand, either in terms of energy, power, or velocity, so that 'what if?' scenarios can be analysed rationally. Most of these models only predict an average power output for a constant velocity or specific race time and distance [Candau et al., 1999, Di Prampero et al., 1979, Bassett Jr et al., 1999, Martin et al., 1998]. Although these models may be fairly accurate for predicting what average power an athlete requires in order to complete a specific race in a certain finishing time, they do not represent what is really happening throughout a race; although an athlete may find that they need to produce an average power of 450W to match previous world hour records [Bassett Jr et al., 1999], these models do not show what pacing strategy the athlete should be using throughout the race. Olds et al. [1993] expanded on the mathematical model by Di Prampero et al. [1979], which only calculates the average evergy expenditure during cycling, and created a new model with one equation for the energy required by an athlete and one equation for the energy produced by an athlete. These equations are then solved iteratively by initialising the elapsed time, t_n, at zero and then iteratively adjusting the instantaneous velocity until supply equals demand. A small value, δt, is then added to t_n and the whole iteration procedure starts again. This process continues until the race distance has been reached. This type of model allows the velocity profile to be calculated, which is more beneficial than just a predicted average power or velocity value for an entire race. Lukes et al. [2006] also created a model to calculate the velocity profile during a race, but used a time stepping technique to determine the acceleration, and therefore change in velocity, over a finite number of time steps from known

SRM power data. The advantage of the model created by Lukes et al. [2006] is that actual race power data is used to predict the velocity, rather than modifying the velocity in order to equate supply and demand without actual race data. Martin et al. [2006] also improved their previous model [Martin et al., 1998] by using forward integration and actual power-time data recorded by an SRM to predict the velocity profile of the cyclist. Although this model assumed a circular track of 250m rather than an oval track, the model still predicted the velocity profile to high accuracy.

The accuracy of mathematical models highly depends on the number of input variables and what assumptions have been made. In track cycling, both human and environmental factors influence power and speed. This includes rider position, rider size, the bike, clothing, helmet, wheels, tyres and components used, the track geometry and surface, temperature, pressure, humidity and wind [Broker et al., 1999]. According to González-Haro et al. [2007], the most important variables that affect power output are displacement speed, overall weight of the rider, bike and wheels, and the aerodynamic variables. Therefore models which exclude some of these factors may be argued to be too simplistic.

All mathematical models for cycling include factors for aerodynamic drag and rolling resistance, as these are the most significant resistive forces to forward motion on flat terrain at a cycling speed greater than 15kph [Martin et al., 2006, Atkinson et al., 2003, Olds, 1998, Martin et al., 2007, Brownlie et al., 2010]. All models also account for the efficiency of the drive chain, as it is common knowledge than no mechanical system is 100% efficient. According to Kyle [2003a] load and gear size are the main contributors to derailleur efficiency. Values for drive chain friction vary from 1.9% for a new, clean chain at 100W power output, to 3.9% at 300W power output for a used chain [Atkinson et al., 2003] and there is currently no agreement of an exact value for drive chain efficiency. However, the discrepancy between values for drive chain friction do not alter the final results for power, velocity or time significantly. It can therefore be assumed that drive chain friction remains constant throughout a race, and would be at the lower end of the scale for elite cyclists, who are more likely to be using a new, clean chain. Reasonably accurate models have been created just using variables for aerodynamic drag, rolling resistance and drive chain efficiency [Bassett Jr et al., 1999, Candau et al., 1999, Lukes et al., 2006]. However, these models are not very useful for making informed recommendations about modifications to equipment, pacing strategy and other factors relating to supply and demand. More detailed models also include terms for the change in potential energy of the system [Di Prampero et al., 1979, Martin et al., 1998, Olds et al., 1993, 1995, Martin et al., 2006], change in kinetic energy of the system [Martin et al., 1998, Olds et al., 1995, Martin et al., 2006], and bearing friction [Martin et al., 1998, 2006]. Although these models can be used to study the effect of the power-time profile on finishing time, they tell us nothing about physical fatigue.

3.1.2.1 Aerodynamic Drag

Aerodynamic drag is by far the most significant variable for track cycling, accounting for 90% of total resistance over 50kph, and is dependent on the air density, ρ, drag coefficient, C_d, frontal area, A, and velocity, V ($D = \frac{1}{2}\rho C_d A V^2$).

Air density is dependent on the temperature, pressure and relative humidity, all of which should be accounted for and be as close as possible to actual race conditions in order for the highest accuracy to be achieved. Di Prampero et al. [1979] and Olds et al. [1993] did not take into account the relative humidity when creating an expresion for the air density for simplicity, and lumped $C_d A\rho$ as a single parameter ($C_d A\rho$=0.404). These

models would therefore only be useful for analysing athletes at the same atmospheric conditions as were used when generating the models. Olds et al. [1995] did update the model to include a correction term for the relative humidity, CF_H, as shown in Equation 3.1, where 1.225 is the density of air at sea level at an ambient temperature of 288.15K, P_B is the absolute pressure (Pa) and T is the temperature (K) at race conditions.

$$\rho = 1.225 \frac{P_B}{760} \frac{288.15}{T} CF_H \tag{3.1}$$

Another common method of calculating air density is by using partial pressures of wet/dry air and the saturation vapour pressure of water, as shown in Equation 3.2, where P_d is the partial pressure of dry air (Pa), P_v is the partial pressure of wet air (Pa), R_d is the specific gas constant for dry air ($JK^{-1}kg^{-1}$), R_v is the specific gas constant for wet air ($JK^{-1}kg^{-1}$), T is the temperature (K), ϕ is the relative humidity, and P_{sat} is the saturation vapour pressure of water (Pa).

$$\rho = \frac{P_d}{R_d T} + \frac{P_v}{R_v T} \tag{3.2}$$

$$P_d = P - P_v$$

$$P_v = \phi P_{sat}$$

$$P_{sat} = 610.78 \times 10^{(7.5T - 2048.625/T - 35.85)}$$

Although this empirical correlation is good for estimating the air density, it does not quite agree with measured data. An alternative method for calculating the air density for moist air is described by Davis [1992], shown in Equation 3.3, where P is the pressure (Pa), M_a is the molar mass of dry air, x_v is the mole fraction of water vapour, T is the temperature (K), R is the molar gas constant, M_v is the molar mass of water, and Z is the compressibility factor. This method calculates the saturation vapour pressure at ambient temperature, an enhancement factor at ambient temperature and pressure, the mole fraction of water vapour, the compressibility factor of air, and finally the air density, using known temperature, pressure and relative humidity data.

$$\rho = \frac{PM_a}{ZRT} \left[1 - x_v \left(1 - \frac{M_v}{M_a} \right) \right] \tag{3.3}$$

Temperature also affects air density, which in turn affects the aerodynamic drag. Di Prampero et al. [1979] suggests that a change in temperature by 3°C will cause a change in drag by 1%. Atkinson et al. [2003] suggests that an increase in temperature by 3°C and a decrease in pressure by 2KPa will cause a reduction in air density, and therefore drag, by 4%. These results highlight the importance of ensuring the temperature and pressure used for modelling are as close as possible to race conditions in order for the results to be as accurate as possible.

Air density changes with altitude, and at a lower air density (higher altitude) the aerodynamic drag decreases, enabling athletes to pedal faster for the same amount of power output. However, there is also a decline in maximal oxygen uptake, VO_{2max}, when the air density is lower, and although athletes can acclimatise to such conditions, a decrease in VO_{2max} will lead to a decrease in power output. The decline in power output can be assumed to be equivalent to the decline in VO_{2max} [Di Prampero et al., 1979, Olds et al., 1995, Bassett Jr et al., 1999] and for a trained, acclimatised subjects this can be described by Equation 3.4 [Davis, 1992, Bassett Jr et al., 1999], where z is the altitude (m) ($r^2 = 0.9729$) . Equation 3.4 is useful for estimating power profiles and finishing times for athletes competing on different indoor velodromes around the world, even when only one set of power or velocity data is available at one known altitude.

$$P = (-1.122)z^2 - (1.8991)z + 99.921 \tag{3.4}$$

An alternative method for comparing race data on similar terms is described by Bassett Jr et al. [1999], who used Equation 3.5 to adjust all hour records to sea level in order to compare past outcomes on equal terms, where ρ is the air density (kgm^{-3}), g is the acceleration due to gravity (ms^{-2}), n is a polytropic gas coefficient (1.235), z is the altitude above sea level (m), R is the specific gas constant for air (287.1Nm) and T is the temperature (K). Bassett Jr et al. [1999] used this equation to generate a correction factor to account for changes in altitude, where sea level = 1.0.

$$\frac{\rho_2}{\rho_1} = [1 - g(n-1)(z_2 - z_1)/(nRT_1)]^{(1/(n-1))} \tag{3.5}$$

Olds et al. [1995] corrects for altitude by using default values for temperature and pressure as described by an iterative appoximation method; using an initial pressure, P_B, of 101325Pa the pressure at a specific altitude, z, is calculated by firstly finding an approximation for the acceleration due to gravity, g, then finding the temperature at this altitude, T, and finally finding the pressure for the ith+1 iteration, P_{Bi+1}:

$g = 9.80665(\frac{6378}{6378+\frac{z}{1000}})^2$

T=288.15-0.0065Z

$P_{Bi+1} = P_B \frac{T}{288.15-0.0065Z} \times \frac{g}{287\times 0.0065}$

Depending on the available data and aim of the mathematical model, any of the above equations are valid for analysing the effects of altitude on cycling performance. The model by Bassett Jr et al. [1999] is more useful for making comparisons between two results at different elevations on equal terms, where as the model by Olds et al. [1995] is more useful for determining the pressure from a known temperature and elevation.

The equation for aerodynamic drag is $D = \frac{1}{2}\rho C_d A V^2$. The drag coefficient, C_d, varies significantly with position and size of riders, ranging from $C_d = 0.35$ for riders on the drops to $C_d = 1.1$ for riders standing on the pedals [Martin et al., 2007]. This results in a wide variety of values for drag coefficient reported in the literature. Estimates of the frontal area of the rider, rider and bike, or rider, bike and wheels also vary widely throughout the literature, as shown in Table 3.1. The frontal area can be determined by photographic weighing, manual planimetry, computerised planimetry or using Computer Aided Software (CAD). Debraux et al. [2009] compared the methods of using CAD, photographic weighing and computerised planimetry to calculate the frontal area of a cyclist and found no significant difference between the three methods, as shown in Table 3.2. It should be noted that the drag coefficient and frontal area will vary between riders, due to differences in body size and shape.

	n	Projected Frontal Area (m^2)		
		Hoods	**Drops**	**Aero**
Capelli et al. (1993)	2			0.394
Davies (1980)	15		0.5	
Faria & Cavanagu (1979)	-	0.5		0.35
Gross et al. (1983)	-	0.399		0.362
McLean (1994)	10		0.387	
	10		0.465	
Neumann (1992)	-	0.6	0.5	0.4
Nonweiler (1956)	3	0.396		0.326
Olive (1996)	17	0.605	0.563	0.493
Pugh (1974)	6	0.47	0.46	0.42
Swain et al. (1987)	5			0.318
	5			0.378
Wright et al. (1993)	10			0.332

Table 3.1: Reported values for the projected frontal area of cyclists [Olds and Olive, 1999]

	Photographic Weighing	**CAD**	**Computerised Planimetry**
Upright Position	0.432	0.430	0.533
Aero Position	0.341	0.338	0.426

Table 3.2: Comparison of three methods to calculate the frontal area of a cyclist (m^2) [Debraux et al., 2009]

Olds and Olive [1999] also carried out a study to compare these three methods and found that all methods showed high precision and reliability, and were similar to within 3.3% of each other. They found that the differences between reported values was most likely due to the perspective and distortion effects of photography; the frontal area changed with displacement of the reference dimension, the distance between the camera and the cyclist, and the focal length of the camera. Therefore it is difficult to compare reported values of frontal area with each other unless these factors are also reported in the literature. Although Olds and Olive [1999] found a valid explanation for the differences in calculated frontal areas for cyclists, it is unlikely that the test subjects in each study adopted exactly the same position as each other, nor had the same equipment or set up. Although two athletes may both adopt a "drops" position it is unlikely that both will be in exactly the same position, resulting in a difference in frontal area. More reliable models are those which allow the frontal area and drag coefficient for the specific athlete, set up and equipment to be input into the model, rather than relying on previously reported values in the literature or even correction factors, such as the model by Bassett Jr et al. [1999].

Olds et al. [1993], Di Prampero et al. [1979] and Bassett Jr et al. [1999] have created expressions to calculate the frontal area from the body surface area (BSA) of the rider and shape of the bike, rather than using photographic weighing, manual planimetry or computerised planimetry. Previous data has shown that there is a linear relationship between body surface area, BSA, and frontal area, A, although the accuracy of this relationship varies from r^2=0.401 to r^2=0.757 [Bassett Jr et al., 1999]. A possible reason for this discrepancy

is explained by Bassett Jr et al. [1999], who state that the slope of the linear regression curve is similar for all studies, but the ratio of BSA to A favours larger subjects and unless this is taken into account the power required for larger subjects to overcome aerodynamic drag will be overestimated. However, a significant change in rider position will have a huge impact on the frontal area regardless of the height and weight of the athlete. Martin et al. [2006] found a 68% difference in drag area for subjects whose body mass and predicted body surface area differed by only 10% and 4% respectively, showing that a difference in drag area is not simply caused by body mass or surface area. Therefore, the method of calculating the frontal area from body surface area should not be used unless no other data is available, and even then this method should take into account differences in body size and only be used as an approximation. The equation by Bassett Jr et al. [1999] used to calculate the frontal area based on body surface area, which does accounts for body size, is shown in Equation 3.6.

$$A = 0.0293m^{0.425}H^{0.725} + 0.0604 \tag{3.6}$$

Barelle et al. [2010] carried out a study to determine the relationship between the frontal area and the body height and mass, and the frontal area and the inclination and length of the helmet. Using nine professional, male cyclists, five different helmets, and three helmet angles (low, usual and high) Barelle et al. [2010] measured the frontal area by computerised planimetry with a reference board located at 0.15m from the crank set; the optimal location of the reference board was determined as a ratio of proportions and distances between body parts. The results showed that the frontal area was sensitive to both body height (H) and mass (m), as shown by Equation 3.7, and related to the helmet inclination (α) and length (L) by a polynomial regression when the helmet was in the usual position, as shown by Equation 3.8.

$$A = A_{cb} + A_{ch}$$

$$A_{cb} = 0.045 \times H^{1.15} \times m^{0.2794} \tag{3.7}$$

$$A_{ch} = 0.329 \times (Lsin\alpha)^2 - 0.137 \times Lsin\alpha \tag{3.8}$$

Martin et al. [1998] recommended using drag area, C_dA, instead of separating the variables of drag coefficient and frontal area, as drag area is dominated by the separation associated with rider position, shape, size, and surface roughness; as the frontal area changes, the flow over the rider and bike will also change. However, there are still large variations is the percentage reduction in drag area from changes in position in the literature, most likely due to the difference in stature between individual riders. Table 3.3 shows a summary of reported values of the reduction in drag area from the stated reference position. Comparing these results for athletes going from a dropped position to a time trial position, an athlete may reduce their drag by anything between 2.2% and 31% depending on their stature. Models which allow actual values for drag coefficient, frontal area, or drag area to be changed for individual riders are more realistic than those which use a correction factor for different riding positions, such as the model by Bassett Jr et al. [1999], or those based on a drag coefficient for a specific riding position, such as the model by Di Prampero et al. [1979] which is only applicable to riders on a racing bike in a fully dropped position.

	Kyle & Burke (1984)	Kyle (1991b)	Kyle (1989)	Richardson & Johnson (1994)	Zdravkovich (1996)	Grappe et al. (1997)
Reference Position	Dropped	Dropped	Cowhorn	Dropped	Dropped	Upright
Dropped-crouch	20%				5%-13%	8%
Speed-skating		12%				
Time-trial			14%-16%	2.2%	24%-31%	12%
Hill descent	28%				24%-31%	
Obree						28%

Table 3.3: Percentage reduction in drag area from stated reference position

Values for drag area can be measured from wind tunnel tests, coast down tests or towing tests. Each of these methods has their own advantages and disadvantages. Martin et al. [2006] used linear regression to calculate the drag area based on field tests using a power meter and compared the results to wind tunnel tests. There was no significant difference between the field derived drag area and the drag area recorded from wind tunnel testing. However, regression analysis precision is limited by the effects of changes in the ambient conditions, especially wind [Candau et al., 1999]. Candau et al. [1999] used coast down tests to determine the drag area of cyclists, the results of which lay within the same range as wind tunnel tests. However, Candau et al. [1999] also suggested that coast down tests have a tendency to overestimate drag because there is no drag interaction between the cyclist and the floor, as there is in wind tunnel testing, and that wind tunnel tests have a higher reproducability even compared to coast down tests carried out in a hallway where there are no effects of wind or changes in temperature or grade.

3.1.2.2 Rolling Resistance

Tyre rolling resistance is the second highest contributor of resistance to motion, and decreases as a function of cycling speed, tyre material, tyre pressure, tyre diameter, tyre width, surface roughness, steering angle, temperature and total load. At 40kph, rolling resistance accounts for 10% of total resistance to forward motion [Atkinson et al., 2003]. Rolling resistance is usually expressed in terms of the coefficient of rolling resistance, C_{rr}, which is equal to the friction force divided by the load on the tyre. Reported values of the coefficient of tyre rolling resistance vary from $C_{rr} = 0.002$ for tyres on a smooth, hard surface to $C_{rr} = 0.010$ for tyres on an uneven, soft surface [Wilson, 2004, p211]. For track cycling the coefficient of rolling resistance will be on the lower end of this scale, as the surface of velodromes used for major competitions is often made from timber, the bikes are lighter than road bikes, and the bicycle tyres are narrower and inflated to a high pressure; an increase in tyre pressure reduces the coefficient of rolling resistance regardless of the size of the wheel [Kyle, 2003a]. Martin et al. [2006] measured the global coefficient of friction on a velodrome, which included tyre and bearing resistance, and found the mean value to be $C_{rr} = 0.0025$. As expected, this value was slightly higher than previously reported values for the friction coefficient on a velodrome due to the inclusion of bearing resistance. Most mathematical models generate equations, albeit different, which include a term for the coefficient of rolling resistance, and then use reported values in the literature close to race conditions or valid assumptions from previous tests to determine the coefficient of rolling resistance to validate the models [Martin et al., 1998, Olds et al., 1993, 1995, Candau et al., 1999, Lukes et al., 2006]. Grappe et al. [1997] calculated the rolling resistance for four different positions (upright, dropped, aero, and Obree) from

plots of total resistance, R_T, against velocity squared for a cyclist performing trials on a velodrome. The results showed that the rolling resistance was 2.79N, 1.25N, 2.51N and 1.24N for the upright, dropped, aero and Obree positions respectively, which gave an average coefficient of rolling resistance of $C_{rr} = \frac{R_T}{mg} = 0.003$. Groot et al. [1995] obtained data for seven cyclists in the dropped position using coast down tests on a flat, asphalt surface. The deceleration due to rolling resistance, a_r, was found to be between $0.035 < a_r < 0.040$, and assuming $a_r = C_{rr}g$, the coefficient of rolling resistance found to be between $0.0036 < C_{rr} < 0.0041$. A summary of values of the coefficient of rolling resistance for low-drag tyres typically used for modelling cycling at an elite level is shown in Table 3.4. Table 3.4 shows that the values for the coefficient of rolling resistance in the literature varies between 0.0016 and 0.00563.

C_{rr}	**Description**
0.0016 - 0.0032	sew-ups on linoleum
0.0023 - 0.0029	clinchers on linoleum
0.0017	track sew-up on concrete
0.0016 - 0.0026	track sew-up
0.0028	Moulton clincher
0.0033 - 0.0037	road sew-up
0.0039	road clincher
0.0039 - 0.0049	road tyres (120psi)
0.0016 - 0.0042	road tyres (120psi)
0.0043	top 700C clincher, 100psi
0.00563	linoleum flooring [Candau et al., 1999]
0.0025	on velodrome (includes bearing resistance) [Martin et al., 2006]
0.0036 - 0.0041	asphalt surface [Groot et al., 1995]
0.003	on velodrome [Grappe et al., 1997]

Table 3.4: Values for C_{rr} for low-drag tyres [Wilson, 2004, p230]

Few models take into account the increase in rolling resistance due to the steering angle. This is significant for track cycling as the track is always banked, even on the straights, so the rider must steer in order to keep the bike straight. Kyle [2003a] measured the steering angle of a bike on a 250m velodrome track during constant pedalling at 48kph. The results showed a variation in steering angle by 2.5° with every pedal stroke, and that on the straights a steering angle of 1° was required to keep the bike straight, and on the bends the steering angle increased to 4°. This corresponds to an increase in rolling resistance of 4.1% in the straights and 28.6% in the bends. Wilson [2004, p211] states that a slope of even 0.001 can increase the tyre coefficient of rolling resistance by 10-50% due to scrubbing. Only those models created by Bassett Jr et al. [1999] and Lukes et al. [2006] include a factor for the increase in rolling resistance due to steering, using those results published by Kyle [2003a].

In addition to tyre rolling resistance, bearings also resist forward motion. According to Martin et al. [2007] bearing resistance accounts for only 2-5% of power, but Wilson [2004, p215] states that bearing resistance is negligible compared to 1-3N tyre rolling resistance. Martin et al. [1998] states that the total power lost due to bearing friction can be calculated from Equation 3.9, where V is the velocity (m/s).

$$P_{bearings} = V(91 + 8.7V)10^{-3} \tag{3.9}$$

Wilson [2004, p214] states that the coefficient of bearing resistance is close to 0.001, and this value can be used to determine an expression for the bearing friction in a similar way to tyre rolling resistance. Bassett Jr et al. [1999] included all losses due to bearing friction in a constant value for dynamic rolling resistance ($0.00775 W.kg^{-2}h^{-2}$) which also included losses due to dynamic tyre deformation and windage of the spinning wheel. Although this model allows a correction factor to be applied for different external conditions, it is not possible to change actual values for tyre diameter, pressure etc.

3.1.2.3 Grade Angle / Potential Energy

Although air resistance and rolling resistance are the greatest opposing forces to forward motion on flat terrain, gravity becomes the greatest resistive force on hilly terrain [Olds et al., 1993]. Most mathematical models for cycling are developed for road cycling, where hills and wind (headwind, tailwind or crosswind) are inevitable. Atkinson et al. [2003, 2007] state that grade and wind greatly affect the relationship between power and velocity, which complicates the pacing strategy. However, a velodrome is oval and symmetrical, and the effect of wind is often negligible [Kyle and Bassett Jr, 2003b]. It can therefore be assumed that the effects of wind can be ignored when calculating the average power or velocity required to complete a track race. However, grade angle should not be ignored; the grade angle differs in the bends compared to the straights, which will in turn affect the power output and velocity. Although the track is symmetrical, the grade angle should be included in order to determine the power/velocity profile throughout the race. The grade angle becomes even more important for races where riders go up the banking, such as the Team Pursuit (TP), as there is a greater variation in grade angle. The calculation of work performed against the grade is related to the total mass of the rider and bike, vertical distance to the contact point, and the grade angle, as shown in Equation 3.10 [Olds et al., 1993, 1995, Martin et al., 1998], where V is the velocity (m/s), m_T is the total mass of the rider and bike (kg), g is the acceleration due to gravity (m/s^2), and G is the grade angle (rise/run). For grades of up to 10%, $\sin[\tan^{-1}(G)]$ is approximately equal to G [Martin et al., 1998], and so Equation 3.10 can be simplified.

$$P_{grade} = V m_T g sin[tan^{-1}(G)] \tag{3.10}$$

3.1.2.4 Kinetic Energy

A separate expression must be created for the acceleration of the bike, as most cycling events are from a standing start and the athlete will not necessarily be travelling at a constant velocity throughout the race. Bassett Jr et al. [1999] generated a model for a flying start rather than taking into account an initial acceleration phase, and only assumed that the power output increased by 10% when accelerating from a standing start. However, this will still exclude any effects of acceleration or deceleration which may occur during the race. A more reliable method would be to calculate the acceleration in terms of changes in kinetic energy. Olds et al. [1993] used first principles to develop an expression for the change in kinetic energy during the acceleration phase; $E_k = \frac{1}{2} m_T (V_f^2 - V_i^2)/(t_i - t_f)$, where f and i relate to the final and initial velocity or time respectively. However, this expression only accounts for the linear kinetic energy and not the rotational kinetic energy of rotating components or the athlete's legs. Olds et al. [1995] updated this model to account for changes in rotational kinetic energy in terms of bike mass, rider mass, rider height, velocity, tyre diameter, cadence and a time constant for acceleration. By using data for the masses and radii

of gyration of the leg segments, leg segment lengths, the kinematics of the relevant joints, measured masses, and estimates of radii of gyration of bicycle components, Olds et al. [1995] was able to estimate the total rotational kinetic energy of the system. The model by Martin et al. [1998] also included expressions for the translational and rotational changes in kinetic energy, where the translational kinetic energy was the same as that by Olds et al. [1993], but the rotational kinetic energy only considered the rotating wheels and not the legs or other components ($E_k = \frac{1}{2}IV^2/r^2$, where I is the moment of inertia and r is the outside radius of the tyre). Although the model Martin et al. [1998] does not exclude the effects of changes in translational and rotational kinetic energy completely, the model by Olds et al. [1993] has the advantage of including the effects of rotating legs and additional bike components.

In order to accurately model the power or velocity profile for track cycling the lean angle must be calculated, as the effects of a banked track and changing radius of curvature will introduce an angular acceleration and centripetal force. The rider must move their centre of mass inwards in order to balance the bike, which will reduce the overall distance travelled by the centre of mass compared to the base of the wheels and result in the centre of mass travelling at a slower velocity than the wheels. Very few models take into account the lean angle of the rider and bike around the bend, most likely because there are very few models which have been created solely for track cycling; most mathematical models are created for road cycling, and although there may be bends on a road, the effects of lean angle are not as important as they are on the track, where a longer proportion of overall time is spent in the bends. The models created by Martin et al. [2006] and Lukes et al. [2006] are the only ones which even mention the importance of lean angle during cycling. Martin et al. [2006] assumed the track was circular, with a length of 250m, rather than oval. Assuming the centre of mass was located at the top of the seat, and that the rider and bike leaned together, the lean angle could be calculated using Equation 3.11. Although this result would not provide accurate results at a specific point because of the assumption of a constant radius of curvature for the straights and bends, a realistic approximation should be achieved.

$$Lean = tan^{-1}(\frac{acc_{centripetal}}{g}) \tag{3.11}$$

Lukes et al. [2006] used a similar formula to calculate the lean angle, and also assumed that the centre of mass was located at the seat height. Lukes et al. [2006] separated the straights and the bends, and assumed that in the straights the lean angle was equal to 90^{o} relative to the horizontal, therefore only calculating the lean angle in the bends. The resulting calculated velocity profile clearly showed the difference in velocity of the centre of mass between the bends and the straights, and is therefore a good representation of what is really happening throughout a race on an indoor velodrome.

3.1.2.5 Assumptions existing models use

Di Prampero et al. [1979]

The mathematical model by Di Prampero et al. [1979] assumes that the total energy required by the athlete is that which overcomes rolling resistance and aerodynamic drag, and assumes that all other factors are negligible. The equation for total resistance is determined by plotting the total resistance against velocity squared for the results from towing tests. Straight line regression is then used to calculate the values for rolling resistance (3.2N) and drag (0.19N) ($R_T = 3.2 + 0.19V^2$). This model assumes a mechanical efficiency

of 0.25, which has been taken from previous literature results. It is assumed that the lateral component of air velocity has no substantial effects on mechanical power output, and when cycling on the level, $\dot{V}O_2$ is essentially proportional to body surface area. All equations formed by Di Prampero et al. [1979] are only valid for level ground, for athletes of average size in the fully dropped posture ($C_dA\rho = 0.404$), and for the weight of the subjects and bikes, and for the same rolling resistance conditions used to generate the equations.

Bassett Jr et al. [1999]

Bassett Jr et al. [1999] measured the power during cycling and compared the results of the mathematical model to these field derived values. The reduction in power at altitude was estimated by measuring the power at five different altitudes and finding the relationship between these to create correction factors for the change in power with altitude. The general equation for power output given by Bassett Jr et al. [1999] is P=$A_1V + A_2V^2 + A_3V^3$. The static rolling resistance, A_1, is assumed to be equal to 0.35% of the down force applied to the tyre, found to be A_1=0.00953M from experimental data, where M is the total mass of the system. The dynamic rolling resistance, A_2, is assumed to be proportional to the increase in rolling resistance, where measured data by Richard Moore of General Motors found A_2=0.00775. The drag, A_3, is solved based on experimental data for power and velocity and the given values for static and dynamic rolling resistance, resulting in $A_3 = 0.002582$. The general equation for power output is therefore P=$K(0.00953MV + 0.00775V^2 + K_1(A_f)0.007551V^3$, where K is the correction factor for surface roughness, and $K_1$is the correction factor based on position, bike used, clothing, helmet and altitude. The values for K and K_1 are given for a range of scenarios based on previous literature results. Bassett Jr et al. [1999] assume the frontal area is related to body surface area by $A = 0.0293H^{0.725}M^{0.425} + 0.0604$, and this equation includes the effect of different body sizes. It is also assumed that the drag coefficient is constant as long as position, equipment, and environmental conditions are constant. Therefore, air drag increases linearly with frontal area, so it can be assumed that drag is proportional to the frontal area. The mathematical model assumed a flying start and a steady speed during the entire race, which excludes the initial acceleration phase. However, Bassett Jr et al. [1999] state that the power can be increased by 10% to take into account the initial acceleration for a standing start.

Lukes et al. [2006]

Lukes et al. [2006] used their model to analyse the power output for Chris Boardman, who had an average power of 520W and power at constant speed of 474W (taken from Broker et al. [1999]). The assumed value for drag area, C_dA, was taken from previous literature results of wind tunnel testing with an earlier version of the bike, and the frontal area was calculated using the equation based on body surface area by Bassett Jr et al. [1999], resulting in a drag coefficient of C_d=0.52. Although Lukes et al. [2006] state that the values for rolling resistance, bike efficiency, and climate conditions were selected to be as close as possible to actual race conditions, no actual values are given.

Martin et al. [1998]

The mathematical model by Martin et al. [1998] mainly uses measured variables to generate equations for supply and demand. It is assumed that the coefficient of rolling resistance does not vary with velocity, and

is taken to be the average of the results for 10 high-pressure clincher bike tyres on smooth asphalt previously recorded in the literature (Crr=0.0032). It is also assumed that for road grades of up to 10%, the equation for potential energy can be simplified from $P_{grade} = Vm_T gcos[tan^{-1}(G)]$ to $P_{grade} = Vm_T gG$ (as $cos[tan^{-1}(G)]$ is approximately 1 at grade angles less than 10%). The moment of inertia for both wheels was taken to be 0.14kgm^2 and efficiency was assumed to be constant at 97.698% across the range of powers measured.

Martin et al. [2006]

This updated model by Martin et al. used multiple linear regression to determine the drag area, C_dA, and global coefficient of friction (tyres and bearings), μ, from measured results and compared these to the literature. The efficiency of the drive chain was assumed to be 97.9%, as determined from previous findings, and the authors assumed a circular track of 250m with constant radius of curvature in the straights and bends to model the power profile around the track. A 1s moving average of the sine of the lean angle was generated to account for the transistions between the bends and straights to provide continuous wheel speed. It was assumed that the velocity predicted by the model was the velocity of the centre of mass, which was assumed to be located at the height of the seat measured vertically from the ground up. Any excess power/speed/mass was assumed to go to accelerating the system.

Olds et al. [1993]

The model created by Olds et al. [1993] used mainly measured variables, except for the coefficient of rolling resistance and drag coefficient, which were both assumed to be similar to those found by Di Prampero et al. [1979]. For the demand side, it was assumed that the frontal area was a constant fraction (25%) of the body surface area, there was no drafting involved, acceleration was constant up to steady velocity, steady velocity was maintained once achieved, and the friction from moving bike parts was negligible. On the supply side, it was assumed that the sustainable fraction of maximum oxygen consumption VO_{2max}=1 for less than ten minutes, that the mechanical efficiency was similar at submaximal and supramaximal levels, that mechanical efficiency measured on the ergometer was similar to that seen on the track, and that the mechanical efficiency during the acceleration phase was similar to the steady state phase.

Olds et al. [1995]

The updated model by Olds et al. assumed that the acceleration pattern was monoexponential rather than constant up to steady state velocity. This results in a high power demand during the acceleration phase, and the rate of increase in aerobic energy supply may not necessarily mirror the rate of decrease in anaerobic energy supply. Although this is unimportant for long races, it should be accounted for in shorter races such as the individual pursuit. For this model it was assumed that C_d=0.592, that the time constant for oxygen consumption was 0.667 minutes, that the time constant for deficit kinetics was 0.417 minutes, and that the time constant for acceleration was 10 seconds. It was also assumed that the cadence was 100rpm, and the correction factor for an asphalt and concrete surface was 1 and 0.87 respectively.

3.1.2.6 Accuracy of existing models

Out of all the main mathematical models used for high performance cycling, the model by Lukes et al. [2006], with a time error of only 0.5s (0.2%), is reported to be the most accurate. However, this model was only validated using one set of data, so the reliability could be questioned. The model by Martin et al. [1998] was validated using six subjects, and showed an average of 2.7W difference in power between actual and predicted average power outputs. This is equivalent to an average difference of 3.3%. This model was updated in 2006 to generate a velocity profile rather than an average power output value [Martin et al., 2006]. Not only is this updated model more useful in terms of identifying modifications in set up and equipment, but the accuracy also improved; the predicted velocity profile generated by Martin et al. [2006] had a standard error of only 0.25m/s and a high correlation ($r^2 = 0.989$). The model created by Bassett Jr et al. [1999] was also fairly accurate, with an estimated 4% absolute error and 1.6% time error between actual and predicted values. This model used correction factors for differences in altitude, position, bikes and components, clothing, and helmets, to compare hour record performances under similar conditions. The two models created by Olds et al. [1993, 1995] predicted the finishing time of athletes based on aerobic and anaerobic energy. The 1993 model was validated using 18 elite, male track cyclists, and showed an accuracy of 4.6s (1.3%) mean difference with a high correlation (r=0.809). The 1995 model was validated using 41 subjects, made up of a mixture of recreational, club, state, national, male and female cyclists. The overall accuracy of this model was 1.65min (1.73%) mean difference with a high correlation (r=0.89). However, when the difference between actual and predicted times was predicted for the sub-groups (recreational, club, state and national) a significant variation among groups was seen; the recreational mean difference was 1.9min, the state mean difference was 0.09min, the club mean difference was 0.38min, and the national mean difference was 0.01min. These results suggest that there is more consistency in position or power output between tests where input variables are measured for high end cyclists. A summary of the accuracy of the existing high performance cycling models is shown in Table 3.5.

Model	Accuracy	Number of Cases Tested for Validation
Martin et al. (1998)	3.3% power difference	6
Martin et al. (2006)	0.25m/s velocity difference	3
Lukes et al. (2006)	0.2% time difference	1
Bassett Jr et al. (1999)	1.6% time difference	1
Olds et al. (1993)	1.3% time difference	18
Olds et al. (1995)	1.73% time difference	41

Table 3.5: Accuracy of existing high performance cycling models

3.1.3 Team Pursuit Models

There are very few mathematical models for Team Pursuits (TP) that currently exist in the literature. There is an added complexity to TP models, as there are more riders, the effects of drafting and changeovers come in to play, and there are many unknown variables for which assumptions have to be made, such as the exact trajectory of the riders. Some authors have attempted to generate a mathematical model for drafting events, based on previous models created for individual races [Broker et al., 1999, Olds et al., 1995, Olds, 1998].

Broker et al. [1999] states that the effectiveness of drafting depends on the rider size, position, and the order of the paceline. Drafting is more effective when a smaller rider is drafting a larger rider, although during TP races each rider spends approximately the same amount of time in the lead position as they do drafting. However, it is worth considering if there may be an optimal paceline order, which allows for smaller riders to draft larger riders as much as possible throughout the race. There is currently no literature which addresses this factor, most likely due to the complexity of modelling TP events. The average power output of four TP riders is 75% of that of an IP rider, with riders in second, third and fourth position saving 30%, 36%, and 36% of power compared to the lead rider respectively [Atkinson et al., 2003, Broker et al., 1999, Martin et al., 2007]. This is equivalent to an overall reduction in aerodynamic drag of 38% [Martin et al., 2007, Olds, 1998]. However, the actual reduction in power and drag is also dependent on wheel spacing between riders when in a paceline, with no benefit for any rider who is more than 3m away from the wheel in front [Olds et al., 1995, Olds, 1998]. It has been found to be more beneficial for riders to draft directly behind rather than laterally, with a reduction in drag of 0-30% for laterally displaced riders, and 44% for riders directly behind [Olds, 1998]. More specifically, Olds et al. [1995] reported that riders who were 0.2m, 0.5m, 1m and 2m directly behind the wheel in front showed a reduction in finishing time of 14.1%, 13.6%, 11.9%, and 6.8% respectively. Zdravkovich et al. [1996] carried out a wind tunnel study to determine the optimal position of drafting cyclists by testing twenty different positions in staggered and tandem arrangements. The maximum reduction in drag was found to be 49% in the closest tandem arrangement, but Zdravkovich et al. [1996] suggest that riding so close is too dangerous and that safer positions are at 10cm apart in either a staggered or tandem arrangement, yielding a reduction in drag by 37% and 35% respectively. These results highlight the importance of efficient drafting for all members of a Team Pursuit.

Olds et al. [1995] adapted the model for individual road cycling performance to include a drafting factor, CF_{draft}. This factor was based on a quadratic fit of empirical data from previous literature results for the reduction in time depending on wheel spacing, as shown in Equation 3.12, where x is the wheel spacing (m).

$$CF_{draft} = 1 - 0.3835 + 0.0104x + 0.0405x^2 \tag{3.12}$$

This model for drafting was updated to allow the speed that a group of riders maintain for any remaining distance to be calculated, as well as the maximum time any one rider is able to spend at the front of the paceline. A description of the model process is described in Olds [1998], but the model uses the supply equations for time to exhaustion and demand equations for mean power output respectively. The supply side variables for this model take into account the relationship between the metabollic power production as a fraction of maximum oxygen consumption, fVO_{2max}, and time to exhaustion, T_{lim}; a strong relationship between the log of time to exhaustion and log of sustainable fraction of maximum oxygen consumption was seen, with the line of best fit described by Equation 3.13 [Olds, 1998].

$$ln(T_{lim}) = -6.351ln(fVO_{2max}) + 2.478 \tag{3.13}$$

The demand side for this model was solely based on aerodynamic drag, tyre rolling resistance, and grade angle. It was assumed that each rider took equal turns at the front of the paceline, that all riders were identical and that they rode close enough for the effects of drafting to be significant, that the riders maintained the same power output as if they were riding alone, and that there were negligible effects of acceleration or deceleration, or mechanical and bearing friction. For a specific time, t, if riders spend an equal amount of

time in lead position each rider will spend tn^{-1} at the front and $t(n-1)n^{-1}$ either dropping back or drafting. The mean power output at any velocity can then be calculated using Equation 3.14 [Olds, 1998], where P_{air} is the power to overcome air resistance, P_{roll} is the power to overcome rolling resistance, P_{grade} is the power to overcome gradient, and n is the number of riders in the group.

$$P_{mean} = P_{air}\{[CF_{draft}(n-1)+1]n^{-1}\} + P_{roll} + P_{grade} \tag{3.14}$$

This model serves as a fairly accurate tool for analysing scenarios during breaking away and chasing in cycling. However, this model does rely on a number of assumptions, which although may not yet have shown to violate the predictive power of the model significantly, they restrict the use of this model considerably.

Broker et al. [1999] also created a mathematical model for drafting, based on the model for single track endurance cycling by Bassett Jr et al. [1999]. Assuming all four cyclists in a TP produce the same amount of power that they would in an IP, and using the results for the percentage reduction in power output depending on the position in the paceline, the model for the individual pursuit can be multiplied by the average power factor in the four positions ((1+0.708+0.641+0.640)/4=0.743) to give an expression for the average power produced by each member of the team [Broker et al., 1999]. However, Broker et al. [1999] state that this prediction would be lower than the actual power produced because, even for experienced riders, two riders will be exposed to the wind during a changeover and the energy required for TP riders to accelerate is 1.6% higher than for IP riders. To account for the additional exposure to wind, Broker et al. [1999] estimates a changeover lasts for one-fifth of a lap (15.625s) and that the riders would be completely unsheltered for 8 seconds of this time; this would increase the energy consumption by 1.4% and the acceleration by 3%, resulting in an average power factor of 0.7697 ($1.03 \times 0.743 = 0.7697$). Therefore the average team pursuit power calculated by Broker et al. [1999] can be shown by Equation 3.15, where V is the velocity (kph), M is the total mass of the rider and bike (kg), A is the frontal area (m^2), K is an adjustment factor for track and external conditions, and K_1 is a factor accounting for all aerodynamic variables.

$$P_{av} = 0.7697K(0.00953MV + 0.00775V^2 + K_1(A)0.007551V^3) \tag{3.15}$$

Both drafting models created by Broker et al. [1999] and Olds [1998] are valid yet simplified models, which can be used to analyse the effects of drafting, and chasing and breaking away in cycling. The model by Broker et al. [1999] is more applicable to track cycling, but still lacks the ability to determine the effects of different rider stature in a team, or even analyse the power or velocity profile throughout a TP.

3.1.4 Pacing Strategy

The existing literature on pacing strategies for cycling is also limited. Pacing strategy is related to the energy expenditure of an athlete, and is described as the optimal allocation of physiological resources for a physical task of known or unknown duration [Atkinson et al., 2007]. By regulating the rate of energy expenditure athletes can vary their velocity over a race [Hettinga et al., 2006]. Therefore, mathematical models can be useful for identifying the optimal pacing strategy for an event of any distance.

High performance athletes can vary their power output in a number of ways, the choice of which depends on the race distance and terrain on which the race takes place. Abbiss and Laursen [2008] classify pacing strategies as follows:

1. Negative - an increase in speed and power output towards the end of a race.
2. Positive - a reduction in power output towards the end of a race.
3. All-out - maximum power output during the initial acceleration phase, followed by a gradual decline in power for the remainder of the race.
4. Variable - an increase in power during uphill sections and when riding into a headwind, and a decrease in power during downhill sections and when riding with a tailwind. The power output is varied to counteract external conditions, which affect performance.
5. Even - an initial acceleration to an average velocity and power output, which is then maintained for the remainder of the race.
6. U Shaped Parabolic - instant acceleration to 130% of the average power output, followed by a decrease in power in a parabolic fashion to 80% of the average power output at 50% of the race distance, followed by an increase in power output in the same parabolic fashion to 130% of the average power output at the end of the race.
7. J-Shaped Parabolic - instant acceleration to 95% of the average power output, followed by a decrease in power output in a parabolic fashion to 90% of the average power output at 30% of the completed race distance, followed by an increase in power output in the same parabolic fashion to 130% of the average power output at the end of the race.
8. Reverse-J-Shaped Parabolic - instant acceleration to 130% of the average power output, followed by a decrease in power output in a parabolic fashion to 90% of the average power output at 70% of the completed race distance, followed by an increase in power output in the same parabolic fashion to 100% of the average power output.

In road cycling, the terrain on which the race takes place is the most important factor for analysing pacing strategies, as hills and wind create variations in speed when power output is constant [Swain, 1997]. Many authors have shown that by varying power output on hills and in the wind, specifically increasing power output in uphill and headwind sections and reducing power in downhill and tailwind sections, the time to finish a race can be reduced [Atkinson et al., 2003, 2007, Abbiss and Laursen, 2008, Swain, 1997]. Swain [1997] used the mathematical model developed by Di Prampero et al. [1979] to model a time trial course with equal uphill/downhill segments and equal headwind/tailwind segments. The results showed that the finishing time could be reduced by varying the power output in the hills and wind so that velocity remained as constant as possible; by increasing the power on uphill sections and in headwind, and reducing power on the downhill and tailwind sections to keep mean power constant, athletes completed the race in a faster time compared to a constant power output throughout the whole race.

For flat terrain with no wind, a variable pacing strategy is not necessarily the most optimal. The choice of pacing strategy under such conditions is dependent on the length of the race. By classifying short distance as those less than 1km or 2 minutes, medium races as those greater than 2 minutes or 1km but less than 10 minutes or 10km, and long distances as those greater than 10 minutes or 10km, literature results for the optimal pacing strategy can be grouped more easily. In general, an all-out strategy is best for short races when the kinetic energy loss is less than the aerodynamic resistance, an even strategy is best for medium races where there is a lower percentage of overall time spent in the initial acceleration phase, and an even or

negative pacing strategy is best for longer races, as shown in Table 3.6 [Abbiss and Laursen, 2008, Atkinson et al., 2003, 2007, De Koning et al., 1999]. For short events, a high proportion of the overall time is spent in the initial acceleration phase, so any gains made during this time will outweigh any losses towards the end of the race, even if the athlete begins to fatigue and power production decreases. De Koning et al. [1999] investigated the pacing strategy for 1km and 4km events using the mathematical model created by van Ingen and Cavanagh [1990], which was based on the flow of energy. The results from this study showed that for the 1km event an all-out strategy was optimal, regardless of peak power output, with an optimal time to constant aerobic power being less than 60 seconds. For the 4km event, the optimal pacing strategy was an all-out strategy for 12 seconds followed by an even strategy, where the time to constant aerobic power was 12 seconds, as this resulted in an evenly paced race. De Koning et al. [1999] found that the time to constant aerobic power was critical for the 4km event, and that small variations in pacing strategy had substantial effects on performance.

It has also been observed that athletes tend to reserve some anaerobic energy, and pace themselves so that near zero values are reached at the very end of the race [Foster et al., 2003, Atkinson et al., 2007]. This will only be true for high performance athletes, who are aware of their own boundaries and who are familiar with their race.

Study	Duration (min)	Distance (m)		Athlete/Model	Pacing Strategy	Observed or Optimal
Foster et al (2004)	0.67	500	short	Trained cyclists	Negative	Observed
	1.45	1,000	short	Trained cyclists	All-out	Observed
	2.23	1,500	medium	Trained cyclists	Positive	Observed
	4.93	3,000	medium	Trained cyclists	Even	Observed
	-	4,000	short/medium	Trained cyclists	Even	Observed
van Ingen Schenau et al.	0.97	1,000	short	Model	Negative (all-out)	Optimal
(1992)	4.27	4,000	short/medium	Model	All-out (<0.14min) then even	Optimal
de Koning et al. (1999)	0.97	1,000	short	Model	All-out	Optimal
	-	4,000	short/medium	Model	All-out (0.2min) then even	Optimal
Atkinson & Brunskill (2000)	27.68	16,100	long	Elite cyclists	Even	
Atkinson et al. (2003)	-	>4km	medium	Summary	Even	
	-	<1km	short	Summary	All-out	
	-	10-60km	long	Summary	Even or Negative	Optimal
Atkinson et al. (2007)	>10	-	long	Model	Even	Optimal
	<10	-	medium	Model	Positive	Optimal
	<2	-	short	Model	All-out	Optimal
Swain (1997)	2-4	-	medium	Model	Even	Optimal
Abbiss & Laursen (2008)	>2	-	medium		Even	
Perry et al. (2003)	30	-	long	Trained triathletes	Even	Observed
Padilla et al. (2000)	60	53,000	long	Elite cyclist	Even	Observed
Neumayr et al. (2004)	1645	525,000	long	Elite cyclist	Positive	Observed

Table 3.6: Summary of reported optimal pacing strategies for cycling [Abbiss and Laursen, 2008]

Summary

The first part of this chapter has shown that accurate models for cycling do exist, each with their own unique way of predicting performance variables. The most significant variables, which are included in all, current mathematical models for cycling, include the drag area (frontal area and drag coefficient), rolling resistance, and power or velocity output. The more accurate models however, are those which involve additional variables for grade angle, kinetic energy, bearing resistance, air density, and altitude. Models which predict the power or velocity profile throughout the entire race are more useful than those models which only predict an average power, speed or time. There is limited current research on mathematical models for the team pursuit, primarily due to the complexity of additional riders, wheel spacing, and changeovers. Although some research has been carried out on optimal pacing strategies for cycling, this research is also limited and the results vary between studies.

3.2 Literature Review: Aerodynamics

Aerodynamic drag is the resistive force to motion of an object travelling through the air. Aerodynamic drag consists of pressure drag and skin friction drag, and is the most significant resistive force in cycling. Air resistance increases as the squared function of velocity, so as speed increases the importance of wind resistance compared to rolling resistance increases [Atkinson et al., 2003, Lukes et al., 2005, Oggiano et al., 2008]. At 50kph, aerodynamic resistance accounts for 90% of the total resistance [Grappe et al., 1997, Broker, 2003, Lukes et al., 2005, Oggiano et al., 2008, Zdravkovich et al., 1996]. Of this aerodynamic resistance, the rider accounts for 75-80% and the bike and components the rest [Broker, 2003, Defraeye et al., 2010, Oggiano et al., 2008, Zdravkovich et al., 1996]. This highlights that body position is the most important factor when it comes to reducing overall resistance at race speeds.

3.2.1 Background

3.2.1.1 Pressure Drag, Skin Friction Drag and Base Drag

Pressure drag is caused by the difference in pressure at the front of the object compared to the rear of the object and is strongly correlated to the object's shape. The pressure drag is proportional to the frontal area of the object, so is therefore large for blunt bodies, small for streamlined bodies, and zero for thin, flat plates parallel to the flow.

Base drag is part of the pressure drag and occurs at the base of projectile shaped objects. Base drag largely depends on the the length of the forebody, its surface conditions, and the ratio of base-to-body diameter [Hoerner, 1965, p3-19]. For bodies with a base diameter smaller than that of the forebody, the drag may be considered similar to that of a parallel-sided shape. For three-dimensional bodies the base drag coefficient is a function of the forebody drag coefficient, as shown in Figure 3.1.

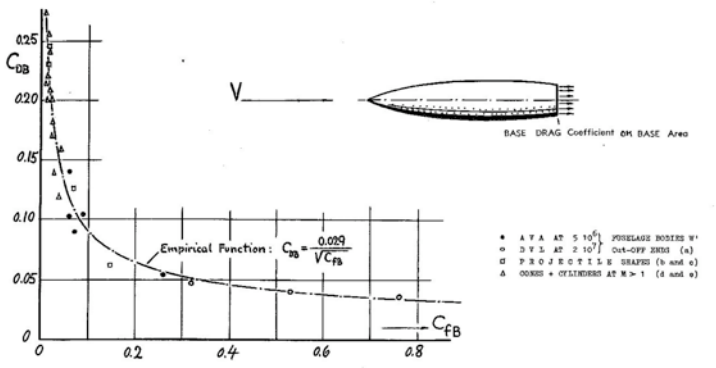

Figure 3.1: Base Drag Coefficient as a Function of Forebody Drag Coefficient [Hoerner, 1965]

Skin friction drag is caused by shear stress on the wall of the object as the air molecules collide with the surface of the object. Friction drag depends on the orientation of the object as well as the surface roughness,

and the friction drag is nearly zero for flat surfaces normal to the flow and maximum for flat surfaces parallel to the flow. Skin friction drag is also dependent on the viscosity of the fluid, and increases with increasing viscosity. For laminar flow over flat plates the skin friction coefficient can be calculated using Equation 3.16, where Re is the Reynolds number and x is the distance from the leading edge at which the Reynolds number is taken.

$$(C_f)_{laminar} = \frac{0.664}{\sqrt{Re_x}} \tag{3.16}$$

For the transition-to-turbulence region the skin friction drag, D_{SF}, for a flat plate of length 1m can be determined using Equation 3.17:

$$D_{SF} = qA_s \left[\frac{0.074}{Re_L^{\frac{1}{5}}} - \frac{1740}{Re_L} \right] \tag{3.17}$$

where q is the dynamic pressure, $q = \frac{1}{2}\rho V^2$, and A_s is the surface area. Equations 3.16 and 3.17 can be used to calculate the skin friction drag for an athlete, where $A_s = 0.2025H^{0.725}m^{0.425}$ [Pendergast et al., 2006].

At low speeds or high viscosity (low Reynolds number) viscous stress is the predominant parameter determining the drag of a body so skin friction drag will contribute to a higher proportion of overall drag, as can be seen in Figure 3.2 [Hoerner, 1965, p2-1].

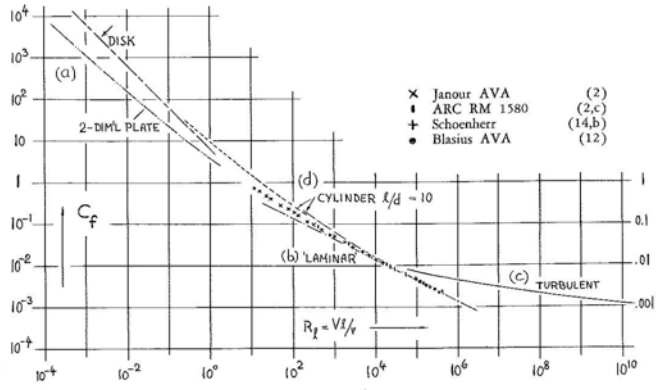

Figure 3.2: Skin Friction Coefficient; (a) in viscous flow, (b) with laminar, (c) with turbulent boundary layer flow, (d) cylinder in axial flow [Hoerner, 1965, p2-1]

In general, for a flat plate parallel to the flow drag is due almost entirely to skin friction drag; for a flat plate normal to the flow drag is due entirely to pressure drag; and for a cylinder normal to the flow drag is due to a combination of skin friction and pressure drag, although pressure drag dominates.

The total drag coefficient, C_d, is a dimensionless quantity that is used to quantify the total drag of an object, comprising of pressure drag and skin friction drag, and is calculated by $C_d = \frac{D}{\frac{1}{2}\rho AV^2}$, where D is the drag (N), ρ is the air density (kg/m^3), A is the frontal area (m^2) and V is the velocity (m/s). The total drag coefficient is lowest for a parallel plate normal to the flow, highest for a plate normal to the flow, and in between for a

cylinder (although closer to the drag coefficient of a flat plate normal to the flow). The drag coefficient is also related to the Reynolds number, as shown in Figure 3.3, where the minimum drag coefficient for both the long, flat plate parallel to the flow and circular cylinder in the spanwise orientation occurs of order $Re = 10^5$.

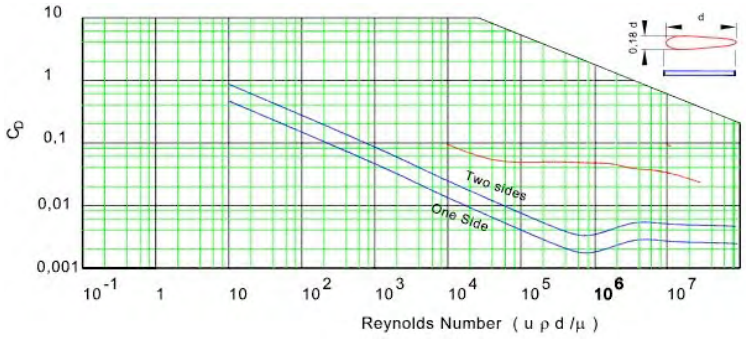

(a) Flat Plate [Roymech, 2011]

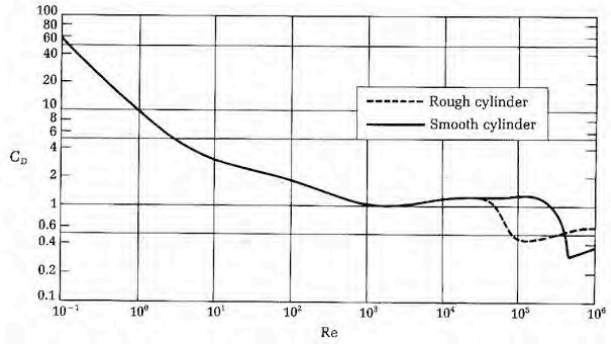

(b) Circular Cylinder in the Spanwise Orientation [Propeller-Guard, 2011]

Figure 3.3: Drag Coefficient as a Function of Reynolds Number

For spanwise cylinders of finite length, the relationship between drag coefficient, C_d, and diameter to span ratio, $\frac{d}{l}$, can be seen in Figure 3.4 [Hoerner, 1965, p3-16].

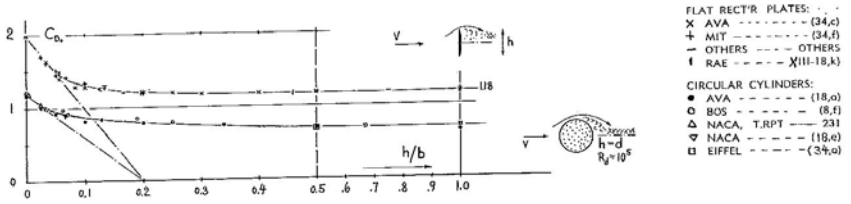

Figure 3.4: Drag Coefficient of Rectangular Plates and Circular Cylinders as a Function of Height (or Diameter) to Span Ratio [Hoerner, 1965, p2-1]

For parallel sided shapes, such as those shown in Figure 3.5, the total drag consists of frictional drag on the surface of the body and base drag [Hoerner, 1965, p3-12]. Figure 3.5 shows the relationship between drag coefficient, C_d, and fineness ratio, $\frac{l}{d}$, for cylindrical bodies in axial flow. It is clear that as the ratio $\frac{l}{d}$ increases, the total drag comprises of a greater proportion of friction drag than base drag.

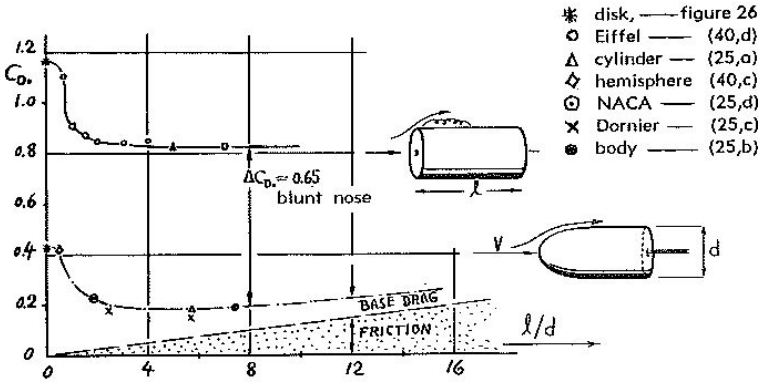

Figure 3.5: Drag Coefficients of Cylindrical Bodies in Axial Flow as a Function of Fineness Ratio

The Reynolds number of the parts of the body of a cyclist can be calculated using $Re = \frac{UD}{\nu}$, where U is the cycling speed (m/s), D is the characteristic linear dimension (m), and ν is the kinematic viscosity (m^2s^{-1}). The calculated Reynolds numbers for each body part at cycling speeds between 40kph and 70kph are shown in Table 3.7. A comparison between the calculated Reynolds numbers for the body parts of a cyclist (Table 3.7) and the drag coefficient as a function of Reynolds number for flat plates and cylinders (Figure 3.3) shows that all body parts of a cyclist at cycling speeds between 40kph and 70kph lie within the drag crisis region. Using Table 3.7 and Figures 3.3, 3.4 and 3.5, a drag coefficient of $C_d = 0.0012$ would be expected for the torso, where as for the upper arms, thighs and calves a drag coefficient of $C_d = 0.6 - 1.2$ would be expected, depending on the surface roughness, diameter and cycling speed.

						Re (x10^5)			
Body Part	**Shape**	**Length (m)**	**Diameter (m)**	**l/d**	**d/l**	**40kph**	**50kph**	**60kph**	**70kph**
Head	Sphere	NA	0.28	NA	NA	2.05	2.57	3.08	3.59
Torso	Flat plate	0.8	NA	NA	NA	5.86	7.33	8.8	10.26
Forearm	Streamwise cylinder	0.37	0.076	4.9	0.2	2.71	3.39	4.07	4.75
Upper Arm	Spanwise cylinder	0.25	0.09	2.8	0.4	0.66	0.82	0.99	1.15
Thigh	Spanwise cylinder	0.4	0.16	2.5	0.4	1.17	1.47	1.76	2.05
Calf	Spanwise cylinder	0.4	0.1	4.0	0.3	0.73	0.92	1.1	1.28

Table 3.7: Calculated Reynolds numbers for body parts of a cyclist

3.2.1.2 Separation

The pressure drag becomes most significant when separation of the fluid becomes too high for the flow to be able to stay attached to the body. At this point the fluid separates from the body, creating a large,

low pressure region at the rear of the object. The point of separation depends on the Reynolds number, surface roughness, fluctuations in the free stream, and the shape of the object, as shown in Figure 3.6. In the low pressure region the flow begins to recirculate, and the greater this region of separation the greater the pressure drag. The separation of air creates turbulence and results in pockets of low and high pressure that leave a wake behind the object. It is the pressure on the surface that retards the body. Flow separation is primarily caused by an adverse pressure gradient. Therefore, flow separation primarily occurs on blunt bodies, such as cyinders and spheres, due to the steep pressure curve, although complete separation can also occur on streamlined bodies such as airfoils at high angles of attack. For flow past a blunt body separation will occur at low speeds because the boundary layer particles lose so much kinetic energy that they cannot overcome the increasing pressure near the rear of the blunt body. When separation occurs a wake forms, the flow becomes reversed, and the aerodynamic drag increases. At higher speeds the boundary layer becomes turbulent, so the boundary layer particles have more energy to stay attached to the body and the point of separation is delayed, reducing the aerodynamic drag. Separation does not occur on flat plates parallel to the flow because no backflow takes place; the flow becomes turbulent without separation occurring.

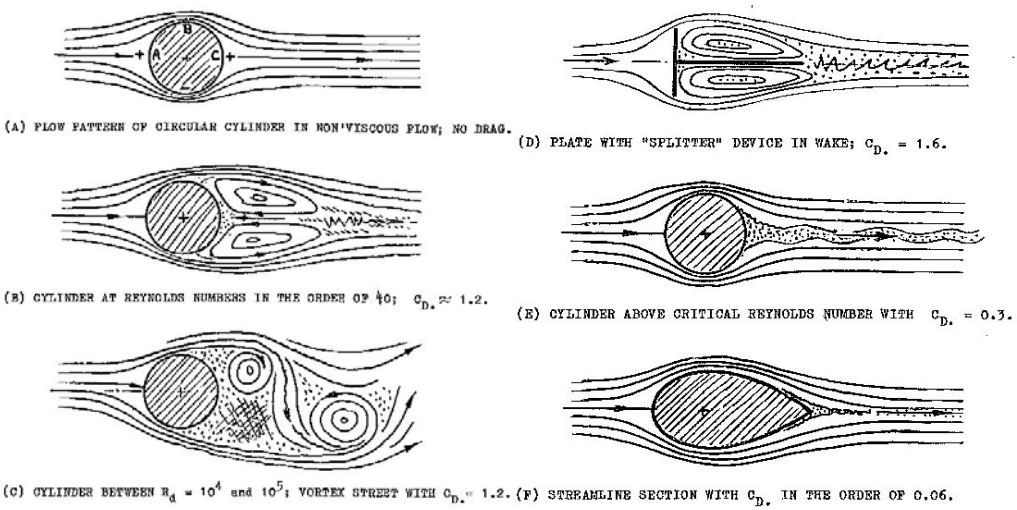

Figure 3.6: Flow Pattern over Different Shapes [Hoerner, 1965, p3-2]

Hyun Paul and Kwang [1988] collated experimental and theoretical data for the separation angle for circular cylinders in axial flow, the results of which are shown in Table 3.8. They state that separation occurs at approximately 80° from the point of stagnation for a laminar boundary layer between Re=$10^3$to 10^6. However, a much larger separation angle of 108.8° has been computed by Schlichting [1979, p215], who carried out numerical calculations on a digital computer programmed to solve the differential equations directly with a Blasius series containing eleven terms rather than just first three terms, as was the case for Heimenz's solution. Schlichting [1979, p215] argues that a Blasius series containing only the first three terms is inadequate to represent the solution of the point of separation.

Contributor	Analysis	Separation angle
Thwaites (6)	Integral	78.5°
Smith and Clutter (13)	Finite difference	80.0°
Howarth (10) Tifford (18)	Series composed of 19 terms	83.0°
Stratford (5)	Stratford prediction	79.8°
Shvets (12)	Approximation	79.7°
Hyun and Chang	Eq. (23)	81.0°
Hiemenz (15)	Measurements	80.5°

Table 3.8: Separation Angles for a Circular Cylinder in Axial Flow Hyun Paul and Kwang [1988]

A more recent study by Miau et al. [2011] concluded that differences in reported separation angles for flow around circular cylinders in the spanwise orientation may actually be a result of unsteady flow, particularly in the one-bubble state, as well as the difference in surface roughness of the cylinders. Miau et al. [2011] conducted experiments on acrylic and stainless steel cylinders of similar diameter, with a relative surface roughness of $2.43\text{x}10^{-6}$ and $3.88\text{x}10^{-5}$ respectively, and used pressure taps, pressure transducers, and hot-wire probes to analyse the flow around the cylinders in the critical regime ($1.73\text{x}10^5$<Re<$5.68\text{x}10^5$). In general, Miau et al. [2011] found that initial transition from the subcritical to critical regime took place at Re=$2\text{x}10^5$ for both cylinders, and at Re=$4\text{x}10^5$ the flow had reached the two-bubble regime where reattachment downstream of a separation bubble had occurred. In the initial transition from the subcritical to critical regimes (Re=$3.1\text{x}10^5$) the acrylic cylinder showed flow separation at $\theta = +60°$ and $\theta = -52.5°$ (+ is one side of the cylinder and - is the other side, with 0° being the stagnation point), where as the stainless steel cylinder showed flow separation at $\theta = \pm$75-85°, suggesting that flow separation would occur further upstream on the acrylic cylinder compared to the stainless steel cylinder. For both cylinders the flow was found to be unsteady in this region (upstream of $\theta = 90°$) with the development of a separation bubble, and Miau et al. [2011] suggest that this unsteadiness contributes to the differences in separation angles for circular cylinders reported in the literature. In the one-bubble regime (Re=$3.5\text{x}10^5$) the results for the stainless steel cylinder suggested that a separation bubble developed on one side of the cylinder at $\theta = -110°$ to -130°, and then switched to the other side at $\theta = 110°$ to 130°. However, for the acrylic cylinder the results suggested that a separation bubble only formed on one side of the cylinder, at $\theta = 90°$. In the two-bubble regime ($3.9\text{x}10^5$) where reattachment occurs, the results suggested that reattachment regions were not uniform along the span of the cylinders, and that the three dimensionality of the flow reattachment was very pronounced and would conceivably affect the wake flow development downstream.

Boundary layer separation is undesirable for cycling purposes because of the large increase in pressure drag. A number of methods can be used to delay flow separation and keep the boundary layer flow attached to the object for as long as possible, which will in turn lower the overall drag on a cyclist. These methods will be described after a brief description of the boundary layer.

3.2.1.3 Boundary Layer Theory

The boundary layer is the region in which the velocity of the fluid increases from zero at the wall (no-slip condition) to free stream velocity, and where the viscous effects of the fluid are confined. Outside the boundary layer the viscosity does not have a noticable effect on the motion of the fluid particles. The boundary layer

thickness is the point at which the free stream velocity of the fluid reaches 99% of the actual free stream velocity. The thickness of the boundary layer decreases with decreasing viscosity, and at large Reynolds numbers a thin boundary layer exists where the effects of viscosity become confined to narrow regions near the solid walls [White, 1991, p218]. For flat plates with zero pressure gradient the boundary layer thickness can be calculated using Equation 3.18 for laminar flow [Hoerner, 1965, p2-2] and Equation 3.19 for turbulent flow [Hoerner, 1965, p2-3], where x is the distance from stagnation to the point at which the boundary layer is to be determined (m), and Re_x is the Reynolds number at the distance x.

$$\delta_{laminar} = \frac{5.5x}{\sqrt{Re_x}} \tag{3.18}$$

$$\delta_{turbulent} = \frac{0.154x}{Re_x^{\frac{1}{7}}} \tag{3.19}$$

The boundary layer thickness for a thin, flat plate at zero incidence is the most simple case because the velocity profiles at various distances from the leading edge of the plate can be assumed to be similar to each other. The boundary layer thickness for a cylinder in axial flow is not so simple because the velocity profiles change with the angle from the leading edge. The boundary layer thickness over a flat plate and displacement thickness around a circular cylinder in axial flow (δ_1) are shown in Figure 3.7.

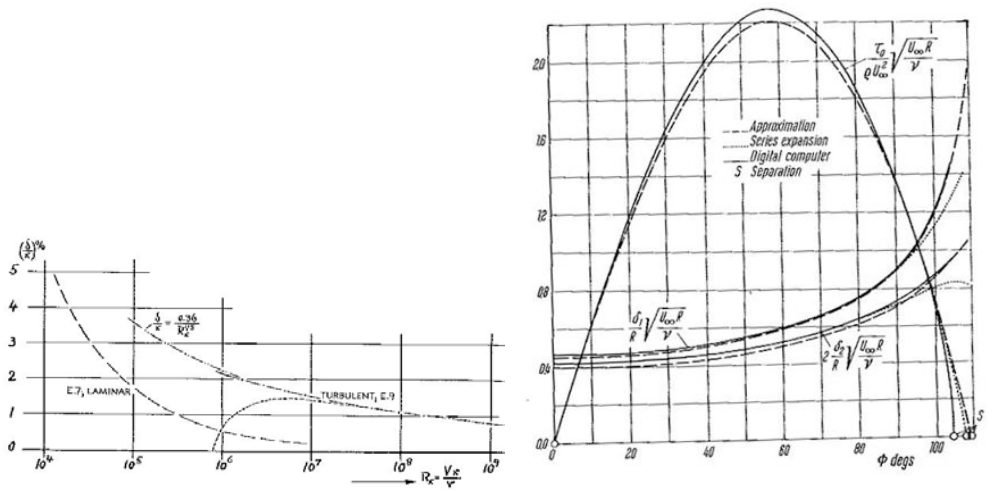

(a) Boundary Layer over a Flat Plate

(b) Displacement Thickness over a Cylinder in Axial Flow

Figure 3.7: Boundary Layer Thickness and Critical Reynolds Number over a Plate and Cylinder

The displacement thickness is a measure of how far the undisturbed flow is removed from the wall due to reduced velocities within the boundary layer, and can be determined using Equation 3.20 for a laminar boundary layer and Equation 3.21 for a turbulent layer [Çengel and Cimbala, 2006], where x is the distance from stagnation to the point at which the boundary layer is to be determined (m), and Re_x is the Reynolds number at the distance x.

$$\delta*_{laminar} = \frac{1.72x}{\sqrt{Re_x}} \tag{3.20}$$

$$\delta*_{turbulent} = \frac{0.02x}{Re_x^{\frac{1}{7}}} \tag{3.21}$$

For a boundary layer originating on a smooth, plane, constant-pressure wall, the inertial flow forces become predominant over the viscous forces at a critical Reynolds number of $Re_{crit} = 10^6$ and the laminar boundary layer shows signs of a wave motion. This motion then breaks up into turbulent oscillations and is the point of transition from laminar to turbulent flow within the boundary layer [Hoerner, 1965, p2-8]. The actual point of transition is dependent on the amplitude of the disturbing influence, which can be caused by surface roughness, sound waves, or by the turbulent oscillations in the artificial stream of a wind tunnel [Hoerner, 1965, p2-8]. However, for bluff bodies, such as spheres and cylinders, eddies begin to form at moderate Reynolds numbers and separated regions occur at the rear of the body. The flow past smooth spheres was analysed by Achenbach [1972] who measured the total drag, local static pressure and local skin friction distribution of a 200mm diameter sphere in a wind tunnel. In the subcritical region (Re=1.62x10^5) Achenbach [1972] observed that the boundary layer separated linearly at 82° from the stagnation point, and that recirculation occurred downstream of this point of separation. An increase in the Reynolds number to Re=2x10^5 caused the boundary layer to shift downstream, and at Re=2.8x10^5 separation occured at 95° from the stagnation point. A further increase in the Reynolds number to Re_{crit}=3x10^5 resulted in the formation of a separation bubble, with immediate laminar separation and the turbulent shear layer reattaching to the wall further downstream, which is typical for the critical flow regime. At Reynolds numbers greater than the critical flow regime but less than the transcritical regime (3x10^5<Re<1.5x10^6) immediate transition from laminar to turbulent flow occurred at 95° from the stagnation point without the formation of a separation bubble, and in the transcritical regime (Re>1.5x10^6) immidiate transition occurred in the front part of the sphere. Although thin boundary layer theory does not apply for separated regions, it is useful for understanding the boundary layer up to the point of separation.

3.2.1.4 Tripping the Boundary Layer and the Significance of Surface Roughness

Separation occurs earlier for laminar flow than turbulent flow because the turbulent boundary layer transports more momentum towards the surface at a greater rate, so the flow is able to reattach itself to the surface of the body. Therefore by inducing turbulence before the laminar boundary layer separates, separation can be delayed. Transition occurs at a lower Reynolds number on a rough surface compared to a smooth surface, so increasing surface roughness is one way of delaying separation and reducing the wake behind an object. As the height of the roughness element is increased, the point of transition moves continuously upstream until it reaches the position of the roughness element itself [Schlichting, 1979, p536]. However, if the degree of roughness is too small then there will be no effect on transition. It can be concluded that there must be a critical height of roughness element below which no influence on transition is seen, and that there is also a limiting height of the roughness elements which causes transition to occur at the element itself.

Surface Roughness on a Flat Plate

Roberts and Yaras [2005] carried out experiments on flat plates of different surface roughness to determine the effects of surface roughness, skewness, and spacing of the roughness elements on the transition of the boundary layer. They found that increased surface roughness, increased spacing between the roughness elements, and negative skewness all caused transition to move upstream, although spacing and skewness had a secondary effect on the location of transition inception compared to the height of the roughness elements.

For single, 2D roughness elements in incompressible flow, such as a trip wire, the critical height of the roughness element is a function of the height ratio $\delta/\delta*$, where δ is the boundary layer thickness and $\delta*$ is the boundary layer displacement thickness. As the height of the roughness element, k, or free stream velocity, U, is increased until $k/\delta* > 0.3$, the point of transition moves closer to the roughness element until they meet, at which point $x_{tr} = x_k$. The value of $Re_{\delta*,tr}$ drops along a hyperbolic curve, as shown in Figure 3.8, and the criterion for a wire to 'trip' a flow into turbulence is given by Equation 3.22 [White, 1991, p386], where U is the free stream velocity (m/s), k is the height of the roughness element (m), and ν is the kinematic viscosity of the fluid (m^2/s).

$$Re_{\delta*,tr} = \frac{Uk}{\nu} \approx 850 \tag{3.22}$$

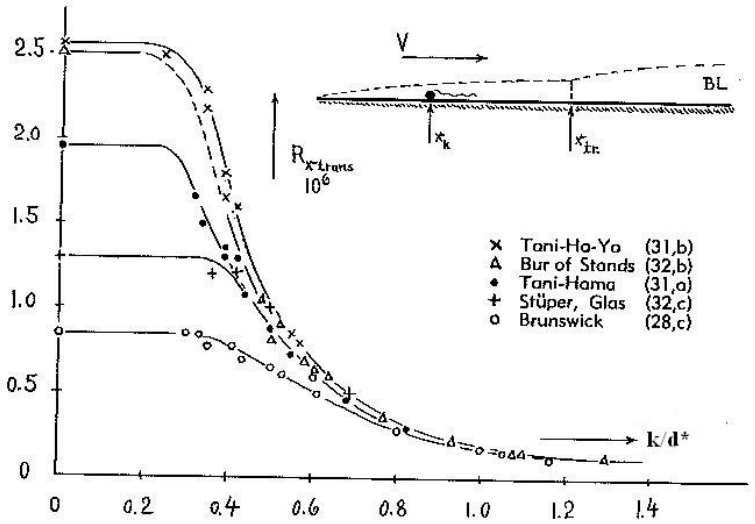

Figure 3.8: The Transition of Plane Surfaces for Single Protuberances placed in the Forward Part of the Surface [Hoerner, 1965]

A similar trend is seen for uniform roughness on a flat plate, where the critical Reynolds number decreases as the roughness grain size, $\frac{k}{x}$, increases, as shown in Figure 3.9.

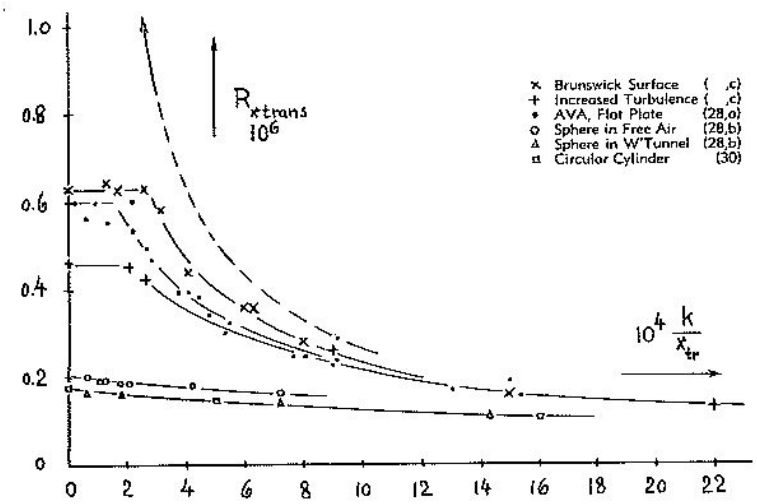

Figure 3.9: Transition Reynolds Number as a Function of Overall Surface Roughness [Hoerner, 1965]

For single, 2D roughness elements the minimum distance between the point of transition, x_{tr}, and location of the wire itself, x_k, can be determined using Equation 3.23 (Figure 3.10) [Schlichting, 1979, p539].

$$\frac{U(x_{tr} - x_k)}{\nu} = 2 \times 10^4 \tag{3.23}$$

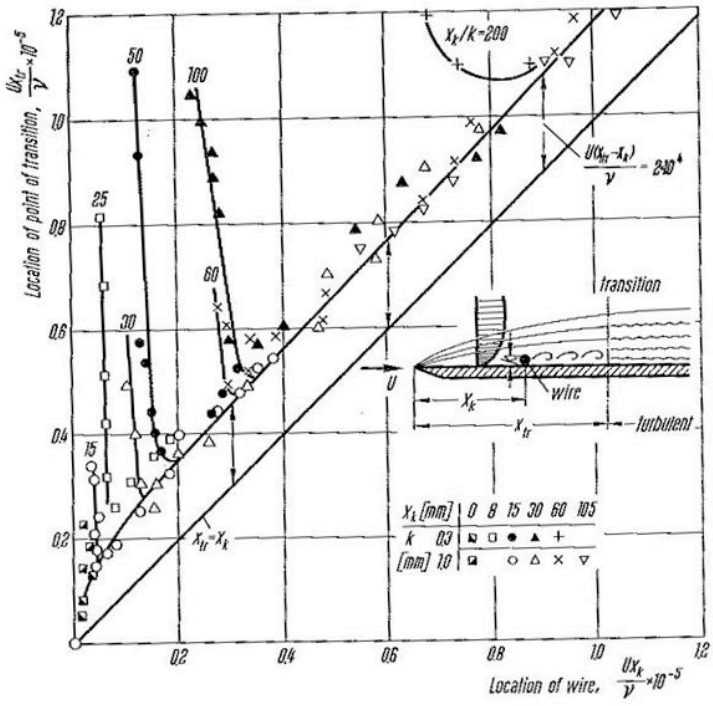

Figure 3.10: Distance between Point of Transition and the Position of the Tripping Wire for Fully Effective Operation [Schlichting, 1979]

It is also possible to determine the height of the roughness element with different intensities of turbulence, as the ratio $\frac{(Re_{xtr})_{rough}}{(Re_{xtr})_{smooth}}$ is a function of $\frac{k}{\delta_k*}$, as shown in Figure 3.11 [Schlichting, 1979, p541], where $(Re_{xtr})_{rough}$ is the Reynolds number of the rough element, $(Re_{xtr})_{smooth}$ is the Reynolds number of the flat plate at the roughness element, k is the height of the roughness element, and δ_k* is the displacement thickness of the boundary layer at the roughness element.

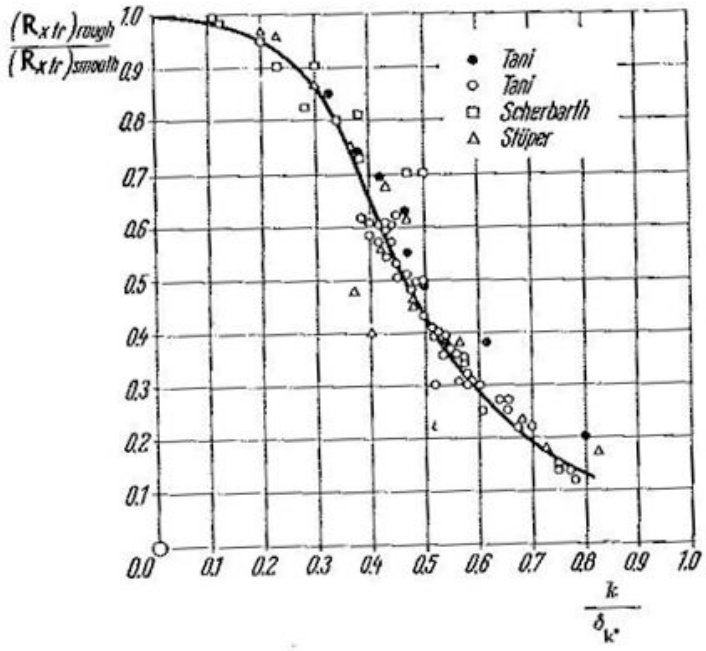

Figure 3.11: Ratio of Critical Reynolds Number on a Flat Plate at Zero Incidence with a Single Roughness Element to that of a Smooth Plate [Schlichting, 1979]

Surface Roughness on a Circular Cylinder

The influence of surface roughness on circular cylinders in the spanwise orientation is shown in Figure 3.12 [Hoerner, 1965, p3-10], where k is the sand grain size and d is the diameter of the cylinder (m). It is clear that the reduction in drag coefficient using surface roughness is dependent on the Reynolds number between $5x10^4 < Re < 4x10^5$, either side of which surface roughness has no effect on the drag coefficient. An increase in grain size or a reduction in cylinder diameter causes a drop in drag coefficient (the drag crisis) to occur at a lower Reynolds number, but the drag coefficient post-crisis is greater. A similar trend has been observed for spheres [Achenbach, 1972].

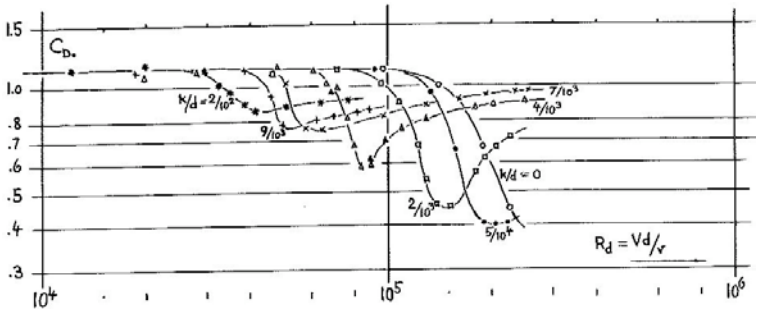

Figure 3.12: Drag Coefficient of Cylinders with Varying Degrees of Surface Roughness [Hoerner, 1965]

Experimental results for a cylinder covered in sand placed axially in a convergent and divergent channel are reported in Schlichting [1979, p542], which show that the critical Reynolds number decreases steeply after $\frac{Uk_s}{v} = 120$, where k_s is the roughness, concluding this value as the critical roughness for distributed rough surfaces (Figure 3.13). These results also show that an increase in roughness causes transition at a lower Reynolds number.

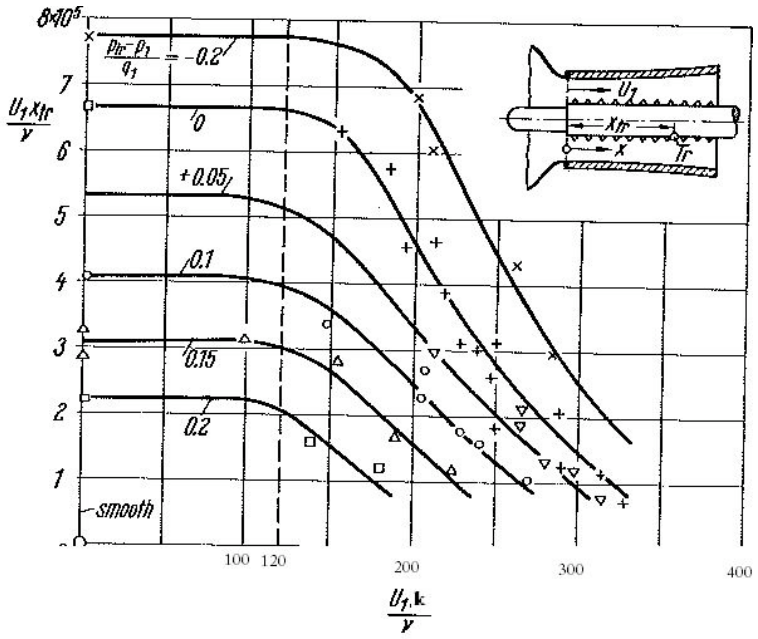

Figure 3.13: Influence of Surface Roughness on Sand-Covered Walls on the Position of the Point of Transition for Incompressible Flow

Analysis of non-random surface roughness of circular cylinders is limited in the literature. Achenbach [1971] observed the influence of surface roughness on the cross-flow around circular cyinders in a wind tunnel at $4x10^4 < Re \leq 3x10^6$ by measuring the local pressure and skin friction distributions. The test cylinder was 150mm in diameter and 500mm in length, and was covered with emery paper to simulate different surface roughnesses, as well as with 2.5mm spheres using glue. Achenbach [1971] found similar results to those published by [Hoerner, 1965, p3-10], the results of which can be seen in Figure 3.14. The surface roughness did not appear to have any influence on the subcritical flow regime, and in a large range of Reynolds numbers the drag coefficient appeared nearly constant. An increase in the Reynolds number to the critical flow regime caused a sudden drop in the drag coefficient, the lower limit of which was dependent on the surface roughness. An further increase in the Reynolds number past the drag crisis and to the supercritical region caused an increase in the drag coefficient to a constant value. The post crisis drag coefficient increased with increasing surface roughness. Achenbach [1971] also observed the behaviour of the boundary layer from the local pressure and skin friction distribution results. The results showed that in the drag crisis region, where there was a sudden drop in drag coefficient due to the formation of a separation bubble, an increase in the

surface roughness reduced the range in Reynolds number at which this drag crisis occurred. In addition, an increase in surface roughness caused strong disturbances, leading to earlier transition of the flow from laminar to turbulent. These results can be seen in Figure 3.15. In terms of the percentage of friction force to the overall drag on a circular cylinder, Achenbach [1971] found that friction forces contributed to only a few percent to overall resistance, but in the transcritical range (Re>1.5x10^6) the percentage of friction forces to overall drag diminishes for smooth cylinders with increasing Reynolds number, but remains relatively constant for rough cylinders. This can be seen in Figure 3.16.

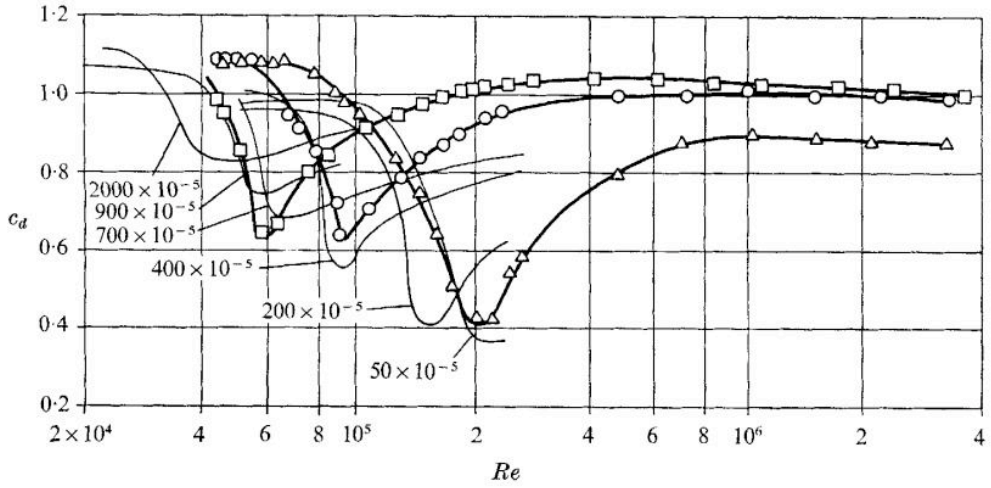

Figure 3.14: Drag coefficient of a 150mm diameter cylinder covered with different surface roughness (corrected for blockage effects) [Achenbach, 1971]

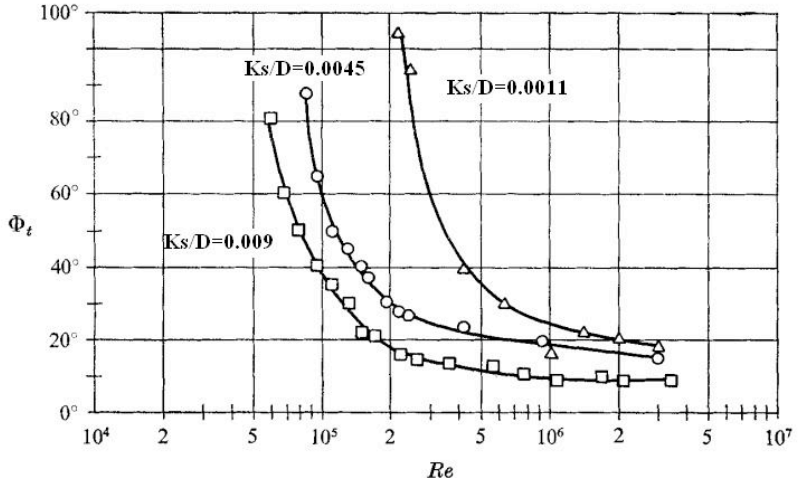

Figure 3.15: Angular position of transition from laminar to turbulent flow for circular cylinders of different surface roughness [Achenbach, 1971]

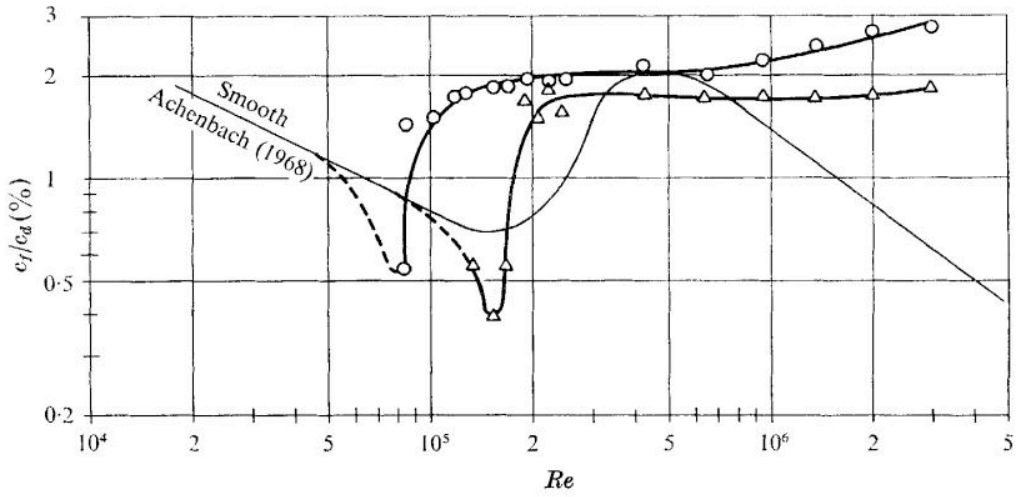

Figure 3.16: Contribution of friction force to overall drag for circular cylinders [Achenbach, 1971]

3.2.2 Factors Affecting Aerodynamic Drag of Cycling

A brief discussion on the background of drag, the boundary layer, and separation has been provided above, and so the remaining part of this chapter will concentrate on the main factors that affect aerodynamic drag and ways in which drag can be reduced.

In order to reduce the aerodynamic drag for a cyclist travelling at constant speed in the same conditions, a reduction in drag coefficient, C_d, and/or frontal area, A, is required. These two variables can be combined into one single variable for drag area, C_dA, as changes in the frontal area will also affect the flow over the bike and rider. A reduction in drag area can be achieved through changes in athlete position, helmet choice and position, clothing, and equipment. The influence of and ways in which these factors can reduce drag will be discussed individually, followed by a discussion of the effect of environmental conditions on the aerodynamic drag.

3.2.2.1 Athlete Position

Kyle [2003a] states that body position is the single factor in achieving low aerodynamic drag, and that a low crouch with the torso as close to the horizontal as possible and a front arm profile narrower than the rest of the body is important. Body position affects pressure drag, which dominates on a cyclist, so a reduction in frontal area and pressure drag is more beneficial than a reduction in skin friction drag. Many authors state that a low position with a flat back, forearms parallel to the horizontal, and a tucked head help streamline the shape of the rider on the bike, resulting in a reduction in aerodynamic drag [Burke and Pruitt, 2003, Broker, 2003, Mestdagh, 1998]. Burke and Pruitt [2003] also state that narrow arms, particularly the elbows, help direct the wind around the body and reduce the aerodynamic drag. The significance of body position on aerodynamic drag became well known when Graham Obree broke the hour record in 1993 and 1994 in the Obree position (arms tucked into the chest) and the individual pursuit record in 1995 in the Superman

position (arms straight out in front). By flipping the handlebars and folding the arms into the chest, Obree was able to shield these factors from the influence of aerodynamic resistance. Since then, many studies have been carried out to quantify the reduction in drag with different body positions using either wind tunnel tests, field tests, or through CFD analysis.

Most studies have focused on comparing 'standard' cycling positions, such as the dropped, upright, aero and Obree positions (see Figure 3.17).

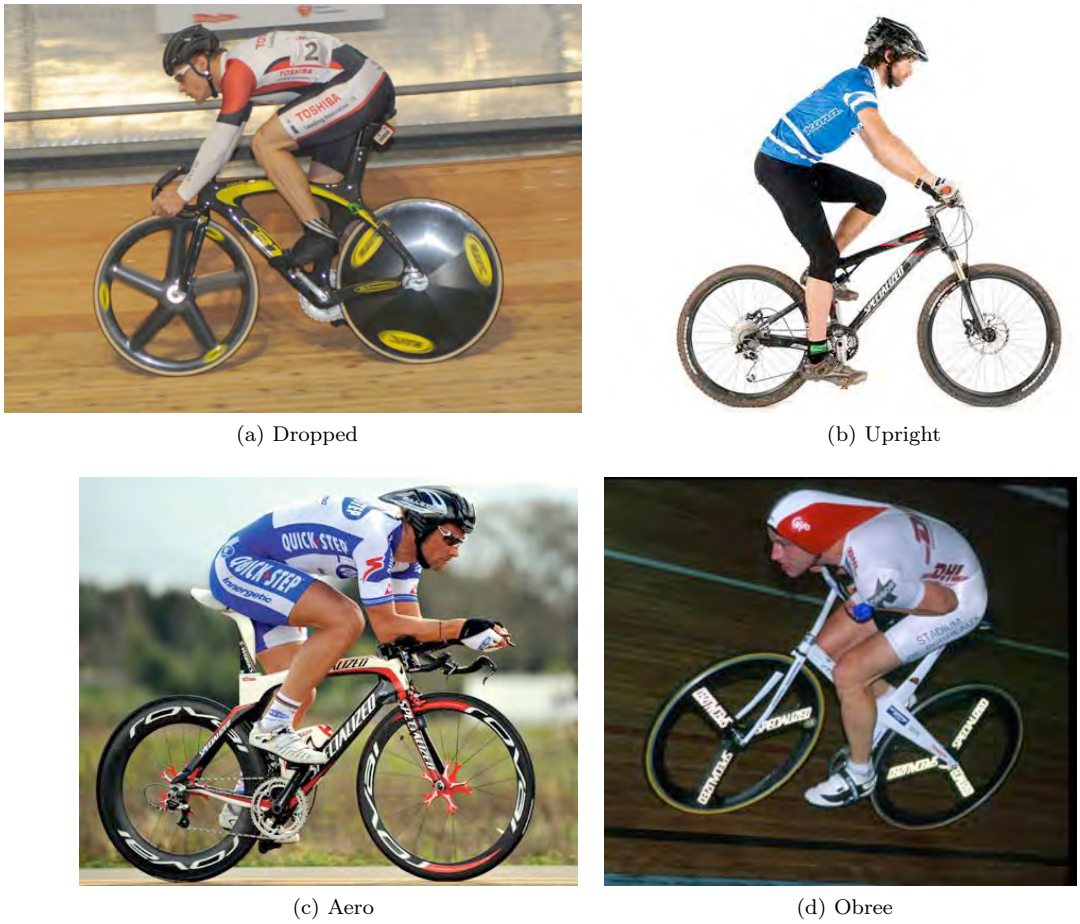

(a) Dropped (b) Upright

(c) Aero (d) Obree

Figure 3.17: Standard Cycling Positions

Defraeye et al. [2010] carried out wind tunnel tests on three static cycling positions (upright position, dropped position with arms straight, and time trial position) and determined that a reduction in frontal area results in a reduction in drag. Garcia-Lopez et al. [2008] found a trend in optimal position for athletes tested in a wind tunnel, where the drag was reduced by lowering the handlebars and moving the elbow pads forwards. This study also found a significant correlation (r=0.42) between the torso angle and drag area, where drag area was reduced with a reduction in the angle of the torso to the horizontal. Grappe et al. [1997] studied four different positions (upright, dropped, aero, and Obree) using one athlete who performed 12 laps on a velodrome at speeds from 5.5m/s to 11m/s, increasing by 0.5m/s every lap for each position. The athlete

changed position at each velocity before increasing the velocity by 0.5m/s. The total resistance was measured, and the results plotted against velocity squared. A line of best fit was then drawn for each position, and the equation of the line calculated to determine the drag area, C_dA, for each position using $R_T = \alpha V^2 + \beta$, where $\alpha = \frac{C_d A}{0.5\rho}$. The results showed that the Obree position had the lowest drag area of C_dA=0.216, followed by the aero position, dropped position and then the upright position. This is in agreement with other wind tunnel tests, as bringing the arms closer together and dropping the body (from an upright position to an aero position) helps to streamline the body, and tucking the forearms in and bringing the torso horizontal (Obree position) reduces the drag even further. However, it is likely the athlete fatigued towards the end of the testing, as each position was tested for 12 laps consecutively. This may have affected the athlete's ability to hold each position, particularly towards the higher velocities. Zdravkovich et al. [1996] used dummy models to determine the drag coefficient for six different riding positions tested in a wind tunnel. Although Zdravkovich et al. [1996] state that the difference in drag results for a cyclist would be greater than for a dummy due to the inadequate posture of the dummy, the results showed that the lowest, crouched position reduced the drag the most (17% drag reduction) compared to an upright position.

Oggiano et al. [2008] compared six different positions on eleven, elite cyclists using wind tunnel tests at speeds between 0.5m/s and 30m/s, by changing only the seat and handlebar positions. The advantage of this study was that quantitative changes were made to the bike set up rather than using 'standard' cycling positions. The results showed that changes in handlebar position had a greater reduction in drag than changes in seat position, and by moving the handlebars both down and forwards by 20mm reduced the average drag by 5.8%, which is in agreement with statements that a forward, low position is best. However, although this position resulted in the greatest reduction in drag for all athletes, the benefit of adopting this position was not the same for all athletes as there was a scatter in the results. This highlights that although a trend may be seen, results do differ between athletes for each position tested.

Lukes et al. [2005] summarised some of the existing literature on cycling aerodynamics, and highlighted the importance of body position, with a horizontal torso and horizontal forearms being the optimal position. However, having the handlebars tilted up by 30 degrees and 45 degrees, and lowering the head and extending the handlebars also showed to reduce the drag, which suggests that there is not necessarily one single optimal position for all athletes. It should be noted that the UCI rules now state that the forearms must be horizontal, so tilting the handlebars upwards is now illegal. Lukes et al. [2005] also state that differences in body size affect the aerodynamic drag, with larger cyclists having more absolute air resistance but a lower air resistance relative to body mass. Oggiano et al. [2008] agree that a cyclist's position is related to anthropometric characteristics, with body mass and body size having an effect on athlete position. Craig and Norton [2001] estimated that an increase in body mass by 2kg without any corresponding increase in power would increase the finishing time for a 4000m individual pursuit event by 1.5 seconds, which shows how significant body mass can be. In addition, the frontal area of smaller athletes is less than that of bigger athletes. Faria et al. [2005] state that a cyclist's frontal area represents 18% of their body surface area, so a smaller frontal area would result in smaller cyclists having a larger body surface area to frontal area ratio, which means they are at a disadvantage in flat time trials where air resistance is the dominant force. However, Garcia-Lopez et al. [2008] state that frontal area is not necessarily a fixed proportion of body surface area, because the body surface area to body mass ratio is lower for heavier cyclists.

Defraeye et al. [2011] carried out a CFD study to compare the drag of a cyclist in an upright position, dropped position with straight arms, and TT position. The bike was excluded in the study, but instead of just considering the cyclist as a whole, the cyclist's body surface was subdivided into 19 body segments so

that the contribution of each body segment to the overall drag could be analysed. A standard $k-\omega$ model was used with a low turbulence intensity and uniform velocity profile to simulate velodrome conditions, and the free stream wind speed varied from 10-100kph in 10kph increments. The drag area of the individual body segments to the overall drag area of the cyclist was compared for the three different positions at 60kph, where the drag areas for the upright, dropped and TT positions for the overall cyclist were calculated to be $C_dA = 0.239$, 0.193 and 0.149m^2 respectively at 60kph. The highest drag area values were found to be for the head, legs and arms, as these areas contribute the most to the frontal area of the cyclist and have a relatively large surface area. The drag area of the head in the TT position was higher than for the other positions because the head was the most protruding body segment in this position, consequently contributing significantly to the total frontal area. The upright position showed a higher drag area for the back and chest, due to their greater contribution to the frontal area in this position. This study highlights that the optimal position of a cyclist can be achieved by considering body segments as opposed to the entire body. This study also included an analysis of convective heat transfer, the results of which indicated that drag area and convective heat loss are not necessarily correlated. This finding is useful for knowing that changes made to an athlete's position will not affect heat loss; heat loss is more likely dependent on the thermal properties of the clothing and not the athlete's position.

Although many studies have concluded that a low, crouched position where the frontal area is reduced also reduces the aerodynamic drag, there is limited literature on the optimal angles of the major joints used in track cycling, such as the hip, torso, shoulder, elbow, knee and wrist angles. Savelberg et al. [2003] looked at the effect of trunk angle on muscle recruitment pattern and found that trunk angle is a factor in producing power output and not just an aerodynamic factor. Their study revealed that trunk angle affects the kinematics of leg movement and the activity of the muscle, not only at the hip, but at the knee, ankle, and muscles spanning these joints. Too and Landwer [2004] also attempted to determine the optimal trunk angle in terms of power production, by varying the trunk angle from 90° to 60° and 120° whilst maintaining a constant hip orientation and seat-to-pedal distance to control joint kinematics. However, the results of this study provided limited information on the optimal trunk angle, joint kinematics, or hip orientation needed to optimise cycling performance. Garcia-Lopez et al. [2008] tested five professional, male cyclists in different positions in a wind tunnel, pedalling at 90% VO_{2max} for 10 minutes. Although this study did not determine optimal joint angles either, a significant correlation was found between the torso angle and drag area (r=0.42), and between the torso angle and drag area to body mass ratio (r=0.4). However, they found that the minimum drag area did not coincide with the minimum drag area to body mass ratio. Minimum drag area values were between C_dA=0.255 and 0.299m^2.

Some athletes may find it more difficult to adopt certain positions due to their build, which in turn affects their aerodynamics and power output. Although many studies have been carried out on different positions of athletes, not all athletes will be able to adopt exactly the same position. This suggests that although trends can be seen by comparing different general positions, individual testing is needed in order to identify the optimal position for a specific athlete.

When watching track cycling races, it is clear that athletes adopt different hand and forearm positions on the aerobars. This could be due to the type of aerobar used, perhaps for individual reasons relating to stability and comfort. An investigation into the relationship between power output and grip style was carried out by Baker et al. [2001], but this study did not consider the grip style in terms of aerodynamics. Similarly, Bressel and Cronin [2005] looked at the relationship between the position of the hands on the tops and drops of the handlebars in terms of how this affects the pressure on the seat, but there is no mention of how these positions

affect the aerodynamic drag of a cyclist. There is also limited data on the position of the elbow pads on aerobars or the influence of the shape of the handlebars and/or handlebar extensions on aerodynamic drag. Although some authors mention that narrow, parallel forearms, or forearms tilted upwards by 30 degrees reduces aerodynamic drag [Kyle, 2003a, Burke and Pruitt, 2003, Broker, 2003, Lukes et al., 2005] there is no quantifiable data to back up these statements.

A summary of the reported values of drag area, C_dA, and best positition from the literature are shown in Tables 3.9 and Table 3.10. The difference in drag area values is likely to be a result of athletes using different equipment during tests, adopting a slightly different posture even though the general position may be the same, and individual differences between body size and shape.

Author	Position					
	TT	**Obree**	**Drops**	**Upright**	**Aero**	**Touring**
Gibertini et al. [2008]	0.223		0.275			
Garcia-Lopez et al. [2008]	0.260 (static)					
	0.341 (dynamic)					
	0.293 (low bars, advanced pads)					
Grappe et al. [1997]		0.216	0.276 0.251 to 0.370	0.277 0.299 to 0.390	0.262 0.191 to 0.262	
Groot et al. [1995]			0.262 to 0.365 (static)			
Zdravkovich et al. [1996]	0.172 to 0.234		0.227 to 0.338 (arms straight)	0.258 to 0.383 (arms straight)		
			0.198 to 0.322 (arms bent, body crouched)			
Edwards and Byrnes [2007]			0.246 to 0.379			
Nonweiller (1956)	0.283 to 0.325					0.362 to 0.374
Candau et al. [1999]				0.355 (with backpack)	0.262 to 0.304 (trunk angle 10°)	
					0.333 (trunk angle 35°)	

Table 3.9: Summary of drag area, C_dA, values reported in the literature

Author	Best Position	Source
Kyle [2003a]	Flat back, elbows narrower than rest of body, forearms horizontal If on drops, hold in descent position, tuck in elbows, low crouch, knees to top tube	Comments
Burke and Pruitt [2003]	If on drops, put hands around top of brake level hood, width of bars same as shoulders Aerobars help to narrow the arms Lower the chin and bring knees in	Comments
Broker [2003]	Flat back, tucked head, forearms parallel to bike	Comments
Defraeye et al. [2010]	TT position	Wind tunnel tests
Gibertini et al. [2008]	TT position	Wind tunnel tests
Mestdagh [1998]	Knee angle $<150°$ when in BDC and $>65°$ when in TDC, saddle height 107° Extreme forward, steep posture and lower the trunk	
Lukes et al. [2005]	Tri bars better than cow horn bars, elbows close together, lower the head, extend the bars Hands and forearms level or tilted up by 30°, arms and torso parallel to ground	Literature review
Oggiano et al. [2008]	Handlebars down and forward by 20mm	Wind tunnel tests
Garcia-Lopez et al. [2008]	Lower handlebars and advance pads	Wind tunnel tests
Grappe et al. [1997]	Obree position	Velodrome
Zdravkovich et al. [1996]	TT position, hands on aerobars	Wind tunnel tests
Nonweiler (1956)	Racing position better than touring	Wind tunnel tests
Candau et al. [1999]	Racing aero position better than standard aero position	Coast down tests

Table 3.10: Summary of best position reported in the literature or from experimental results

3.2.2.2 Drafting

The benefits of drafting in terms of aerodynamics and oxygen consumption are well known. More research is being carried out to quantify the savings when drafting another cyclist, although few of these studies involve wind tunnel tests. The aerodynamics of drafting is complex, due to the position and equipment of both the lead cyclist and the drafter. Changes made by the lead cyclist will inevitably affect the drafter, but the optimal position and equipment for both the lead cyclist and drafter is yet to be determined. According to Broker [2003], who summarised data from field trials and wind tunnel tests, a drafting rider produces 61-66% of the lead power in second position, and 57-62% of the lead power in third or fourth position. Lukes et al. [2005] report power savings of 33% for a drafting rider at 40kph during coast down tests, with little difference between the drafter in second position and last in line. Lukes et al. [2005] also state that the reduction in drag is greatest when the drafting rider is as close to the wheel as possible, with a 47% reduction in drag with no gap between the leader and drafter, but a significant reduction in efficiency when the drafting rider is 20-30cm from the lead rider. Olds et al. [1995] and Olds [1998] used a mathematical model, which incorporated a drafting factor dependent on the spacing between the wheels, and concluded that when the drafting rider is 3m from the wheel in front there is no benefit from drafting.

Zdravkovich et al. [1996] compared the position of a drafting cyclist in different tandem and staggered arrangements in a wind tunnel. The results showed that the best position in terms of aerodynamics was for the drafter to be directly behind the lead rider in the closest tandem arrangement (49% reduction in drag). However, Zdravkovich et al. [1996] suggests this position may be too dangerous and a safer position, which has nearly the same aerodynamic benefits, is for the drafting rider to position themselves 10cm away in a staggered arrangement (37% reduction in drag). Zdravkovich et al. [1996] also found that the effect of shielding is reduced abruptly when the drafting cyclist is 20-30cm away.

Edwards and Byrnes [2007] also compared the position of a drafting cyclist, but used 13 trained cyclists performing 4 trials at 45kph on a velodrome. Of the thirteen cyclists, the lead riders were selected as those who had the maximum, medium and minimum drag areas during individual trials so that the effect of drag area of the lead rider on the drafting cyclists could be analysed. The remaining riders drafted each of the lead riders, and the lead riders also performed a trial where they drafted another lead cyclist. The riders were asked to maintain a wheen spacing of 0.5m and minimise lateral movement. The results showed an average of 33.25% reduction in power when drafting, and an average reduction in drag coefficient of 42.44%. The drafting effect was found to be the least when drafting the lead cyclist with the minimum drag area, and the most when drafting the lead rider with the maximum drag area. However, not all drafting riders experienced a significant reduction in drag when drafting the lead rider with the maximum drag area compared to the lead rider with the minimum drag area. The results showed that the characteristics of the drafter were important when drafting a less aerodynamic leader, and that the effect of changing the leader was specific to the drafter. The frontal area of the lead cyclists was found to be significant, but the frontal area of the drafting rider was not. This study highlights the complexity between drafters and leaders, as a high variability was seen depending on the frontal area of the lead rider, the drag area of the lead rider, and the drafter's characteristics when drafting a less aerodynamic leader. In order for the greatest gains to be made for a drafting cyclist, the lead cyclist should have a large frontal area, high power output, but a low drag coefficient. This study did not take into account the lateral displacement of the drafting cyclists, nor their ability to maintain wheel spacing or alignment, all of which influence the aerodynamic effect of drafting. Contradictory results were found by Gardner et al. [2009], who also carried out a study to determine the reduction in drag area while drafting

behind riders with different frontal areas on a velodrome. The drag area was determined by regression of power-speed data collected from the SRM during the trials, and the riders were paired so that the three smallest and three largest riders led during fourteen trials each. Although the results found that individual drag areas reduced by 36% when drafting, there was no difference in the reduction of drag area for smaller riders following a large leader compared to larger riders following a small leader. Therefore, Gardner et al. [2009] suggest that although drag can be reduced by drafting, the rider size does not have any effect on this reduction in drag.

Iniguez-de-la Torre and Iniguez [2009] carried out a two dimensional fluid dynamics simulation of elliptical 'cyclists' composed of 5 riders at 15m/s in a paceline with a 20cm gap between them. The simulation showed that the lead rider also gains an aerodynamic benefit when being drafted, with the average power of the lead rider dropping to 95-96% in a team of 2 riders or more. The simulation also showed that the average power output of the team reduced as more riders joined the team; for 2 riders in a team the average power output was found to be 85% and with 9 riders in a team the average power output was found to be 70%. Although this study highlights the benefits of drafting, the simulation does not take into account individual differences between riders, as the riders are assumed to be elliptical, and the 20cm gap chosen for the simulation has been shown to be the point at which the effect of shielding abruptly reduces [Zdravkovich et al., 1996].

Although a number of studies have shown that drafting provides benefits for both the drafting cyclists and the lead cyclist, there are very few studies which have considered the position and equipment of both the drafter and leader to draw sound conclusions. For events where the lead rider changes, such as the Team Pursuit, the effect of drafting becomes even more complex and the effects of rider position, drag area and changeovers are still not completely understood.

3.2.2.3 Helmets

For endurance athletes cycling in a velodrome, where there is no external wind and the athletes maintain one head position, a teardrop shaped 'aero' helmet has been found to have a 7% lower drag than a rounded helmet, due to the elimination of the void between the head and upper back, which delays separation and prevents recirculation [Lukes et al., 2005]. Kyle [2003a] states than an aero helmet with no ventilation holes is the most aerodynamic, but also that each helmet has an optimal position at which the drag is minimal. This may also vary depending on the shape and position of the athlete wearing the helmet and how the helmet sits on the rider's head. Kyle [2003a] suggests that having the bottom of the helmet parallel to the upper back so that there is a gap between the back and the helmet, or by having a helmet with a tail which fits the back, are the best helmet positions. However, it is almost impossible to design a standard aero helmet that will fit all cyclists, due to the large difference in body shape of individual riders.

Alam et al. [2008a] states that vents in a helmet increase the aerodynamic drag, and that the helmet provides 2-8% of the overall drag of a cyclist travelling at 30kph. Alam et al. [2008b] carried out a study to compare a number of different helmets fixed to a dummy head at speeds between 20kph and 60kph and at different yaw and pitch angles in a wind tunnel. All helmets tested were standard, rounded road helmets; no aero helmets were tested. One helmet was selected to compare the effect of open vents to having the vents blanked off. The geometry, orientation and surface protrusion (helmet surface roughness) of the vents were classified, and the results showed that helmets with high protruded vents and/or large channelled vents increased the aerodynamic drag, and that by blanking off vents the aerodynamic drag was reduced.

Blair and Sidelko [2008] also carried out wind tunnel tests on three different helmets, all of which were aero helmets, using an upper body mannequin in the time trial position at 48kph, and at four different yaw angles (0°, 5°, 10° and 15°). All helmets were tested with and without the visor, and were tipped up from having the tip on the back to having the tip upwards in the air. The results showed that for all three helmets the drag was greater when the tip was up in the air compared to having no helmet on at all. The drag reduction resulting from the helmet that performed in the median in each test condition was 7.2%, 5.8%, 5.7%, and 4.5% at yaw angles of 0°, 5°, 10° and 15° respectively, which shows the benefit of wearing an aero helmet compared to a standard road helmet. However, no helmet showed a consistantly high performance in all head positions or yaw angles, as the rank of the helmets varied depending on the test condition. These results highlight that the aerodynamic drag of an aero helmet is dependent on the position and angle at which the rider wears it, and if a rider cannot maintain the position which results in the lowest drag for one helmet, they may need to change the helmet they are wearing. These results may also have varied with different riders; the helmet which had the lowest drag in one test condition on the mannequin may not have had the lowest drag for the same test condition on an athlete. Although Blair and Sidelko [2008] tested helmet visors, there is no mention the effect of the visor on the aerodynamic drag.

Chabroux et al. [2010] analysed the wake at seven distances from the tip of three very different aero helmets on a mannequin fixed to a bike in a wind tunnel at 50kph. The helmets were placed on the head so that they were 140mm from the back of the mannequin, which Chabroux et al. [2010] states is the 'natural orientation of the head when cycling'. The helmets differed in length, height and width; Helmet 1 had two recesses on the rear, Helmet 2 was similar to a tear drop, and Helmet 3 had a single kink. Different flow features were observed, as the helmet geometry generated a specific wake. The results showed that Helmet 2, shaped like a tear drop, had the lowest aerodynamic drag because the number of kinks and recesses were minimised, limiting the height of the wake. In addition, the helmets with a smaller width and a non-rounded trailing edge resulted in a wake that was not as wide.

Further studies have been carried out on the effect of vents for ventilation purposes rather than aerodynamic purposes. Sznitman et al. [2005] used colour dyes for visualising the flow over four bicycle helmets attached to a glass head replica in a closed-circuit water tunnel. The helmets tested represented the best available in terms of ventilation at the time or had little angle dependence. Therefore none were aero helmets. The equivalent air speed was only 6.8kph, which is only representative of uphill riding situations. Although the aim of this study was to analyse the ventilation characteristics of the helmets, the testing procedure also provided an insight into the flow characteristics around the helmets at different tilt angles. When the surface of the helmet was normal to the incoming streamline, the flow deviated towards the rider's face. These results highlight the significant influence of the front profile of a helmet on the rest of the flow. The results also showed that the presence of a visor can alter the front profile; providing there are no gaps between the visor and helmet the incoming streamline entered one of the vents, preventing the flow from being deflected towards the rider's face. The size of the vents and tilt angle of the helmet also affected the streamline, with larger, longitudinal vents which were exposed to the flow resulting in the flow entering the vents. Helmets with these type of vents would therefore have a greater aerodynamic drag compared to helmets with horizontal vents located at the side or rear of the helmet, where they are hidden from the flow. Sznitman et al. [2005] state that the size, location, orientation, and complex shape of the vents, as well as the inter-vent connections and the presence of hair all affect the flow over a helmet.

3.2.2.4 Clothing

The design, fit and aerodynamic attributes of athlete clothing can all contribute to an improved athlete performance, with a reduction in drag of 10% seen for athletes wearing appropriate clothing [Oggiano et al., 2009, Kyle, 2003a]. The design of an aerodynamic skinsuit should have seams parallel to the flow or in separated flow zones where they will not increase the drag, be close fitting to minimise wrinkles, be made of smooth, rubberised material, cover body hair, and have any graphics out of the airflow [Oggiano et al., 2009, Kyle and Weaver, 2004, Brownlie et al., 1991]. A cyclist is a bluff body for which pressure drag dominates. Separation at low speeds can be delayed by inducing turbulence in order to minimise the aerodynamic drag. This can be achieved by introducing trip wires, surface roughness, or dimples slightly upstream of the point of separation. As the torso of a cyclist is nearly horizontal, smooth fabric should be applied in this area where the flow is parallel as skin friction dominates [Brownlie et al., 2009]. However, on the upper arms and legs, which are similar to circular cylinders in the spanwise orientation, the introduction of surface roughness, trips or dimples can induce turbulence and delay laminar separation. The use of zoned fabric, with smooth and rough materials being placed strategically on different parts of the body, has shown to reduce the drag by 5-8% [Kyle and Weaver, 2004, Oggiano et al., 2009]. The critical Reynolds number for a circular cylinder where the boundary layer undergoes transition from laminar to turbulent flow is $3x10^5<Re<5x10^5$, at which point there is a decrease in the size of the wake and the drag coefficient, C_d, decreases from 1.2 to 0.3 [Brownlie et al., 1991, Hoerner, 1965]. However, by inducing turbulence through surface roughness, dimples, or trips, turbulence will be induced at a lower Reynolds number and the same reduction in drag coefficient will be seen.

The Reynolds number of parts of the body of a cyclist can be determined using Equation 3.24, where D is the length for streamwise elements and diameter for cylindrical, spanwise elements (m), υ is the kinematic viscosity (m^2/s) and U is the cycling speed (m/s). A table of the Reynolds number of body parts for an average, male cyclist at cycling speeds between 40kph and 70kph is shown in Table 3.11.

$$Re = \frac{UD}{\upsilon} \tag{3.24}$$

Body Part	**Shape**	**'D' (m)**	**Reynolds Number ($x10^5$)**			
			40kph	**50kph**	**60kph**	**70kph**
Head	Sphere	Diameter = 0.28	2.05	2.57	3.08	3.59
Torso	Flat Plate	Length = 0.80	5.86	7.33	8.80	10.26
Forearm	Streamwise Cylinder	Length = 0.37	2.71	3.39	4.07	4.75
Upper Arm	Spanwise Cylinder	Diameter = 0.09	0.66	0.82	0.99	1.15
Thigh	Spanwise Cylinder	Diameter = 0.16	1.17	1.47	1.76	2.05
Calf	Spanwise Cylinder	Diameter = 0.10	0.73	0.92	1.10	1.28

Table 3.11: Reynolds numbers of different parts of the body of an average, male cyclist at different speeds

A number of studies have been carried out to identify the best way to reduce the aerodynamic drag through the use of surface roughness, trips or dimples, all of which can be applied to cycling apparel. These will each be discussed separately.

Surface Roughness

The use of surface roughness is the most popular method of inducing turbulence on cylindrical elements in terms of sports aerodynamics. The legs and arms of an athlete are approximately cylindrical elements, so many studies have been carried out on circular cylinders placed in a wind tunnel covered in a number of different fabrics [Oggiano et al., 2006, 2009, Brownlie et al., 2009, Oggiano and Sætran, 2010, Brownlie et al., 1991, Chowdhury et al., 2010]. Some studies have used a complete mannequin in a racing position [Seatran and Oggiano, 2008, Oggiano and Sætran, 2010, Brownlie et al., 1991, Auteuil et al., 2010], or used a number of cylinders placed in a sequence to represent the actual location of the arms and legs during a race [Oggiano and Sætran, 2010].

The effect of surface roughness on the critical Reynolds number and drag crisis for circular cylinders in the spanwise orientation can be seen in Figure 3.18. This shows that the minimum drag coefficient depends on both the Reynolds number and surface roughness, and that an increase in grain size or reduction in cylinder diameter causes the drag crisis to occur at a lower Reynolds number. Once the minimum drag coefficient has been reached, an increase in Reynolds number causes the drag coefficient to increase again for a specific cylinder and surface roughness combination. In this post-crisis region, the drag coefficient is greater for rougher surfaces.

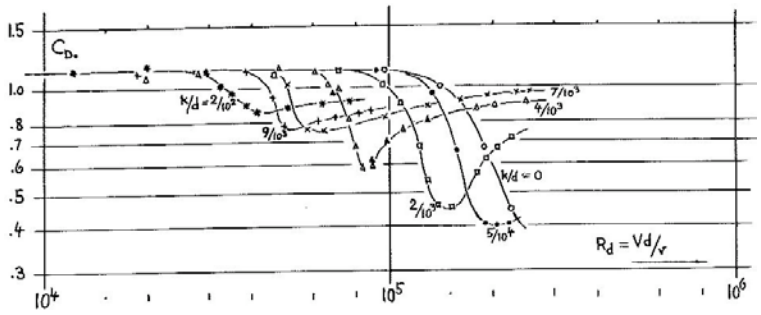

Figure 3.18: Drag coefficient of Cylinders with Varying Degrees of Surface Roughness [Hoerner, 1965]

Oggiano et al. [2006] tested a number of textiles with different surface roughness on three cylinders, 11cm, 20cm and 31cm in diameter and 120cm long, in a wind tunnel placed in the spanwise orientation. A roughness factor was defined as $k = \sqrt{w.d}$, where w and d were the width and depth of the roughness elements, and a dimensionless roughness coefficient defined as $r = \frac{k}{D}$, where D was the diameter of the cylinder. The results showed that by increasing the roughness, transition to turbulence occurred at a lower Reynolds number, and the drag coefficient was reduced by 40% on the 11cm and 20cm diameter cylinders and 10-20% on the 31cm diameter cylinder. These results are in agreement with those published by Hoerner [1965] (Figure 3.18). Oggiano et al. [2009] also analysed the effect of knitted fabric roughness on a circular cylinder and leg model in a wind tunnel at 20-80kph and found that all fabrics tested acted like rough cylinders, with rougher fabrics shifting to the turbulent regime at a lower speed compared to the smoother fabrics. The minimum drag coefficient for all fabrics tested was C_d=0.592 to 0.692, showing a drag reduction of 22-36% compared to smooth cylinders at speeds between 37kph and 70kph. A higher reduction in drag was seen at speeds up to 50kph, but the drop in drag coefficient for the rougher samples was less than that for the smooth samples.

Brownlie et al. [2009] states that there is a limited range of velocities for which rougher surfaces provide an aerodynamic advantage to separated flow, and tested 200 stretch fabrics on spanwise cylinders of diameter 8.9cm, 10cm and 20.3cm, as well as on a leg model in a wind tunnel at 48-52kph. The friction of the fabrics were also measured by placing the 10cm diameter cylinder in the streamwise orientation in the wind tunnel. Brownlie et al. [2009] also found that the rougher fabrics caused boundary layer transition earlier at lower Reynolds numbers compared to the smoother fabrics, but found that the smoother fabrics caused boundary layer transition earlier at higher Reynolds numbers compared to the rougher fabrics. An increase in the diameter of the cylinders caused the minimum drag coefficient to shift to a higher Reynolds number. These results agree with those published by Hoerner [1965] (Figure 3.18) who found that for $3x10^4<Re<1x10^5$ a larger grain size or smaller cylinder diameter caused earlier transition because the roughness to diameter ratio is greater on smaller cylinders; rougher fabrics cause boundary layer transition earlier at lower Reynolds numbers. Brownlie et al. [2009] also found that a stretch knit fabric with a dimpled surface caused early transition with a minimum drag coefficient of C_d=0.62 at $Re=1.2x10^2$, but the drag coefficient then increased to C_d=0.72 at a higher Reynolds number. The smoother fabrics provided the least frictional drag, and similar trends were found when a comparison of seams was made; low-profile, flat, bonded or taped seams had a lower drag than exposed seams. These results suggest that a smooth fabric should be used for the horizontal body parts, and rougher fabrics should be used for narrow diameter limbs, such as the upper arms, rather than wider limbs, such as the thigh, due to the difference in results for the different diameter cylinders. Brownlie et al. [2009] highlights that the human body is a complex combination of cylinders, where the flow of each cylinder will affect others and where transition is initiated on larger diameter cylinders first. The complexity of the moving legs will also reduce the effectiveness of surface roughness induced transition on the leg region.

Seatran and Oggiano [2008] used a doll in a speed skating position to analyse suits of different surface roughness at speeds between 28.8kph and 64.8kph. The suits were made of different material on the lower leg, upper leg, trunk, head and arms. They found that the suit that was moderately rough on the legs and smooth on the trunk and head had the lowest drag, and the suit that was totally smooth had the highest drag. The smooth material on the worst suit did not allow transition to take place, causing separation of the boundary layer and an increase in drag. A different behaviour was seen for the suit that was made from totally rough material for men and women because the shift to transition for such a rough material was at lower speeds compared to all the other suits tested; women race at slower speeds than men, so this suit would be more beneficial for women speed skaters. These results again show that an increase in surface roughness causes transition to occur at a lower speed and lower Reynolds number, but the drag then increases again at higher speeds.

A comprehensive study by Brownlie et al. [1991] included testing a number of different types of surface roughness elements, including stretch fabrics, sandpaper (grit 30 to 600), fibreglass window screen, 0.1cm diameter plastic tubing, polyurethane surgical dressing, and 3M ribbed tape. These were applied to small and large spanwise cylinders and a mannequin in various postures in order to analyse the effect of surface roughness on boundary layer transition. Drag was measured in both a small and large wind tunnel, with a wind speed between 28.8 and 113kph in the small wind tunnel and between 18 and 75.6kph in the large wind tunnel. The drag coefficient of the bare cylinder was similar to other results published in the literature (C_d = 0.95 to 1.06) and transition did not occur. Sandpaper, 3M ribbed tape, polyurethane surgical dressing, fibreglass window screen and 0.1cm diameter plastic tubing did not cause flow transition to take place in the range of Reynolds numbers tested, as the drag coefficient did not reduce. However, various types of stretch materials did cause transition to occur, all of which showed a unique critical Reynolds number at which

the drag coefficient was minimised. When the stretch fabrics were applied to three cylinders placed in an orientation as to represent two arms and a torso, a reduction in drag was seen but it was not as great as for a single cylinder. However, when the three cylinder model was placed in the large wind tunnel no reduction in drag coefficient was seen. This implies that turbulence induced changes are more important than surface roughness induced changes when analysing the aerodyanmics of a human model. Brownlie et al. [1991] also carried out tests on a mannequin and found that certain fabrics did provide a reduction in drag coefficient, although these reductions were not as great compared to a single cylinder model.

Auteuil et al. [2010] also used a mannequin to analyse the effect of different materials on different parts of the body on the drag coefficient, specifically looking at the formation of separation bubbles. In general, for flow around cylinders of the same diameter in axial flow, the surface pressure distribution depends on the Reynolds number, as shown in Figure 3.19; at low Reynolds numbers transition occurs in the wake then moves forwards to the shear layer. As the Reynolds number increases to $1x10^5$ transition takes place in the boundary layer and there is a reduction in drag coefficient, which is associated with an asymmetrical pressure distribution caused by a laminar separation bubble on one side of the cylinder. With a slightly higher Reynolds number the minimum drag coefficient is achieved because of the formation of a separation bubble of either side of the cylinder.

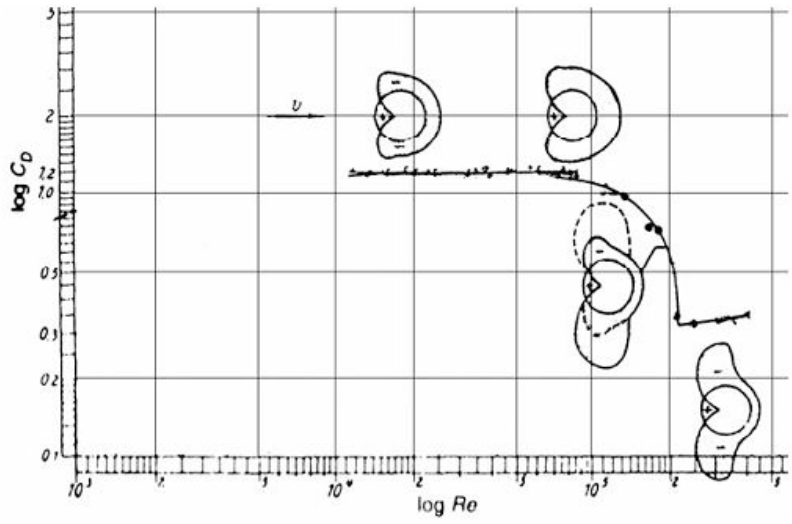

Figure 3.19: Surface pressure distribution around cylinders in axial flow

When the naked mannequin was placed in a speed skating position in the wind tunnel at wind speeds between 30-65kph Auteuil et al. [2010] found that the surface pressure distribution differed at the calf and knee at 58.7kph, with the calf entering the one bubble regime but not the knee, even though the diameters were the same. This suggests the flow around the knee was influenced by the calf, delaying transition of the boundary layer from laminar to turbulent flow at the knee. When smooth fabric was placed on the mannequin in laminar flow a reduction in drag occurred between 50-60kph, which was consistent with the presence of the asymmetrical separation bubble on the calf. However, the thigh did not enter the one bubble regime until

75kph, which suggests that the flow around the thigh was affected by other near by parts of the body and did not undergo transition at a lower velocity, as would be expected for a bigger diameter cylinder when tested on its own. When rough fabric was placed on the mannequin in laminar flow the whole leg was in the single bubble regime at 48.8-58.6kph and not just the calf. This suggests that a greater surface roughness promoted transition at a lower velocity. When a combination of rough and smooth fabric was applied to the mannequin in laminar flow, with rough material on the lower legs and arms and smooth material on the rest of the body, transition occurred on the arms due to the surface roughness, which then affected the flow seen by the thigh. At 64.5kph the calf and knee reached the end of the two bubble regime, with the calf contributing significantly to the reduction in drag compared to the knee even though both went through flow transition. The results differed significantly when the naked mannequin was placed in turbulent flow, with all cylindrical elements (calf, thigh, knee and arm) entering the two bubble regime. When smooth material was placed on the mannequin in turbulent flow the minimum drag coefficient was reached at 60kph, compared to 80kph in laminar flow. When rough fabric was placed on the mannequin in turbulent flow there was actually an increase in drag at 64.1kph because the right leg had already gone through the two bubble regime and the base pressure was beginning to increase again. This study by Auteuil et al. [2010] highlights the importance of simulating the correct flow and using the correct model in order to identify how drag can be reduced through the use of different types of material on different parts of the body. For velodrome conditions there is no external wind, resulting in a low turbulence intensity (laminar) flow. However, many road races involve a side wind, head wind or tail wind to some extent, in which case a turbulent flow should be created for wind tunnel experiments in order for the correct flow to be simulated.

Chowdhury et al. [2010] also analysed the effect of surface roughness on cylinders by placing a cylinder 110mm in diameter and 300 long at different angles in a wind tunnel to simulate the effects of different materials on different parts of the body. The wind speed was set at 20-120kph in 10kph increments, and the cylinder placed at 30°, 60° and 90° from the horizontal. Four different fabrics, two rough and two smooth, were placed on the cylinder at each orientation. The results showed that for the bare cylinder at 90°, 60° and 30° the boundary layer flow was laminar at 90kph, 80kph and 30kph respectively. When the rough fabrics were placed on the cylinder at 90° and 60° the boundary layer underwent transition earlier at 40kph and 30kph respectively. These results are slightly lower than those recorded by Auteuil et al. [2010], who found transition of the whole leg occurred at 48.8-58.6kph for rough fabric in laminar flow. The difference is most likely due to the influence of other body parts on the flow for the mannequin model compared to the cylinder model. When the smooth fabrics were placed on the cylinder at 90°, 60° and 30° the boundary layer underwent transition later at 70kph, 60kph and 30kph respectively. These results are similar to those reported by Auteuil et al. [2010], who found that the calf of the mannequin, which was of similar diameter to the cylinder, went through transition at 50-60kph when covered in smooth material.

Although cyclists are predominantly made up of a combination of cylinders, many studies have been carried out on flat plates and spheres to analyse the effect of surface roughness on boundary layer transition. Roberts and Yaras [2005] analysed the effects of surface roughness and free stream turbulence on boundary layer transition by performing experiments in a closed circuit wind tunnel on a flat test surface parallel to the flow and covered with different surface roughness, upon which streawise pressure gradients were imposed using a countoured wall to form the ceiling of the test section. A perforated plate at the inlet to the test section in the flow path was used to control the level of free stream turbulence. The flat plate was covered with countertop laminate, tar paper, fine asphalt shingle and coarse asphalt shingle with surface roughnesses of $31\mu m$, $53\mu m$, $107\mu m$ and $185\mu m$ respectively. For $3.5\text{x}10^5 < \text{Re} < 4.7\text{x}10^5$ they found that at less than 0.5m

from the leading edge (laminar boundary layer) the surface roughness or Reynolds number had no influence on the boundary layer displacement thickness or boundary layer shape factor. At 0.5-0.6m from the leading edge of the flat plate there was a rapid growth in boundary layer displacement thickness, indicating the presence of a separation bubble, at which point the boundary layer displacement thickness was maximum (0.55m). An increase in surface roughness caused the thickness of the separation bubble to reduce, indicating that surface roughness is an important parameter in flow transition; the $53\mu m$ tar paper was more effective at suppressing the separation bubble compared to the $107\mu m$ fine asphalt shingle. In addition, Roberts and Yaras [2005] found that the larger spacing of the $31\mu m$ countertop laminate was more effective at initiating transition that the more densely packed $53\mu m$ tar paper, where transition occurred further upstream. A further study concluded that the increase in surface roughness was more successful at causing earlier transition than the spacing effect [Roberts and Yaras, 2006].

Haake et al. [2007] found that a slightly roughened surface on a sphere, with the ratio of roughness diameter to sphere diameter k/D=0.025% caused transition of the boundary layer from laminar to turbulent to occur earlier at Re=2.7x10^5 compared to Re=4x10^5, while maintaining the minimum drag coefficient. When k/D=1.25% transition occured even earlier at Re=8x10^4, but the drag coefficient significantly increased. Therefore only a small amount of surface roughness is required in order for transition to occur at a lower velocity, and this relationship is roughly exponential; an increase in size of the roughness elements has less and less of an effect. This study indicated that there is a critical level of roughness which will cause the boundary layer to become turbulent, and although some studies have been carried out to try and identify that critical size, the majority of these studies have been carried out on trips rather than complete surface roughnesses.

Trips

An alternative method for inducing turbulence is to use one or more trip slightly upstream of the point of separation. Trips have been used on speed skating and skiing suits for a number of years, with zigzag trips on the legs and even the head proving to be successful at reducing the drag [Kuper and Sterken, 2008]. Thompson et al. [2001] compared different trips including simple wire, sandpaper tape, dimples, tape ridges up to 15mm thick, and saw-tooth sandpaper strips, and mounted them on the back and inner thigh of skiers in a wind tunnel. An 8% reduction in drag was seen when a 6mm diameter wire or cloth ridge was sewn into the suit, delaying the point of separation, but the location of the trip was dependent on the athlete and the helmet. However, a simple, straight wire placed 75mm behind the trailing edge of the helmet was shown to reduce the drag of all athletes tested. With the right combination of trip wires placed on the shoulders, on the back upstream of the buttocks, and on the inside of the thighs, a drag reduction as big as 11% was seen.

Similar applications of trips have been used for swimsuits, where vortex generators and riblets covering the torso has shown to reduce the energy demand of male swimmers [Pendergast et al., 2006]. Vortex generators 10-20% of the height of the boundary layer have shown to be the most effective, although trips wires with a wire diameter to body diameter ratio of 0.013 to 0.02 have also shown to be successful at reducing the drag [Pendergast et al., 2006]. Using the results for wire diameter to body diameter for a body width of 24cm, a trip wire should be 3-5mm thick. Using 10-20% of the boundary layer thickness, Pendergast et al. [2006] calculated the vortex generator height to be 0.9-1.9mm on the upper back, and 1.7-3.3mm on the buttocks. These results differ from each other and as vortex generators that are larger than required will actually increase the drag, the size and location of the trips is crucial. Pendergast et al. [2006] analysed the effect

of placing 3.4mm turbulators on the upper back, chest and buttocks and found that the drag was reduced on both men and women. A significant drag reduction of 19-41% was seen regardless of gender, weight or height, but the placement of the turbulator was scaled according to the variable height of the subjects with differently sized suits. These results tend to imply that the location of the trip is more significant than the height of the trip wire, as the trip used for this study was greater than 10-20% of the boundary layer thickness. However, Huber II and Mueller [1987] found that both the height and location of a trip wire affect the drag on an airfoil. Trips at a length to chord ratio, x/c, of 1% caused a higher minimum drag coefficient, but when placed further downstream the minimum drag coefficient actually reduced. The lowest recorded drag coefficient was found when the trip with the smallest roughness height was placed at the location of maximum airfoil thickness.

Other types of trips include low-profile vortex generators, which have a height greater than 10% but less than 50% of the boundary layer thickness. Lin [2002] found that low-profile vortex generators can actually be more beneficial than convential vortex generators, which are designed to produce an array of streamwise trailing vortices, because low-profile vortex generators have a lower device drag and do not create strong vortices that cause pockets of recirculating flow. However, Lin [2002] found that the reduction in drag ranged from 24-38% and was dependent on the shape, height, location, separation, angle of inclination, and vortex height to boundary layer thickness ratio (h/δ) of the low-profile vortex generators, as well as the Reynolds number. A rectangular low-profile vortex generator with $h/\delta = 0.2$ reduced separation by 90% when placed at $10h$ upstream of the baseline separation. Vane-type low-profile vortex generators were found to be more favourable than wishbone or doublet types, as these were more effective in separation control and had a lower device drag. However, the forwards wedge shape had 40% of the drag of counter-rotating vane types at zero pressure gradient. The device drag of the counter-rotating vanes could be reduced by increasing the spacing, and Lin [2002] found that each type of low-profile vortex generator had its own favourable spacing. All low-profile vortex generators tested were found to reduce the drag at an angle of inclination of 4°, although the smaller height wishbone and ramp cone types with $h/\delta = 0.3$ and 0.4 respectively were more effective than the larger wishbone with $h/\delta = 0.8$ because of their lower device drag and larger spacing. However, at Re>3.75x10^5 a grit strip of glass beads of 0.31mm diameter was found to be the most effective at reducing the drag ($d/\delta = 0.2$), which according to Lin [2002] is the optimum bead diameter to cause induce transition, and any increase in diameter would make the bead's performance unacceptable.

Torres [1999] also found that the shape of trips was important for drag reduction, and analysed the effectiveness of six different turbulator geometries on an airfoil with chord length 152.4mm and span of 609.6mm placed in a wind tunnel, with the objective of assessing different turbulators at a fixed, free stream condition. The patterns tested included circular arcs, wedges, and waves, as shown in Figure 3.20. All trips were made from 3M scotch tape, 0.076mm thick. For Re=0.35x10^6 transition to turbulent flow would occur at distance/chord length, x/c=0.63-0.67. Therefore, each trip was placed at x/c=0.43 so that they were upstream of the point at which transition would occur. The results showed that an inwards arc shape on the leading edge with a straight trailing edge (configuration #5) was the optimal shape for a trip at this location on an airfoil. Even though configuration 4 had the same leading edge, it was thought that the wavy trailing edge of this trip counteracted the benefits of the leading edge.

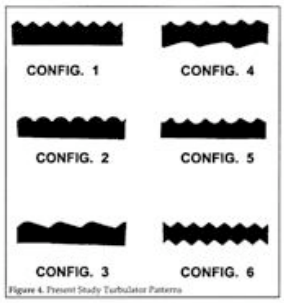

Figure 3.20: Different configurations of trip wires tested on an airfoil [Torres, 1999]

Similar studies have been carried out on spheres to identify the point of separation and how the drag can be reduced by the use of trips. For a sphere at Re<2x10^5 the boundary layer flow is laminar, separation occurs at 80° and the drag coefficient is almost constant at $C_d = 0.5$ [Jeon et al., 2004]. At 2x10^5<Re<3.7x10^5 the drag coefficient reduces rapidly to $C_d = 0.07$ and a separation bubble exists above the surface, and at Re>3.7x10^5 the drag coefficient increases again slowly [Jeon et al., 2004]. Jeon et al. [2004] attached a trip of 2 wires, 0.5mm in diameter and 60° from the front of a sphere, and found that drag could be reduced by 30%. The presence of the trip induced turbulent flow and delayed separation until 110-120°. Jeon et al. [2004] also found that dimples can reduce the drag coefficient of a sphere even further to $C_d = 0.25$, where it remains almost constant.

A summary of the published results for trip heights that have successfully reduced the aerodynamic drag on a flat plate can be seen in Table 3.12. However, the critical height of a 2D element to satisfy the criterion by White [1991], where $Re_{d*tr} = \frac{Uk}{\nu} \approx 850$, for cycling speeds between 40-70kph is shown in Table 3.13. These results show that a 2D element need only be around 1mm thick in order to induce turbulence on a flat plate at typical cycling speeds.

Published trip height (m)	**Author**
0.0030	Pendergast et al. [2006]
0.0050	Pendergast et al. [2006]
0.0009	Pendergast et al. [2006]
0.0033	Pendergast et al. [2006]
0.0060	Thompson et al. [2001]
0.0031	Lin [2002]

Table 3.12: Summary of published results of successful trip heights on flat plates

	40kph	**50kph**	**60kph**	**70kph**
Critical height of trip (mm)	1.2	0.9	0.8	0.6

Table 3.13: Critical height of a 2D element to induce turbulence according to White [1991]

Dimples

The majority of research carried out on the effect of dimples on the aerodynamic drag has been carried out on spheres. The presence of dimples on a golf ball has been known to cause the boundary layer to transition from laminar to turbulent flow, causing a reduction in pressure drag and enabling the ball to travel further. The reduction in drag due to dimples is caused by the generation of separation bubbles inside the dimples, which delays separation of the boundary layer. Choi et al. [2006] found that drag could be reduced by 50% by placing dimples on a sphere at Re=0.9x10^5 (dimples 0.6mm deep, 13mm surface diameter and 392 dimples distributed uniformly on the surface of a sphere 150mm in diameter). Unlike surface roughness, dimples fix the transition point further upstream, keeping a constant separation angle regardless of the Reynolds number, resulting in a constant drag coefficient. Choi et al. [2006] found that the Reynolds number range for which the drag coefficient would be constant was dependent on the depth, surface area and shape of the dimples, and at Re=0.5x10^5 the reattached flow did not have enough momentum near the wall to overcome the strong adverse pressure gradient. Haake et al. [2007] found that increasing the number of dimples decreased the critical Reynolds number while retaining the minimum drag coefficient. Deepening the dimples caused a further decrease in the critical Reynolds number while retaining the minimum drag coefficient, but as the Reynolds number increased the drag coefficient also increased, probably due to a thickening of the turbulent boundary layer and earlier separation. Transition was found to occur earlier through either an increase the number of dimples or an increase in their depth. However, by increasing the number and the depth of dimples at the same time there would be no net gain, as the benefits of each cancel each other out. In terms of drag, an increase in the number of dimples from 104 to 184 actually increased the drag by 0.05, probably because more densely packed dimples causes thickening of the boundary layer, inducing earlier separation and a larger drag coefficient.

Other studies have been carried out on dimples on circular cylinders, which is more applicable to cycling applications as the legs and arms can be treated as cylindrical elements. Yamagishi and Oki [2004] compared triangular and arc grooves placed at the same intervals in the vertical direction on a circular cylinder using experiments, numerical analysis and visualisation. The cylinder was 420mm long and 48mm in diameter, and the triangular and arc grooves were 3.6mm wide, 0.5mm deep and attached to the surface at intervals of 11.25° in the vertical direction. Tests were carried out between 1x10^4<Re<1x10^5 and the velocity measured using a hot-wire anemometer and the drag coefficient recorded from the output signals. The results showed that the drag coefficient dropped abruptly to C_d = 0.59 at Re=4x10^4 with the triangular grooves, then increased slightly to a constant value of C_d = 0.8. This was a 15% greater reduction in drag coefficient compared to the cylinder with arc grooves. It was also found that the pressure in the concave grooves was greater than in the convex grooves, and that separation occurred at θ =100 to 103° for the cylinder with triangular grooves, but at θ = 82 to 90° for the cylinder with arc grooves. The later separation for the cylinder with triangular grooves was as a result of a larger convex part of the velocity in the boundary layer beyond θ = 90°, and a more upstream location of reattachment. Owen and Bearman [2001] also studied the effect of dimples on a spanwise circular cylinder at 10<Re<3.4x10^5 through drag measurements and found that the drag was reduced by attaching hemispherical bumps to the forward face of a straight cylinder in the spanwise orientation with endplates at each end. By applying the bumps in a spiral pattern around the cylinder with constant longitudinal spacing and at an angular separation of 45°, the drag was reduced by 25%. Owen and Bearman [2001] also compared the height of different bumps, 25%, 33% and 50% of the cylinder diameter, but found that the small bumps were just as effective at reducing the drag as the larger

bumps. These results suggest that by creating a dimpled pattern in a spiral formation the drag can be reduced significantly, regardless of the height of the dimples. Bearman and Harvey [1993] studied the effect of dimples on a horizontal cylinder using 12 equally spaced dimples with a depth of 0.91mm, which appeared as ellipses due to machining them with a spherical cutter. The dimples were spaced 11.15mm in the major axis and 9.65mm in the minor axis, and this pattern was repeated along the cylinder in steps of 6.35mm. In comparison to a golf ball, the density of dimples was about half. The minimum drag coefficient was found at Re=1x10^5, which increased to a constant value of $C_d = 0.7$ with an increase in Reynolds number.

Summary of Reducing Drag through the use of Clothing

The literature has highlighted a number of ways to reduce the aerodynamic drag of athlete's attire, including placing surface roughness, trips, or dimples upstream of the point of separation. Dimples appear to be the most effective at reducing the drag coefficient, particularly on spheres where there is a sudden drop in drag coefficient at a particular Reynolds number, after which point the drag coefficient remains relatively constant. However, the literature does highlight the importance of choosing the right material, trip, or dimple according to the velocity and conditions at which the athlete is racing. An increase in surface roughness causes transition to occur at a lower Reynolds number, but after the critical Reynolds number the drag coefficient then increases. The distribution of surface pressure coefficient has been shown to differ for smooth flow compared to turbulent flow, and the results from single cylinder tests do not always agree with full scale mannequin tests because body parts influence the flow around other near by body parts. Only a small amount of surface roughness is required to induce transition, although the location of surface roughness is dependent on the roughness particles, speed and individual athlete. Height, location, spacing and shape of trip wires are all important parameters, and these may differ between athletes and helmet types. Similar to surface roughness, only a small trip height of 10-20% of the boundary layer thickeness is sufficient to induce tubulence. The height of bumps has not shown to be an important parameter, as bumbs of different heights have shown to have the same effect on drag. However, the shape, number and depth of dimples seems to be more significant, with an increase in the number or depth of dimples causing transition to occur at a lower Reynolds number. For all methods of reducing aerodynamic drag on skinsuits the Reynolds number is the critical factor; the correct choice of trip, surface roughness or dimpled surface applied at the point at which the critical Reynolds number occurs will result in a significant reduction in drag coefficient. The extent of reduction in drag coefficient will depend on the location, shape, spacing and size of the surface roughness, trip or dimpled surface.

3.2.2.5 Pedals and Footwear

Most cyclists wear a shoe that is comfortable and appropriate for their event, rather than one that is aerodynamic. Kyle [2003a] suggests that a shoe with a smooth upper surface will help reduce the drag, but that aerodynamic shoes are not necessary because shoe covers made from smooth fabric are more beneficial; shoe covers help streamline the flow over straps, seams, ridges and thick soles. Gibertini et al. [2010] carried out a study to compare two different types of bike shoe, one laced and one strap fastened, and also compared the drag for the strapped shoe with and without a shoe cover. The test setup consisted of putting each shoe on a clipless pedal, which was mounted on a foot hinged to a beam with the top extremity shaped like a shank. The clipless pedal extended 33mm below the sole of the shoes. The forces and moment obtained

at four different crank arm angles (0, $\frac{\pi}{2}$, π and $\frac{3\pi}{2}$) were recorded and the power to overcome aerodynamic effects over the shoes calculated from $P = F_x V_B + M_y \dot{\theta}$. The results showed that the power to overcome air resistance over the two shoes was approximately 8% of the total air resistance. The required power increased by 2.5W per foot (1% of the total power) for the strap shoe with the shoe cover on compared to without the shoe cover. Gibertini et al. [2010] suggests this increase in power is due to an increase in frontal area, as the laced shoe was a tighter fit and resulted in the lowest power required to overcome air resistance. The limited number of tests of shoe and shoe cover combinations carried out by Gibertini et al. [2010] is not a representative sample, and the results contradict the statements by Kyle [2003a], who suggests that shoe covers are beneficial for reducing aerodynamic drag. It should be noted that since this thesis was submitted, the UCI have changed the rules so that shoe covers are no longer allowed to be worn in competitions, placing a greater importance on the development of cycling shoes in the future.

Hamill and Hardin [2001] state that proper cycling shoes are important for optimising cycling performance, as the interface between shoe and pedal are important for transmitting forces from the cyclist to the pedal. However, the aerodynamics of the shoe and pedal combination is something that is not often published in the literature.

3.2.2.6 Bike Frame

The UCI rules state that the bike frame must be a traditional double triangle frame, but the elements can be streamlined providing they have a maximum length and width of 8cm and 2.5cm respectively for the main frame, or 8cm and 1cm respectively for the forks, seat and chain stays, and maximum length to diameter ratio of 3 [Regulations, 2009, Edition July 2009]. A full description of the UCI rules can be seen in Appendix A. Lukes et al. [2005] state that an aerodynamic frame is 3% faster than a normal frame, and by shielding the components the drag can be reduced. Kyle and Weaver [2004] also state that by hiding the screws, bolts, fastenings and other external components, covering the under saddle, smoothing the cranks and sprockets, and having long, thin aero elements for the frame, the drag can be reduced by as much as 14%. According to Lukes et al. [2005] the handlebars contribute to 10% of the total drag on the frame and components (excluding the wheels, saddle and seat post) which is equivalent to approximately 3% of the total drag on a cyclist (the frame, wheels and components account for only 30% of the total drag on a cyclist). Although the contribution of the handlebars to overall drag may be small, handlebars are important for helping the athlete to obtain the best possible position on the bike. Handlebar extensions allow athletes to get into a low, crouched, streamlined position and the elbow pads help riders maintain this position throughout an event [Kyle and Weaver, 2004].

3.2.2.7 Wheels

Although many bike wheels are stiff, strong, and durable, not all wheels are necessarily light or have a low aerodynamic drag. The wheels influence the flow around the rest of the bike and rider, so it is important for athletes to use the most aerodynamic wheels as possible. According to Jermy et al. [2008] the wheel drag accounts for approximately 10% of the total aerodynamic drag on a cyclist at speeds between 30kph and 50kph, and the rear wheel dissipates only 60% of the drag of the front wheel due to shielding from the front wheel Kyle [2003a]. The UCI rules state that wheels for track cycling must be of the same diameter, eliminating the possiblity of athletes using a smaller wheel at the front to try and reduce aerodynamic drag.

Kyle [2003a] states that small wheels are lighter and stronger, but have a higher rolling resistance than larger wheels. Results of wind tunnel tests of a number of different bike wheels of different size, weight, and structure are reported in Kyle [2003a], where results showed that the difference in drag between wheels of 24 inch diameter and 27 inch diameter was only 29g at 30kph (approximately 1.5% of the total drag). Bicycle wheels can be either spoked or disc wheels. Spoked wheels experience pressure drag from separation on the rear facing surfaces of the rim, the hub, and the spokes themselves, which causes spoked wheels to have a higher drag than disc wheels at zero yaw [Lukes et al., 2005, Kyle, 2003a, Kyle and Weaver, 2004, Tew and Sayers, 1999, Jermy et al., 2008]. Disc wheels have been shown to reduce the drag by 4-26% compared to spoked wheels, and Kyle [2003a] showed that composite aero wheels had a lower drag than the best oval, bladed, or round spoked wheel by 35-50g per wheel (approximately 1.75-2.5% of the total drag per wheel). However, front disc wheels become unstable in crosswinds. The yaw angle at which disc wheels become unstable varies in the literature between 8 degrees to 25 degrees [Kyle, 2003a, Lukes et al., 2005]. Spoked wheels, especially 3 or 4 spokes, can actually reduce the drag in crosswind because the spokes provide lift [Lukes et al., 2005]. Advanced carbon fibre composite constuction has allowed ultra lightweight wheels with a low spoke count to evolve, and by tapering the rims to delay separation, streamlining the non-cylindrical spokes, reducing the number of spokes, and creating a smaller hub, the aerodynamic drag on spoked wheels can be reduced [Jermy et al., 2008].

In order to minimise the drag the width of the tyres should be equal to the width of the rim, otherwise separation will occur [Lukes et al., 2005, Kyle, 2003a]. Lukes et al. [2005] also state that the ratio of wheel diameter to tyre tube cross sectional diameter, known as the shape factor, influences the drag on the wheel, where a higher shape factor (large wheel with narrow tyre) increases the drag. However, Kyle [2003a] states that wider tyres increase the drag.

Tew and Sayers [1999] carried out wind tunnel tests on six different wheels (5 spoked and 1 disc) at speeds between 30-60kph and yaw angles of 0-30 degrees. The wheels tested were a standard 36 spoke wheel, Campagnolo Shamal wheel, Mavic Cosmic wheel, Spinergy wheel, Specialized Trispoke wheel, and a disc wheel. The Mavic, Spinergy and Specialized wheels were streamlined with solid material behind the rim forming an aerofoil profile section, where as the Campagnolo was built up behind the rim but with a triangular cross section. The projected area of the wheels was $0.38m^2$, based on a wheel diam of 695mm with the tyre fitted. Both the effect of the wind speed with the wheel rotating at a constant speed, and the effect of wheel speed with constant wind speed were analysed. The results showed that the disc wheel had the lowest drag with no side wind, but not with high crosswinds at low axial velocities, and that the aero wheels had a lower axial drag force than the Standard 36 spoke wheel. The aerodynamic forces were only weakly affected by the rotational speed of the wheel.

Jermy et al. [2008] tested disc, composite compression spoked, and wire spoked wheels in a closed section wind tunnel at 50kph. The drag was measured on a custom built 2-axis force balance, where each wheel was suspended by rigid forks housed in streamlined fairings and spaced 100mm or 120mm apart for front or rear wheels respectively. The wheels were driven by a drive belt running on toothed pulleys, and the whole set up could be rotated to analyse the effect of yaw angle. The spoked wheels tested were front wheels and the disc wheels tested were rear wheels, and the same tyre was used on all wheels. The power required to translate and rotate the wheels was analysed at all yaw angles. The results showed that at zero yaw the disc wheels require more power to translate than rotate; rotational power for disc wheels was 25-50% of total power. The Zen disc wheels required the least amount of power overall and the flat disc wheels required the most amount of power overall at all wind speeds. However, different wheels had the lowest/highest translational

or rotational drag at different speeds, and the difference between translational and rotational power differed by 12% and 40% respectively between the disc wheels. The convex and flat disc wheels had different hub widths, but there was little difference in translational power between these wheels, and rotational power did not correlate with curvature. It appearred that the hub and tyre contributed most to the drag on the disc wheels. For the spoked wheels at zero yaw angle the Zen 3-spoke wheel had the lowest overall drag and the lowest translational drag at all speeds. The wire spoked wheels had a higher rotational power loss than the compressed spoked wheels; 45-55% rotational power for wire spoked wheels and 37-55% rotational power for compression spoked wheels. The wire spoked wheels also had a higher overall power loss than the compression spoked wheels at all speeds. There was no significant difference between translational and rotational power loss between the spoked wheels (both compression and wire spoked) and all spoked wheels had a similar rim profile. This suggests the rim profile dominates translational drag for spoked wheels. For the spoked wheels at yaw angles less than 30 degrees the rank of the wheels in order of longitudinal force was dependent on both the yaw angle and wind speed. However, at yaw angles between 40-50 degrees the rank of the wheels was the same at all speeds. This study shows that rotational power strongly influences total power, and that at zero yaw angles disc wheels or aero spoked wheels have a lower drag than wire spoked wheels. However, the choice of wheel for conditions involving crosswind is dependent on both the angle of the crosswind and the speed of the athlete. Hopkins et al. [1990] also looked at the translational and rotational drag of different bike wheels by using a strain gauge and motor power power consumption. The results showed that the rotational drag only comprised of 10-20% of the total wheel drag. The differences between the results of Jermy et al. [2008] and Hopkins et al. [1990] could be due to the difference in testing techniques and different wheels used for the testing.

Godo et al. [2009] carried out a CFD study on a Zipp 404 wheel with continental tubular tyre. The model included the contact area of deflection of the tyre on the road, which was measured using a rider on a bike. The model was split into two parts: one for the spokes, hub, and inner edge of the wheel rim, and another for the remaining wheel surface, ground contact, and surrounding volume. A no slip condition at the ground plane was assumed, and a uniform velocity profile upstream of 20mph and 30mph was applied. The effect of yaw angle between 0 and 20 degrees was analysed at both 20mph and 30mph. The results showed that at all speeds and yaw angles the contribution of viscous drag force was less than 3% of the total force, which implies all forces are a result of pressure drag. The drag coefficient of the wheels at zero yaw was calculted to be 0.0308 at 20mph and 0.0311 at 30mph, which was similar to results by Greenwell et al. [1995] and Tew and Sayers [1999], who found the drag coefficient of similar wheels to be 0.0389 and 0.028-0.03 respectively. Godo et al. [2009] observed a delayed increase in drag force as the yaw angle increased, and found that the wheel itself was responsible for the majority of the drag force. The spokes did account for drag forces comparible to those found at the hub of the wheel, even though the spokes had a small projected frontal area. The side force on the wheel increased nearly linearly with an increase in yaw angle. Flow features showed a vortex forming at the top of the wheel at all yaw angles, due to the collision of air being dragged forwards by the outer edge of the surface of the rotating wheel into the oncoming flow. This vortex was seen to be nearly vertical at zero yaw, becoming more horizontal as the yaw angle increased. At low yaw angles (0, 2 and 5 degrees) vortex shedding was also seen from the inner rim along the leading edge of the wheel.

The literature on bicycle wheels has shown that disc wheels are more aerodynamic in zero crosswind situations, but 3 or 4 spoked aero wheels are more aerodynamic when crosswind occurs. It has been found that the hub and tyre contribute the most to the drag on disc wheels, but the rim profile contributes the most to the drag on spoked wheels. The choice of wheel is therefore dependent on the speed of the cyclist and the angle of

the crosswind. Although there is some variability between the contribution of rotational drag to the overall drag on bicycle wheels, it is clear that pressure drag is the dominant force.

3.2.2.8 Air density and Altitude

A reduction in air density causes a reduction in aerodynamic drag due to the fewer air particles per square meter. Air density is calculated by using the ambient temperature, pressure, and relative humidity, as shown by Equation 3.25, where P_d is the partial pressure of dry air (Pa), P_v is the partial pressure of wet air (Pa), R_d is the specific gas constant for dry air ($JK^{-1}kg^{-1}$), R_v is the specific gas constant for wet air ($JK^{-1}kg^{-1}$), T is the temperature (K), ϕ is the relative humidity, and P_{sat} is the saturation vapour pressure of water (Pa).

$$\rho = \frac{P_d}{R_d T} + \frac{P_v}{R_v T} \tag{3.25}$$

$$P_d = P - P_v \tag{3.26}$$

$$P_v = \phi P_{sat} \tag{3.27}$$

$$P_{sat} = 610.78 \times 10^{(7.5T - 2048.625/T - 35.85)} \tag{3.28}$$

Equation 3.25 can be used to show that:

- An increase or decrease in temperature by 3°C causes a decrease or increase in air density by 2% respectively.
- An increase or decrease in relative humidity by 5% causes a decrease or increase in air density by 0.5% respectively.
- An increase or decrease in pressure by 1KPa causes an increase or decrease in air density by 1% respectively.
- An increase in temperature by 3°C and a decrease in pressure by 2KPa causes the air density to be reduced by 4%.
- It should be noted that a 2% reduction in air density is equivalent to a 0.57s reduction in finishing time.

These results are similar to those reported by Di Prampero et al. [1979] and Atkinson et al. [2003], who suggest that a change in temperature by 3°C will cause a change in drag by 1%, and an increase in temperature by 3°C and a decrease in pressure by 2KPa will cause a reduction in air density, and therefore drag, by 4%. These results show that temperature and pressure have a significant effect on air density, and therefore drag, but relative humidity has a much smaller effect. However, it should be noted that relative humidity can change by a much greater amount (>50%) than absolute temperature (<10%) from race to race.

The air density, and therefore drag, also reduces with an increase in altitude, enabling athletes to pedal faster for the same amount of power output. According to Wilber [2003] the optimal altitude for cycling between

2km and 40km time trials is 3200m to 3500m, resulting in a reduction in finishing time by approximately 4% compared to sea level. Although at such high altitudes VO_{2max} is significantly reduced, the improvement in cycling aerodynamics exceeds the reduction in VO_{2max}, resulting in faster cycling speeds at altitude [Wilber, 2003].

Di Prampero [2000] suggests the relative gain in speed for a cyclist riding at altitude can be predicted by Equation 3.29, where V_a is the velocity at altitude (m/s), V_1 is the cycling speed at measured conditions (m/s), A is the fractional decrease of VO_{2max}, and k is the fractional decrease of energy expenditure per unit distance due to altitude. However, Equation 3.29 assumes that athletes can maintain the same VO_{2max} at altitude as they can at sea level, which is not strictly true.

$$\frac{V_a}{V_1} = \sqrt[3]{A/k} \tag{3.29}$$

3.2.2.9 Summary

The review of literature on the factors that affect the aerodynamic drag of cycling has shown that athlete position is by far the most significant factor, with a low, crouched position that reduces the frontal area being the most advantageous for individual riders. When multiple riders are considered, drafting can significantly reduce the aerodynamic drag of both leading and drafting riders, although this benefit is lost once the spacing between riders exceed about 3m. The priority for athletes and coaches looking to gain a competitive advantage should therefore be optimising athlete position in order to reduce the aerodynamic drag and maximise cycling speed. Once position has been optimised, the focus can then turn to improvements in the frame and wheel design, the choice of helmet, pedals, footwear, and clothing, and then to making improvements to the design of clothing to consider surface roughness, trips, dimples, and zoned fabric. It is impossible to have any external influence on the air density and altitude at which races take place, and although athletes can train in extreme conditions to maintain the same VO_{2max} at altitude as they can at sea level, altitude and air density can be considered dependent variables.

The literature has shown that the drag of bike frames and wheels has already reached a point where only minimal gains can be made through further changes in their design. Therefore the focus of this thesis will concentrate primarily on individual athlete position, followed by an analysis of helmets, pedals, skinsuit design, and fabric choice.

Chapter 4

Mathematical Model of the Individual Pursuit

Introduction

Presented in this section is a mathematical model for the Individual Pursuit (IP) event for track cycling on an indoor velodrome. This model takes into account leaning in the bends and the actual position of the rider on the track by using data collected by the SRM training system. As mentioned in Chapter 2 (Background) performance in track cycling is effectively only dependent on factors which affect power supply and power demand, and the overall aim of competitive track cycling is to minimise the demand of power so that less power output is needed to match this demand and as little energy as possible is wasted. As the interaction between the power supplied by the rider and the bike is direct, any excess power produced by the athlete will result in acceleration of the system; the larger the excess power the greater the acceleration and the faster the finishing time. This mathematical model uses supply and demand equations to determine the surplus power of an IP athlete for a particular race, and assumes this surplus power leads to acceleration of the centre of mass of the rider.

The optimal path for the IP is to follow the black line, as this is the shortest distance around the track. However, it is almost impossible for athletes to follow this path exactly, so the actual distanced travelled by the athlete is likely to be slightly greater than the race distance. Although there is a small discrepency between the actual distanced travelled and the race distance, the mathematical model is based on the assumption that athletes follow the black line, as this value is known.

The mathematical model will be used to analyse the effect of changing a number of variables on the predicted finishing time, and for generating theoretical pacing strategies in order to identify the optimal pacing strategy for IP athletes.

Although the model is similar to those created by Lukes et al. [2005] and Martin et al. [2006], it is unique in the way that it is designed specifically for track cycling, uses actual SRM power data rather than average power or generated power profiles, uses actual velodrome data and does not assume a circular track, includes separate losses for tyres and bearings, and the equations used to form the mathematical model are described in terms of power rather than force, as this is more appropriate measure of cycling intensity.

4.1 Fundamental Equations

Assuming that the bike and rider are one system, the Free Body Diagram (FBD) of the forces acting on the system on a banked velodrome track can be shown by Figure 4.1, where F_D is the aerodynamic drag force (N), F_A is the force to overcome acceleration or deceleration of the bike (N), F_T is the transmitted force as a result of the power supplied by the athlete (N), F_R is the rolling resistance (N) where r denotes the rear wheel and f denotes the front wheel, F_N is the normal force at the point of contact between the wheel and track (N) where r denotes the rear wheel and f denotes the front wheel, F_F is the lateral friction force between the wheels and track (N), F_C is the centripetal force (N), m is the mass of the bike and rider system (kg), g is the acceleration due to gravity (m/s^2), COM is the centre of mass of the system, δ is the leaning angle (rads), ψ is the gradient of the track (rad), and θ is the banking angle of the track (rad). H is the height of the seat (m).

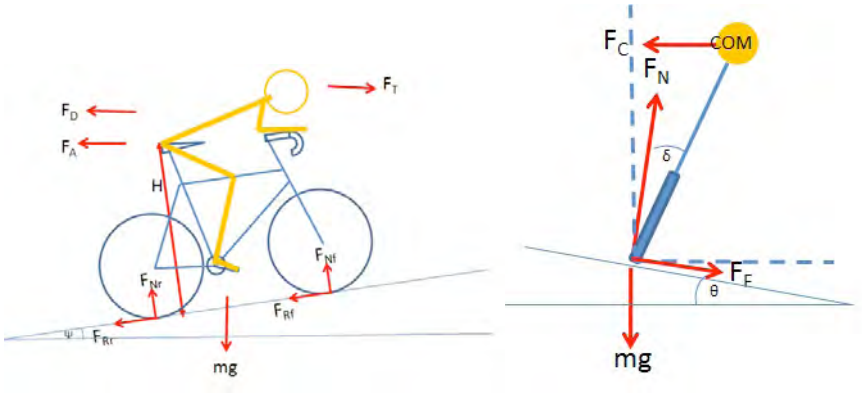

(a) Side view (b) Rear view

Figure 4.1: Free body diagram of the forces acting on a bike and rider system

Resolving forces in Figure 4.1a in the horizontal direction gives:

$$F_A = mgsin\psi + F_T - F_D - F_N sin\psi - F_R cos\psi \tag{4.1}$$

and in the vertical direction gives:

$$F_N cos\psi = mg + F_R sin\psi \tag{4.2}$$

Resolving forces in Figure 4.1b in the horizontal direction gives:

$$F_F cos\theta + F_N sin\theta = F_C \tag{4.3}$$

and in the vertical direction gives:

$$F_N cos\theta = mg + F_F sin\theta \tag{4.4}$$

Although it is possible that there is a very slight grade angle (ψ) on the track when riding on the black line, it will be assumed that $\psi = 0$ for simplicity, and also because the velodrome is a symmetrical track and any slight incline will be offset by a decline at the same angle. This will simplify Equation 4.1 to $F_A = F_R - F_D - F_R$, and Equation 4.2 to $F_N = mg$.

4.1.1 Power

Power is a more appropriate measure of cycling intensity than velocity because power takes into account the amount of work delivered per unit of time. Knowing that $Force = Power \times Velocity$, the power required by an athlete to produce a force to overcome resistance for a given velocity, V, can be determined. Therefore the following equations used to form a mathematical model of the IP will be described in terms of power.

4.1.2 Demand Side Equations

4.1.2.1 Power to Overcome Aerodynamic Drag Force ($\mathbf{F}_D$)

The aerodynamic drag accounts for the majority of the resistance acting on the bike and rider system. Assuming still air inside a velodrome (i.e. zero wind speed) the velocity of the air over the bike and rider system is equal to the velocity of the bike. The power required to overcome the aerodynamic drag force, F_D can therefore be written as:

$$P_D = \frac{1}{2}\rho C_d A V^3 \tag{4.5}$$

where ρ is the air density (kg/m^3), C_d is the drag coefficient, A is the frontal area of the system (m^2), and V is the velocity of the system (m/s).

4.1.2.2 Power to Overcome Tyre Rolling Resistance ($\mathbf{F}_R$)

Rolling resistance is the resistance to a wheel's steady motion, caused by power absorption in the surfaces of the wheel and surface on which it rolls [Wilson, 2004, p208]. Typical values of the coefficient of rolling resistance, C_{rr}, range from 0.002 to 0.010 for bicycle tyres, depending on track surface, cycling velocity, tyre inflation pressure, wheel diameter, tyre thickness, tyre material, inner tube material, tyre-rim interface, steering angle, temperature, and lean of bike [Wilson, 2004, p211]. A value of $C_{rr} = 0.002$ was used for the coefficient of tyre rolling resistance in the mathematical model because the model was created primarily for elite, track cyclists who would be at the most efficient end of the scale due to their narrow, smooth tyres inflated to high pressures, and the hard, wooden surface of indoor velodromes on which they race.

According to Kyle [2003a] tyre rolling resistance increases when cornering, primarily because the tyre deforms laterally to set up an elastic stress which provides the centripetal acceleration. Tyre rolling resistance increases further if steering (scrubbing) occurs. As the track is always banked on a velodrome, Kyle [2003a] found athletes adjust the steering angle by 1° in the straights and 4° in the bends. This corresponds to a 4.1%

and 28.6% increase in tyre rolling resistance in the straights and bends respectively, as shown in Figure 4.2. A scrubbing factor, C_s, should therefore be included in the calculation of power to overcome tyre rolling resistance, where C_s=1.04 in the straights and C_s=1.28 in the bends.

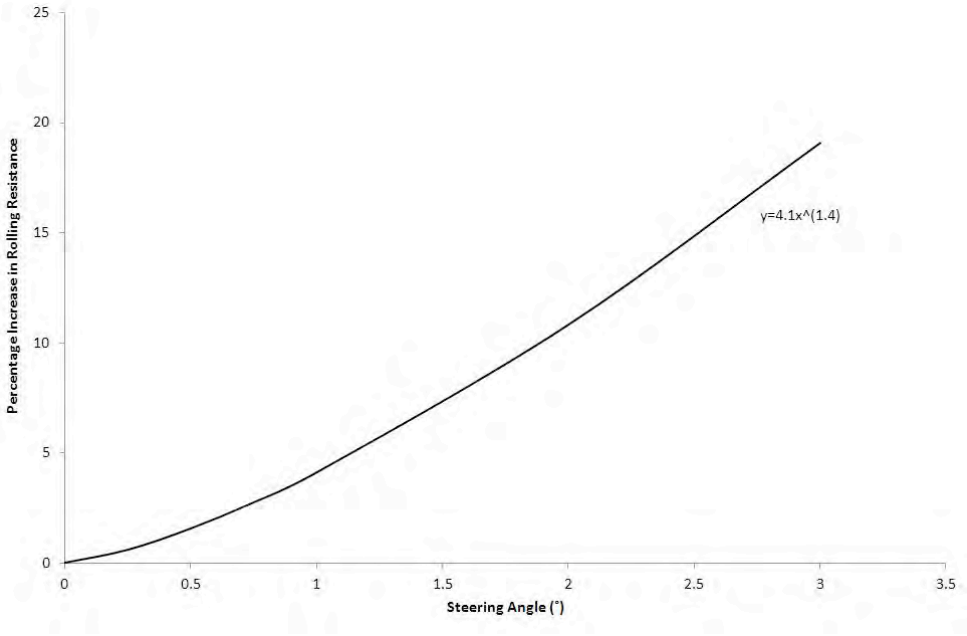

Figure 4.2: Increase in rolling resistance due to steering angle

The power required to overcome tyre rolling resistance can be written as:

$$P_{rr} = (F_N C_{rr} V C_s)\, cos\theta cos\psi \tag{4.6}$$

where F_N is the normal force acting on the wheel (N), C_{rr} is the coefficient of rolling resistance, V is the velocity of the system (m/s), θ is the banking angle (rad), and ψ is the gradient of the track (rad).

As it is assumed that $\psi = 0$, the power required to overcome tyre rolling resistance can be simplified to $P_{rr} = (F_N C_{rr} V C_s)\, cos\theta$.

4.1.2.3 Power to Overcome Bearing Rolling Resistance

There is a small resistance from the bearing seals around the axle of a bike caused by the scrubbing motion of the rolling elements, which should not be ignored. Typical values for the coefficient of bearing rolling resistance, C_{br}, are less than 0.001 [Wilson, 2004, p214], so $C_{br} = 0.001$ was used in the model for each bearing. The power required to overcome bearing rolling resistance can be written as:

$$P_{br} = F_N C_{br} r_b \omega cos\theta cos\psi \tag{4.7}$$

where C_{br} is the coefficient of bearing rolling resistance, r_b is the bearing radius (m), ω is the wheel rotational speed (rad/s), θ is the banking angle (rad), and ψ is the gradient of the track (rad).

As it is assumed that $\psi = 0$, the power to overcome bearing rolling resistance can be simplified to $P_{br} = F_N C_{br} r_b \omega cos\theta$.

4.1.2.4 Power to Overcome Weight Resistance

The power to overcome resistance from the weight of rider, bike frame and the wheels, assuming $\psi = 0$, can be expressed as:

$$P_g = mgV \tag{4.8}$$

where m is the mass of the whole system (kg), g is the acceleration due to gravity (m/s^2), and V is the velocity of the system (m/s).

4.1.2.5 Power to Overcome Wheel Aerodynamic Resistance

The aerodynamic drag of bike wheels has been studied since the early 20th Century [Jermy et al., 2008]. Wind tunnel tests are often used to determine the drag area of cyclists, but it is not always the case that cycle rigs for wind tunnel testing enable both the front and rear wheels to be rotating. For cases when the front wheel is stationary, the aerodynamic power term associated with rotating wheels is not measured. Therefore by calculating the power required to overcome wheel resistance separately from the aerodynamic resistance of the bike frame and rider (excluding both wheels) a more accurate model can be created. Jermy et al. [2008] describe the method by which they determine the aerodynamic drag on both spoked and disc wheels, leading to the following equation for the power required to overcome this resistance depending on the type of wheel used, where α , β and γ are the coefficients used to fit a quadratic to the power absorbed by the drag of the wheel ($\alpha = 0.2118$, $\beta = -0.7388$, $\gamma = 0$ [Jermy et al., 2008]). Wheel drag is assumed to be zero at low velocities, as wheel drag cannot be negative.

$$P_w = \alpha V^2 + \beta V + \gamma \tag{4.9}$$

For cases where wind tunnel tests of cyclists include both the front and rear wheel rotating, the power term associated with rotating wheels is measured so Equation 4.9 can be eliminated, providing that the calculated drag area, C_dA, includes the rider, frame and both wheels.

4.1.3 Supply Side Equations

4.1.3.1 Power Produced by the Athlete (Transmitted Force ($\mathbf{F}_T$))

Some of the power supplied by the athlete will be lost due to inefficiencies of the bike. These include drive chain losses, stiffness losses, and bearing losses. These losses are minimal compared to aerodynamic resistance, however, they should not be ignored. Therefore, the total power transmitted by the athlete can be expressed as:

$$P_T = \eta P_{input} \tag{4.10}$$

where P_{input} is the instantaneous power supplied by the athlete (W), and η is the efficiency of the bike.

Drive chain efficiency has been shown to be 95-98% efficient [Kyle, 2003a], and for elite, track racing cyclists the efficiency will be at the higher end of the scale as there are no gears, the chain will be well lubricated and aligned, and the athletes will pedal fast. Therefore the drive chain efficiency for the mathematical model was chosen to be 98% efficient.

The instantaneous power supplied was input into the model by using SRM data taken for a specific race for an individual athlete. This allows the actual position of the rider on the track to be accounted for, as the power output will vary depending on whether the rider is in the bends or straights. The SRM training system logs power output every 0.5 seconds. The instantaneous power is determined by a linear interpolation of two SRM power readings taken 0.5 seconds apart, as shown in Equation 4.11 and Table 4.1, where $P^i_{athlete}$ is the instantaneous power produced by the athlete (W), t_i is the instantaneous time (s), P^p_i and t^p_i are the power output (W) and time (s) at the previous SRM reading, and P^s_i and t^s_i are the power output (W) and time (s) at the subsequent SRM reading.

$$P^i_{athlete} = P^p_i + \frac{t_i - t^p_i}{t^s_i - t^p_i}\left(P^s_i - P^p_i\right) \tag{4.11}$$

t_i	t^p_i	P^p_i	t^s_i	P^s_i	$P^i_{athlete}$
0	0	0.00001	0.5	657	0.00001
0.005	0	0.00001	0.5	657	6.57
0.01	0	0.00001	0.5	657	13.15
0.015	0	0.00001	0.5	657	19.73
0.02	0	0.00001	0.5	657	26.30

Table 4.1: Interpolation of SRM power data

4.1.4 Power Associated with Acceleration or Deceleration of the Bike ($\mathbf{F}_A$)

The power required to overcome acceleration or deceleration of the bike can be split into separate terms; one for the wheels of the bike, and another for the legs of the athlete. The power to overcome the acceleration of the wheels arises from translational motion based on the translational velocity (Equation 4.12) and rotational motion based on moments of inertia and wheel radius (Equation 4.13), where P_t is the power to overcome translational acceleration of the wheels (W), m is the mass of the whole system (kg), V is the velocity of the system (m/s), P_r is the power to overcome rotational acceleration of the wheels (W), ω is the angular velocity (rad/s), I is the moment of inertia of the wheels (kg/m^2), and r_w is the radius of the wheel (m).

$$P_t = mV \tag{4.12}$$

$$P_r = I\frac{\omega}{r_w} \tag{4.13}$$

The legs can be subdivided into thighs, calves and feet, each of which has its own mass, radius of gyration, and moment of inertia. Therefore the total power required to overcome acceleration from the legs can be written as $P_L = P_{Th} + P_{Ca} + P_F$, where:

$$P_{Th} = I_{Th}\frac{C}{r_{gTh}} \tag{4.14}$$

$$P_{Ca} = I_{Ca}\frac{C}{r_{gCa}} \tag{4.15}$$

$$P_F = I_F\frac{C}{r_{gF}} \tag{4.16}$$

where P_L, P_{Th}, P_{Ca}, and P_F are the powers required to overcome acceleration of the legs, thighs, calves and feet respectively (W), I is the moment of inertia (kg/m^2) where Th, Ca and F represent the thighs, calves and feet respectively, C is the pedalling cadence (rpm), and r_g is the radius of gyration (rad/s) where Th, Ca and F represent the thighs, calves and feet respectively.

The pedalling cadence, C, is the ratio of the rear wheel rotational speed, ω, to the gear ratio:

$$C = \frac{\omega}{gearing} \tag{4.17}$$

In order to determine the moment of inertia and radius of gyration of the legs, two athletes (one male 1.93m in height and 82kg in weight, and one female 1.68m in height and 59kg in weight) were asked to pedal on a bike fixed to the cycle rig so that their pedal strokes could be captured by high speed video. Markers were placed on the foot, calf and thigh, as shown in Figure 4.3, and the athletes told to pedal at 100rpm for 1 minute. The location of the markers was then tracked using Matlab to locate the x and y coordinates of each marker in each frame. The coordinates were then plotted for the foot, calf and thigh for each athlete to illustrate the motion of each part of the leg throughout one revolution, as shown in Figures 4.4 and 4.5.

Figure 4.3: Location of markers on the foot, calf and thigh

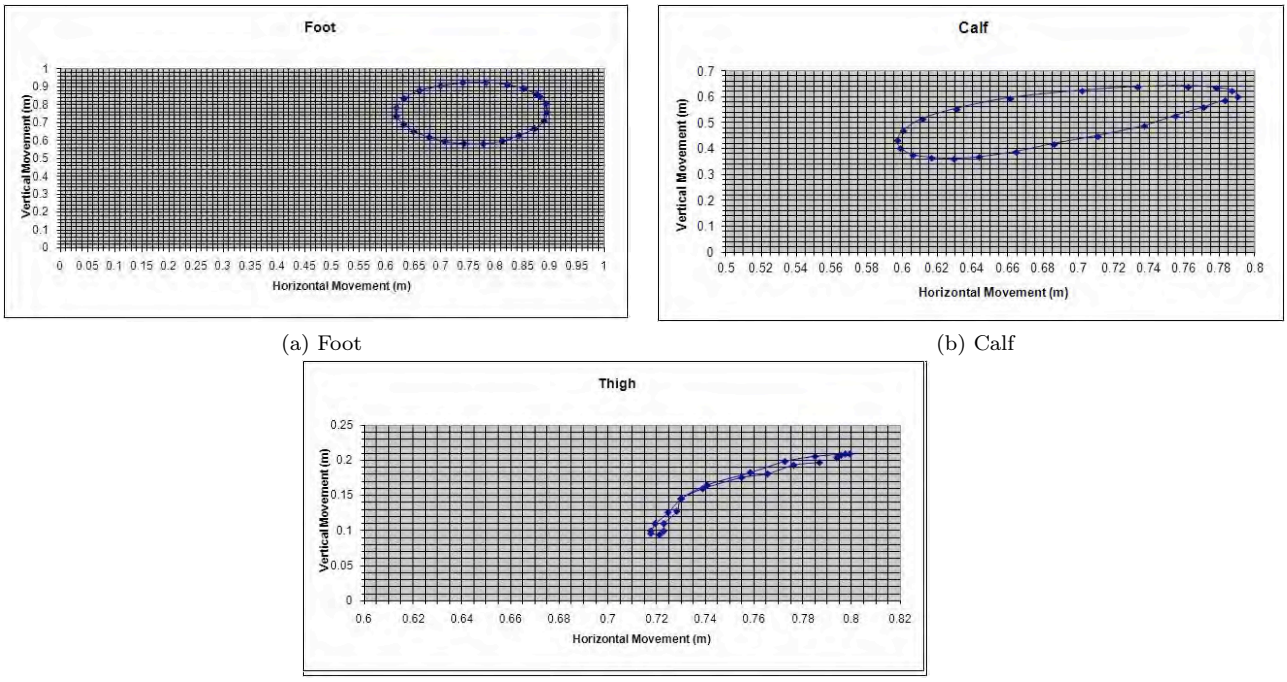

(a) Foot

(b) Calf

(c) Thigh

Figure 4.4: Motion of the Foot, Calf and Thigh for the Male Athlete

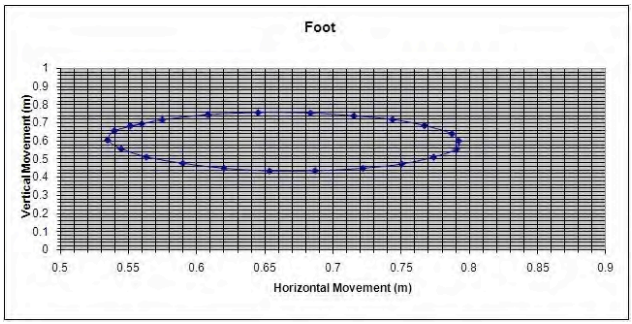

(a) Foot

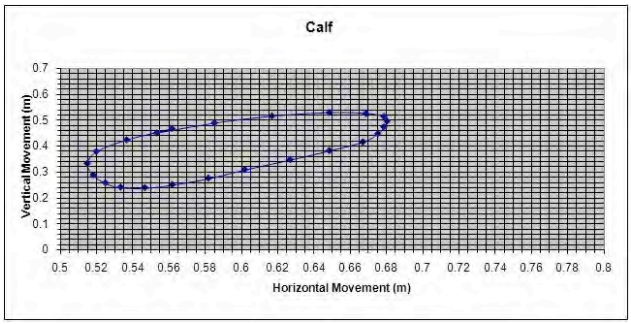

(b) Calf

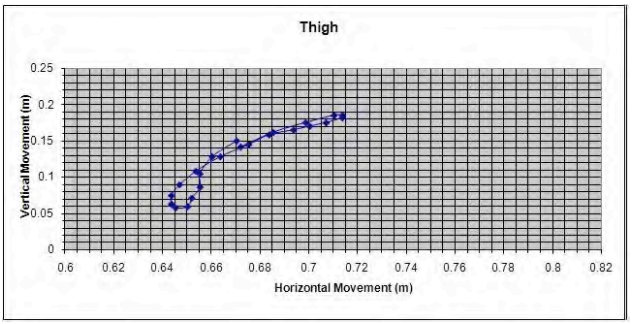

(c) Thigh

Figure 4.5: Motion of the Foot, Calf and Thigh for the Female Athlete

The motion of the foot and calf is similar to that of an ellipsoid, where the radius of gyration can be expressed by Equation 4.18, where a and b are the distances from the centre of the ellipsoid in the horizontal and vertical directions respectively. The motion of the thigh is similar to a pendulum, where the radius of gyration is equal to the length of the thigh.

$$r_{o_{foot}} = \frac{1}{2}\sqrt{(a^2 + b^2)} \tag{4.18}$$

The moment of inertia for both ellipsoids and pendulums can be expressed by Equation 4.19.

$$I = mr_o^2 \tag{4.19}$$

The lengths of the leg segments for the two athletes were measured, and the mass of each segment calculated by multiplying the total body mass by the average ratio of segment mass to total body mass [Drillis et al., 1964]. The radius of gyration and moment of inertia for the two athletes were calcluated using Figure 4.4 and Equations 4.18 and 4.19, and the average values calculated for a rider of 75kg body mass. These average values (Table 4.2) were inserted into the mathematical model to calculate the power required to overcome acceleration of the legs.

	Segment Mass to Total Mass (%)	Mass (kg)	Radius of Gyration (m)	Moment of Inertia (kgm^2)
Foot	2.75	2.0625	0.107	0.0238
Calf	9.49	7.1175	0.083	0.0484
Thigh	25.11	18.83	0.366	2.5227

Table 4.2: Average mass, radius of gyration, and moment of inertia data for a 75kg human [Drillis et al., 1964]

4.1.5 Governing Equation

The mathematical model is generated by calculating the surplus power from total power supplied minus total power demand, and then equating acceleration to surplus power; in other words it is assumed that any additional power supplied results in acceleration of the centre of mass. The power equation is initially solved to determine acceleration in terms of current velocity ($a = \frac{dV}{dt}$) and once the initial acceleration has been calculated it is possible to calculate the new velocity for a small increment, which in turn updates the power equation to yield a new value for dV/dt. A description of the complete calculation process can be seen in Section 4.1.8.

4.1.6 Additional Parameters

4.1.6.1 Motion in the Bends and Straights

In order to prevent a bike from tipping, the FBD must be balanced. For steady, horizontal motion this will be when the COM is vertically above the seat of the bike. However, when travelling around a bend or during an acceleration phase, the combination of the vertical, gravitational force and horizontal, centripetal force (the elastic force in the laterally deformed tyre) results in a tipping angle, as shown in Figure 4.6a. This results in the centre of mass travelling a shorter distance than the wheels when in the bends, as shown in Figure 4.6b.

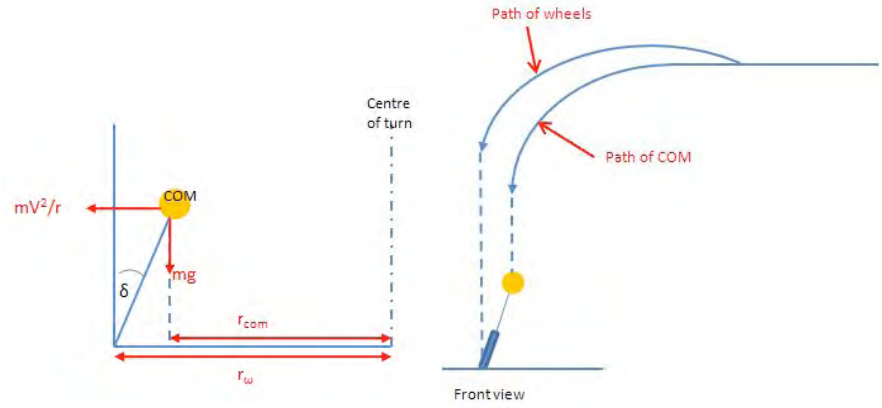

(a) Tipping of the bike when travelling around a bend or during an acceleration phase

(b) Path of the wheels and COM

Figure 4.6: Motion in the bends

The radius of curvature of the COM, r_{com}, can be expressed in terms of the radius of curvature of the wheels, r_w, as shown in Equation 4.20, where H is the distance of the COM from the contact point between the wheels and track surface (m), and δ is the leaning angle (rad).

$$r_{com} = r_w - Hsin\delta \tag{4.20}$$

The leaning angle, δ, can be determined by resolving forces acting on the COM, as shown in Figure 4.7 and Equation 4.21, where m is the mass of the system (kg), V_w is the velocity of the wheels (m/s), r_{COM} is the radius of curvature of the centre of mass (m), and g is the gravitational acceleration (m/s^2).

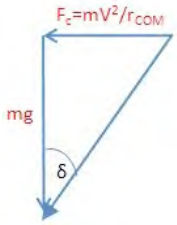

Figure 4.7: Leaning angle

$$tan\delta = \frac{mV_w^2}{r_{com}mg}$$

$$\delta = tan^{-1}\left(\frac{V_w^2}{r_{com}g}\right) \tag{4.21}$$

As both equations 4.20 and 4.21 include terms for the lean angle and radius of curvature of the COM, an iterative procedure is used to determine appropriate values for the lean angle and radius of curvature of the centre of mass; assuming initially that $r_{com} = r_w$, an initial approximation of the lean angle, δ, can be found using Equation 4.21, which is then used to give an improved value for r_{com}. This process is repeated three times in order to find suitable values for r_{com} and δ; trial and error identified that any more than three iterations did not reduce the finishing time any more, as shown in Figure 4.8.

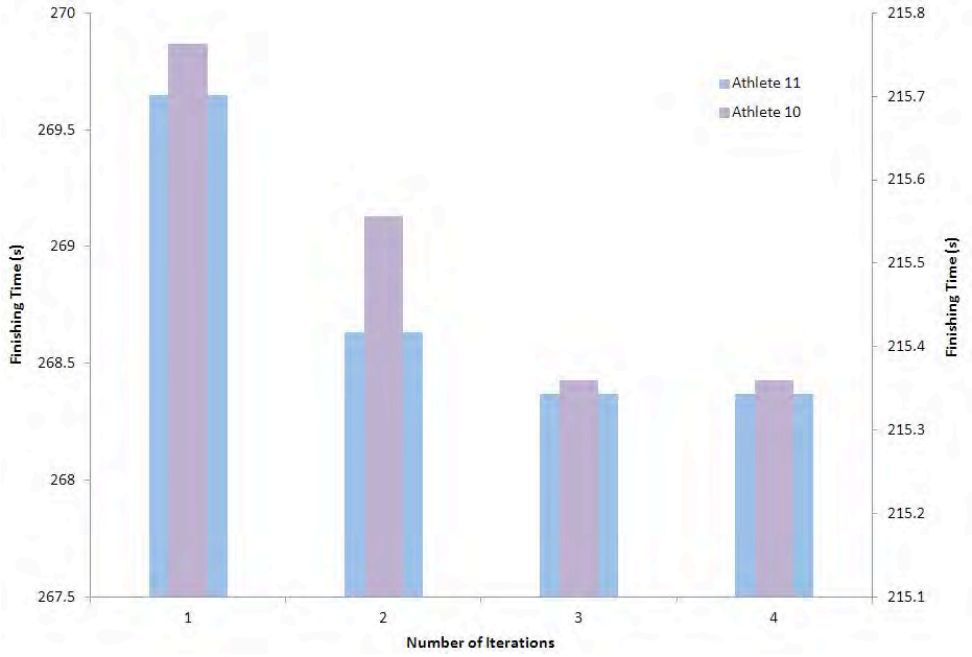

Figure 4.8: The dependence of the finishing time on the iterative procedure for the leaning angle and radius of curvature of the centre of mass

4.1.6.2 Normal Force Acting on the Wheels and Bearings

By taking moments about the COM from Figure 4.1b, the normal force, F_N, can be determined:

$$F_N H sin\delta = F_F H sin\left(\frac{\pi}{2} - \delta - 2\theta\right) \tag{4.22}$$

or

$$F_F = \frac{F_N sin\delta}{sin\left(\frac{\pi}{2} - \delta - 2\theta\right)}$$

and from Equation 4.22, F_F can be eliminated:

$$F_N = \frac{mgsin\left(\frac{\pi}{2} - \delta - 2\theta\right)}{cos\theta sin\left(\frac{\pi}{2} - \delta - 2\theta\right) - sin\delta sin\theta} \tag{4.23}$$

4.1.6.3 Air Density

The air density was calculated using Equation 4.24 for air density for moist air described by Davis [1992], where p is the pressure (Pa), M_a is the molar mass of dry air, x_v is the mole fraction of water vapour, T is the temperature (K), R is the molar gas constant, M_v is the molar mass of water, and Z is the compressibility factor.

$$\rho = \frac{pM_a}{ZRT}\left[1 - x_v\left(1 - \frac{M_v}{M_a}\right)\right] \tag{4.24}$$

At a lower air density the aerodynamic drag decreases, and therefore athletes can pedal faster for the same amount of power output. However, there is also a decline in maximal oxygen uptake, VO_{2max}, when the air density is lower (at higher altitudes) and although athletes can acclimatise to such conditions, a decrease in VO_{2max} will lead to a decrease in power output. The decline in power output can be assumed to be equivalent to the decline in VO_{2max}, and for an acclimatised subject this can be described by Equation 4.25 [Davis, 1992].

$$P = (-1.122)x^2 - (1.8991)x + 99.921 \tag{4.25}$$

Equation 4.25 is useful for estimating finishing times for an athlete on different indoor velodromes, especially when the only available instantaneous power output data is from one specific velodrome.

The temperature was taken from SRM data, and the atmospheric pressure and relative humidity taken from recorded data for the closest airport to the velodrome on which the race was taking place [Underground, 2009]. Although climatic conditions are often controlled in velodromes, this was the most consistent method of obtaining atmospheric data for each athlete without actually being present at the race.

4.1.6.4 Frontal Area

The drag coefficient and frontal area of the system both depend on the shape of the body involved, so can be combined as a single variable for drag area. The overall drag area, C_dA, was determined from wind tunnel data and the frontal area of the rider, bike and wheels was determined using the digitizing method, as described in Section 5.1.2.2, during the wind tunnel tests. As the wind tunnel tests carried out at the University of Canterbury do not allow rotation of the front wheel, it is necessary to include the term for power to overcome wheel resistance, which has already been described in Section 4.1.2.5. In order to avoid accounting for the wheel drag twice, the drag area for the athlete and bike, excluding the wheels, was determined and this value used in Equation 4.5 to determine the power required to overcome aerodynamic drag.

$$C_dA_{rider+bike} = C_dA_{rider+bike+wheels}\frac{A_{rider+bike+wheels} - A_{wheels}}{A_{rider+bike+wheels}} \tag{4.26}$$

Equation 4.26 and the separate contribution for wheel drag could be omitted, but this would mean all the information on wheel and rider drag comes from one drag area measurement in the wind tunnel. Although this is more simple, wheel rotational aerodynamic resistance would not be accounted for those wind tunnel tests carried out at the University of Canterbury.

For athletes not tested in a wind tunnel, the drag area, C_dA, can be determined by calculating the quantities for the left and right sides of Equation 4.27 using SRM data, and using linear regression to determine the drag area for a constant coefficient of friction [Martin et al., 2006]. This equation includes wheel drag, so it is not necessary to include the extra term for power to overcome wheel resistance (Equation 4.9) in this case.

$$C_dA\frac{1}{2}\rho V^3 + \mu F_N V = P_{av} \times Efficiency - \frac{\triangle KE}{\triangle t} - \frac{\triangle PE}{\triangle t} - mgC_{rr}V \tag{4.27}$$

where P_{av} is the average power from SRM data (W), $\frac{\triangle KE}{\triangle t}$ is the change in kinetic energy of the system over the total finishing time (J/s), $\frac{\triangle PE}{\triangle t}$ is the change in potential energy of the system over the total finishing time (J/s), ρ is the air density (kg/m^3), V is the average velocity (m/s), μ is the coefficient of friction, F_N is the normal force (N), m is the total mass of the system (kg), g is the acceleration due to gravity (m/s^2), and C_{rr} is the coefficient of rolling resistance.

4.1.6.5 Initial Velocity

Although in reality the initial velocity is zero, the mathematical model requires a positive initial velocity to be stated to prevent the governing equation from tending to infinity as the velocity tends to zero. An initial velocity that is too high will generate an artificial surge at the start of the mathematical model, so in order to determine the optimal initial velocity the dependence of the initial velocity on the finishing time was explored. It was found that an initial velocity of 0.0003kph provided the smallest starting velocity without generating an artifical surge, and also resulted in the most accurate predicted finishing time, as shown in Table 4.3. Details of all other parameters used to identify the optimal initial velocity are given in Table 4.4.

	Predicted Finishing Time (s)	
Initial Velocity (kph)	**Athlete 11 (Actual T=265.023s)**	**Athlete 6 (Actual T=267.566s)**
0.0002	223.038	224.845
0.0003	264.887	267.612
0.0004	266.859	269.597
0.0005	267.597	270.302
0.0006	267.937	270.625
0.0007	268.122	270.796
0.0008	268.230	270.900
0.0009	268.301	270.965
0.0010	268.349	271.010

Table 4.3: Effect of initial velocity on the finishing time

Athlete Data		**Wheel Data (each wheel)**	
Height (m)	1.85	Power coefficient α	0.2118
Weight (kg)	75	Power coefficient β	-0.7388
C_dA (m^2)	0.198	Power coefficient γ	0
Race distance (m)	4000	C_{rr} tyre	0.001
		C_{rr}bearing	0.001
Track Data		**Environmental Data**	
Lap distance (m)	250	Temperature ($^\circ$C)	24
Banking angle straights (rad)	0.22	Pressure (mbar)	1016.86
Banking angle bends (rad)	0.733	Relative humidity (%)	56
Radius of curvature straights (m)	$1x10^{21}$		
Radius of curvature bends (m)	26.101		

Table 4.4: Parameters used to determine the optimal initial velocity

4.1.6.6 Time Step

A first order Euler time integration technique was used to determine the finishing time, where the equations described above were solved at every time step starting from t=0s. The time step should be small enough so the results don't change, but a time step which is too small will take longer for the equations to be solved. The mathematical model was generated in Microsoft Excel, which has a limit to the number of iterations that can be performed. Therefore, the smallest possible timestep which could be used for the model in Excel was dt=0.005s.

4.1.6.7 Accounting for SRM Delay

The SRM Training System does not start recording data until one complete revolution, causing a delay at the start of approximately 3 seconds. In order to account for this delay, a linear interpolation was applied between zero and the first recorded power output, so that the first recorded power output was input into the model at 3 seconds, as shown in Table 4.5.

Time (s)	**Power (W)**
0	0.0001
0.5	108
1	216
1.5	325
2	433
2.5	541
3	649*

Table 4.5: Interpolation of initial power recorded by SRM
* This is the first recorded power output by the SRM.

4.1.7 Assumptions

1. Stiffness losses are combined with drive train losses, which have been approximated as a reduction in instantaneous power output by 2%, and drive train losses do not vary with power output.
2. All types of bearing losses are incorporated into losses due to bearing rolling resistance.
3. Tyre rolling resistance increases by 4.1% in the straights and 28.6% in the bends.
4. Grade angle is assumed to be zero.
5. About 40% of the weight of the frame acts on the front wheel and bearings; the remaining 60% acts on the rear wheel and bearings. Therefore, the normal force acting on the front and rear wheels and bearings will be 40% and 60% of Equation 4.23 respectively.
6. The rear wheel dissipates only 60% of the power of the isolated front wheel due to shielding by the frame [Jermy et al., 2008].
7. The centre of mass is taken to be equal to the height of the seat, measured vertically from the ground. The mathematical model is relatively insensitive to the centre of mass position, and a method to estimate the centre of mass of a seated bike and rider was developed by Moore et al. (2009), giving the location of the centre of mass for a 75kg rider to be 1.06m vertically from the ground, which is comparable to seat heights of 1-1.2m used for the mathematical model.
8. There is negligible effect of wind on an indoor velodrome, as on a circular, symmetrical track any head and tail winds cancel each other out. This eliminates any equations for sidewind, which would be applicable in a mathematical model for road cycling.
9. The coefficient of rolling resistance does not vary with velocity, tyre or track surface.
10. The athlete travels on the black line throughout the event.

4.1.8 Calculation Procedure

The model was compiled in a Microsoft Excel Spreadsheet, and the calculation procedure used a time-stepping technique where by the equations were solved in a certain order at every time-step starting from t=0s. The calculations were performed in the following order:

1. Calculate the initial acceleration

For an initial velocity of 0.0003kph, the power to overcome losses, P_{losses} , the instant power produced by the athlete, $P^i_{athlete}$, and the power to overcome acceleration, $P_{acceleration}$, can be determined at t=0s. The initial acceleration can then be determined by:

$$a = \frac{P_{surplus}}{P_{acceleration}} \tag{4.28}$$

where $P_{surplus} = P^i_{athlete} - P_{losses}$.

2. Calculate the change in velocity, the velocity of the centre of mass and velocity of the wheels

Once the initial acceleration has been determined, the change in velocity can be calculated by $dV = a\Delta t$. It is assumed that the surplus power leads to acceleration of the centre of mass, so the calculated change in velocity is the change in velocity of the centre of mass. The velocity of the centre of mass at the next time-step can then be determined using the velocity at the the previous time-step plus the calculated change in velocity:

$$V_{i+1} = V_i + dV \tag{4.29}$$

The velocity of the wheels can be determined by:

$$V_w = \frac{V_{com}}{r_{com}} \times r_w \tag{4.30}$$

where V is the velocity (ms^{-1}), r is the radius of curvature (m), w represents the wheels and com represents the centre of mass.

3. Calculate the distance of the centre of mass and distance of the wheels

The distance travelled by the centre of mass over each time-step is calculated using a discrete version of the kinematic formula $d = ut + \frac{1}{2}at^2$, where $u = V_i$ and $a(t_{i+1} - t_i) = dV$. The cumulative distance can then be found by adding the distance travelled over the previous time-step to the total distance travelled until that point, as shown in Equation 4.31.

$$d_{i+1} = d_i + V_i(t_{i+1} - t_i) + \frac{dV}{2}(t_{i+1} - t_i) \tag{4.31}$$

The distance of the wheels can then be determined by:

$$d_w = \frac{d_{com}}{r_{com}} \times r_w \tag{4.32}$$

4. Calculate the finishing time

The finishing time is taken to be the time at which the overall racing distance is reached (3000m for women IP and 4000m for men IP).

4.1.9 Validation

The accuracy of the mathematical model was determined by comparing finishing times for eleven, IP athletes for specific World Championship events (five 4000m male races and six 3000m female races). The power profile for each athlete was taken from SRM training systems, which were placed on the bike during the event.

4.1.9.1 Input Parameters

The temperature (°C), pressure (Pa), body weight (kg), athlete height (m), seat height (m) and gear ratio were determined for each athlete at the time of the race. The frame, wheel and bearing masses and radii were obtained from the manufacturer, and the velodrome data obtained from the velodrome database

(www.fixedgearfever.com). The range of these variables are shown in Table 4.6. The drag area for each athlete was calculated using Equation 4.27, as not all athletes were able to be tested in the wind tunnel. The calculated drag areas are shown in Table 4.7.

Variable	**Maximum**	**Minimum**	**Range**
Temperature ($^\circ$C)	28	22	6
Pressure (mbar)	1021	1005	16
Relative humidity (%)	60	45	15
Body weight (kg)	78.0	54.5	23.5
Athlete height (m)	1.90	1.64	0.26
Seat height (m)	1.1	1.0	0.1
Gear ratio	3.8	3.2	0.6
Frame mass (kg)	8.0	8.0	0
Wheel mass (kg)	1.255	1.145	0.11
Wheel radius (m)	0.3315	0.3315	0
Bearing radius (m)	0.012	0.012	0
Track banking angle in bends (rad)	0.750	0.733	0.017
Track radius of curvature in bends (m)	26.101	26.101	0
Track banking angle in straights (rad)	0.22	0.22	0
Track radius of curvature in straights (m)	$1x10^{21}$	$1x10^{21}$	0

Table 4.6: Range of variables used in the mathematical model

	Athlete										
	1	**2**	**3**	**4**	**5**	**6**	**7**	**8**	**9**	**10**	**11**
C_dA	0.194	0.201	0.195	0.192	0.210	0.174	0.172	0.174	0.209	0.203	0.195

Table 4.7: Calculated drag area for each athlete

The following parameters remained the same for all athletes because all velodromes on which the races took place had a lap length of 250m and it was assumed that the grade angle was zero, and the foot, calf and thigh parameters were averages determined from video analysis of pedal strokes, as described in Section 4.1.4:

Parameter	
Lap length (m)	250
Grade angle (rad)	0
Foot mass (kg)	1.0875
Foot radius of gyration (m)	0.10745
Foot moment of inertia (kgm^2)	0.01256
Calf mass (kg)	3.4875
Calf radius of gyration (m)	0.0825
Calf moment of inertia (kgm^2)	0.09489
Thigh mass (kg)	7.5
Thigh radius of gyration (m)	0.366
Thigh moment of inertia (kgm^2)	1.00467
Wheel moment of inertia (kgm^2)	0.065
Coefficient of tyre rolling resistance (both tyres)	0.002
Coefficient of bearing rolling resistance	0.002
Power coefficient α	0.2118
Power coefficient β	-0.7388
Power coefficient γ	0

Table 4.8: Input parameters recorded prior to the event

4.1.9.2 Results

A comparison between the predicted finishing time and actual finishing time for each athlete is shown in Table 4.9. These results show that the average difference between actual and predicted finishing times is 0.31 seconds (0.16%). As the mathematical model under-predicted the finishing time for 6 of the athletes but over-predicted the finishing time for 5 of the athletes there is no clear indication as to whether the model is likely to under or over predict the finishing time for any given athlete.

Athlete	Actual finishing time (s)	Predicted finishing time (s)	Difference (s)	Difference (%)
1	222.080	220.583	-1.497	-0.67
2	221.597	222.064	0.467	0.21
3	222.990	222.634	-0.356	-0.16
4	222.819	220.228	-2.591	-1.16
5	276.640	277.263	0.623	0.23
6	267.566	267.612	0.046	0.02
7	233.255	232.695	-0.560	-0.24
8	267.789	269.747	2.181	0.81
9	268.118	268.476	0.358	0.13
10	215.212	213.306	-1.906	-0.89
11	265.023	264.887	-0.136	0.05
		RMS	*1.30*	*0.56*

Table 4.9: Results of actual and predicted finishing times

A comparison of actual and predicted lap times for Athlete 10 (3000m female race) is shown in Table 4.10. These results show that the greatest error is seen during the first lap, where the model underpredicts the

lap time by 3.214 seconds. This could be due to the increased drag area during the standing start in reality, which is not accounted for in the model. It also takes one complete revolution before the SRM Training System begins to store the data, and although this was accounted for using a linear interpolation between zero and the first recorded power output, which was assumed to be at 3 seconds, it would be more realistic to have power data that recorded more frequently than 0.5s intervals. It was also assumed that the riders would travel exactly 3000m or 4000m during their race, which as previously mentioned would not be exactly true, as athletes are not able to stay on the black line throughout the entire race.

	Distance (m)	**Actual Lap Time (s)**	**Predicted Lap Time (s)**	**Difference (s)**
Lap 1	250	23.299	20.085	-3.214
Lap 2	500	17.115	17.032	-0.083
Lap 3	750	17.615	17.101	-0.514
Lap 4	1000	17.873	17.327	-0.546
Lap 5	1250	17.796	17.646	-0.150
Lap 6	1500	17.674	17.540	-0.134
Lap 7	1750	17.726	17.580	-0.146
Lap 8	2000	17.831	17.535	-0.296
Lap 9	2250	17.958	17.652	-0.306
Lap 10	2500	18.191	17.820	-0.371
Lap 11	2750	18.209	17.939	-0.270
Lap 12	3000	18.239	18.049	-0.190

Table 4.10: Comparison between actual and predicted lap times for Athlete 10

A comparison of the velocity profiles for the predicted velocity of the wheels and the actual velocity recorded by the SRM data for one male and one female athlete (Athlete 11 and Athlete 7) is shown in Figure 4.9. This clearly shows the increase in velocity throughout the bends compared to the straights. In general, the model predicts a slightly lower velocity in both the bends and straights compared to the SRM data, a difference of approximately 0.2m/s. The mathematical model tends to underpredict the time to complete the first lap by approximately 3-4s for each athlete, which is probably due to the increase in aerodynamic drag when athletes stand during the standing start, which is not accounted for in the mathematical model. After the initial acceleration phase, the mathematical model either under-predicts or over-predicts lap times by anything from 0.003s to 0.5s. However, there is no clear trend as to when the model may under or over-predict lap times, as it appears to vary between athletes.

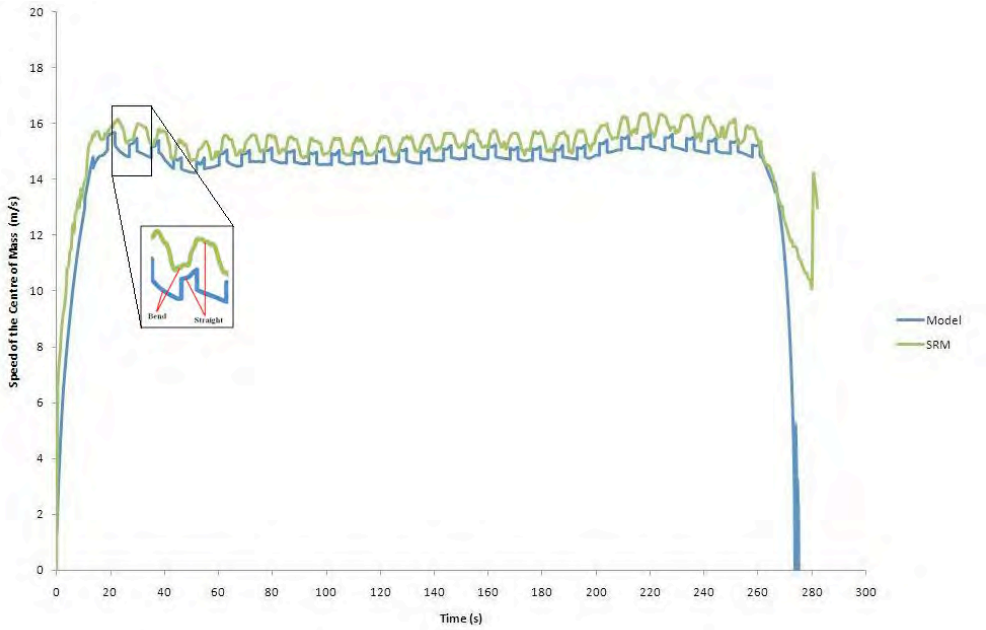

(a) Athlete 11

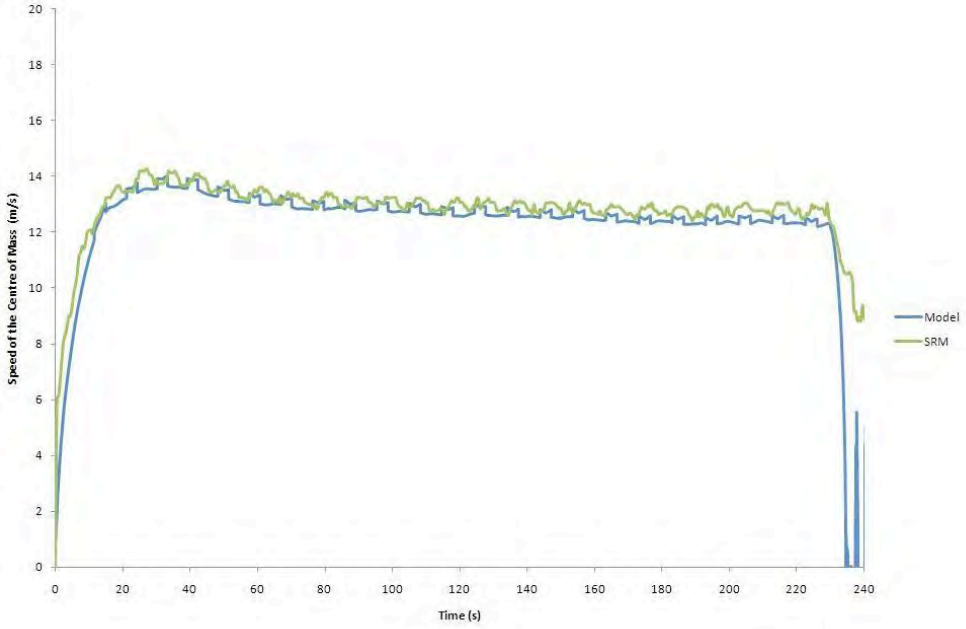

(b) Athlete 7

Figure 4.9: Comparison of the predicted velocity of the wheels to the actual velocity recorded by the SRM data

These results show that the mathematical model can be used to predict the finishing time for IP athletes to a high degree of accuracy. Although improvements can be made, such as better atmospheric data and more frequent power and velocity data, the model is more than capable of being used to predict 'what if' scenarios

without the need for athletes to simulate such conditions on the track.

4.1.10 Relative Contribution of resistive forces

The mathematical model can also be used to identify the relative contribution of the resistive forces to the instantaneous power output, as shown in Figure 4.10. From Figure 4.10 it is clear to see that the aerodynamic drag contributes the most to the overall resistive force, with bearing resistance being the minimal resistance. It is also clear that the contribution of all resistive forces varies between the bends and the straights, and there is a significant increase in resistive forces in the first 20s, which is most likely due to the standing position of the rider during the standing start. A comparison between the contribution of the resistive forces calculated from the model and compared to the literature can be seen in Table 4.11. Table 4.11 shows that the results are similar between the model and the literature, although the effect of scrubbing appears to be slightly greater in the literature. The contribution of bearing rolling resistance calculated in the model tends to agree with Wilson [2004], who states that the effect of bearing rolling resistance is thought to be negligible compared to the other resistive forces in cycling. The contribution of aerodynamic drag to overall resistance is lower in the bends due to the increase in the contribution of rolling resistance and scrubbing, but drag is still the highest contributor to resistance in both the bends and straights.

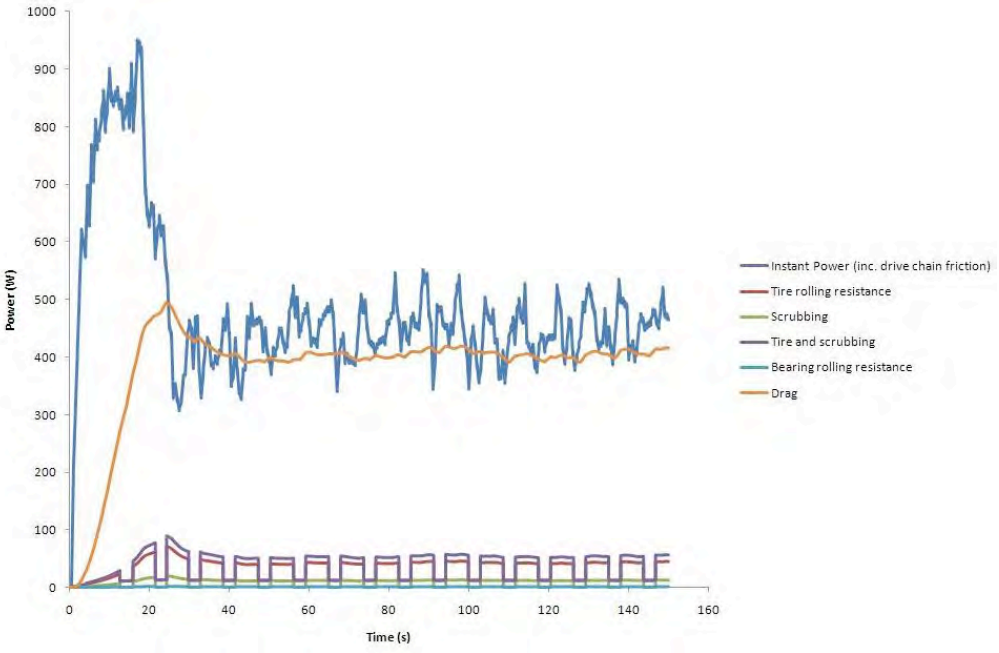

Figure 4.10: Contribution of resistive forces

	Drag	**Tyre RR**	**Scrubbing**	**Bearing RR**
Straights	94%	2.5%	0.02%	0.08%
Bends	80%	8%	0.7%	0.3%
Literature (at V>40kph)	90% [Oggiano et al., 2008]	<10% [Atkinson et al., 2003]	0.4% straights [Kyle, 2003a]* 2.9% bends [Kyle, 2003a]* 1 to 5% [Wilson, 2004]*	negligible [Wilson, 2004] 2-5% [Martin et al., 2007]

Table 4.11: Contribution of resistive forces as a percentage of instant power

* According to Kyle (2003a) scrubbing increases the tyre rolling resistance by 4.1% in the straights and 28.6% in the bends, which is equivalent to 0.4% and 2.9% of the 10% contribution of tyre rolling resistance. Similarly, Wilson (2004) states that scrubbing can increase the tyre rolling resistance by 10-50%, which is equivalent to 1-5% of the 10% contribution of tyre rolling resistance.

4.1.11 Errors and Improvements

The main source of error is the low frequency of data collection by the SRM system. The SRM only records data every 0.5 seconds, limiting the frequency of the input power for the athlete. In addition, the SRM does not start recording data until one complete revolution has been completed, which in turn will cause a delay at the start of the race. Although a linear interpolation was applied for the first three seconds to account for this error, it cannot be guaranteed that this represents the actual power output of the athlete for the first three seconds. It would be more useful to be able to gather power and data from t=0s and at a higher sampling rate.

As mentioned previously, the time-step size and the initial velocity both affect the stability and accuracy of the mathematical model. The chosen values were those which produced realistic and stable finishing times. Also, the Euler time integration scheme has an inherent error which is related to the timestep. A future recommendation would be to trial more accurate time integration schemes, such as the 4th order Runge-Kutta method, to see if the accuracy of the mathematical model can be improved further.

The pressure and relative humidity data was taken from online weather for the airport closest to the velodrome on which the race was taking place. Climatic conditions are often controlled in velodromes, so although this method of collecting atmospheric data is consistent, it is not as reliable as obtaining real time data. The temperature was taken from SRM data, and it would also be useful to have a similar system that logged pressure and relative humidity with the SRM data for future analysis. In addition, more accurate measurements of rolling and scrubbing resistance for the tyres used would lead to an improved accuracy for the mathematical model.

One of the assumptions of the mathematical model was that the overall distance travelled by the athlete was equal to the race length. However, in reality the athlete is not able to keep to the black line throughout the race, which will cause the cumulative distance travelled to be slightly greater than the race length.

The results shown for the model used a calculated drag area, C_dA, rather than a drag area recorded in the wind tunnel. This was because not all athletes had been involved in wind tunnel testing close to the time of their race, and the drag area has a significant affect on the results; if the athlete adopts a very different position on the day of the race compared to when they were in the wind tunnel, the mathematical model would not be as accurate. All IP events have a standing start, where the athlete adopts a standing position

for approximately three-quarters of the first lap. This would increase the drag area during this time, which has not been included in the model. This is a likely cause of the large difference between predicted and actual lap time for the first lap. An improvement on the drag area calculation would be to use the digitizing method to calculate the frontal area of an athlete during the race for which the SRM data is collected for. This would ensure the most recent and accurate drag area would be calculated for each athlete, which would then be used for the model. In some cases the bike wheels used for racing were not tested in the wind tunnel, and so only available data for similar wheels could be used in the model. It would be beneficial to build up a database of data for different bike frames and wheels so that users of the model can select the type of bike and wheels used by the athlete, which would automatically input the relevant data into the model.

4.1.12 Effect of Changes on Finishing Time

The mathematical model can be used to predict what effect changes to model parameters have on cycling performance. A number of parameters were reduced by 2% and the finishing time calculated and compared to the original predicted finishing time. Table 4.12 shows the effect of these changes on the finishing time for Athlete 10 (female, 3000m IP athlete, original predicted finishing time 213.306s), categorised into athlete, bike, and environment or track parameters. Note that the seat height changes the position of the centre of mass but not the drag area in the model, but in reality a change in seat height would also change the drag area.

Input Parameter		**Decrease by 2%**		
		Predicted Finishing Time (s)	**Difference from Original Finishing Time**	
Athlete	C_dA	212.130	-1.176s	-0.55%
	Seat height	213.306	0.000s	0.00%
	Body mass	213.053	-0.253s	-0.12%
	Athlete height	213.306	0.000s	0.00%
	Body mass and C_dA	211.881	-1.425s	-0.67%
Bike	Gear ratio	213.318	0.012s	0.01%
	Tyre rolling resistance	213.243	-0.063s	-0.03%
	Bearing rolling resistance	213.305	-0.001s	0.00%
	Wheel radius	213.327	0.021s	0.01%
	Frame weight	213.274	-0.032s	-0.02%
	Wheel weight	213.296	-0.010s	0.00%
Environment/Track	Air density	212.092	-1.214s	-0.57%
	Temperature	213.416	0.110s	0.05%
	Pressure	212.106	-1.200s	-0.57%
	Relative humidity	213.320	0.014s	0.01%
	Banking angle	212.291	-1.015s	-0.48%
	Grade angle*	213.262	-0.044s	-0.02%

Table 4.12: Effect of changes in model parameters on cycling performance
* The grade angle was changed to -0.006 for half of a straight section of the track and 0.006 for the other half of a straight section to represent a 'dip' in the straight sections of the track, which is what may actually be experienced by athletes [Palmer, 2009]. This only affected the predicted finishing time by 0.044s, so it is therefore acceptable to assume a grade angle of zero throughout the track.

The results in Table 4.12 show that a change in drag area, C_dA, and body mass together had the most significant effect on cycling performance, reducing the finishing time by 0.67%. The reduction in finishing time from combining these changes was similar to, but slightly greater than the reduction seen from making these changes individually. Therefore it should not be assumed that the gains or losses from multiple changes in position are a summation of the individual gains or losses, which would be in agreement with results published by Martin et al. [2006]. Out of all individual changes, air density, drag area, and banking angle had significant affects on the predicted finishing time, with reductions in finishing time of 0.57%, 0.55% and 0.48% respectively. However, it should be noted that a 2% reduction in air density is a significant change compared to a 2% reduction in tyre or bearing rolling resistance. Table 4.12 also shows that changes made to the athlete and environment/track parameters have a greater effect on cycling performance than changes to the bike and components, though of course changes to the environment and track will affect all riders in a given race. This highlights the importance of optimising athlete position in order to maximise cycling velocity and performance.

A comparison between a decrease in temperature, pressure and relative humidity shows that changes in temperature have the greatest influence on the air density, with a 1°C decrease in temperature causing the air density to rise by 0.005kgm^{-3}, and therefore increasing the finishing time by 0.248s.

- Decrease in temperature by 1°C = rise in air density by 0.005kgm^{-3}
- Decrease in pressure by 1kPa = reduction in air density by 0.001kgm^{-3}
- Decrease in relative humidity by 1% = rise in air density by 0.001kgm^{-3}
- Decrease in temperature by 1°C and increase in pressure by 1kPa = rise in air density by 0.006kgm^{-3}

Di Prampero et al. [1979] and Atkinson et al. [2003] state that a change in temperature by 3°C is equivalent to a change in drag of 1%. When the mathematical model was used to simulate both an increase and decrease in temperature and drag area by 3°C and 1% respectively (Table 4.13) the results suggested that a change in temperature by 3 $^\circ$ C had a slightly greater effect than a change in drag area by 1%.

Change	Predicted Finishing Time (s)	Difference from Original Finishing Time (s)
Increase temperature by 3 $^\circ$ C	212.645	-0.661
Decrease temperature by 3 $^\circ$ C	213.981	0.675
Increase C_dA by 1%	213.915	0.609
Decrease C_dA by 1%	212.705	-0.601

Table 4.13: Effect of temperature and drag on cycling performance

4.1.13 Conclusion

The ability to simulate changes to different parameters both individually and together using the mathematical model is a useful tool for both athletes and coaches to help analyse the effect of these changes on performance, without the need for these changes to actually be made in reality. The model is also useful for predicting the

finishing time for different athletes competing in the same race and conditions; for example a comparison can easily be made between riders racing on the same velodrome on the same day, but who have different drag areas and masses.

In addition to changes made to the athlete, bike, and environment or track, it is possible to modify the power output whilst maintaining all other parameters to simulate different strategies and the effect of pacing strategy on performance.

4.2 Optimal Pacing Strategy

The Individual Pursuit (IP) is a closed-loop event, in which athletes must complete a certain distance in the shortest possible time. The regulation of power output is a clear indication of performance, and pacing profiles can be analysed to determine the optimal strategy which should be used for a particular race. High performance athletes can vary their power output in a number of ways, the choice of which depends on the race distance and the terrain on which the race takes place. According to Abbiss and Laursen [2008] the main types of pacing profiles that have been observed for different forms of exercise in a variety of conditions are negative, all-out, positive, even, parabolic and variable. A description of these models can be found in the literature review and in Abbiss and Laursen [2008].

The mathematical model described above was used to simulate different pacing strategies by generating specific power profiles that related to those pacing strategies described by Abbiss and Laursen [2008]. The data for one of the eleven athletes used for validating the model was used for all other inputs into the model, details of which can be seen in Table 4.14. Each power profile was modified slightly to ensure the overall work done was the same as that produced during the actual race, so that all generated pacing strategies were realistic and comparable. Anaerobic reserves are fixed for a given athlete (and deplete to zero in a good pacing strategy for elite athletes) but whether the aerobic work done increases, decreases, or remains constant for different pacing strategies is not yet clear. Although it may not necessarily be true that athletes can only produce a certain amount of energy regardless of the pacing strategy used (it is possible that athletes could increase their total work done when adopting a specific pacing strategy by increasing the efficiency with which anaerobic capacity is used during the race) the assumption that athletes produce the same work done for all pacing strategies enables fair comparions to be made with the information available. The mathematical model also excluded psychological (motivation) effects, which may increase the total work output of a rider when optimised. A better understanding of athlete fatigue and total work done for different strategies is required before being able to included these changes in the model.

The actual finishing time for the race was 265.023s and the predicted finishing time using the mathematical model with actual SRM power data was 264.887s (-0.136s). The maximum power output was 1044W, reached at 11s into the race, the average power was 466W, and the calculated work done for the entire race was 128.3KJ (work done = sum over all SRM sample of instantaneous power x time interval). An analysis of the power profile for the SRM data suggests that the athlete used an all-out strategy for the first 14s of the race, followed by a variable strategy with a higher power output in the bends compared to the straights. The actual SRM power profile can be seen in Figure 4.11.

According to Abbiss and Laursen [2008] if an athlete's power or velocity drops below their critical fatigue threshold or critical power, then performance will be compromised regardless of whether the athlete increases their power or velocity during other sections of the race in order to make up for lost time.

Athlete Data		**Environmental Data**	
Height (m)	1.85	Temperature (°C)	28
Weight (kg)	75	Pressure (mbar)	1021
C_dA (m^2)	0.195	Relative humidity (%)	60
Race distance (m)	4000		
Track Data		**Frame and Wheel Data (each wheel)**	
Lap distance (m)	250	Power coefficient α	0.2118
Grade angle (rad)	0	Power coefficient β	-0.7388
Banking angle straights (rad)	0.22	Power coefficient γ	0
Banking angle bends (rad)	0.733	Crr tyre	0.001
Radius of curvature straights (m)	$1x10^{21}$	Crr bearing	0.001
Radius of curvature bends (m)	26.101	Wheel radius (m)	0.3315
		Front wheel mass (kg)	1.145
		Rear wheel mass (kg)	1.255
		Frame mass (kg)	8

Table 4.14: Rider and bike characteristics used for generating pacing strategies

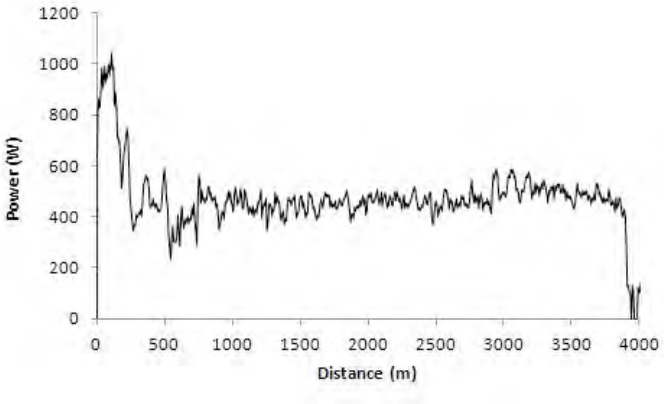

Figure 4.11: Actual SRM power profile

4.2.1 Negative Pacing Strategy

A negative pacing strategy is one in which athletes show a significant increase in the speed and power towards the end of a race (Figure 4.12). It is believed that athletes adopting this strategy use all their anaerobic energy reserves, as they are aware of the remaining distance for completing the race [Abbiss and Laursen, 2008].

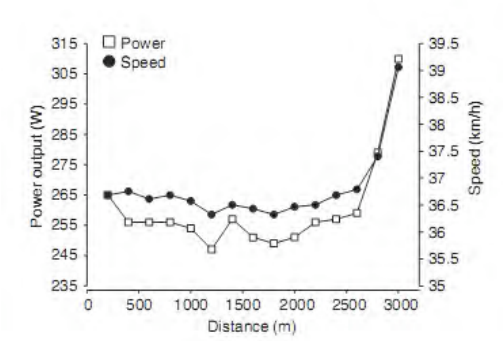

Figure 4.12: Negative Pacing Strategy

A negative strategy was simulated using the mathematical model by increasing the power to 466W instantly and maintaining this power until 3500m, at which point the power was increased in a linear fashion from 466W to 695W at 4000m (P=0.458d-1137). The simulated negative strategy can be seen in Figure 4.13.

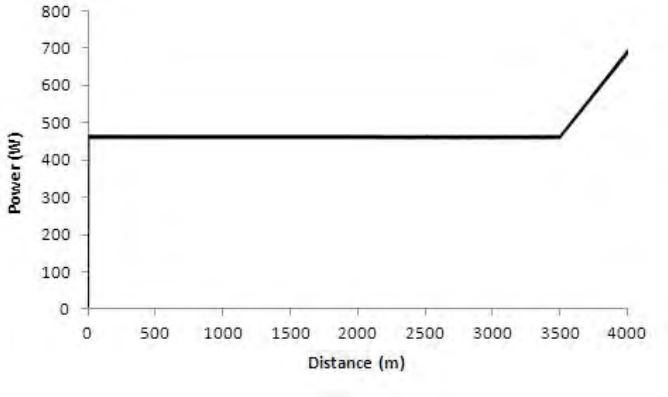

Figure 4.13: Modelling a negative pacing strategy

4.2.2 All-Out Pacing Strategy

For events where the majority of time is spent in the initial acceleration phase it is important for an athlete to maximise their power output during this phase. This is the understanding behind all-out pacing strategies, where a high initial power output is followed by a gradual decline (Figure 4.14).

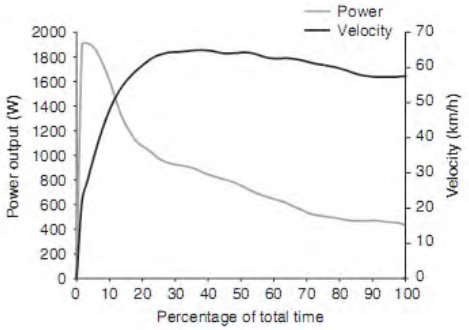

Figure 4.14: All-Out Pacing Strategy

According to Abbiss and Laursen [2008] the initial acceleration phase lasts for approximately 10-20% of the total time to complete the race. However, De Koning et al. [1999] state that time at which the change between an all-out strategy to an even strategy takes place is critical and depends on anaerobic energy kinetics of the athlete. De Koning et al. [1999] suggest that a 12s initial acceleration phase is optimal for the 4000m event. In order to analyse the length of the initial acceleration phase on the predicted finishing time, an initial acceleration phase lasting 10s, 12s, 14s, 16s and 18s with a maximum power of 1044W, followed by a linear decrease in power to a final power that resulted in a total work done of 128.3kJ was simulated using the mathematical model. A parabolic profile was used for the all-out phase, where the maximum power of 1044W was reached in the middle of the all-out phase and the power output at the end of the all-out phase was 600W, as this was similar to the actual SRM power data and would therefore be realistic. The simulated all-out strategy with an 14s initial acceleration phase is shown in Figure 4.15.

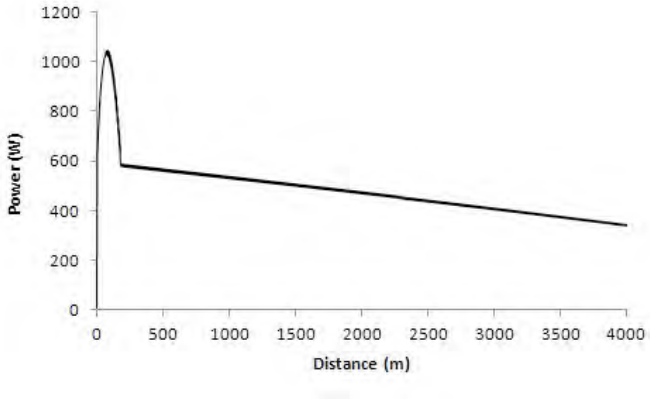

Figure 4.15: Modelling an all-out pacing strategy

An all-out strategy with a parabolic initial acceleration phase of 10s, 12s, 14s, 16s, and 18s followed by an even strategy, where the power output during the even phase was such that the total work done was 128.3KJ, was simulated using the mathematical model to identify the effect of a linear decrease in power output for the remainder of the race. The simulated all-out and even strategy is shown in Figure 4.16.

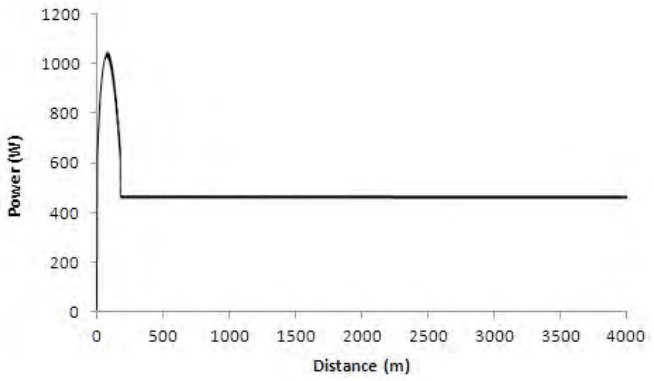

Figure 4.16: Modelling an all-out and even strategy

4.2.3 Positive Pacing Strategy

Abbiss and Laursen [2008] describe positive pacing strategies as those with a reduction in speed and heart rate throughout an event, as shown in Figure 4.17. They suggest positive pacing strategies are often adopted for races where fatigue is likely to kick in, such as an ironman.

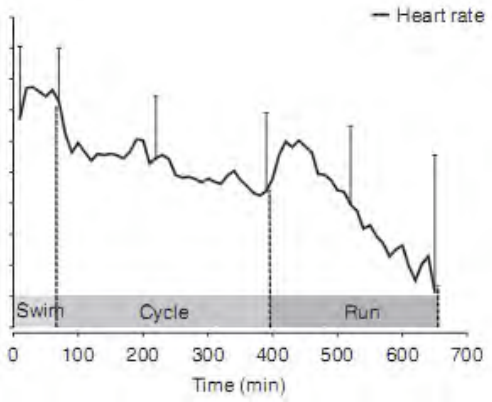

Figure 4.17: Positive Pacing Strategy [Abbiss and Laursen, 2008]

Abbiss and Laursen [2008] suggest a positive pacing strategy is one in which athletes accelerate to 110% of the average power for the first 25% of the race, reduces to 98% of the average power for the next 50% of the race, and reduces to 97% of the average power for the remaining 25% of a race (there is a rounding error of $<$1% which is corrected for by scaling the power to achieve the same work done to within 0.1%. This power profile was simulated for the male athlete using the mathematical model, as shown in Figure 4.18, but the power profile was modified slightly to ensure the total work done was 128.3kJ by setting the power output to 527W (113% of the average power) for the first 1000m, 471W (101% of the average power) for the next 2000m, and 466W (100% of the average power) for the final 1000m.

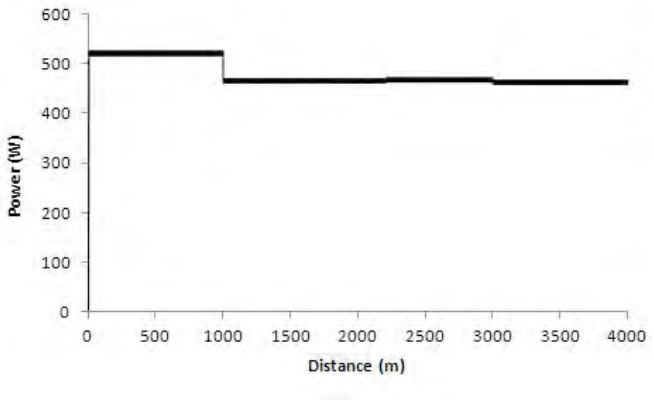

Figure 4.18: Modelling a positive pacing strategy

4.2.4 Even Pacing Strategy

Even pacing strategies are often adopted when the starting strategy has less of an effect on performance, due to the smaller percentage of overall time spent in the initial acceleration phase [Abbiss and Laursen, 2008]. Such strategies show an initial acceleration to an average velocity and power output, which is then maintained for the remainder of the race (Figure 4.19).

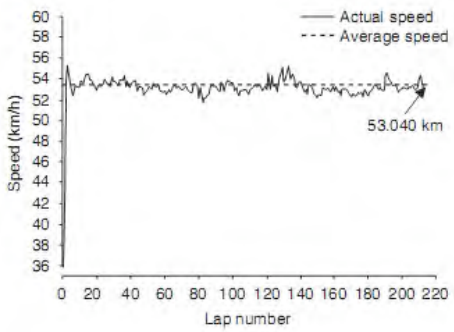

Figure 4.19: Even Pacing Strategy [Abbiss and Laursen, 2008]

In order to maintain the total work done at 128.3KJ, an even strategy with a power output of 482.5W was simulated using the mathematical model. The simulated even strategy is shown in Figure 4.20.

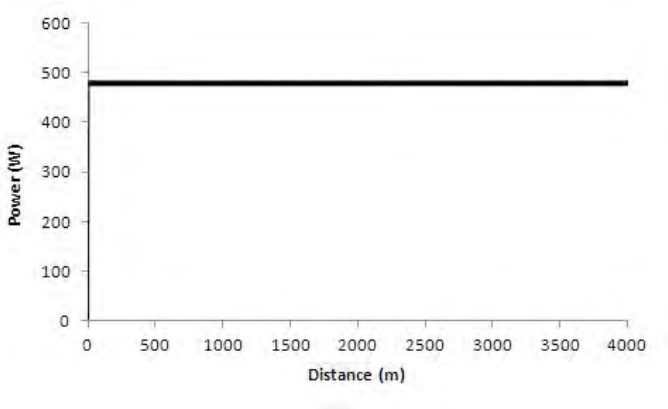

Figure 4.20: Modelling an even pacing strategy

4.2.5 Parabolic Pacing Strategy

Parabolic pacing strategies show a difference in power and velocity between the first and second half of an event, and can be described as U-shaped, J-shaped or reverse J-shaped (Figure 4.21) [Abbiss and Laursen, 2008]. As can be seen by Figure 4.21 the velocity, and hence power output, is dependent on the distance travelled. Parabolic pacing strategies were simulated using the model by creating parabolic equations for power output to represent the curve pattern required whilst ensuring the total work done was 128.3kJ.

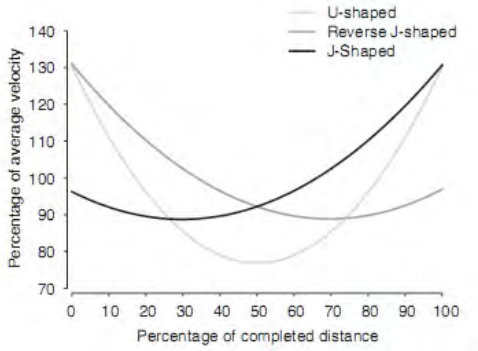

Figure 4.21: Parabolic Pacing Strategies

4.2.5.1 U-Shaped Parabolic Pacing Strategy

The U-shaped strategy defined by Abbiss and Laursen [2008] requires the power output to be increased to 130% of the average power at the start of the race, followed by a decrease in power in a parabolic fashion to 80% of the average power at 50% of the total race distance, followed by an increase in power in a parabolic fashion to 130% of the average power at the end of the race. In order to maintain the total work done at 128.3kJ the power profile simulated for this strategy involved a power output of 631W at the beginning of the race (135.5% of the averager power) and 398W in the middle of the race (85.5% of the average power), as shown Figure 4.22 ($P = 0.00006dt^2 - 0.233d + 631$).

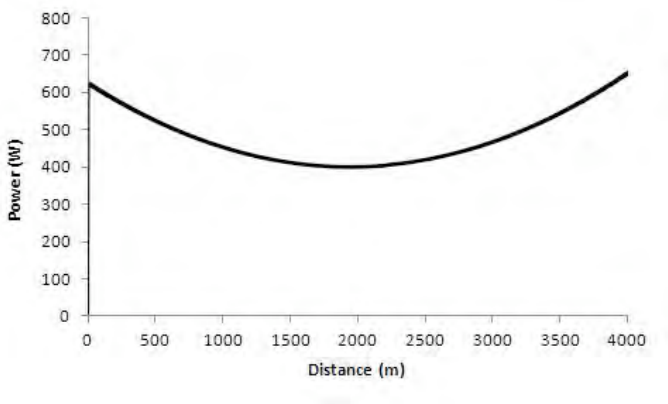

Figure 4.22: Modelling a U-shaped parabolic pacing strategy

4.2.5.2 J-Shaped Parabolic Pacing Strategy

The J-shaped strategy defined byAbbiss and Laursen [2008] requires the power output to be increased to 95% of the average power at the start of the race, followed by a decrease in power in a parabolic fashion to 90% of the average power at 30% of the completed distance, followed by an increase in power in a parabolic fashion to 130% of the average power at the end of the race. Again, in order to maintain the total work done at 128.3kJ the power profile simulated for this strategy involved a power output of 466W at the start of the race (100% of the average power), 443W at 1200m into the race (95% of the average power) and 629W at the end of the race (135% of the average power), as shown in Figure 4.23 ($P = 0.00002d^2 - 0.046d + 466$).

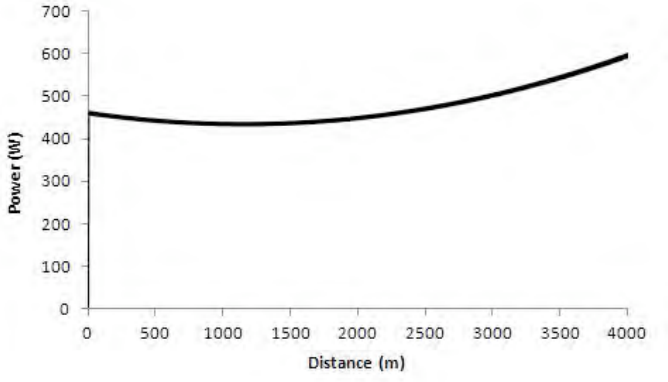

Figure 4.23: Modelling a J-shaped parabolic pacing strategy

4.2.5.3 Reversed J-Shaped Parabolic Pacing Strategy

The reverse J-shaped strategy defined byAbbiss and Laursen [2008] requires the power output to be increased to 130% of the average power at the start of the race, followed by a parabolic decrease in power to 90% of

the average power at 70% of the total race distance, followed by a parabolic increase in power to 100% of the average power at the end of the race. Again, in order to maintain the total work done at 128.3kJ the power profile simulated for this strategy involved a power output of 607W at the start of the race (130.3% of the average power), 421W at 2800m into the race (90.5% of the average power) and 467W at the end of the race (100.3% of the average power), as shown in Figure 4.24 ($P = 0.0003d^2 - 0.14d + 607$).

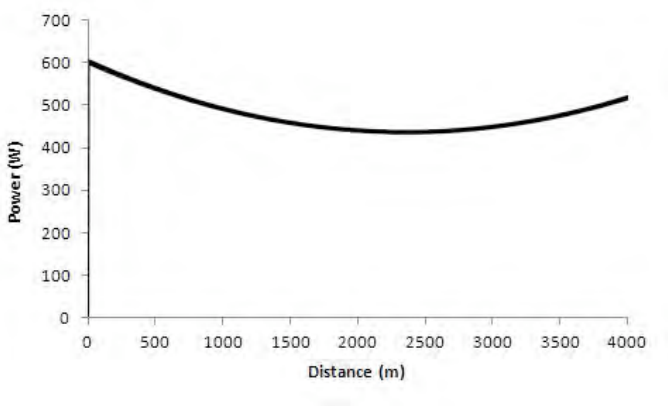

Figure 4.24: Modelling a reverse J-shaped parabolic pacing strategy

4.2.6 Variable Pacing Strategy

According to Abbiss and Laursen [2008] a variable pacing strategy is usually adopted in order to counteract external conditions which have an affect on performance. It is not always possible for an athlete to maintain a constant power output during an event, although it is not yet clear where power should be increased or reduced in order to maximise efficiency. For IP races the effects of external conditions are minimal; it can be assumed that the effects of wind are negligible in controlled conditions and gradient effects cancel out on an oval, symmetrical track where athletes remain on the black line throughout the event. However, IP athletes can vary their power output in the bends compared to the straights.

Therefore, a variable strategy was simulated using the mathematical model by generating a power profile with 415W in the straights and 515W in the bends, and also generating a power profile with 549.5W in the straights and 449.5W in the bends, to compare the difference between a high power in the bends or straights whilst maintaining a total work done of 128.3kJ. A difference in power of 100W between the bends and straights was chosen as this was similar to the actual variation in power recorded by the SRM, and so was assumed to be a realistic power variation. The simulated variable pacing strategy, with a higher power output in the bends, is shown in Figure 4.25.

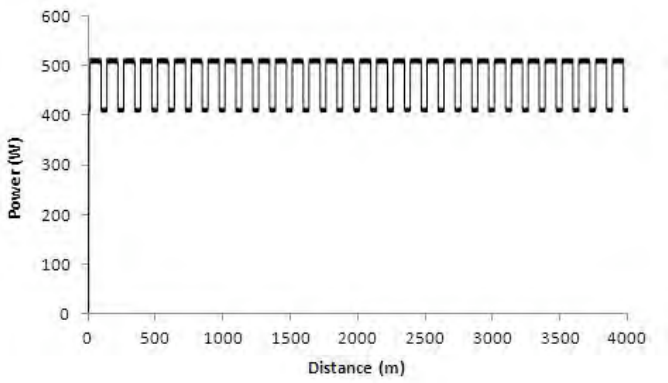

Figure 4.25: Modelling a Variable Pacing Strategy

4.2.7 All Out and Variable Pacing Strategy

The actual SRM data is similar to an all-out and variable strategy, with an initial acceleration phase of 14s and a higher power output in the bends compared to the straights. An all-out strategy for 10s, 12s,14s, 16s and 18s followed by a variable power output with a higher power in the bends and also with a higher power in the straights (again with a 100W difference in power between the bends and straights) was simulated using the mathematical model. A parabolic power profile was used for the all-out phase, the same as described in Section 4.2.2 for the all-out strategy, and it was ensured that the selected variable power output resulted in a total work done of 128.3kJ. The simulated all-out and variable strategy with a 14s initial acceleration phase and a power output of 531.5W in the straights and 431.5W in the bends is shown in Figure 4.26.

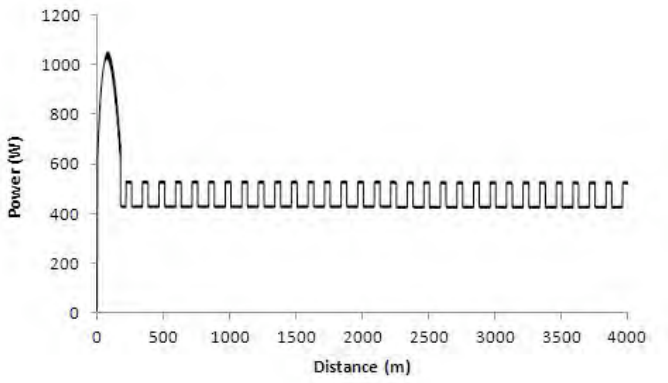

Figure 4.26: All out and variable strategy with a 14s initial acceleration phase and a higher power in the straights

4.2.8 Summary of Predicted Finishing Times

The predicted finishing times for all pacing strategies simulated using the mathematical model are shown in Table 4.15. The results are ranked from fastest finishing time to slowest finishing time. A summary of all the power profiles generated and their corresponding power outputs and equations can be seen in Appendix C.

Strategy	**Predicted Finishing Time (s)**
SRM data	264.887
All-out 12s even	265.336
All-out 12s variable higher bends	265.358
All-out 14s variable higher bends	265.387
All-out 10s variable higher bends	265.406
All-out 10s even	265.421
All-out 14s even	265.460
All-out 12s variable higher straights	265.464
All-out 14s variable higher straights	265.481
All-out 10s variable higher straights	265.516
All-out 16s even	265.582
All-out 16s variable higher bends	265.606
All-out 16s variable higher straights	265.642
All-out 10s linear decline	265.750
All-out 12s linear decline	265.765
All-out 18s variable higher bends	265.814
All-out 18s even	265.830
All-out 14s linear decline	265.844
All-out 18s variable higher straights	265.858
All-out 16s linear decline	266.192
All-out 18s linear decline	266.379
Reverse J-Shaped	266.697
Positive	267.731
Variable higher straights	268.037
Even	268.889
Variable higher bends	269.807
Negative	270.627
J-shaped	270.767
U-shaped	271.929

Table 4.15: Predicted finishing time and calculated work done for all pacing strategies modelled

A comparison between the actual SRM data and the simulated all-out strategy for 14s followed by a variable strategy, with a higher power output in the bends, is shown in Figure 4.27.

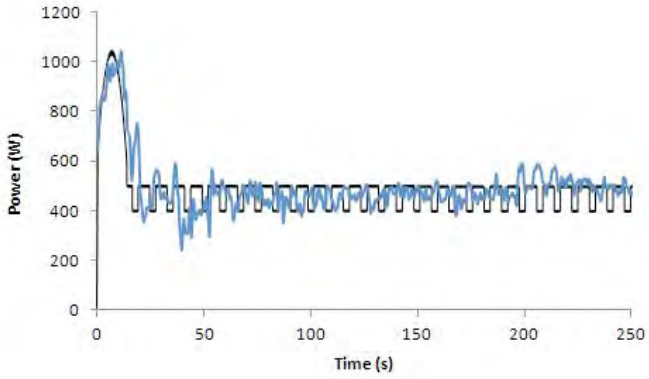

Figure 4.27: Comparison between actual SRM power data and a simulated all-out and variable pacing strategy

The comparison between the actual SRM power data and the simulated all-out and variable strategy shown in Figure 4.27 indicates that there is some variation in the actual power produced by athletes during a race and the theoretical power output for the simulated pacing strategy which, of those tested here, most closely represents the actual SRM power. Although this variation will depend on athlete ability, with elite riders being more likely to reproduce theoretical pacing strategies compared to recreational riders because of greater riding experience and training, it is unlikely that any athlete will be able to reproduce theoretical pacing strategies exactly. This should be kept in mind when analysing different pacing strategies, because it may be possible that one pacing strategy is more easily achieved than another. The actual SRM data will be excluded for the following comparison of pacing strategies for the IP.

Assuming that an athlete has a given quantity of total work to expend, the best strategy is the one which delivers the quickest finishing time for the given work. Of the strategies simulated, this is the all-out and even or all-out and variable strategy (with a higher power output in the bends) with an initial acceleration phase of 12s. The initial acceleration phase is of course a period of time in which the rider is travelling below the average speed for the race, and it is expected that a long acceleration phase will result in a slow finishing time. However, the results show that for an all-out and variable or all-out and even strategy with an initial acceleration phase of 10s to 14s resulted in a slower finishing time than a longer acceleration phase. It is possible that a long initial acceleration phase will result in athletes reducing their power output significantly for the rest of the race for the same total work done. On the other hand an initial acceleration phase that is too short ($<$12s) may not provide a large enough speed gain to overcome any losses towards the end of the race. De Koning et al. [1999] state that for short races a high proportion of time is spent in the initial acceleration phase, so any gains made during this time will outweigh any losses towards the end of the race, even if the athlete begins to fatigue. This may be true in very short races ($<$1000m), but the results from this study have shown that for slightly longer races (4000m) the longest initial acceleration phase did not result in the fastest finishing time. It is possible that athletes exceed the mean velocity during this time, and therefore use extra energy to overcome a higher aerodynamic drag, which would result in a lower power output for the remainder of the race. The significance of the initial acceleration phase on finishing time shown in this study is in agreement with De Koning et al. [1999], who found that that the time to constant aerobic power was critical for the 4km event and that small variations in pacing strategy had substantial effects on performance.

The very small difference in finishing time between the all-out and even and all-out and variable (with a higher power output in the bends) strategies with an initial acceleration phase of 12s (only 0.022s difference in finishing time between these two strategies) suggests that either one of these strategies are suitable for a 4000m IP, and that it is the length of the initial acceleration phase that has the greatest influence on finishing time rather than which out of the even or variable strategies are used for the remainder of the race.

De Koning et al. [1999] and van Ingen and Cavanagh [1990] found that for a 4000m race an all-out and even strategy with an initial acceleration phase of 12s resulted in the fastest finishing time, which is in agreement with the present results, even though the models, assumptions, athlete and track data used do differ between the studies; the model used by De Koning et al. [1999] was based on the flow of energy, including expressions for power production and dissipation, used a drag coefficient of 0.202m^2, used a coefficient of rolling resistance of 0.004, and was solved by calculating the rate of change of kinetic energy (Equation 4.33) by using a variable step size second-order predictor, third-order corrector integration algorithm using the Runge-Kutta method.

$$\frac{d(\frac{1}{2}mV^2)}{dt} = P_0(t) - P_{air}(v) - P_{roll}(v) \tag{4.33}$$

As aerodynamic drag is the dominant resistive force in cycling, and the power required is proportional to velocity cubed, it would be expected that for a rider with a fixed stock of energy whose efficiency is not a function of speed or power output, that the strategy that results in the most even speed would result in the fastest finishing time; an even velocity strategy or variable power strategy. Any other strategy would require the athlete to go faster than the mean speed at some point and use extra energy to overcome a higher aerodynamic drag. However, the results from this study have shown that an even power (variable speed) after a 12s initial acceleration phase results in a slightly faster finishing time compared to a variable power strategy with the same amount of time spend in the initial acceleration phase. A comparison of the wheel velocity for these two strategies can be seen in Figure 4.28, which shows there is only a slight difference in wheel velocity between these two strategies, and this may not be a great enough difference to affect the finishing time significantly. Comparing the strategies with an all-out acceleration phase of 12s followed by either an even or variable power, these differ from each other by no more than 0.5s in 265s or less than 0.25% in finishing time. The total energy expended may vary from strategy to strategy by more than this.

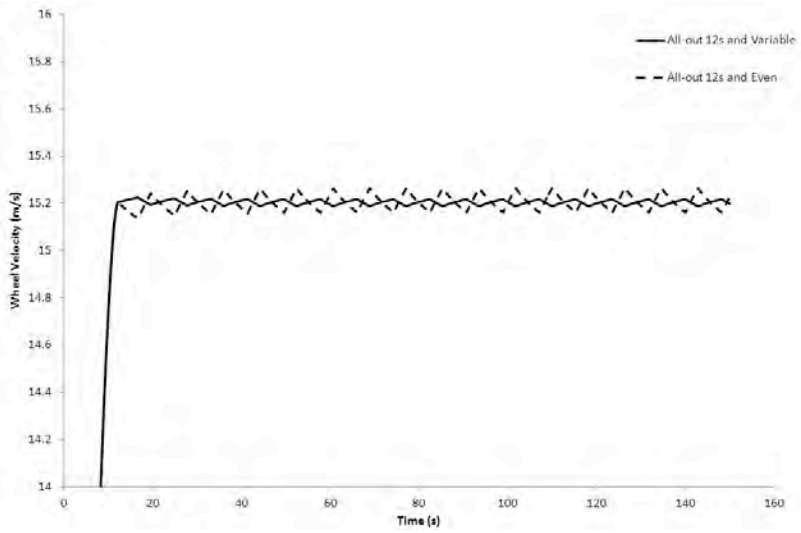

Figure 4.28: Predicted wheel velocity for an all-out and even and all-out and variable pacing strategy with a higher power in the bends (12s initial acceleration phase)

The results in Table 4.15 show that an all-out strategy followed by a linear decline in power resulted in a significantly slower finishing time (+0.4s) compared to an all-out and even or all-out and variable strategy with the same length of time spent in the initial acceleration phase. This suggests that although an initial acceleration phase is important, the power output for the remainder of an IP race is also significant and athlete should maintain a relatively high power output in order to complete the race in the fastest possible time.

The results from this study show that by adopting an all-out strategy IP athletes will gain a significant advantage at the beginning of the race compared to athletes adopting any other strategy, providing their power output does not decline significantly (so that the velocity does not fall below the mean velocity) once the initial acceleration phase is complete. This implies that not only are all-out and even or all-out and variable strategies optimal for the IP in terms of fastest finishing time, but also that these strategies are the ones that are least likely to cause a competitor to catch the rider. For two competing IP athletes both adopting an all-out and even or all-out and variable strategy, the only way for one rider to be caught is if the other rider produces a higher power output in either the initial acceleration phase, the remainder of the race, or throughout the whole event, providing the riders have similar bikes, body masses and drag area.

The results in this study clearly show that an all-out and even or all-out and variable pacing strategy results in a significantly faster finishing time compared to other pacing strategies for IP athletes with a fixed stock of energy whose efficiency is not a function of power output or speed. It would be useful to identify if the same trend in finishing times for different pacing strategies applies to female, IP athletes, as the length of the race is shorter (3000m). It would also be beneficial to generate different scenarios for two different athletes adopting the same pacing strategy, as well as for different combinations of pacing strategies to identify the outcome when two athletes compete against each other. An analysis of the effect of other parameters which were kept constant for this study, such as air density, body position, and body weight, on the predicted finishing time for different pacing strategies would also be useful.

4.2.9 Comparison to Video Analysis of a Team Pursuit

An additional analysis of the effect of the acceleration phase on finishing times can be made by analysing real time video of race data, as shown in Table 4.16 [Phillips, 2011]. Table 4.16 shows that athletes with a faster initial acceleration phase are more likely to have a faster finishing time compared to athletes with a higher average velocity; although the USA had the fastest average speed over the entire race their finishing time was slower than than GBR, who had a faster start and finish split (Table 4.16). These results are in agreement with the results for the optimal pacing strategy for an IP, which showed that the initial acceleration phase has a significant influence on finishing time.

Nation	Av. Speed over 2.875 (kph)	Time over 2.875km (s)	Start Split (s)	Finish Split (s)	Finishing Time (min)
GBR	54.70	3:09.210	8.64	4.40	3:23.642
USA	54.71	3:09.180	8.98	4.50	3:23.965
NZL	54.42	3:10.180	8.76	4.56	3:24.701
AUS	54.51	3:09.870	9.10	4.72	3:25.253

Table 4.16: Video Analysis of Race Data

4.3 Analysis of Team Pursuit Data

Using actual SRM data for a Team Pursuit it is possible to determine the reduction in drag area and power output for drafting cyclists compared to lead cyclists. Power and velocity data for both men and women competing in two World Championship TP events was collected (4 elite male athletes and 3 elite female athletes competing in 2 separate TP events on 2 different tracks) details of which can be seen in Tables 4.17 and 4.18. All athletes maintained a drafting distance that was as close as possible to the rider in front, but the actual distance was not measured. All athletes were elite, TP track cyclists, and so their drafting ability was assumed to be of the highest standard; elite athletes are better at maintaining a close distance from the rider in front when drafting, and also at riding directly behind without deviating from the line of the TP.

	Rider	Weight (kg)	Height (m)	BSA (m^2)*	Bike	Changeover every
Male Athletes 4000m	1	80	1.90	0.90	Avanti	Lap or half lap
	2	75	1.73	0.88	Zen	Lap
	3	74	1.80	0.88	Zen	Lap
	4	78	1.85	0.90	Zen	Lap
Female Athletes 3000m	1	64	1.77	0.86	Zen	Lap
	2	55	1.68	0.84	Zen	Lap
	3	62	1.71	0.85	Zen	Lap

Table 4.17: Details of the riders used for analysis of TP data
*BSA is the Body Surface Area, calculated using using $BSA = 0.0293M^{0.425}H^{0.725} + 0.604$ [Bassett Jr et al., 1999], where M is the weight (kg) and H is the height (m).

	Track 1	**Track 2**
Grade angle ($^\circ$)	0	0
Banking angle bends ($^\circ$)	43	42
Banking angle straights ($^\circ$)	12.6	12.6
Radius of curvature bends (m)	26.101	26.101
Radius of curvature straights (m)	1x10^{21}	1x10^{21}
Lap length (m)	250	250

Table 4.18: Details of the tracks used for analysis of TP data

Using Equation 4.34 the drag area, C_dA, of each competing cyclist when in the lead position, when drafting in each position during a team pursuit (2nd, 3rd or 4th), and when drafting in general can be calculated via linear regression for a given global coefficient of friction, μ (including rolling resistance and bearing friction) [Martin et al., 2006].

$$P \times E - \frac{\triangle PE}{\triangle t} - \frac{\triangle KE}{\triangle t} - \mu V F_n = \frac{1}{2}\rho C_d A V^3 \tag{4.34}$$

The power, P, and wheel velocity, V, were taken from SRM data recorded during the race, and the averages calculated for drafting and leading sections. The mechanical efficiancy, E, was estimated to be 98%, and the global coefficient of friction taken to be $\mu = 0.0025$ as a typical value for riding on an indoor velodrome track [Martin et al., 2006]. The normal force, F_n, is the force exerted by the tyres on the track surface, which is essentially the weight of the rider and the bike, given by $F_n = m_T\sqrt{g^2 + (\frac{V_{com}^2}{r})^2}$, where m_T is the total mass of the system (kg), g is the acceleration due to gravity (ms^{-2}), V_{com} is the velocity of the centre of mass (ms^{-1}), and r is the radius of curvature of the track (m) [Martin et al., 2006]. The velocity of the centre of mass was calculated by $V_{com} = r - Hsin\delta$, where H is the seat height (assumed to be 1.1m), and δ is the lean angle (rad) calculated as $\delta = tan^{-1}(\frac{V^2}{rg})$. The air density, ρ, was calculated from temperature data recorded by the SRM and pressure and relative humidity data taken from online data for the airport closest to the velodrome on the day of the race [Underground, 2009]. The change in kinetic energy, $\triangle KE$, was calculated by $\triangle KE = \frac{1}{2}m_T(V_f^2 - V_i^2)$, where the subscribts f and i represent the final and initial wheel velocity respectively over the timestep. The change in potential energy was calculated by $\triangle PE = VGm_Tg$, where G is the gradient of the track (rad). However, it can be assumed that for TP athletes not making a changeover that the grade angle, and therefore change in potential energy, is zero.

The difference in drag area and power output when in lead position and when drafting (in each position and when drafting overall) was calculated. Power and drag area data during the initial acceleration phase and during changeovers was excluded because during changeovers both the lead rider and the rider in second position are fully exposed to the wind. However, the selection of data for when in lead position and when drafting, as well as when in the bends and straights, was in equal proportion.

The results for the reduction in power output when drafting in each position and when drafting in general for male and female athletes are shown in Figures 4.29 and 4.30 respectively. The results for the reduction in drag area when drafting in each position and when drafting in general for male and female athletes are shown in Figures 4.31 and 4.32 respectively.

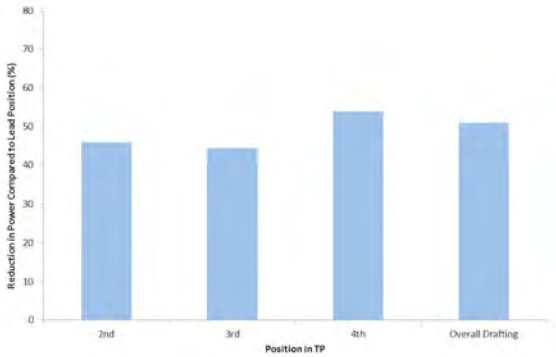

(a) Athlete 1 Race 1

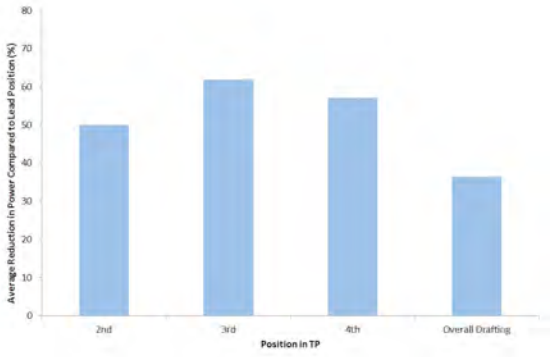

(b) Athlete 2 Race 1

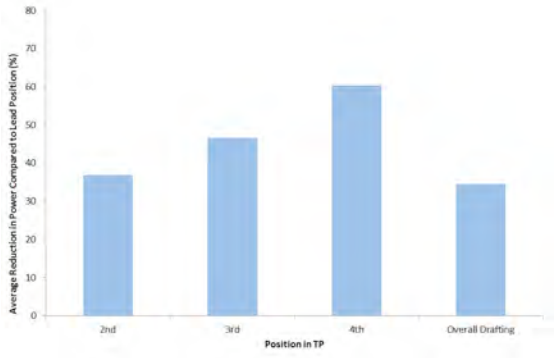

(c) Athlete 3 Race 1

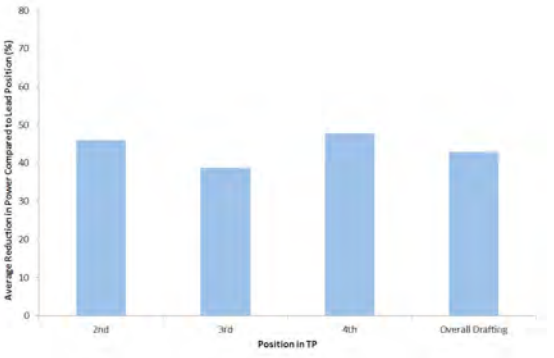

(d) Athlete 4 Race 1

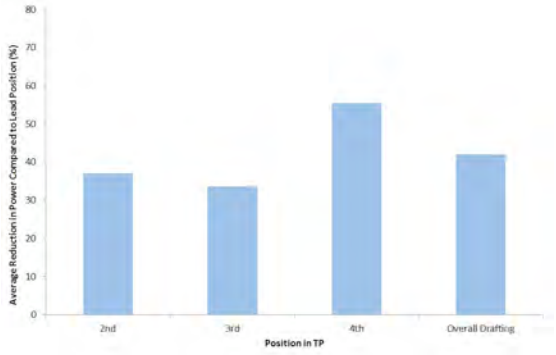

(e) Athlete 1 Race 2

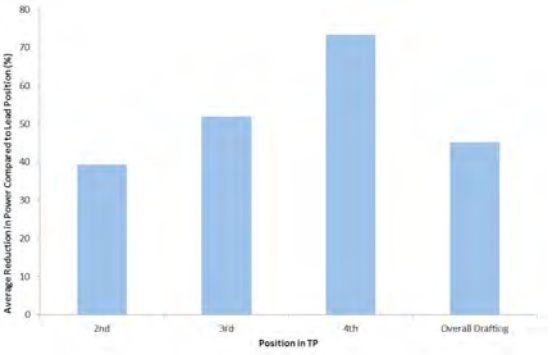

(f) Athlete 2 Race 2

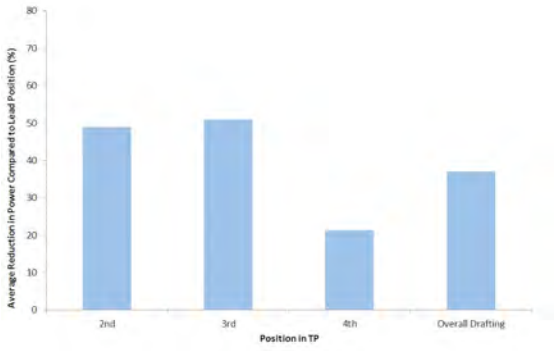

(g) Athlete 3 Race 2

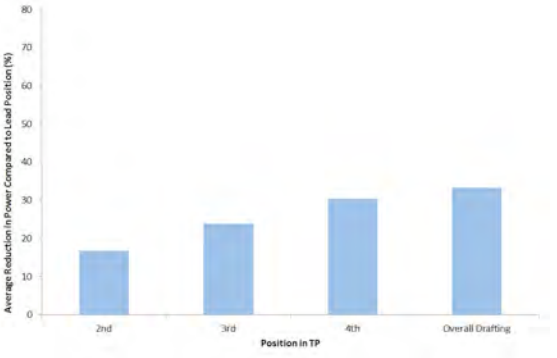

(h) Athlete 4 Race 2

Figure 4.29: Reduction in power output when drafting for male athletes

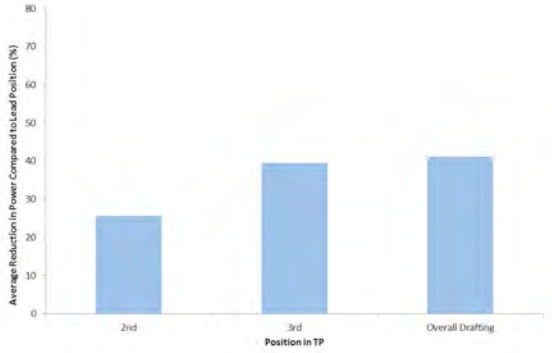

(a) Athlete 1 Race 1

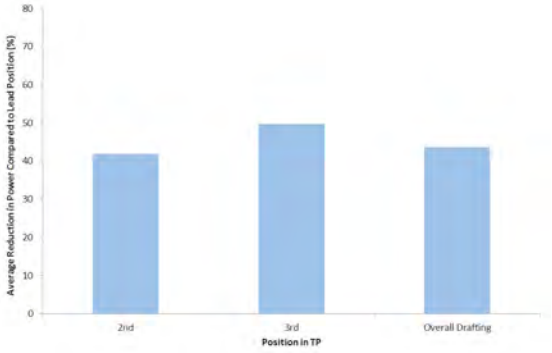

(b) Athlete 2 Race 1

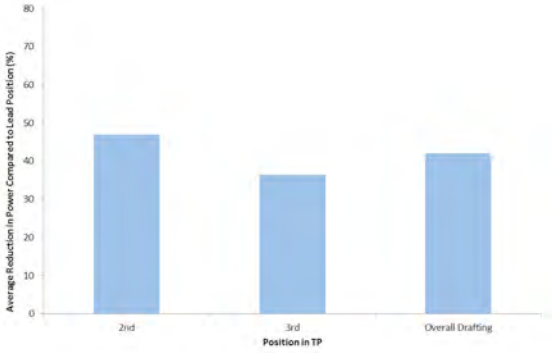

(c) Athlete 3 Race 1

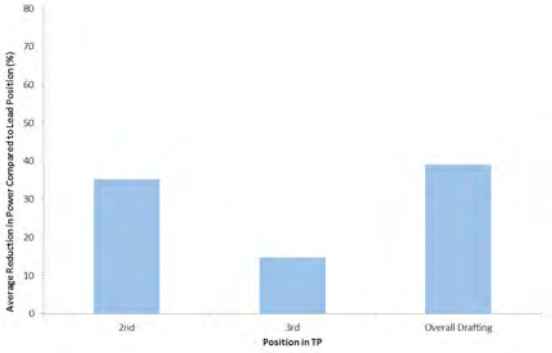

(d) Athlete 1 Race 2

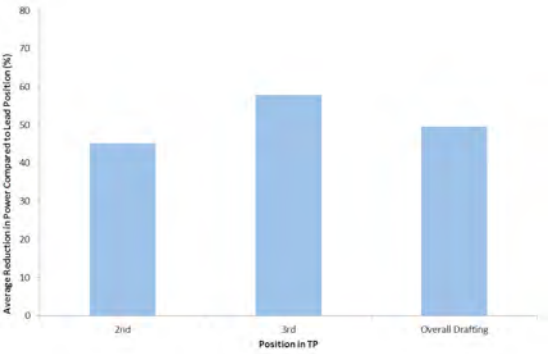

(e) Athlete 2 Race 2

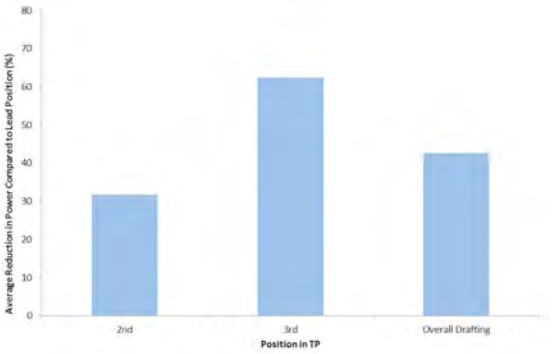

(f) Athlete 3 Race 2

Figure 4.30: Reduction in power output when drafting for female athletes

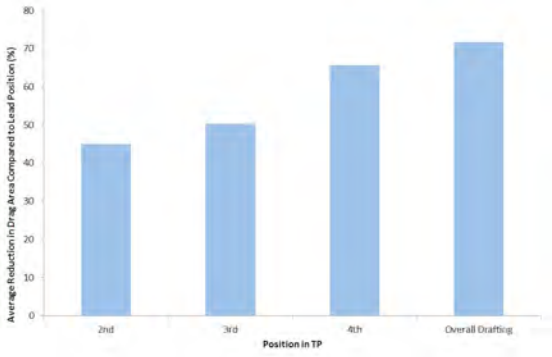

(a) Athlete 1 Race 1

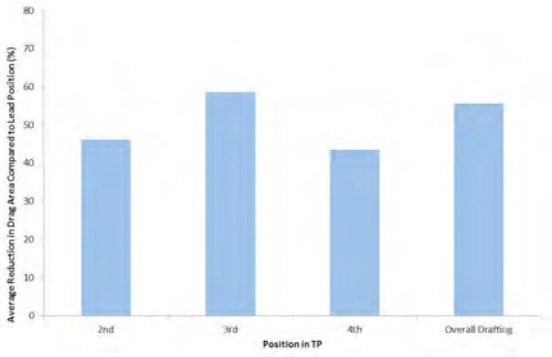

(b) Athlete 2 Race 1

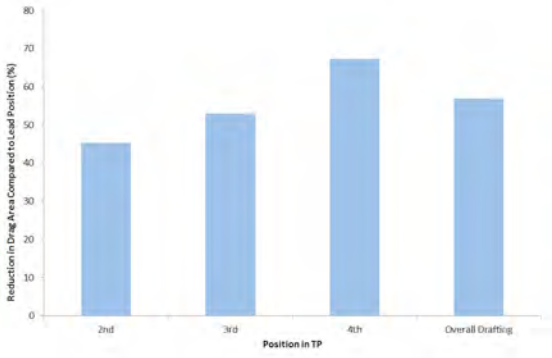

(c) Athlete 3 Race 1

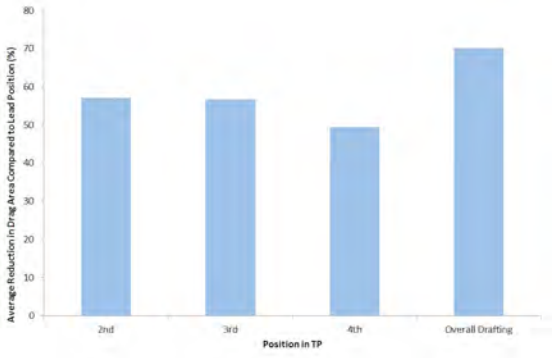

(d) Athlete 4 Race 1

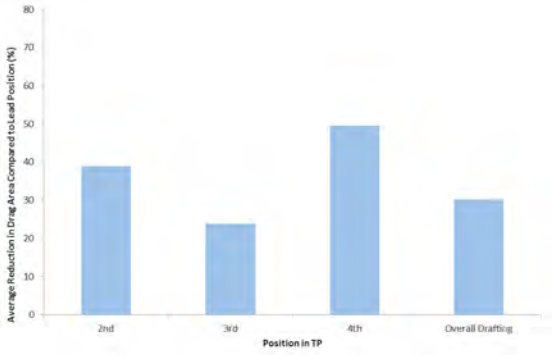

(e) Athlete 1 Race 2

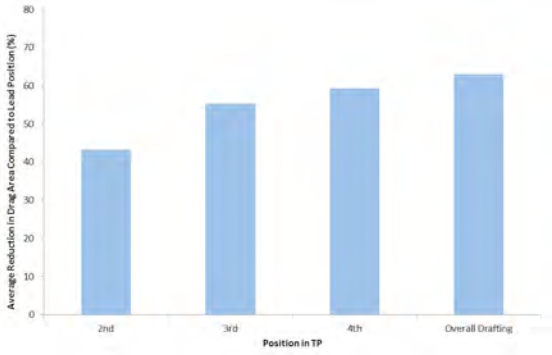

(f) Athlete 2 Race 2

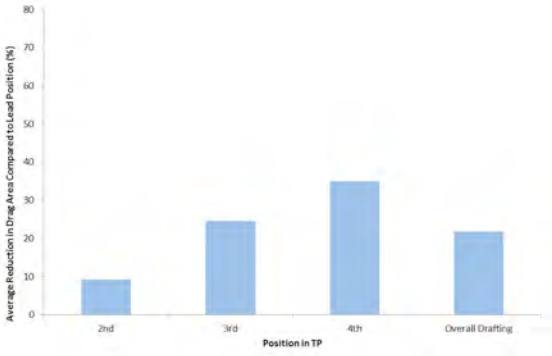

(g) Athlete 3 Race 2

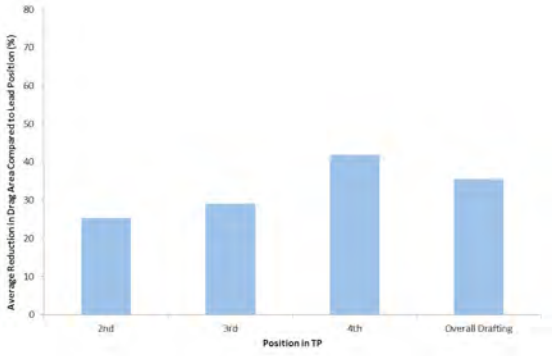

(h) Athlete 4 Race 2

Figure 4.31: Reduction in drag area when drafting for male athletes

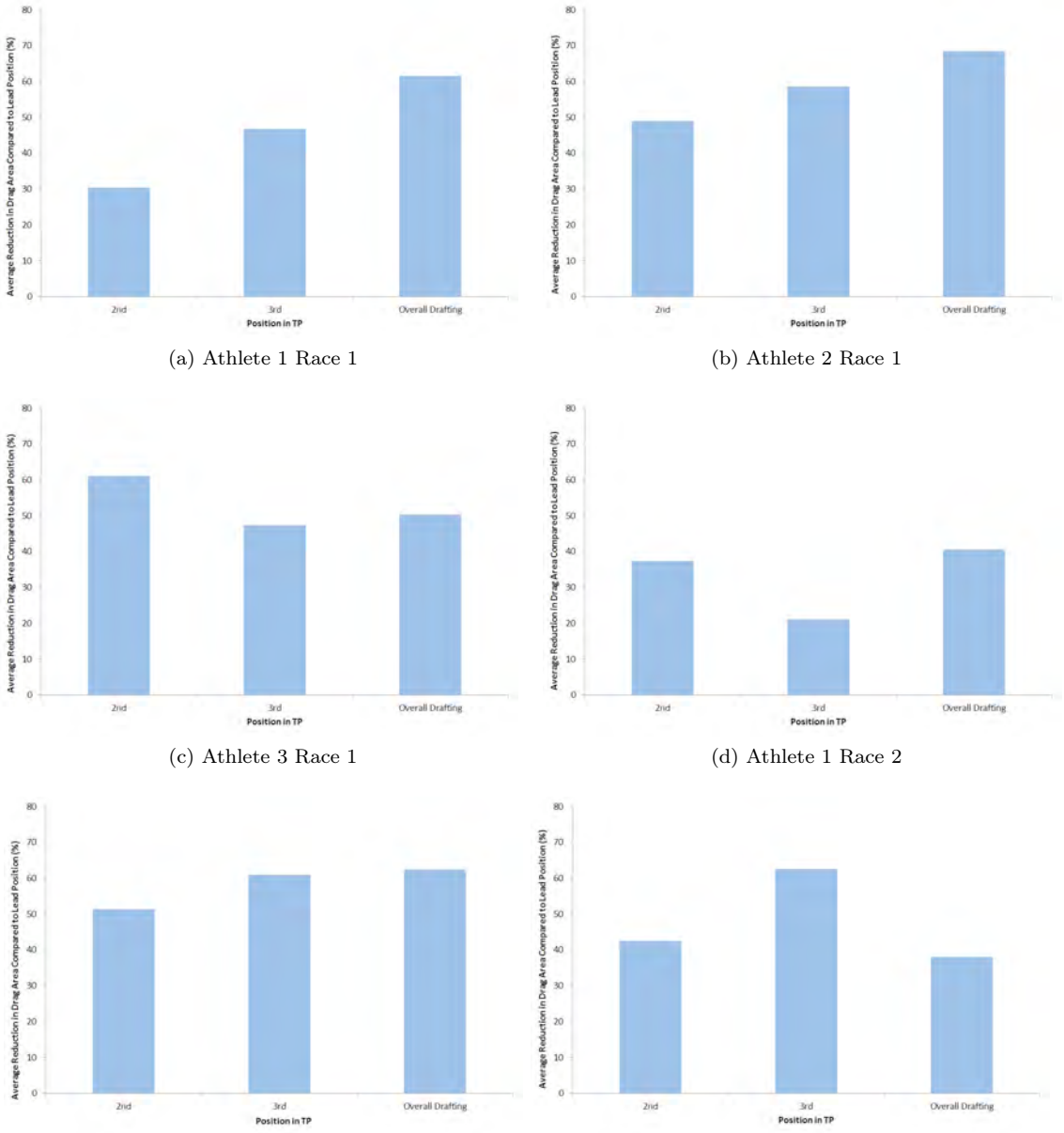

(a) Athlete 1 Race 1

(b) Athlete 2 Race 1

(c) Athlete 3 Race 1

(d) Athlete 1 Race 2

(e) Athlete 2 Race 2

(f) Athlete 3 Race 2

Figure 4.32: Reduction in drag area when drafting for female athletes

These results show that on average, the percentage reduction in both power and drag area for male and female TP riders increases with increasing distance from the lead rider, but not for every rider. The average percentage reduction in both power and drag area for male and female riders in each position and when drafting in general is shown in Table 4.19. These results are slightly higher than results published in the literature, which states that the reduction in drag for drafting riders directly behind the lead rider is 42% to

48% [Lukes et al., 2005, Edwards and Byrnes, 2007, Zdravkovich et al., 1996, Olds, 1998] and the reduction in power when in 2nd, 3rd and 4th position is 29.2%, 35.9% and 36% respectively [Broker et al., 1999]. The discrepancy between these values could be due to the difference in the overall number of drafting riders, differences in body size and shape of riders within a team, difference in distance between riders, or the difference in the drafting ability of riders.

	Male riders				**Female riders**		
	2nd	**3rd**	**4th**	**Overall**	**2nd**	**3rd**	**Overall**
Power	40%	44%	50%	40%	38%	43%	43%
Drag Area	39%	44%	51%	51%	45%	50%	54%

Table 4.19: Average percentage reduction in power and drag area when drafting

The results in Table 4.19 show that the average reduction in drag area is slightly greater than the average reduction in power output for female riders, but not necessarily for male riders. The results in Figures 4.29, 4.30, 4.31 and 4.32 show that on average, riders in 2nd position do not reduce their power output or drag area as much as riders in 3rd or 4th positions. The difference in the actual reduction in drag and power output for individual riders may be due to differences in wheel spacing between riders, differences between the actual line taken by the drafting rider compared to the rider in front, or due to differences in body shape and size of both the leading and drafting riders. Although TP riders aim to follow the wheel in front as closely as possible, athletes are not able to maintain the same distance or follow the line of the wheel in front exactly while drafting continuously. Some riders are better at drafting than other riders, which may explain the greater reductions in power and drag area of some riders compared to others. Edwards and Byrnes [2007] states that interindividual variability is more dependent on the rider's drafting ability at positioning themselves in the wake of the lead rider rather than the aerodynamic or anthropometric characteristics of the drafter.

On average, the overall reduction in power and drag area for male and female athletes while drafting in general was greater than the reduction in power and drag area experienced by individual riders in 2nd position, but not necessarily greater than riders in 3rd or 4th position. These results show the wide variation in power output and drag area of riders in different positions in a team pursuit, highlighting the importance of analysing each position individually rather than looking at the overall power output and drag area when drafting in general.

According to Edwards and Byrnes [2007] the drag area of the lead rider affects the magnitude of the drafting effect, because much of the drafting effect is attributable to the projected frontal area of both riders. In order to determine whether the size of the leading and drafting riders has an influence on the percentage reduction in drag area or power output, the reduction in drag area and power for a small rider drafting a larger leader and for a large rider drafting a smaller leader was compared using the same data as described above. Large and small riders were determined from weight, height and body surface area measurements, as shown in Table 4.20, where the body surface area was calculated using $BSA = 0.0293M^{0.425}H^{0.725} + 0.604$ [Bassett Jr et al., 1999], where M is the weight (kg) and H is the height (m).

	Male Athletes			Female Athletes		
	Height (m)	**Weight (kg)**	**BSA (m^2)**	**Height (m)**	**Weight (kg)**	**BSA (m^2)**
Smaller Rider	1.73	75	0.88	1.68	55	0.84
Larger Rider	1.90	80	0.90	1.77	64	0.86

Table 4.20: Weight, height and body surface area measurements for small and large riders in a TP

The reduction in power output and drag area of the small drafting riders (in 2nd position) behind larger lead riders was compared to the power output and drag area of the smaller rider in lead position, and the reduction in power output and drag area of the large drafting riders behind small lead riders was compared to the power output and drag area of the larger rider when in lead position. These results are shown in Figures 4.33 and 4.34.

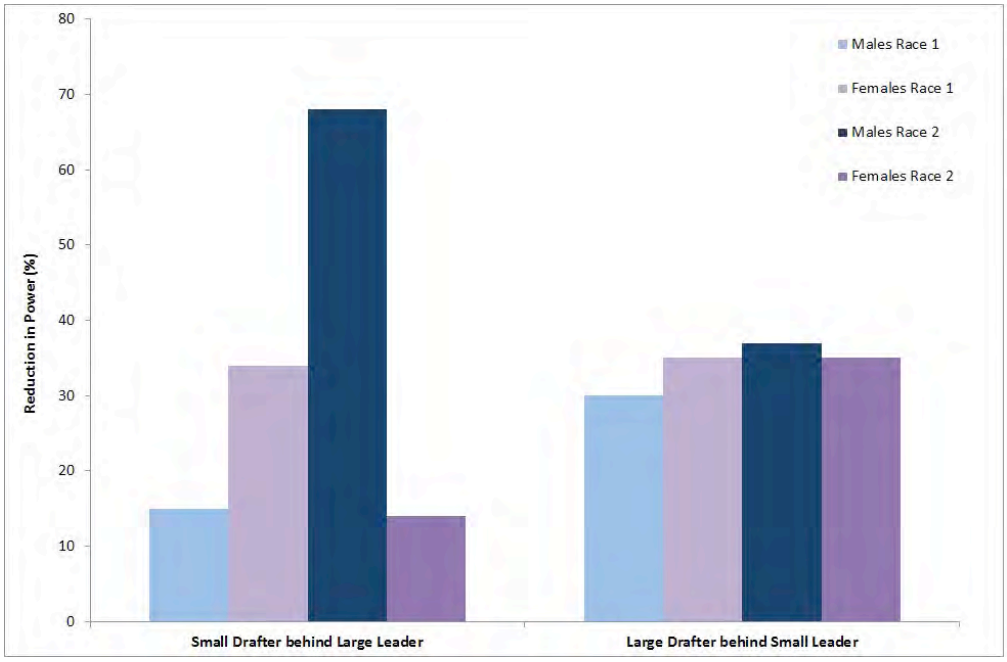

Figure 4.33: Reduction in power for small and large drafting cyclists compared to when in lead position

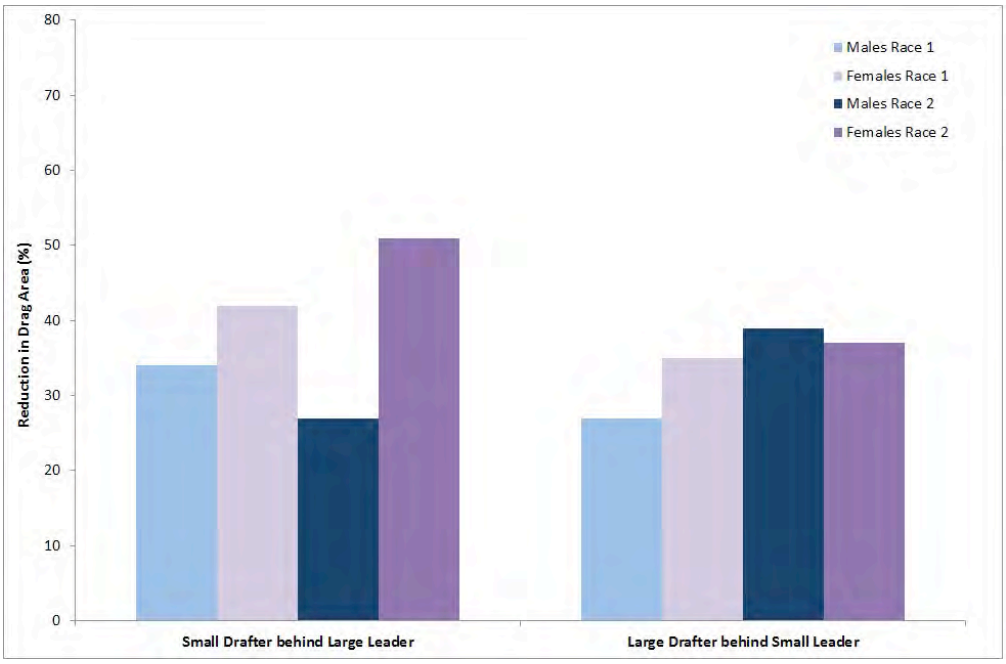

Figure 4.34: Reduction in drag area for small and large drafting cyclists compared to when in lead position

It may be expected that a greater variation in power or drag area would be seen for larger drafters behind smaller leaders due to the reduction in drag area or power being more sensitive to the lateral position of the drafting rider. However, Figure 4.33 shows that larger drafting riders appear to obtain a similar reduction in power, in the region of 30-37%, when drafting a smaller rider, where as the reduction in power for smaller drafters behind large leaders seems to vary significantly, from 14% for some athletes to 68% for others. These results also show that for all but one result there was a slightly greater reduction in power for larger drafting riders compared to smaller drafting riders. It is possible that larger riders produce a greater power output compared to smaller riders in general, and once the drafter has experienced a reduction in drag area they may increase their speed rather than rest and reduce their power. This would result in a greater reduction in power for a large rider when drafting compared to leading, where as smaller riders may still need to maintain a relatively high power output when drafting a large leader so they are not dropped during a TP. It would be useful to collect more data for TP riders of comparable size and also of different sizes in order to validate this hypothesis for future work.

Figure 4.34 shows that the reduction in drag area when drafting compared to leading was greater for most of the smaller riders behind a large leader compared to larger riders behind a small leader. It is possible the frontal area of smaller riders is lower compared to larger riders; smaller riders may be completely out of the wind when drafting a large rider, where as larger drafting riders may actually increase the projected frontal area of that of a smaller rider. This is in agreement with Edwards and Byrnes [2007] who stated that much of the drafting effect is attributable to the projected frontal area of both riders, which is strongly affected by the drag area of the lead rider.

4.4 Summary

In this chapter a mathematical model for the IP race on an indoor velodrome has been described. This model considers the leaning in the bends, and uses actual SRM power data to predict the velocity profile of the athlete and the finishing time for specific conditions. It has been shown that the model is accurate to approximately 0.85% of the actual finishing time, with the greatest error occurring at the start of the race. This could be due to the increase in drag area during the initial acceleration phase, as the IP event is a standing start race, or due to the limited frequency of data collected by the SRM, which also does not start recording data until one complete revolution.

The model has been used to analyse the effect of reducing a number of input parameters by 2% to identify those factors which have the most influence on cycling performance. It was found that changes made to the athlete and environment have a greater influence on the finishing time than changes to the bike, with changes made to the drag area and air density having the greatest individual impact on the finishing time. The model was also used to simulate different pacing strategies to identify the optimal pacing strategy for IP athletes. The power profiles generated for a comparison of pacing strategies ensured the total work done and the position of the athlete was the same as for the actual SRM data because the pattern of energy expenditure during different strategies cannot be modelled using a demand side mathematical model, and because more information is needed before the effects of fatigue and motivation on drag and power output can be modelled accurately. It would be useful for future work to identify an athlete's ability to hold particular power strategies and their aerodynamics position when they are fatigued. It was found that all-out and even or all-out and variable strategy produced faster finishing times for an athlete with a fixed stock of energy whose efficiency is not a function of power output or speed, and that the length of the initial acceleration phase does have an effect the finishing time, although it was not necessarily clear exactly which of these types of strategies was best. A comparison of the actual SRM power profile and the theoretical power profile for the same strategy (all-out and variable) showed a slight difference between the power profiles and finishing times. This was because athletes are never able to reproduce theoretical pacing strategies on the track exactly, but their power output varies more than the idealised theoretical strategies. However, mathematical models are still useful for identifying which pacing strategy athletes should be using without the need for athletes to actually trial these strategies on the track, within the limitations set by the lack of a model of anaerobic power.

An analysis of Team Pursuit data has shown that on average, reductions in both power and drag area increase with distance from the lead rider compared to when in lead position, and that larger drafting riders tend to experience a greater reduction in power when drafting a smaller rider compared to smaller drafters behind a large leader, probably due to the higher power output of larger riders in general. However, it was shown that smaller drafting riders tend to experience a greater reduction in drag area when drafting a larger rider compared to larger drafters behind a small leader, mainly due to the fact that smaller riders are more likely to be completely shielded from the wind when behind a larger rider.

Chapter 5

Wind Tunnel and Testing Procedure

Introduction

This chapter will give a brief summary of the properties of existing wind tunnels and cycle rigs currently used for testing the aerodynamics of cycling, followed by a more detailed description of the wind tunnel and cycle rig at the University of Canterbury that was used for a number experiments to analyse the effect of athlete position on aerodynamic drag. Although in real life track cycling the speed of a cyclist does vary during a race, causing the drag generation to vary, all wind tunnel tests at the University of Canterbury were carried out at at one speed. This was because this thesis was primarily focused around the Individual Pursuit, for which once the initial acceleration phase has been completed the athletes tend to cycle at a fairly constant speed. This chaper will also include a calculation of the boundary layer thickness on the floor of the cycle rig at different distances from the wind tunnel exit.

5.1 Description of Wind Tunnels

5.1.1 Existing Wind Tunnels used for Bike Testing

Wind tunnel testing began in 1870, when Francis Wenham built the first wind tunnel in England to measure the drag and lift forces of various shapes. Wind tunnel designs have become more sophisticated and useful since then due to the growth in the aviation industry, and are now common methods of analysing the aerodynamics for the aerospace industry as well as for a number of sports under controlled laboratory conditions. Although nowadays Computational Fluid Dynamics (CFD) can also be used to analyse airflow and drag, wind tunnel tests are the most common method for obtaining drag data for cycling because although pedalling may introduce noise in the system, the experimental set up is the most realistic to racing conditions. Although Candau et al. [1999] argue that athletes are not able to adopt the same position in a wind tunnel as they would in a race situation, there are many ways in which athlete position can be monitored in a wind tunnel and elite athletes have been shown to reproduce drag values to within a few grams difference when returning to nominally the same position. Experimental testing remains vital for fluid dynamics due to the uncertainties associated with CFD. The complexity of a bike and rider system makes it nearly impossible for

an accurate geometry of the system to be created for CFD studies without the use of a laser scanner. Laser scanners are expensive, and in order to reproduce an accurate bike and rider model the scanning process is very time consuming. The choice of CFD model for simulations also affects the results, with some models failing to provide a converged solution or suffering from instability at steady state. Many CFD models either consistently under predict or over predict results, so experimental testing is still needed to determine a correction factor for CFD results which allow comparisons to be made.

Wind tunnels are either open-circuit, where the air is taken from and expelled back into to environment, or closed-circuit, where the air is repeatedly recirculated in continuous ducts. Some of the well known facilities used for cycle testing are the San Diego Air and Space Technology Center, the Royal Melbourne Institute of Technology (RMIT) wind tunnel, and the A2 wind tunnel in Charlotte, North Carolina.

The San Diego Air & Space Technology Center (http://www.multisports.com/windtunnel_camp.shtml) has a low speed wind tunnel and bike rig set up to measure the aerodynamic drag of cyclists. The bike platform is raised to eliminate ground drag, and can rotate to measure the effects of yaw. Both the front and rear wheel rotate, and are driven by either the cyclist through pedalling, or by a motor if comparisons between bike frames themselves are required. Drag, power, speed, heart rate, and cadence are measured, and front, rear and birds eye images are taken throughout the testing. The wind tunnel is a closed return flow wind tunnel, 2.4m x 3.7m x 4.6m, with a maximum speed of 435kph. The tunnel is powered by a 6m diameter, 1678kW fan. The same trend in drag readings has been seen for both pedalling and static tests at the San Diego Wind Tunnel [Palmer, 2009, Personal Communication], which suggests that both static and pedalling tests are valid ways to compare the aerodynamic drag of cyclists.

The Royal Melbourne Institute of Technology (RMIT) wind tunnel (http://www.rmit.edu.au) has a test section of 3m x 2m x 9m and also has a customised rig for testing the aerodynamic drag of cyclists. The wind speed can reach a maximum of 140kph, and the bikes are fixed to a wooden platform 1.8m x 0.85m x 0.3m by rear stands. A 6-axis force balance (JR3) on a 100mm diameter strut is used to measure drag, lift, force and their corresponding moments.

The A2 wind tunnel in Charlotte (http://www.a2wt.com/Contact.htm) also has a bicycle rig, where the bike is supported by struts attached to the front and rear wheels. The rig is a raised platform, with a turntable to allow yaw effects up to +/-25 degrees to be considered, and both wheels are able to rotate, either with or without a rider. The accuracy of the system is $\pm 0.5\%$ [Salazar, 2011, Personal Communication], and the drag, power, heart rate, wheel speed and cadence are recorded. There is also a smoke testing facility for flow visualisation.

5.1.2 Wind Tunnel and Cycle Rig at the University of Canterbury

The University of Canterbury has a closed-circuit wind tunnel, 1.25m x 0.91m with a 2.5m long working section and maximum air speed of 55m/s (198kph), and an open-circuit, boundary-layer wind tunnel, 1.52m x 1.52m with a 13.2m long working section and maximum air speed of 14m/s (50kph) with low noise working section. The open-section wind tunnel is powered by a 1.2m diameter 50kW Woods two stage contra-rotating fan unit with pneumatic blade pitch control, and this wind tunnel was used for all tests with athletes and mannequins as the closed-circuit wind tunnel is too small. The open circuit wind tunnel facility is shown in Figure 5.1, and consists of a settling chamber, diffuser, fan, contraction, and the cycle rig fixed at the tunnel

exit. The closed-circuit wind tunnel was only used for the material testing described in Section 7.5.2 and the testing of shoe covers on a leg model described in Section 7.6.

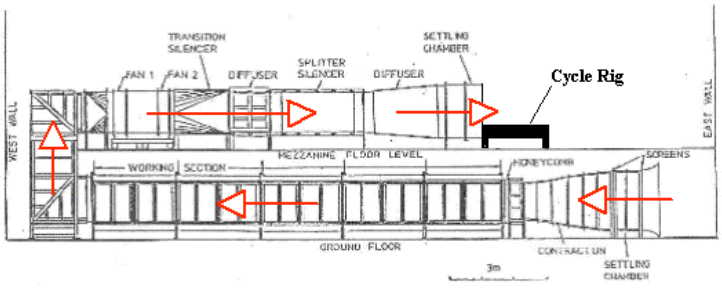

Figure 5.1: Open Circuit Wind Tunnel

The blockage ratio of the open-circuit wind tunnel for cycle testing was calculated using the correction method described by Cooper et al. [1999]. In general, total blockage is a result of (1) solid blockage due velocity increments induced by the displacement effect of the model volume and its separation bubble; (2) wake blockage due to velocity increments induced by the displacement effect of the wake; and (3) incremental forces due to the velocity gradients induced by the wake [Cooper et al., 1999]. As the wake produces no velocity increment in an open wind tunnel, the classical view is that the total blockage for an open wind tunnel only consists of solid blockage [Cooper et al., 1999]. The 3D solid blockage correction for an open section wind tunnel can be calculated using Equation 5.1 [Cooper et al., 1999], where $k_{3s} = -0.032$ and n=2.94 for an open wind tunnel, β is the Mach number correction ≈ 1 for low-speed, boundary layer tunnel studies, B is the tunnel height (m), H is the tunnel width (m), L_m is the model length (m), V is the model volume (m^3), S is the model frontal area (m^2), and C is the tunnel cross sectional area (m^2).

$$\varepsilon_s = \frac{k_{3s}}{\beta^3}\left(\frac{B}{H}+\frac{H}{B}\right)^n\left(\frac{V}{2L_m}\right)^{\frac{1}{2}}\left(\frac{S}{C^{\frac{3}{2}}}\right) \tag{5.1}$$

For an average cyclist in the open circuit wind tunnel at the University of Canterbury, the input values for Equation 5.1 are shown in Table 5.1.

Input	Description	Value*
B	Wind tunnel height (m)	1.52
H	Wind tunnel width (m)	1.52
V	Model volume (m^3)	0.24
L_m	Model length (m)	0.80
S	Model frontal area (m^2)	0.30
C	Wind tunnel cross sectional area (m^2)	2.31

Table 5.1: Inputs for Solid Blockage calculation
*for an average cyclist in the open-section wind tunnel at the University of Canterbury

Using Equation 5.1, the solid blockage for a cyclist in the open section wind tunnel at the University of Canterbury is therefore $\varepsilon_s = -0.013$. Since it is the aerodynamic drag force that is being measured in the open section wind tunnel, the uncorrected drag coefficient, C_{FT}, is determined by $C_{FT} = \frac{F}{\frac{1}{2}\rho V_T^2 A}$, where F is the measured drag force (N), ρ is the air density (kgm^{-3}), V_T is the wind velocity (ms^{-1}), and A is the frontal area of the cyclist (m^2). The actual drag coefficient should be based on the velocity at the position of the cyclist, which is where the solid blockage correction is used to determine the corrected drag coefficient in an open circuit wind tunnel. The uncorrected drag coefficient, C_{FT}, is related to the corrected drag coefficient, C_{FF}, by $\frac{C_{FF}}{C_{FT}} = \left(\frac{V_T}{V_F}\right)^2 = \frac{1}{(1+\varepsilon)^2} = (1-2\varepsilon)$ [Pankhurst and Holder, 1952, p348]. Therefore, the blockage correction for a cyclist in the open section wind tunnel at the University of Canterbury, calculated using the method by Cooper et al. [1999], can be calculated as:

$\frac{C_{FF}}{C_{FT}} = (1-2\varepsilon) = 1.026 = 2.6\%$

The calculated blockage correction is only significant in cases where the actual values of drag coefficient need to be determined, and not for cases where only trends are analysed. In cases where actual drag coefficient values are calculated, these should all be reduced by 2.6% to account for solid blockage correction.

5.1.2.1 Velocity Profile at Tunnel Mouth

The uniformity of the airflow of the open-section wind tunnel was determined at the exit by using a pitot tube to measure the velocity at different locations around the mouth while the wind speed was set at 42kph. Figure 5.2 shows a contour plot of the flow uniformity over the mouth of the wind tunnel, from which it is clear that the flow was slightly faster in the middle of the tunnel exit compared to the outer edges. The velocity of the wind should therefore be taken at the centre of the wind tunnel exit in order to identify the actual wind speed over all objects placed in the boundary layer wind tunnel. An outline of where the athletes lie within this velocity contour plot is shown in Figure 5.3.

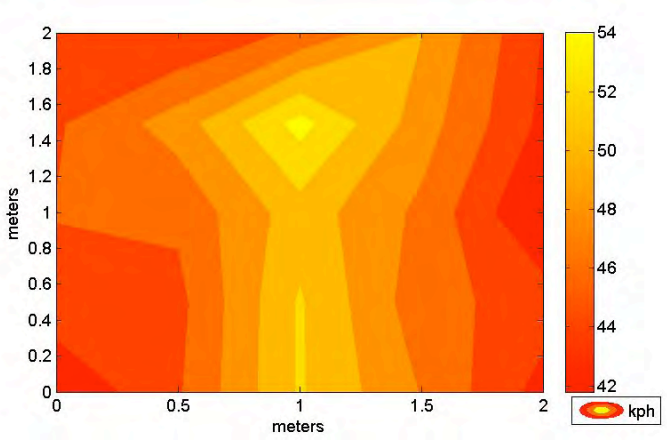

Figure 5.2: Flow Uniformity

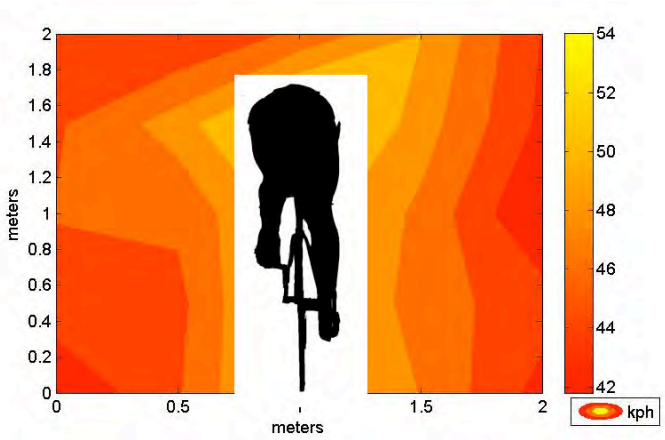

Figure 5.3: Outline of Athlete in the Velocity Contour

The turbulence intensity of the wind tunnel at 42kph was also calculated at the same locations around the mouth of the wind tunnel as the velocity profile using hot wire measurements, and the mean turbulence intensity was found to be 4%.

5.1.2.2 Cycle Platform

Hardware

A platform was built to mount a bike at the exit of the open-circuit wind tunnel to measure the aerodynamic drag of cyclists. The cycle rig consists of a fixed and floating platform, both made from welded, steel RHS. The floating platform is suspended by four, aluminium flexures, 1mm thick, one positioned in each corner of the rig to allow fore-and-aft movement. A single axis, shear beam load cell (50N maximum force, PT Transducers Ltd.) is bolted at the rear centre of the fixed platform to measure the drag as the force from the floating platform is applied. The load cell is aligned with the exit of the tunnel geometrically using a laser level and T-square. A magentic resistance indoor cycle trainer supplies the resistive load to a torque transducer, which measures the torque and angular velocity of a shaft driven by the rear roller so that the power output of the cyclist can be calculated. The rear roller rotates as the cyclist pedals, but the front roller is stationary and only used for stability. Two stands support the rear wheel of the bike on the rear roller. Four springs are located between the fixed and floating platform at the front of the cycle rig to apply a constant compressive force on the load cell to prevent any separation from the contact point, which causes incorrect measurements. A top plate made from MDF is screwed on to the floating platform so that only the two rollers are visible during testing. The cycle rig platform and the key components are shown in Figure 5.4.

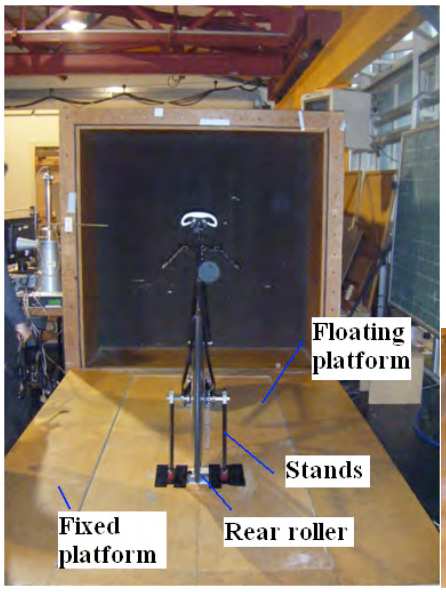

(a) Fixed and Floating Platforms

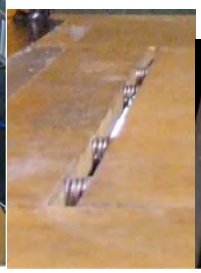

(b) Springs

(c) S-Type Load Cell

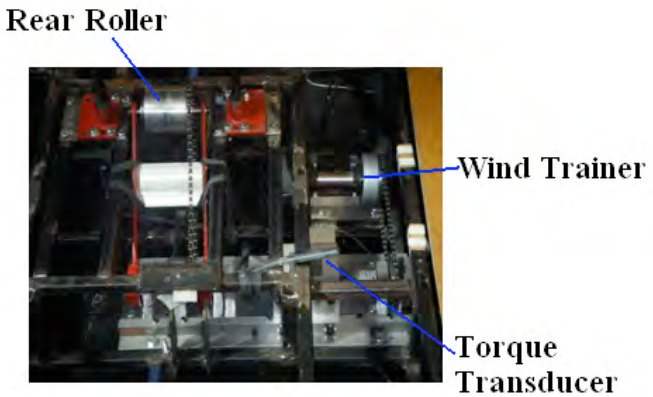

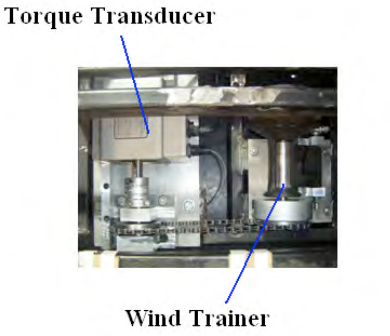

(d) Torque Transducer and Wind Trainer

Figure 5.4: Cycle Rig Platform

The signal from the load cell (mV) is related to the aerodynamic drag on the rider (N) by a calibration constant, which is measured before and after each test. This calibration constant depends on the proportion of the drag force which is resisted by the load cell, which depends on the angle of the rig to the horizontal, the exact shape of the rig, and the alignment of the flexures, frame and cell. Thus deflection of the rig alters the calibration constant. In order to determine the stiffness of the rig, a flexion test was carried out by placing weights ranging from 0kg to 120kg in 20kg increments on the middle of the floating rig. A dial gauge was placed on the side of the rig and then on the middle of the rig to measure the flexion at the side and middle respectively. The deflection results, shown in Figure 5.5, indicate a linear relationship between applied weight

and deflection, and that deflection is greatest in the middle of the rig. The maximum deflection at the side was 1.05mm and in the middle was 1.37mm, both when 120kg was applied.

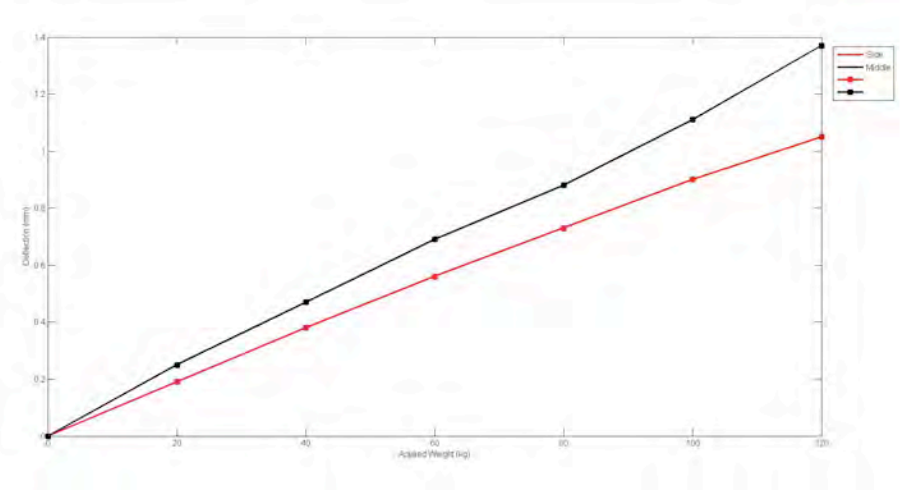

Figure 5.5: Rig Deflection

In order to determine the force needed to move the floating rig, a stiction test was carried out. A dial gauge was used to determine exactly when the floating rig was moving, and a spring balance was used to measure the force required to move the floating rig at this point. This was carried out with no load, as well as when 120kg was placed on the middle of the floating rig. The results showed that 3g was needed to move the floating rig without any weight applied, and 5g was needed to move the floating rig with 120kg placed in the middle.

In early tests, deflection of the mezzanine floor caused high drift and it was necessary for all persons observing the athlete being tested to be seated and as still as possible in order to minimise the drift. However, the floor deflection was reduced by building a stiff, steel frame from the concrete, ground floor up through the mezzanine floor, on which the cycle platform was fixed. This steel frame is shown in Figure 5.6.

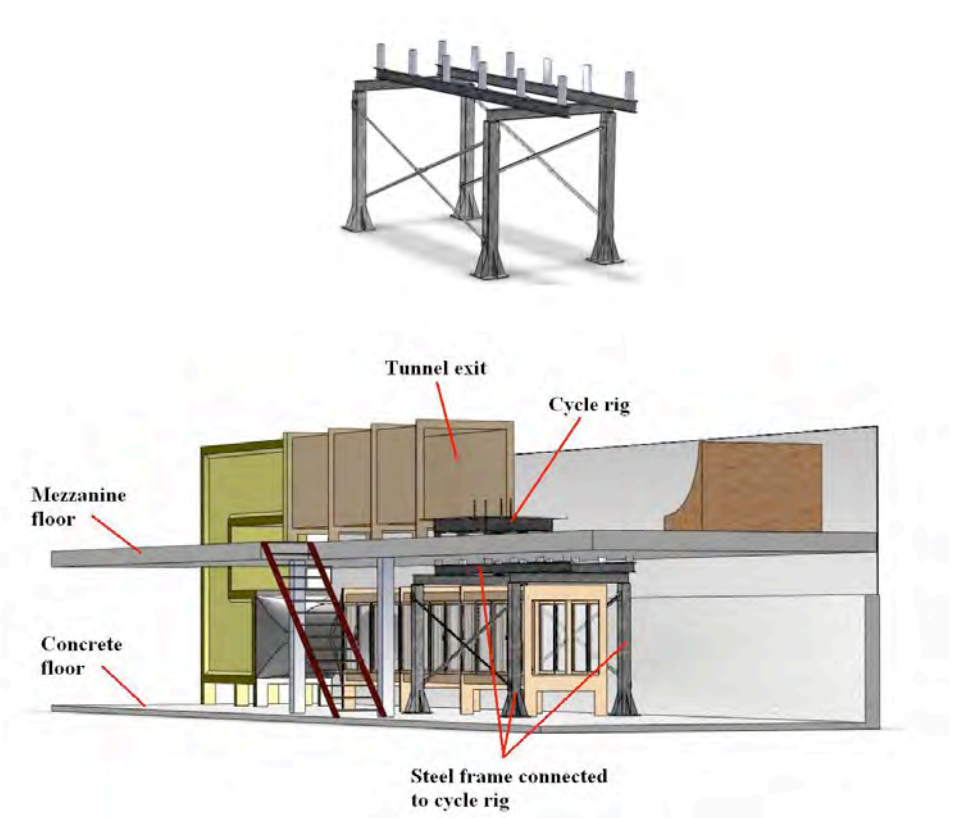

Figure 5.6: Steel frame built to reduce the floor deflection

Software

LabVIEW software was used to capture the signals from the load cell and torque transducer, and a display was created to show real-time data of atmospheric temperature and pressure, wind tunnel speed, drag, torque, power, and the overall length of each test. A separate LabVIEW programme was written to read back the data for analysis, so that comparisons could be made between different positions and equipment for selected intervals. Images of the LabVIEW displays and a description of the testing procedure can be seen in Appendix D. Some of the key points of the testing procedure are described below:

Testing Procedure Key Points

Tracing the Athlete's Outline

The athlete's shadow is projected onto a white board by using a single, bright lamp on the opposite side of the athlete to the board. The outline of the rider or mannequin is then traced around to ensure only the specified changes in position are made and not unintentional position changes, and also to compare athlete position for consecutive tests; for example to compare a low, crouch position to an upright position. An example of this outline is shown in Figure 5.7.

Figure 5.7: Outline of Rider

Force Balance Calibration

The force balance is calibrated before and after each test by using a 2kg weight suspended by fishing wire passing over a pulley on low friction bearings, the other end of which is attached to the floating platform close to the rear roller. A hydraulic system constructed from a pair of disposable syringes is used to load and unload the 2kg weight to ensure the loading and unloading is as smooth as possible. The calibration system can be seen in Figure 5.8.

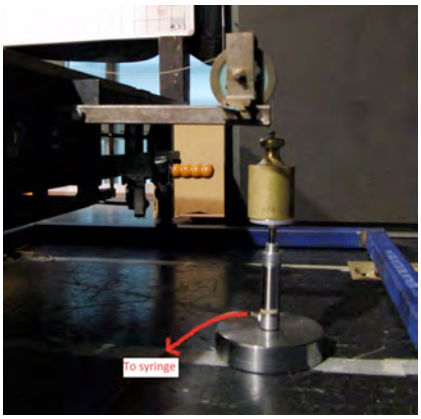

Figure 5.8: Calibration System

Frontal Area Calculation

A rod with a 0.5m white stripe was placed vertically next to the rear of the rider or mannequin and an image taken from the rear and converted into a JPEG format. By selecting the 0.5m white stripe on the rod in the JPEG image, the number of pixels for this 0.5m section can be used to determine the number of pixels

per square meter. The digitizing method was then used to determine the frontal area of the cyclist, bike and wheels. This method involved importing the JPEG image into a computer-based imaging software (Corel Photo-Paint X3) and using the cutout lab to manually select the area of the cyclist, bike and wheels. This image was then converted into black and white and imported into a free image processing tool (ImageTool) for analysis. The image was converted into greyscale in the ImageTool software for binary formatting, and then the thresholding tool used to darken the area. The number of black pixels was then counted. The actual frontal area of the rider, bike and wheels was determined by comparing the number of black pixels to the known number of pixels of the 0.5m white stripe on the rod. The digitizing method is shown in Figure 5.9 and the calculation procedure shown in Table 5.2.

(a) Original FA photo (b) Selecting the FA using cutout lab (c) Selected FA area for analysis

Figure 5.9: Digitizing Method of Frontal Area Calculation

Rod	
Length (m)	0.5
Number of Pixels	572
Pixels per m	2288
Pixels per m^2	5234944
Athlete	
Number of Black Pixels	882901
Frontal Area (m^2)	0.169

Table 5.2: Calculation of Frontal Area of a cyclist

5.1.2.3 Errors and Uncertainties

The greatest error during testing comes from the precision of the force balance system and ensuring the athletes adopt a consistent position during testing. It is important to wait for the wind to die down completely before the second calibration, which was monitored using a cotton tuft attached to the wind tunnel exit using clear, mylar tape. The use of the white board for tracing around the shadow side-on minimises the error associated with a consistent position, but it will be impossible for athletes to hold the exact same position during tests. Therefore comparisons were made for a number of both static and dynamic tests to determine the consistency of drag readings for an athlete or equipment in the same position. Static tests were carried out using a bike placed on the rig at a wind speed of 41kph, and the bike was removed and then replaced in the same position for a total of 7 tests. The results, shown in Table 5.3, indicate that the maximum difference in drag was 9.1g (1.36%).

Test	**Drag (kg)**	**Difference from Lowest Drag (%)**
1	0.6595	0
2	0.6614	0.29
3	0.6617	0.33
4	0.6686	1.36
5	0.6632	0.56
6	0.6644	0.74
7	0.6679	1.26
Mean	0.6638	
SD	0.0034	

Table 5.3: Drag for a stationary bike with 41kph wind speed

Dynamic tests were carried out using three different athletes, each adopting their own reference position for three, pedalling tests. After each test the athlete got off their bike and then back on again, and the white board was used to ensure athletes adopted the same position each time. The results, shown in Table 5.4, indicate that the maximum difference in drag for the same position for these three athletes is between 0.4 and 0.8%.

	Measured Drag (kg)		
Test	**Athlete 1**	**Athlete 2**	**Athlete 3**
1	2.061	2.187	2.060
2	2.078	2.177	2.074
3	2.062	2.178	2.072
Max Difference in Drag (kg)	0.017 (0.8%)	0.009 (0.4%)	0.014 (0.7%)
Mean	2.067	2.181	2.069
SD	0.010	0.006	0.008

Table 5.4: Comparison of drag readings for athletes in the same position

The precision of the force balance system was calculated by measuring the difference between the calibration readings before and after both static and dynamic tests for a total of six tests each. For the static tests the calibration was applied before and after placing and removing a 20kg weight to the middle of the rig. For the dynamic tests, a cyclist adopted their reference position on a road bike fixed to the cycle rig and the calibration was applied, after which point the cyclist began to pedal for 30 seconds and when they stopped the calibration factor was measured again, as shown in Figure 5.10.

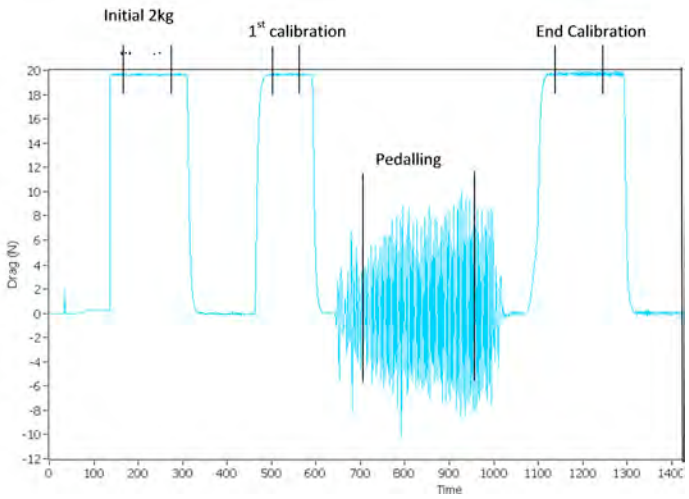

Figure 5.10: LabVIEW display for dynamic testing without wind

For the static tests the maximum drift was 0.015kg and the average drift was 0.0058kg (Table 5.5). An elite cyclist has an approximate overall drag of 2kg, so a drift of 15g is less than 1% error.

Test	**Maximum Drift (kg)**
1	0.0100
2	0.0150
3	0.0006
4	0.0009
5	0.0050
6	0.0030
Mean	0.0058
SD	0.0057

Table 5.5: Drift for static tests

For the dynamic tests the maximum drift was 0.016kg and the average drift was 0.015kg (Table 5.6). This error is slightly higher than for the static tests due to the increased impact on the load cell with every pedal stroke, which would not be present during static tests. However, this error is still less than 1% for a cyclist with an overall drag of 2kg. The drift was not a systematic error, as sometimes the drift would be positive but other times negative. There was no indication as to when a positive or negative drift would be recorded.

Test	Maximum Drift (kg)
1	0.012
2	0.016
3	0.009
4	0.023
5	0.016
6	0.011
Mean	0.015
SD	0.005

Table 5.6: Drift for dynamic tests

The total error associated with athlete position and the force balance is therefore in the region of 2 to 2.5%.

Additional errors are associated with the wind speed, air density, frontal area calculation and human error. The wind speed (in kph) is determined from the change in pressure between the pitot tube and atmosphetic pressure and can be calculated using Equation 5.2, where $\triangle p$ is the manometer reading (mmH_2O), t is the ambient temperature (°C) and P is the ambient pressure (Pa).

$$V = 3.6 \times 7.5034 \times \frac{\left(\triangle p\,(273+t)\right)^{0.5}}{(P \times 0.997)} \tag{5.2}$$

The manometer has an accuracy of ±0.5mm, the temperature an accuracy of 0.1°C, and the pressure an accuracy of 0.005Pa. Therefore the accuracy of the wind speed is 0.06kph (0.13% at 45kph) for an average temperature and pressure of 20°C and 1000mbar respectively, and manometer reading of 8mmH_2O (typical manometer reading for wind tunnel tests at the University of Canterbury) $\left[\frac{\delta V}{V} = \sqrt{\left(\frac{\delta p}{p}\right)^2 + \left(\frac{\delta t}{t}\right)^2 + \left(\frac{\delta P}{P}\right)^2}\right]$.

The air density is calculated by $\rho = \frac{P}{RT}$, where P is the ambient pressure (Pa), R is the universal gas constant (Jkg$^{-1}K^{-1}$) and T is the ambient temperature (K). The accuracy of the temperature and pressure is 0.1°C (1.365K) and 0.005Pa respectively, giving an air density accuracy of 0.004kgm^{-3} (0.4%) at a temperature of 20°C, pressure of 1000Pa, and air density of 1.188kgm^{-3} $\left[\frac{\delta \rho}{\rho} = \sqrt{\left(\frac{\delta T}{T}\right)^2 + \left(\frac{\delta P}{P}\right)^2}\right]$.

The random error associated with the calculation of the frontal area was determined by using the digitizing method to calculate the frontal area for the same athlete in the same position three times. The maximum difference in frontal area calculation was 0.008m^2 (2.5%). There is also a systematic error with the calculation of the frontal area using the digitizing method due to perpective; the image is calibrated in the middle of the depth of field, typically at the hips or ribs of the rider, but for some riders their outline is nearer or farther from the camera. However, this systematic error is not significant for calculations or comparisons that use the drag area, C_dA, calculated from drag measurements, rather than just the frontal area.

The uncertainty of the force balance, wind speed, air density, and frontal area then propagate to the calculation of drag coefficient, as $C_d = \frac{F}{\frac{1}{2}\rho A V^2}$, where F is the measured drag force (N), ρ is the air density (kgm^{-3}), A is the frontal area (m^2) and V is the wind speed (ms^{-1}). The total error for the drag coefficient can therefore be calculated by:

$\frac{\delta C_d}{C_d} = \sqrt{\left(2\frac{\delta V}{V}\right)^2 + \left(\frac{\delta F}{F}\right)^2 + \left(\frac{\delta \rho}{\rho}\right)^2 + \left(\frac{\delta A}{A}\right)^2}$

$$\frac{\delta C_d}{C_d} = \sqrt{(2 \times 0.0013)^2 + (0.025)^2 + (0.004)^2 + (0.025)^2} = 2.6\%$$

It should be noted that this analysis does not include the systematic error in the determination of the frontal area, the variation of wind speed over the tunnel, or the blockage correction. These factors are not important if only trends are to be sought.

5.1.2.4 Athlete and Mannequin Tests

In order to determine whether the trend in drag readings was the same for an athlete compared to a mannequin a comparison was made between four different skinsuits, each worn by a mannequin (FLEXMALE-1 supplied by Artform Mannequins) and a competitve cyclist, both wearing an aero helmet (BELL Meteor II) and shoe covers (Champion Systems). The mannequin was fixed in a racing position to a track bike with handlebar extensions and clip pedals and shoes, with the cranks set at 90^{o} and 270^{o} to the vertical. The athlete adopted their reference racing position on the same track bike and handlebar extensions and was pedalling at 90rpm. The results, shown in Figure 5.11, show that although the actual percentage differences do differ between the athlete and mannequin and are significantly lower for the athlete, the trend between the four different skinsuits was the same. The majority of this difference is likely to be a result of the effect of pedalling, which causes the actual drag values to increase by approximately 3-4% compared to stationary tests for the same athlete, and so the percentage differences in drag will be smaller. Therefore both methods are valid ways of comparing position and/or equipment changes, providing it is understood that the readings for the percentage difference in drag for a pedalling athlete will be much lower than those for a stationary mannequin used.

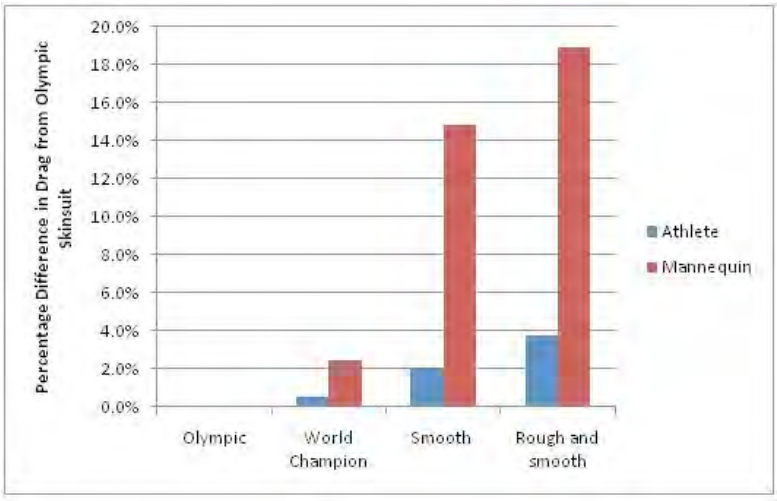

Figure 5.11: Comparison between the results for percentage difference in drag on the mannequin and athlete

5.1.2.5 Boundary Layer Thickness of Cycle Rig

The boundary layer on the cycle rig was determined by measuring the velocity of the wind at different heights above the ground plane using an adjustable height pitot tube connected to a water manometer. The boundary

layer was measured at the front of the rig (15cm from the tunnel exit), at the front roller (60cm from the tunnel exit), in the middle of the rig (115cm from the tunnel exit) and at the rear of the rig (223.5cm from tunnel exit). Equation 5.3 was used to convert the velocity from mmH_2O, read from the manaometer, into kph. The boundary layer thickness is taken to be the vertical distance above the ground plane at which the wind speed reachies 99% of the free stream velocity; when the velocity becomes constant.

$$V = 3.6 \times 7.5034 \times \frac{\left(\triangle p \left(273 + t\right)\right)^{0.5}}{\left(P \times 0.997\right)} \tag{5.3}$$

The velocity profiles at the different points on the cycle rig are shown in Figure 5.12. The boundary layer thicknesses at the front, front roller, middle, and rear of the rig were calculated to be 44.8mm, 68mm, 46mm, and 51mm respectively. These results suggest the boundary layer thickness is no greater than 70mm anywhere along the length of the bike, so any changes in position made will lie in the core flow away from the boundary layer of the cycle rig. It is possible that the raised roller and the gap around it may cause a wake in the flow, which probably dies away further downstream This would explain the higher boundary layer thickness at the front roller compared to the middle of the rig.

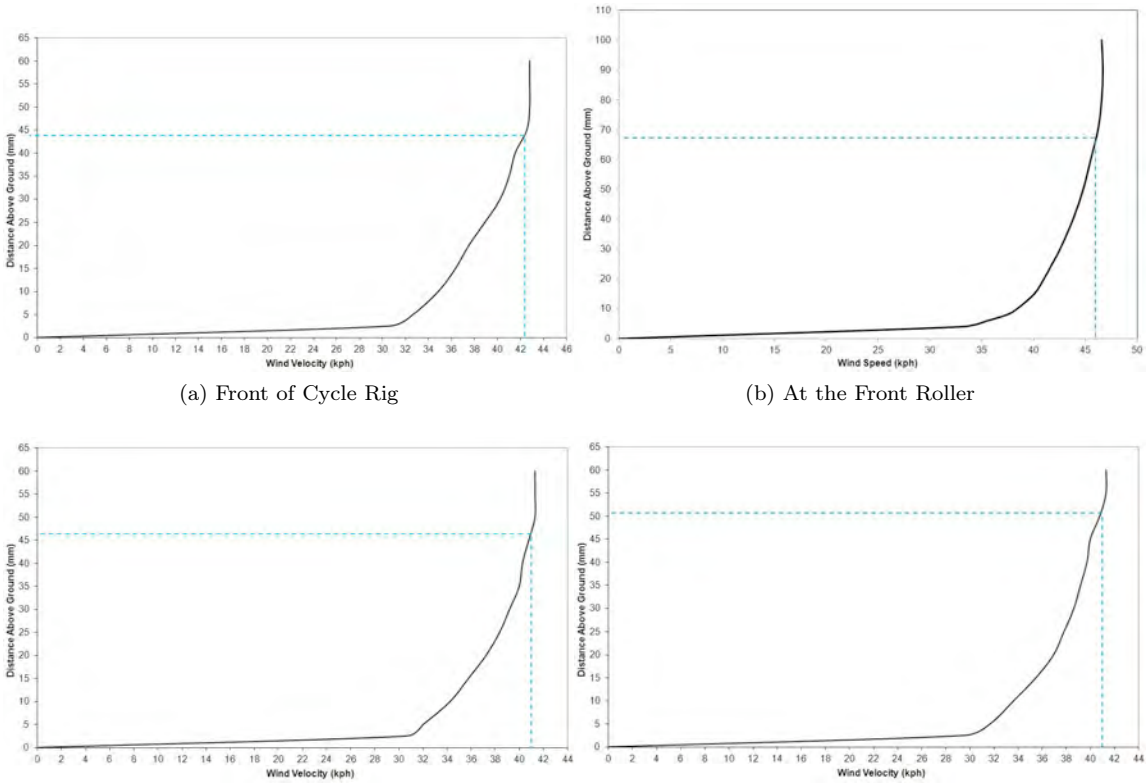

(a) Front of Cycle Rig

(b) At the Front Roller

(c) Boundary layer thickness at the middle of the rig

(d) Boundary layer thickness at the rear of the rig

Figure 5.12: Boundary Layer Thickness of Cycle Rig

5.2 Summary

In this Chapter a description of the wind tunnel and cycle rig used at the University of Canterbury for athlete and mannequin testing has been given. The accuracy of this system is mainly influenced by the force balance accuracy, which has been shown to have an error of around 2 - 2.5%. The calculated drag coefficient is dependent on the accuracy of the force balance, as well as the air density, frontal area of the object involved, and wind speed. The calculated accuracy of the drag coefficient was 2.6%. The wind speed of the boundary layer wind tunnel at the University of Canterbury is lower than the that of other facilities where the aerodynamics of cycling has been investigated. However, as the aerodynamic drag is directly proportional to the velocity squared, it is easy to determine the drag for actual cycling speeds using the data collected at the University of Canterbury; the air flow at the wind speeds simulated in the boundary layer wind tunnel at the University of Canterbury will be at Reynolds numbers similar to those at which racing occurs. For example, for a wind speed of 42kph and a cyclist of length L=1m, the Reynolds number is Re=7.7x10^5. For the same cyclist at a racing speed of 55kph, the Reynolds number is Re=1x10^6. The boundary layer thickness of the cycle rig was found to be less than 70mm, and any changes made to the position of the athlete and/or equipment will occur within the core flow and away from the boundary layer so that the influence of the boundary layer thickness can be ignored.

A comparison between athlete and mannequin tests has shown that the trends in terms of results for aerodynamic drag are similar between the two, but the actual values for drag are lower for a stationary mannequin compared to a pedalling athlete. However, as the trends are the same, both methods are useful for analysing the relative drag for track cycling.

Chapter 6

Flow Analysis over a Cyclist

6.1 Introduction

Aerodynamic drag consists of both pressure and skin friction drag, each of which should be minimised in order to maximise the velocity of a cyclist. The aims of this chapter were to observe the differences in flow over a cyclist due to changes in equipment by measuring the flow velocity at different locations over a stationary mannequin, and to estimate the contribution of skin friction and pressure drag to the overall drag of a cyclist.

6.2 Experimental Set Up

A mannequin (FLEXMALE-1 supplied by Artform Mannequins) was used to determine the flow velocity over a cyclist. The mannequin was fixed to a stationary bike in the aero position in the boundary layer wind tunnel at the University of Canterbury, with the wind speed set at 46kph. The position of the mannequin was monitored by projecting a shadow from side on onto a whiteboard, and although the position of the hands of the mannequin may not truly represent the position of an elite cyclist and may have some effect on the flow, all measurements were made outside of this region and the trends will be unaffected. An adjustable height Pitot tube was used to measure the flow velocity at 5mm increments from the surface of the mannequin's back at the helmet tip, shoulders, mid-back and lower-back. It was ensured that the pitot tube was parallel to the back on all occasions. The flow velocity was measured for (a) two different skinsuits; (b) with and without a helmet on (BELL Meteor II); (c) with the helmet holes taped and untaped; and (d) down the middle and down the side of the back of the mannequin. Velocity profiles were plotted for each comparison at the four selected locations. The experimental set up is shown in Figure 6.1, where the numbers 1 to 4 represent the locations of (1) behind the helmet, (2) on the shoulders, (3) in the middle of the back, and (4) on the lower back. The repeatability of changing the skinsuit or helmet was determined by re-measuring the velocity profile once the skinsuit or helmet had been taken off and put back on the mannequin. The repeatability was found to be between 2 to 4mm. Although the hand position of the mannequin may not be truly representative of an elite cyclist and may have some effect on the flow around the hands, the hand position was consistent from test to test and will not affect the flow in the regions where the velocity profile was measured.

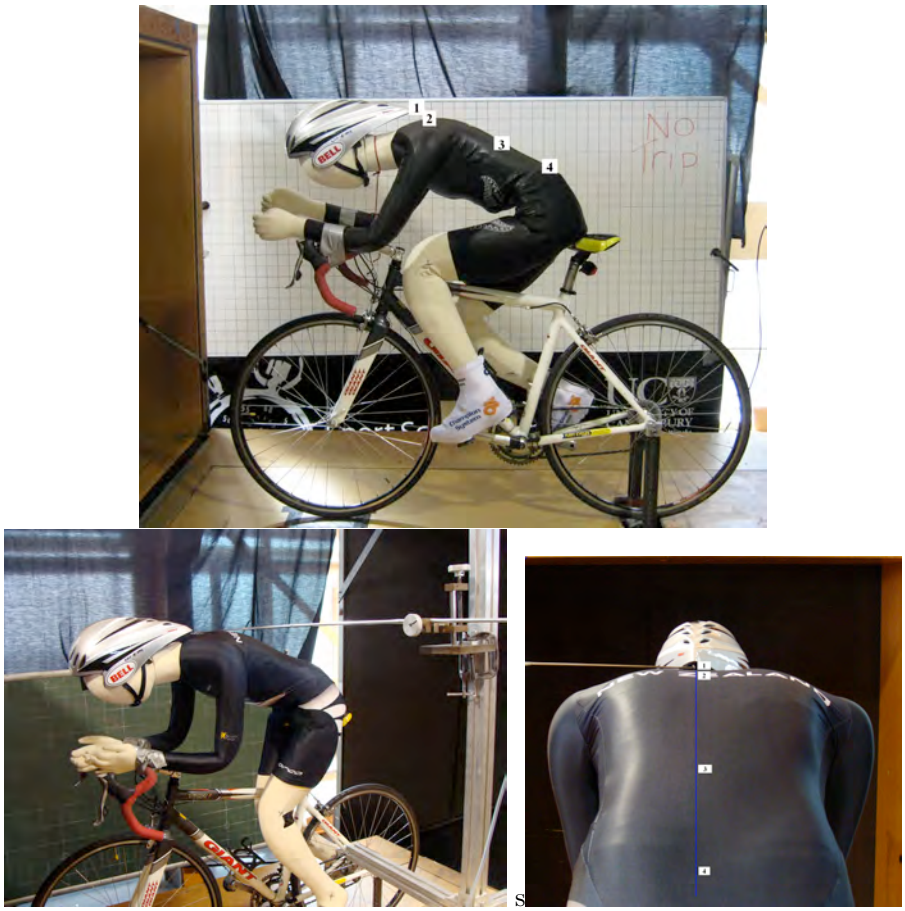

Figure 6.1: Experimental Setup

6.2.1 Flow Velocity Comparison of Different Skinsuits

Details of the two different skinsuits used in this study are shown in Table 6.1. The velocity profiles for the two different skinsuits are shown in Figure 6.2. These profiles show that there is a difference in flow over the two skinsuits, in particular in the region behind the helmet tip. There appears to be a high speed stream that penetrates the flow, caused by the helmet or the gap between the helmet and shoulders. This effect is more significant behind the helmet for Skinsuit 1, but more significant on the shoulders and mid-back for Skinsuit 2. For both skinsuits the effect of this high speed penetration of the flow is not as great the further down the back away from the leading edge.

Skinsuit	**Description**
Skinsuit 1	- Mainly rubberised lycra (nylon laminated)
	- Small patches of lycra on the rear legs, outside of arm, and by the zip
	- Most seams bonded
Skinsuit 2	- 74% polyester, 24% lycra
	- Elastic at the end of the arms and legs

Table 6.1: Details of the skinsuits

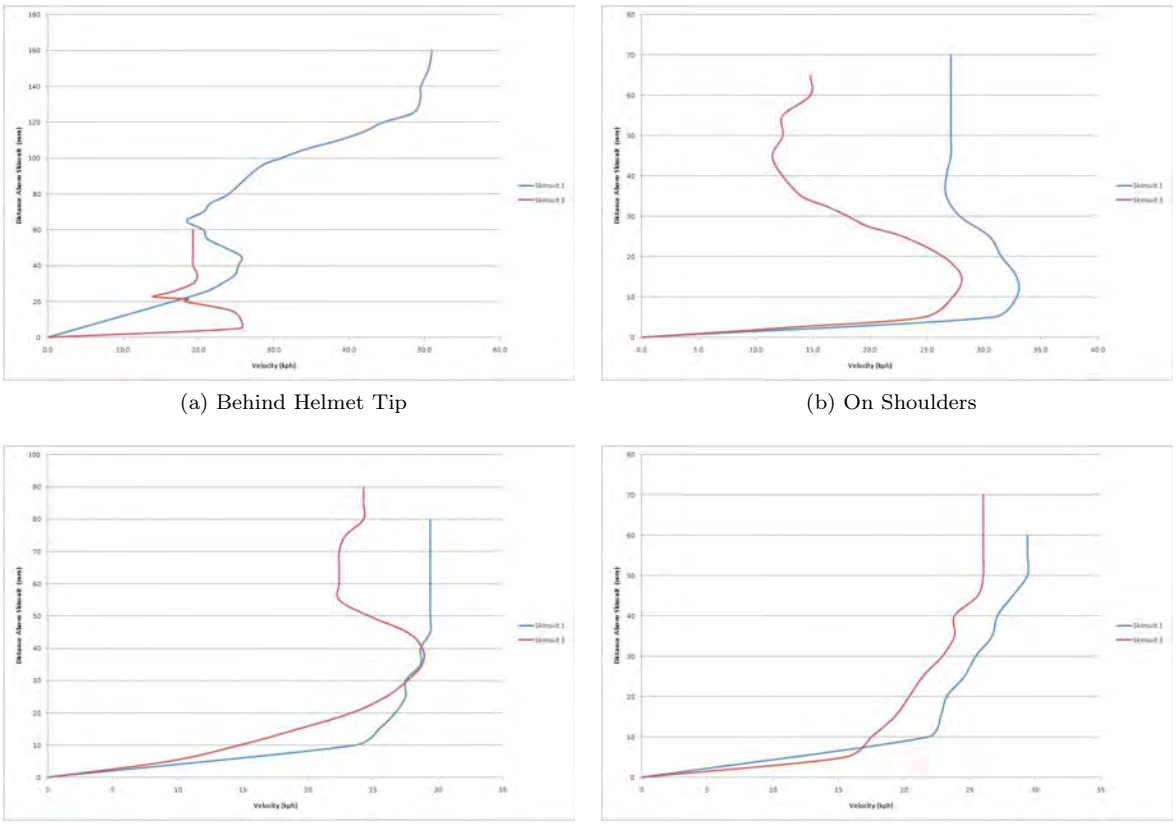

(a) Behind Helmet Tip

(b) On Shoulders

(c) Mid-Back

(d) Lower Back

Figure 6.2: Velocity Profile Comparison of Skinsuits

The main difference between the skinsuits was the type of material used. In general, the flow velocity for skinsuit 2 was lower than for skinsuit 1 at the same locations, which suggests that the drag would be greater for skinsuit 2.

6.2.2 Flow Velocity Comparison of Helmet and No Helmet

A comparison between the flow velocity for the mannequin with and without an aero helmet on was made when the mannequin was wearing skinsuit 1. The velocity profiles are shown in Figure 6.3.

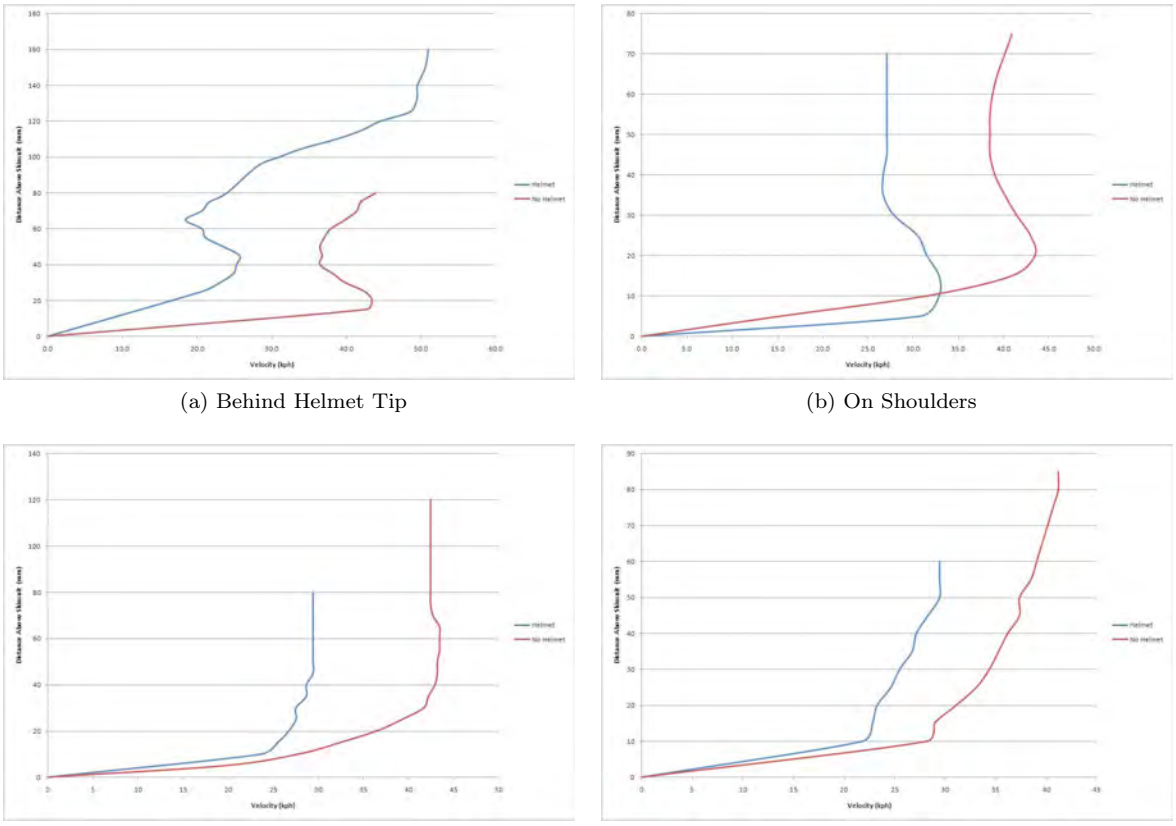

(a) Behind Helmet Tip

(b) On Shoulders

(c) Mid Back

(d) Lower Back

Figure 6.3: Velocity Profile Comparison of Helmet and No Helmet

These results show that the velocity is greater when the mannequin is not wearing a helmet, but the shape of the helmet and head causes the formation of a high speed stream. The head and helmet have a significant influence on the velocity profiles behind the helmet tip and on the shoulders, but their influence becomes less further downstream. The recess shape of the helmet, ventilation holes, and where the neck joins the head of the mannequin when no helmet is worn causes the velocity to decrease. This influence is clearer in Figure 6.4, which shows the location of the recesses and helmet holes on the velocity profiles behind the helmet tip, and is in agreement with results published by Chabroux et al. [2010] who identified a velocity deficit due to helmet recesses using the PIV technique.

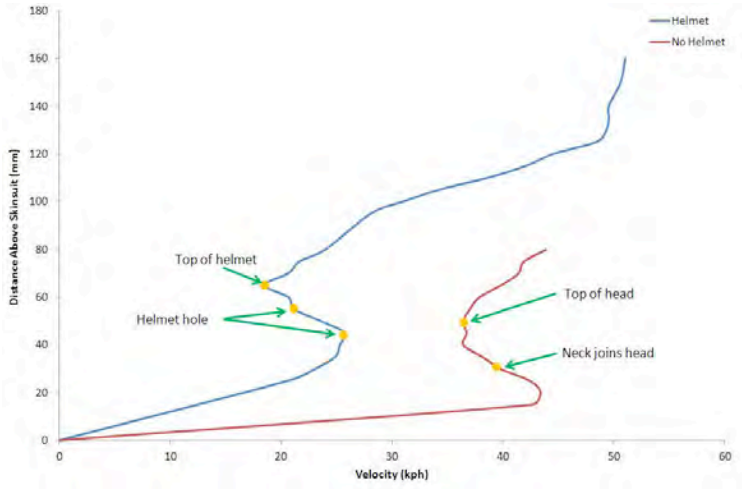

Figure 6.4: Comparison between shape of helmet and head and velocity profiles behind the helmet tip

Although the results show that the flow velocity was lower for when a helmet was worn compared to no helmet, it is likely that the flow velocity was measured in the wake of the helmet and shoulders. Computational Fluid Dynamic (CFD) contour plots of cyclists, shown in Figure 6.5 (www.sportsnscience.utah.edu) clearly show this wake behind the helmet and shoulders, which would have been in the same location as where the velocity profile was measured. However, it is likely that different types of helmets will show different velocity profiles due to their differences in shape and ventilation design. Although the lowest drag helmet can be chosen from an array of ready-made helmets just by measuring the aerodynamics drag, measuring the flow velocity would help understand why one helmet may have less drag than another, and therefore help to design new helmets in the future.

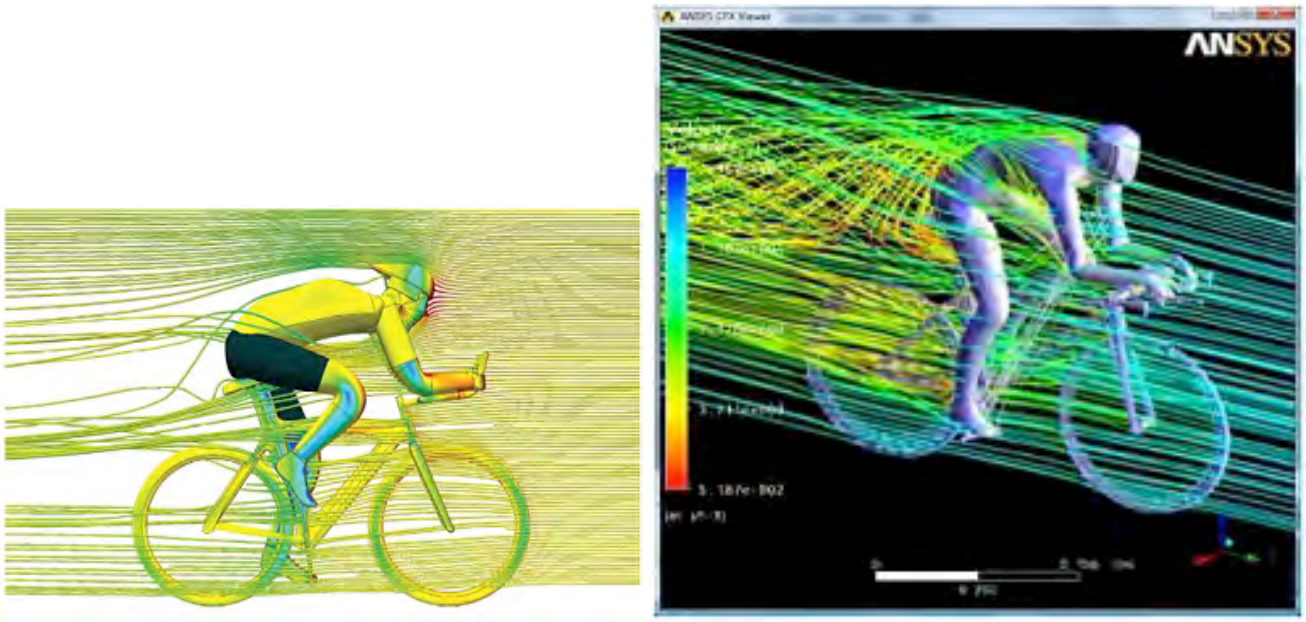

Figure 6.5: CFD Images of Cyclists (www.sportsnscience.utah.edu)

6.2.3 Flow Velocity Comparison of Helmet Holes Taped and Not Taped

The effect of taping the vents of the BELL aero helmet on the flow velocity was analysed using the mannequin wearing skinsuit 1. The velocity profiles are shown in Figure 6.6.

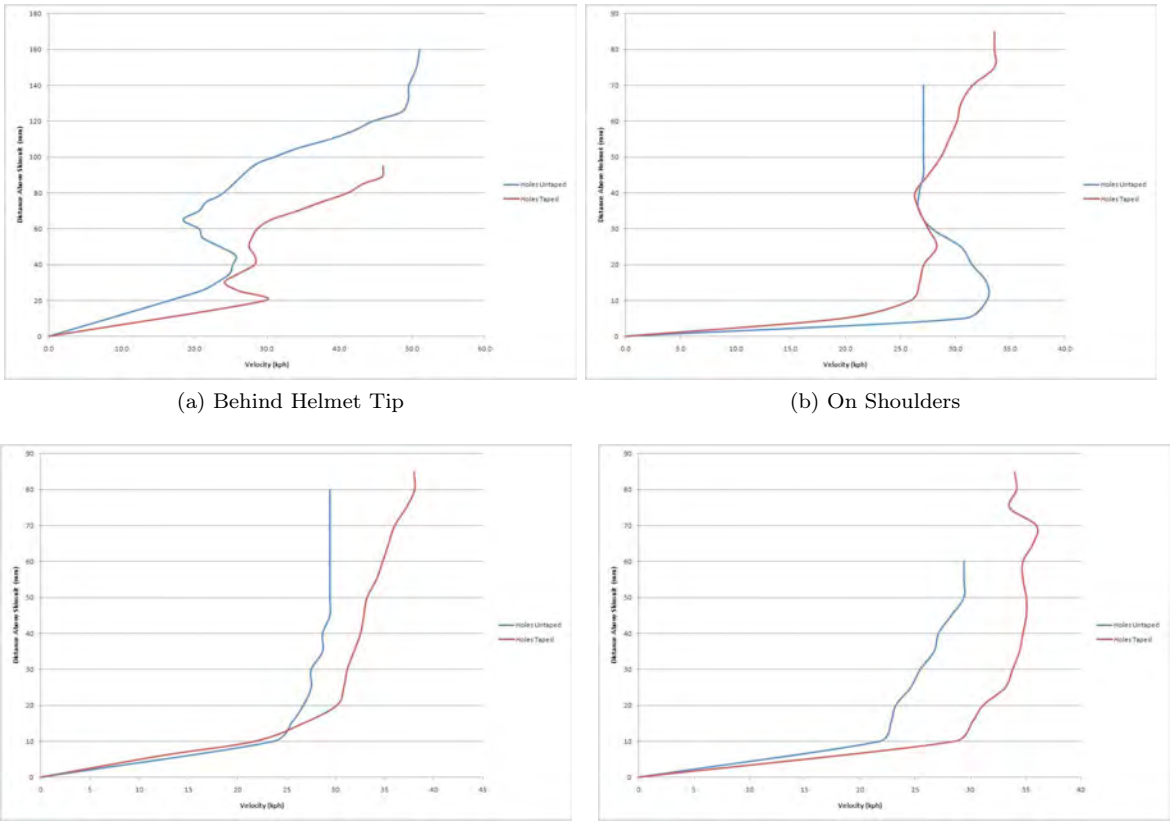

(a) Behind Helmet Tip

(b) On Shoulders

(c) Mid Back

(d) Lower Back

Figure 6.6: Velocity Profile Comparison of Helmet Holes Taped and Not Taped

The results show that the velocity is greater at the same distance above the skinsuit when the helmet holes are taped in all regions, except for on the shoulders. This is probably because by taping the holes the flow can only be directed over the helmet and not through it. When the helmet holes are not taped it is likely that the flow over the top of the helmet mixes with the flow passing through the helmet holes in the shoulder region, causing a greater velocity deficit. The influence of the helmet holes becomes less further downstream. A greater flow velocity observed when the helmet holes are taped suggests that the drag will be lower, which is in agreement with the study by Alam et al. (2008b) who found that drag could be reduced by covering up the vents of road helmets.

6.2.4 Flow Velocity Comparison of Middle and Side of the Back

The flow velocity was measured at the side of the mannequin's back to compare the flow velocity down the side to that down the middle, again using the mannequin wearing skinsuit 1. The velocity profiles are shown in Figure 6.7.

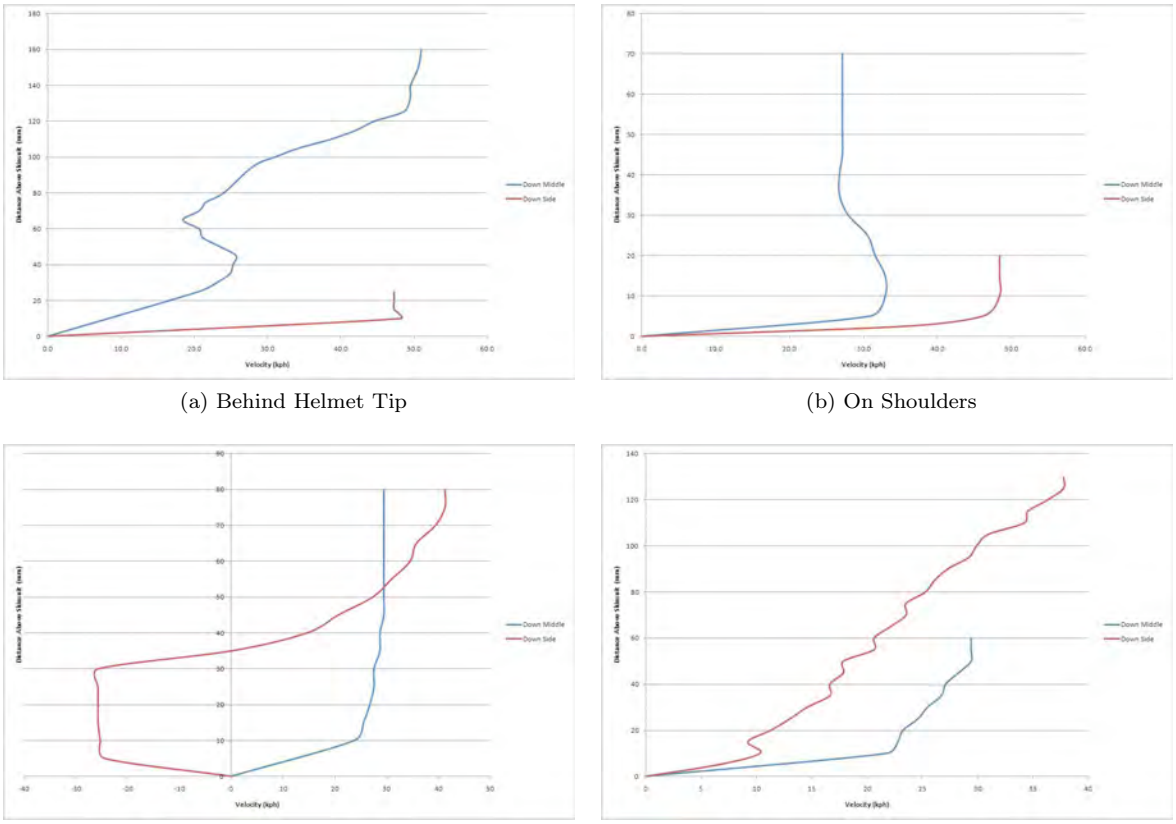

(a) Behind Helmet Tip

(b) On Shoulders

(c) Mid Back

(d) Lower Back

Figure 6.7: Velocity Profile Comparison down the Middle and Side of the Back

These results clearly show the influence of the helmet (and head) on the flow in the regions behind the helmet and on the shoulders; the head and helmet penetrate the flow, causing a significant reduction in the flow velocity in comparison to the flow at the side. However, there appears to be a region of recirculation at the side in the mid-back region, which is probably due to the mixing of the flow from under the armpits with the flow from over the back. This is likely to increase the drag, and should be an area to concentrate on when trying to reduce the aerodynamic drag of a cyclist (by reducing this recirculation).

6.2.5 Contribution of Skin Friction and Pressure Drag

The torso of a cyclist can be thought of as a flat plate to help identify the contribution of skin friction and pressure drag to the overall drag of a cyclist. The skin friction drag can be calculated for a flat plate using

Equation 6.1, where $q = \frac{1}{2}\rho V^2$, $A_s = 0.2025H^{0.725}M^{0.425}$, ρ is the air density (kg/m^3), V is the velcoity (m/s), A$_s$ is the surface area of the athlete (m^2), H is the height of the athlete (m), and M is the mass of the athlete (kg) [Pendergast et al., 2006].

$$D_{SF} = qA_s \left[\frac{0.074}{Re_x^{\frac{1}{5}}} - \frac{1740}{Re_x} \right] \tag{6.1}$$

Assuming the torso of a cyclist can be thought of as a flat plate, a comparison was be made between the contribution of skin friction drag to the overall drag of a cyclist while wearing Skinsuit 1.

The aerodynamic drag was measured in the boundary layer wind tunnel at the University of Canterbury at a wind speed of 41kph using a stationary mannequin on a track bike, as well as for a pedalling athlete on their own track bike in their current racing position. The results were then used to calculate the contribution of skin friction and pressure drag at the shoulders, mid-back, lower back, and rear regions, located at 0.165m, 0.415m, 0.615m, and 0.8m from the leading edge (top of the helmet) respectively. The data used to calculate the contribution of skin friction and pressure drag for the mannequin and athlete are shown in Table 6.2, and the actual results are shown in Table 6.3.

	q	**Height (m)**	**Weight (kg)**	**A$_s$ (m^2)**	**Shoulder Width (m)**
Athlete	75.88	1.80	80	2.00	0.42
Mannequin	75.88	1.83	20	1.12	0.51

Table 6.2: Data used to calculate the contribution of skin friction and pressure drag

	Location	**Overall Measured Drag (N)**	**Re (x10^5)**	**D$_{SF}$**	**% D$_{SF}$**	**% D$_{PD}$**
Athlete	Shoulders	20.10	1.24	-1.05	0	100*
	Mid-back		3.12	0.05	0.25	99.75
	Lower-back		4.62	0.26	1.29	98.71
	Rear		6.01	0.35	1.74	98.26
Mannequin	Shoulders	16.88	1.24	-0.59	0	100*
	Mid-back		3.12	0.03	0.18	99.82
	Lower-back		4.62	0.15	0.89	99.11
	Rear		6.01	0.19	1.13	98.87

Table 6.3: Contribution of skin friction and pressure drag for a mannequin and athlete wearing Skinsuit 1
* Assumed to be 100% pressure drag

It is clear to see from Table 6.3 that skin friction drag contributes to less than 2% of the overall drag at all locations. Although this seems like an insignificant percentage, a reduction in skin friction that causes a reduction in total drag by as little as 1% would have a significant effect on athlete performance and finishing time, and therefore should not be ignored.

6.3 Summary

Clear differences were observed between the flow velocities for different skinsuits, helmet holes taped compared to untaped, and down the side compared to the middle of the back. It appears that a high speed stream was formed by the head and helmet in the regions behind the helmet tip and at the shoulders, which was greater when wearing a helmet compared to no helmet, and with the helmet holes taped compared to not taped. Recirculation began to occur down the side in the mid-back region, most likely due to the mixing of the flow from under the armpits with the flow down the back of the mannequin. The flow then became noisy in the lower back region down the side, and this would therefore increase the drag. A particular observation was the influence of the shape of the helmet and the location and roughness of the helmet holes on the flow velocity. It would be useful to carry out a similar study to compare different helmets in order to identify how the shape and ventilation design (location, orientation and roughness) affects the flow velocity.

Chapter 7

Optimal Equipment and Attire

Introduction

The focus of this thesis was to analyse methods of increasing the speed of track cyclists through changes in position rather than equipment. Therefore, only some simple, initial wind tunnel tests were carried out on cycling equipment in order to identify the contribution of changes to equipment on the overall drag of cyclists compared to the significance of changes in body position. No detailed tests were carried out on different types of wheels used for track cycling, as a full study had already been carried out by Jermy et al. [2008]. However, I was approached to help design a new skinsuit for the London Olympics 2012, which lead to an additional study on materials and patterns for skinsuit design. The focus of this chapter will therefore be on the material selection, design, and identification of the most significant factors for the development of a new skinsuit for track cycling.

7.1 Frames and Wheels

The majority of track cyclists use front and rear disc wheels rather than spoke wheels, due to their lower aerodynamic drag when no external wind is present [Jermy et al., 2008, Lukes et al., 2005]. As previously mentioned, no detailed study was carried out on the aerodynamics of the frame or wheels of a track bike. However, a comparison was made between different track bike frame and disc wheel combinations already used for elite track cycling events to identify their contribution to the overall drag of a cyclist. These comparisons were made both with and without a female rider at a wind speed of 53kph, and the same handlebars and extensions used for all tests (typical Individual Pursuit handlebars). The results, including the contribution of the frame and wheel combinations to the overall drag of a cyclist, are shown in Table 7.1.

Frame (Track bike)	Wheel (Disc)	Without Rider			With Rider			Contribution of frame and wheels to overall drag (%)
		Drag (kg)	Difference in drag		Drag (kg)	Difference in drag		
Zen	Mavic	0.584	0kg	0%	2.488	0kg	0%	25.3
Avanti	Mavic	0.592	0.008kg	1.4%	2.537	0.049kg	1.9%	25.1
Zen	Zen	0.664	0.080kg	12.0%	2.552	0.064kg	2.5%	26.0
Avanti	Zen	0.671	0.087kg	13.0%	2.564	0.076kg	3.0%	26.2

Table 7.1: Drag results for different frame and disc wheel combinations*
*All wheels were disc wheels

The results in Table 7.1 indicate that the trend in difference in drag between the frame and wheel combinations is the same for both with and without a rider, although the absolute difference in drag is slightly greater without a rider than with a rider. For the results with a rider the difference between the frame and wheel combinations is a maximum of 3%. The results also show that the rider contributes to approximately 75% of the overall drag; significantly more than the contribution of the frame and wheels.

An additional analysis of simple modifications made to a current, racing track bike (Zen TK8 frame) was carried out to determine whether some simple improvements could be made to the shape of the frame in order to reduce the aerodynamic drag. This included attaching shaped pieces of polestyrene, covered in electrical tape, to the regions by the stem, fork, and seat tube, as shown in Figure 7.1.

(a) Stem modification

(b) Fork modification

(c) Seat tube modification

Figure 7.1: Modifications to a track bike frame

The frame was placed on the cycle rig in the boundary layer wind tunnel at the University of Canterbury and the wind speed set at 41kph. The drag was measured for the frame without any modifications, and then for each modification made to the stem, fork, and seat tube individually whilst a competitive cyclist was pedalling at 90rpm. The results, shown in Table 7.2, indicate that any modifications made to the frame resulted in a change in drag of less than 0.3%, which is less than the repeatability of the cycle rig.

Modification	**Measured Drag (kg)**	**Δdrag from normal frame (%)**
Normal frame	2.0257	0
Fork	2.0221	-0.2
Stem	2.0271	+0.1
Seat tube	2.0204	-0.3

Table 7.2: Results for modifications made to the frame

The results shown in Tables 7.1 and 7.2 clearly indicate that the cyclist contributes significantly more to the overall drag on a cyclist than the frame and wheel combination, and that in order to increase the velocity of a track cyclist the focus should be on improving athlete position rather than the design of the frame or wheels.

7.2 Helmets

Although no specific helmet analysis was carried out, six athletes compared the drag of different helmets in the wind tunnel in order to identify the significance of a change in helmet on the aerodynamic drag. These helmets were a combination of aero helmets (Giro, Spiuk, Uvex, Rocket and Bell) and non-aero helmets (Casco and MET Road), images of which can be seen in Figure 7.2. Details of each athlete can be seen in Table 7.3.

(a) Giro (b) Spiuk (c) Uvex

(d) Rocket (e) Bell (f) Casco

(g) MET Road

Figure 7.2: Helmets Tested

Athlete	Road/Track	Experience	Gender
1	Track	Elite	Male
2	Track	Elite	Male
3	Road	Elite	Female
4	Road	Competitive	Male
5	Road	Competitive	Male
6	Road	Competitve	Male

Table 7.3: Athlete Details

The number of helmets tested by each athlete was dependent on the fit of the helmet, and the presence of a visor was dependent on athlete preference. Athletes were wearing sunglasses if no visor was worn. All tests were carried out in the boundary layer wind tunnel at the University of Canterbury at a wind speed of 42kph. The athletes adopted the same position and used the same equipment for each helmet comparison, which consisted of their current racing position on their current racing bike. The results are shown in Figure 7.3.

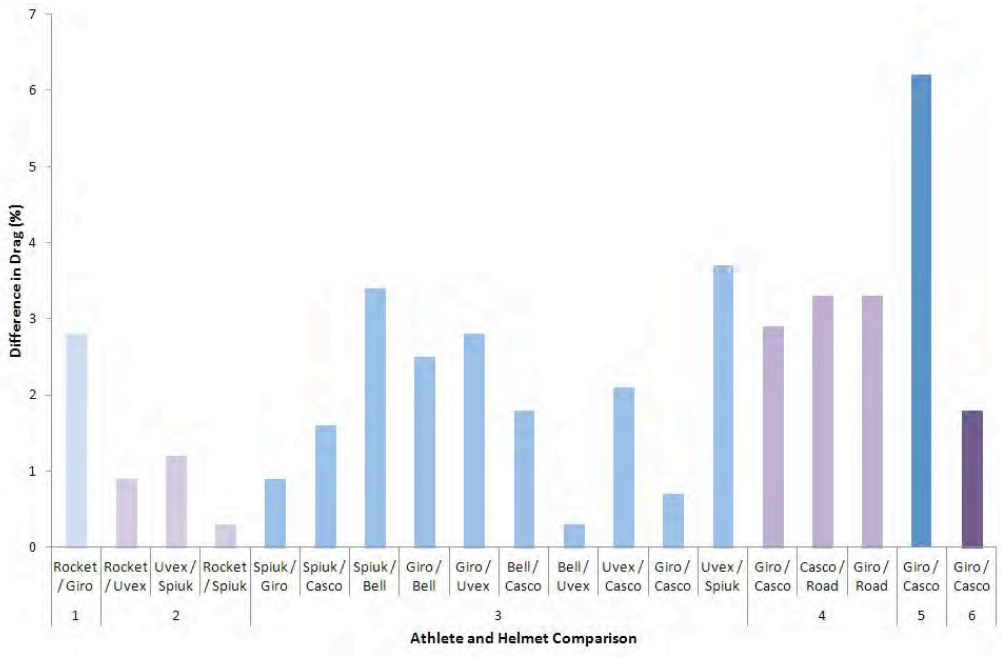

Figure 7.3: Comparison between helmets for different athletes, where the number indicates the athlete identity

These results show that there is a wide variation in percentage difference in drag between helmets for different athletes. The greatest difference in drag was seen between the Giro and Casco helmets for Athlete 5. However, this same comparison was made with three other athletes, for which a smaller difference in drag was seen. Although it was expected that the greatest difference in drag for all athletes would be seen between an aero and non-aero helmet, this was not the case for Athlete 3; the greatest difference in drag for Athlete 3 was seen between the Uvex and Spiuk helmets, both of which are aero helmets. The most aerodynamic helmet for each athlete differed between them, most likely due to the difference in body shape and size, and in the way athletes held their heads during testing. This highlights the importance of individual testing in order to identify the most aerodynamic helmet for a specific athlete.

The presence of a visor or sunglasses will also affect the flow around the face and helmet, so a comparison was made between the presence of a visor or no visor on eleven athletes, all wearing their own helmet and adopting their current racing position on their own racing bike. The aerodynamic drag was measured in the wind tunnel at a speed of 42kph while the athletes were pedalling at 90rpm. The aim of this test was to determine if, in general, a visor has any significant effect on the aerodynamic drag and not to compare different helmets with or without visors. The results are shown in Table 7.4.

Athlete	Drag with visor (kg)	Drag without visor (kg)	△Drag (%)
1	2.178	2.130	-2.2
2	2.208	2.169	-1.8
3	2.147	2.213	+3.0
4	2.528	2.524	-0.2
5	2.093	2.191	+4.5
6	2.204	2.267	+2.8
7	3.314	3.354	+1.2
8	3.106	3.000	-3.4
9	2.943	3.014	+2.4
10	2.115	2.119	+0.2
11	2.464	2.533	+2.7

Table 7.4: Effect of a visor on the aerodynamic drag

The results show that the presence of a visor affects each athlete differently, with some athletes finding an increase in drag with a visor, but some athletes finding a decrease in drag. There is also no noticable trend between the degree to which a visor may or may not affect the aerodynamic drag; the difference in drag between a visor and no visor varies from an insignificant 0.2% to a significant 3.4% between the athletes. These results indicate that the presence of a visor should be tested along with the type of helmet for each athlete individually in order to find the best possible combination.

The majority of aero helmets have vents to allow heat to tranfer from the body to the air in order to keep the athlete cool. All aero helmets used in this study had vents, but the size and shape of these vents varied between the helmets. Alam et al. [2008b] showed that protruded and/or large chanelled vents in a helmet increased the aerodynamic drag, and that the drag could be reduced by covering up the vents. However, the study by Alam et al. [2008b] was only carried out on road helmets, where there are a large number of vents compared to aero helmets. The analysis of the boundary layer thickness over a cyclist described in Chapter 6 also suggested that the drag could be reduced by taping over helmet vents, as in general a lower boundary layer thickness was observed when the helmet holes were taped compared to untaped. Two of the athletes in the helmet comparison study described above also compared the Bell helmet with and without the vents taped over with electrical tape. Both athletes found that the drag was lower when the vents were untaped (0.7% and 1% lower drag), which differs from those results published by Alam et al. [2008b]. It is difficult to draw any sound conclusions about the effect of vent size, shape or location using the results from 2 athletes because it is not known whether the difference in drag is due to the helmet shape, the vents, or a combination of both the helmet and vents. Therefore a more detailed study would be needed to compare the presence, size, shape, and location of vents on helmets of a similar size and shape. Due to limited time constraints and the fact that this was not the main aim for this thesis, the effect on helmet vents on the aerodynamic drag was not carried out, but is recommended as a future study.

7.3 Pedals and Straps

Wind tunnel tests were carried out on different combinations of pedals and straps used by track sprinters to identify the most aerodynamic combination. The tests were carried out using a sprinter on a track, sprint

bike in their reference position, but the tests were stationary; previous tests showed that the trends between pedalling and stationary tests were the same, and that a greater percentage difference in drag could be seen with stationary tests due to the absence of pedalling, which increases the drag readings by 3-4%. To ensure the feet were in the same position for each test a silhouette was drawn on a white board and photos were taken from the side and analysed prior to each test. The straps were covered by a shoe cover during testing, and electrical tape was placed over the bottom of all the pedals, as is commonly done in racing. The wind speed was set at 46kph. Images of the pedals and straps are shown in Figure 7.4, images of the pedal/strap combinations during testing are shown in Figure 7.5, and the results are shown in Table 7.5.

(a) Shimano Pedal

(b) Keywin Pedal

(c) Look Pedal

(d) G-race Straps

(e) Double Leather Straps

Figure 7.4: Images of pedals and straps

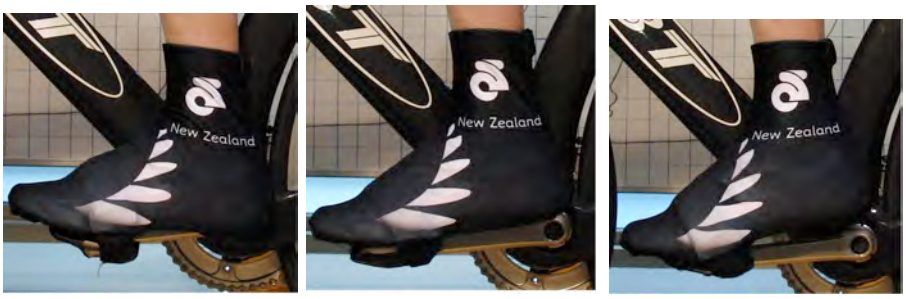

(a) Shimano Pedals with G-Race Straps (b) Keywin Prototype Pedals with G-Race Straps (c) Look Pedals with G-Race Straps

(d) Shimano Pedals with Double Leather Straps (e) Look Pedals with Double Leather Straps

Figure 7.5: Pedal and Strap Combinations

Pedal	Strap	Drag (kg)	Difference in Drag (g)	Difference in Drag (%)
Shimano	G-race	2.6002	0	0
Keywin prototype	G-race	2.6073	7	0.3
Look	G-race	2.6075	7	0.3
Shimano	Double Leather	2.6215	21	0.8
Look	Double Leather	2.6559	56	2.1

Table 7.5: Drag results for different pedal and strap combinations

The results show that the drag is significantly higher when using chunky, double leather straps compared to smoother, G-race, velcro straps under the booties. Out of the pedals tested, the smoother, Shimano pedals were the most aerodynamic. The difference in drag between pedals (same straps) was 1.3% and the difference in drag between the straps (same pedals) was 1.8%. These results suggest that it is more beneficial to have aerodynamic straps compared to pedals, although the right combination of pedals and straps could reduce the drag by as much as 2.1%.

7.4 Gloves

Different types of gloves used for road and/or sprint racing were tested in the wind tunnel to identify whether there was any significant difference in drag between no gloves, smooth, lycra gloves, and larger Kieran gloves.

Images of the typical hand and forearm position on drop bars, and of the different gloves tested are shown in Figure 7.6. The gloves were worn by a road, sprint cyclist, who adopted their current racing position and same hand position for all tests, and all tests were stationary; previous tests showed that the trends between pedalling and stationary tests were the same, and that a greater percentage difference in drag could be seen with stationary tests due to the absence of pedalling, which increases the drag readings by 3-4%. The wind speed was set at 46kph and the uncertainty of the measurements for stationary tests was ±5g. The results, shown in Table 7.6, show that the drag was lowest when no gloves were worn. Out of the three types of gloves tested, the golf type gloves had the lowest drag. These gloves were the closest fitting and did not crease around the wrists like the lycra, Champion System gloves. They were also not as chunky as the Carbon Kieran gloves. Although it would be more aerodynamic for riders not to wear gloves, sprint riders often find that gloves assist with gripping the handlebars during a race. If gloves must be worn, these results suggest they should be as tightly fitting as possible with minimal wrinkles and seams positioned out of the oncoming airflow.

(a) Typical Hand Position

(b) Easton Gloves

(c) Carbon Kieran Gloves

(d) Champion Systems Gloves

Figure 7.6: Type of Gloves Tested

Glove	Drag (kg)	Difference in Drag (g)	Difference in Drag (%)
No Glove	2.6073	0	0
Easton	2.6188	11	0.4
Carbon Kieran	2.6340	27	1.0
Champion Systems	2.6409	34	1.3

Table 7.6: Drag results for different gloves

7.5 Optimal Skinsuit Design

As previously mentioned, the focus of this thesis was to determine the optimal position of a track cyclist in order to maximise their speed. However, I was also approached to help design a new skinsuit for the New Zealand Track Cycling Team, primarily for the endurance athletes, for the London 2012 Olympics. Therefore the remaining part of this Chapter will focus on material selection, seams, and patterns for a skinsuit and shoe covers. Although track cyclists are allowed to wear a two piece garment, consisting of shorts and a jersey, the reduction in aerodynamic drag from wearing a one-piece, long sleeved skinsuit can be as much as 8.4% [Kyle, 2003a, p39]. Therefore, the aim was to develop a new design for a one-piece skinsuit and not a two-piece garment.

In order to create an aerodynamic skinsuit it is necessary to understand the significance of the material type, seam placement, seam type, fit, and comfort. It is also necessary to ensure skinsuits obey the UCI Cycling Regulations, who state that all racing skinsuits for track cycling must have sleeves, and the shorts must come above the knee [UCI Regulations, 2009, version 1.07.2011]. Non essential items of clothing, or items designed to primarily influence the performance (reduce air resistance, compression, stretching, support) are forbidden.

7.5.1 Initial Skinsuit Analysis

An initial visual analysis of the flow around a cyclist was carried out on four, current New Zealand racing skinsuits by taping cotton tufts, 30mm in length, all over the skinsuits. The same athlete wore all skinsuits and adopted their current racing position on their current racing bike for all tests. A description of the skinsuits and images during testing are shown in Table 7.7 and Figure 7.7 repectively. The four skinsuits varied by material type, seam type, seam placement, and use of elastic, although the fit of each skinsuit was tight on the athlete used as the subject for testing. The aerodynamic drag of the skinsuits was also compared for a pedalling athlete in the wind tunnel, at a wind speed of 46kph and pedalling speed of 90rpm.

Skinsuit	**Description**
Skinsuit 1	- Mainly rubberised lycra (nylon laminated)
	- Small patches of lycra on the rear legs, outside of arm and by the zip
	- Most seams bonded
Skinsuit 2	- 80% polyester, 20% lycra (dyed black)
	- Mesh panels under the armpits and on the rear outside of the legs
	- Most seams on the inside
Skinsuit 3	- 74% polyester, 26% lycra
	- Elastic at the end of the arms and legs
Skinsuit 4	- 80% nylon (dimpled) and 20% lycra (smooth) (Figure 7.7e)
	- Elastic on the arms and legs
	- Dimpled sections on the arms, back and bottom of legs

Table 7.7: Description of Skinsuits

(a) Skinsuit 1

(b) Skinsuit 2

(c) Skinsuit 3

(d) Skinsuit 4

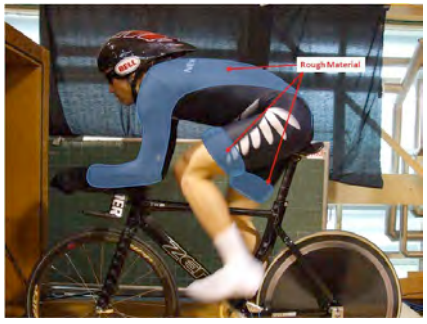

(e) Regions of rough and smooth material for Skinsuit 4

Figure 7.7: Existing New Zealand Skinsuits

Regions of separation were identified on both the outside and inside of the upper arms, under the armpits, on the underside of the torso to the side, and on the lower back and rear of the legs for all skinsuits (Figure 7.8). This analysis quickly identified areas of improvement on these skinsuits in terms of aerodynamic drag.

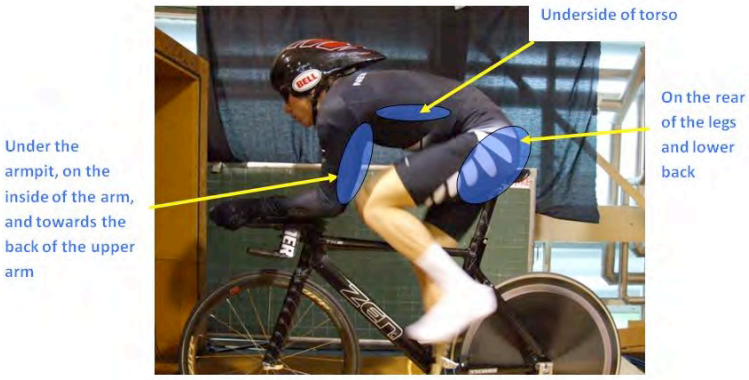

Figure 7.8: Regions of Separation

The results for the measured aerodynamic drag of the skinsuits are shown in Table 7.8. These results show that there is a 3.8% difference in drag between the best and worst skinsuit, with the nylon laminated, rubberised lycra skinsuit having the lowest drag. Most of the seams on skinsuit 1 were bonded, which may have helped reduce the drag compared to the other skinsuits. However, it is also likely that the type of material had a strong influence on the drag, as the material used for skinsuit 1 was very different from the other skinsuits. The skinsuit with the highest drag was made from two different materials, one of which was dimpled. Although it has been suggested that skinsuits with zoned fabric have a lower drag [Kyle and Weaver, 2004, Oggiano et al., 2009] it is possible that the type of material or location of the dimpled fabric on skinsuit 4 was not placed strategically. Alternatively, the influence of the elastic on the arms and legs of skinsuit 4 may have had a negative effect on drag. Although this initial test has shown that there is a significant difference in drag between skinsuits, it is impossible to determine which factor out of the material type, seam type, seam placement, or use of elastic has the greatest influence on drag. It is therefore necessary to analyse the effect of each of these factors on the aerodynamic drag in isolation.

Skinsuit	**Drag $\pm$ 0.02 (kg)**	**Difference in Drag (%)**
1	2.049	0
2	2.060	0.5
3	2.092	2.0
4	2.129	3.8

Table 7.8: Drag results for skinsuits

7.5.2 Material and Seam Placement Analysis

A cyclist can be thought of as a combination of roughly cylindrical arms, thighs, and calves, a roughly spherical head, and a torso with characteristics similar to that of a flat plate. A simple model like this is useful for analysing different types of materials that could be used to make up a skinsuit. Three circular cylinders with diameters of 56mm, 69.6mm, and 111mm, and rounded heads at the leading edge with an axial

extent of 1.5, 1.6, and 1.7 respectively were manufactured to represent a forearm, upper arm and thigh of a cyclist. Each cylinder was placed in the high speed wind tunnel at the University of Canterbury in both a streamwise and spanwise orientation and the drag measured for the cylinders covered with different material sheath samples, as well as without any material on, at wind speeds between 50kph and 80kph; elite endurance riders travel at 53-65kph and elite sprinters can reach speeds of 75-80kph when racing. Each material sample had only one simple, stitched seam in the longitudinal direction to join the sheath together, with no finish (seam, elastic or fold) at the ends; the ends were raw. When in the spanwise orientation the seam was placed at the rear of the cylinder out of the flow, and in the streamwise orientation the seam was placed underneath the cylinder. The location of the seam on all material samples in the spanwise orientation was then compared using the 69.6mm and 111mm diameter cylinders in 30° increments. It was not deemed necessary to analyse the seam placement on the streamwise cylinders, as the flow would be the same regardless of the location of the seam when in this orientation. The drag of the rods without the cylinders attached was also measured by suspending the cylinders in front of, but not connected to the rod, as shown in Figure 7.9, so that only the drag of the cylinders was used to determine the drag coefficient, $C_d = \frac{D}{\frac{1}{2}\rho A V^2}$, where D is the measured drag of the cylinder (N), ρ is the air density (kgm^{-3}), A is the frontal area (m^2), and V is the wind speed (ms^{-1}). The dimensions of the three cylinders used for material testing are shown in Figure 7.10, and the position of the material samples on the cylinders are shown in Figure 7.11.

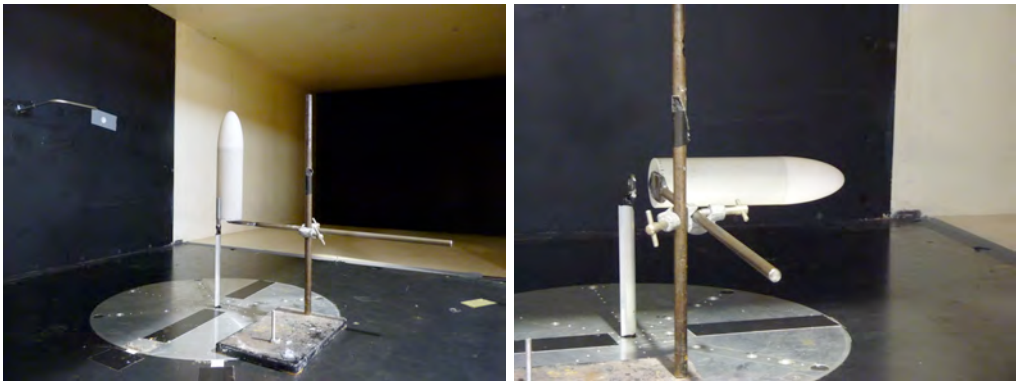

Figure 7.9: Measuring the Drag of the Rod

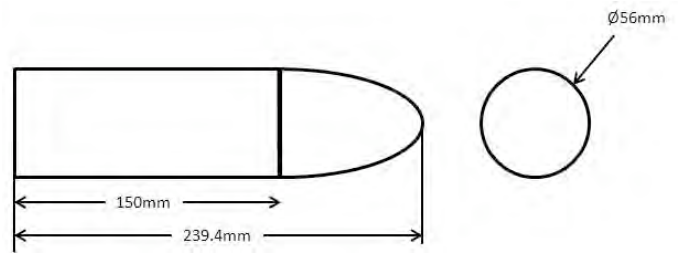

(a) Small Cylinder

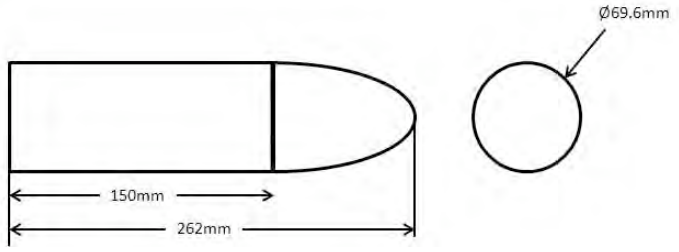

(b) Medium Cylinder

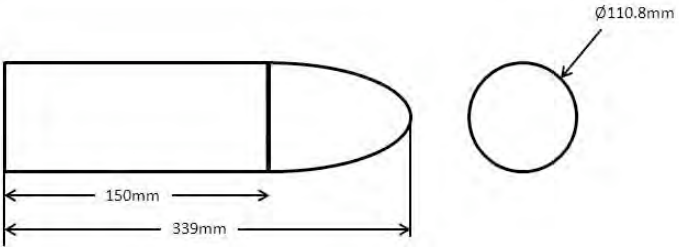

(c) Large Cylinder

Figure 7.10: Dimenstions of Circular Cylinders

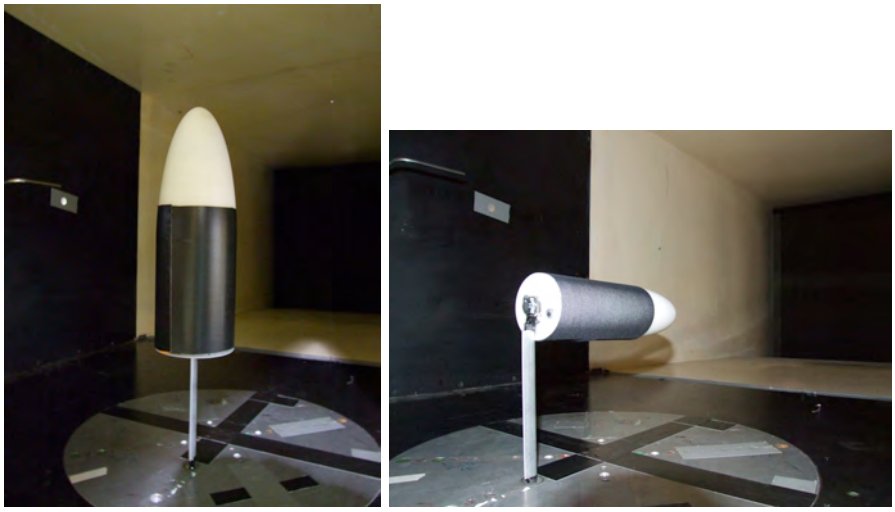

Figure 7.11: Position of the Material Samples on the Cylinders

7.5.2.1 Repeatability and Relative Uncertainty

The greatest error comes from the force balance measurements and ensuring the cylinders and sheaths are repositioned in the same position for each test. For each cylinder/material combination the tests were repeated at 53.8kph and 64.3kph by recovering the cylinder again after all the initial tests had been carried out. This enabled the accuracy of removing and recovering the cylinder with the different material samples to be analysed. The maximum difference between repeat material/cylinder combinations and the corresponding initial material/cylinder combination was ±0.002kg, implying all drag measurements were accurate to 0.002kg. Drag readings in the streamwise orientation ranged from 0.018kg to 0.087kg on the small and large cylinders respectively, and in the spanwise orientation from 0.11kg to 0.61kg for the small and large cylinders respectively. This corresponds to an accuracy of ±2% and ±11% on the large and small cylinders respectively in the streamwise orientation, and only ±0.3% and ±2% on the large and small cylinders respectively in the spanwise orientation.

Additional errors are associated with the wind speed, air density, frontal area calculation, and human error. The wind speed was determined in the same way as for the boundary layer wind tunnel, for which the uncertainty was calculated to be ±0.06kph (±0.075% at 80kph and ±0.1% at 50kph). The air density was also calculated to be accurate to ±0.4% at a temperature of 20°C and pressure of 1000mbar. The frontal area of the cylinders was calculated using the digitizing method when in the spanwise orientation, and assumed to be equivalent to the diameter of the cylinder when in the streamwise orientation. To determine the error associated with the digitizing method the frontal area was calculated for the small and large cylinder three times each, and the maximum difference between frontal area calculations found to be ±0.001m^2 for the large cylinder and ±0.0001m^2 for the small cylinder. This is equivalent to an accuracy of ±3% on the large cylinder and ±0.8% on the small cylinder. The error associated with calculating the diameter of the cylinders (for calculating the frontal area in the streamwise orientation) was accurate to ±0.05mm (±0.09% on the large cylinder and ±0.045% on the small cylinder).

The uncertainties mentioned above are all propagated to the calculation of drag area, $C_d = \frac{F}{\frac{1}{2}\rho A V^2}$, so the total error for the drag area can be calculated by:

$$\frac{\delta C_d}{C_d} = \sqrt{(2\frac{\delta V}{V})^2 + (\frac{\delta F}{F})^2 + (\frac{\delta \rho}{\rho})^2 + (\frac{\delta A}{A})^2}$$

As the errors associated with the different cylinder diameters, orientations, and wind speeds differs, it is necessary to calculate the maximum and minimum error in both the spanwise and streamwise orientations:

$$\frac{\delta C_d}{C_d}_{StreamwiseMax} = \sqrt{(2 \times 0.001)^2 + (0.11) + (0.004)^2 + (0.0009)^2} = 12\%$$

$$\frac{\delta C_d}{C_d}_{StreamwiseMin} = \sqrt{(2 \times 0.00075)^2 + (0.02)^2 + (0.004)^2 + (0.00045)^2} = 2\%$$

$$\frac{\delta C_d}{C_d}_{SpanwiseMax} = \sqrt{(2 \times 0.0001)^2 + (0.018)^2 + (0.004)^2 + (0.03)^2} = 3.5\%$$

$$\frac{\delta C_d}{C_d}_{SpanwiseMin} = \sqrt{(2 \times 0.0001)^2 + (0.003)^2 + (0.004)^2 + (0.008)^2} = 0.9\%$$

The results above show that the maximum error of 12% is associated with the small cylinder at 50kph in the streamwise orientation. Although this appears to be a large error, it is primarily due to the accuracy of the force balance, of only ±0.002kg, on such small drag readings on the small cylinder in the streamwise orientation at low speeds. A summary of the error associated with each cylinder in both the spanwise and streamwise orientations at all wind speeds is shown in Table 7.9.

Cylinder		Wind Speed (kph)						
Orientation	**Diameter (m)**	**49.5**	**53.8**	**57.6**	**61**	**64.3**	**71.5**	**78.8**
Streamwise	0.0560	11.6	10.0	8.8	7.8	7.1	5.8	4.9
	0.0696	10.5	8.9	7.9	6.9	6.3	5.1	4.3
	0.1108	5.8	4.9	4.4	3.9	3.6	2.9	2.4
Spanwise	0.0560	3.5	3.4	3.3	3.2	3.2	3.1	-
	0.0696	2.4	2.3	2.2	2.1	2.1	2.1	2.0
	0.1108	1.2	1.1	1.0	1.0	1.0	0.9	-

Table 7.9: Percentage error for each cylinder in the spanwise and streamwise orientations at all wind speeds tested

7.5.2.2 Material Samples

Cycling skinsuits need to be elastic, have good recovery properties, have good breathability and temperature regulation, be resistant to mechanical wear, be able to wick sweat away from the body to keep the body dry, and also be comfortable. The most common materials used for making skinsuits are lycra (spandex, polyeurothane), polyamides (nylon) and polyester, as these materials satisfy the textile parameters for a high performing cycling skinsuit. Lycra is a particularly popular skinsuit material because of its built-in, lasting elasticity that allows the garment to fit like a second skin without being uncomfortable and binding [Apparel, 2012]. Polyester is durable, elastic, and lightweight with a comfortable, smooth feel, but is often chemically treated so that the material is able to wick moisture away from the skin [Chaudhari et al., 2004]. Nylon is lightweight, has a high strength and softness with good durability, and has a much higher moisture regain than polyester [Chaudhari et al., 2004]. It is most often used in tightly woven outerwear, which can trap heat because of low air permeability [Chaudhari et al., 2004].

One of the most popular technical fabric manufacturers are Eschler, a Swiss company who have developed functional fabrics for a number of applications, including sports apparel. The majority of the materials developed by Eschler for sports apparel are knitted fabrics, with unique polyamide/elastane constructions with different levels of elasticity and different layers for sweat absorption, climate regulation, and protection from wind and water [Eschler, 2012]. Knitted fabrics are also often prefered over woven fabrics for tight-fitting garments [Oggiano et al., 2009]. It is not always possible to obtain all the desirable attributes of functional sportswear using a simple structure of any single fibre or blend, so often a two-layer structure is used to create a layer close to the skin using a material that wicks moisture away from the skin, such as fine, dense polyester fibres, and an outer layer that absorbs and evaporates the moisture [Chaudhari et al., 2004].

The tightness of knitted and woven fabrics is often defined by the ratio between the area covered by yarns to the total area of the web, known as the Cover Factor (CF) [Tapias et al., 2010]. Methods of determining the Cover Factor for different fabrics include using image processing of a microscope image of a fabric sample and tallying the pixels in binarized images produced by thresholding [Tapias et al., 2010] or using the information of yarn count (Tex) and length of a stitch provided by the manufacturer, where $CF^2 = \frac{Tex}{L^2}$ $(\text{g}/(\text{km mm}^2))^{0.5}$ [Oggiano et al., 2009]. In general, the Cover Factor gives an indication of the extent to which the area of a fabric is covered by the yarn, and of the relative looseness or tightness of the knitted structure [Oggiano et al., 2009]. Typical Cover Factor values obtained from image processing of a microscope image of a woven fabric sample range from 0.4 to 0.9 [Tapias et al., 2010].

Six different material samples provided by an independent skinsuit and wetsuit manufacturer were selected on the basis that they would satisfy the required attributes for a skinsuit material (elastic, breathable, regulate temperature, resistant to mechanical wear, and wick sweat away from the body) and were tested on all three cylinders in both the streamwise and spanwise orientations. An additional sample of the material from the best existing New Zealand skinsuit described in Section 7.5.1 (Skinsuit 1, named Material 7 for the material testing) was also tested on the 69.6mm diameter cylinder for comparison. The micro surface of the inside and outside of each material sample was viewed under a microscope at magnification 5X, images of which are shown in Figures 7.12 and 7.13, and the Cover Factor was determined for each sample using a free image processing tool (ImageTool) whereby the microscope images were converted to grayscale for binary formatting and then manually thresholded before counting the number of black and white pixels, as shown in Figure 7.14. The Cover Factor is the ratio of black or white pixels of the yarn to the total number of pixels in the image. A description of each material sample and the area mass is given in Table 7.10. The calculated Cover Factor (CF) values for each material sample is given in Table 7.11. These results show that the material samples were a combination of woven and knitted fabrics, some of which had a significant coating on the outer surface, and that Material 4 was the most compact (tightest) sample and Material 1 was the least compact (loosest) sample. Images of the outer micro surface of the material samples (Figure 7.12) show that materials 1, 2, 3 and 7 have more defined pores on their outer surface compared to the other materials, but the size and pattern of these pores varies between the materials. The inner microsurface does not vary significantly between all woven or all knitted samples.

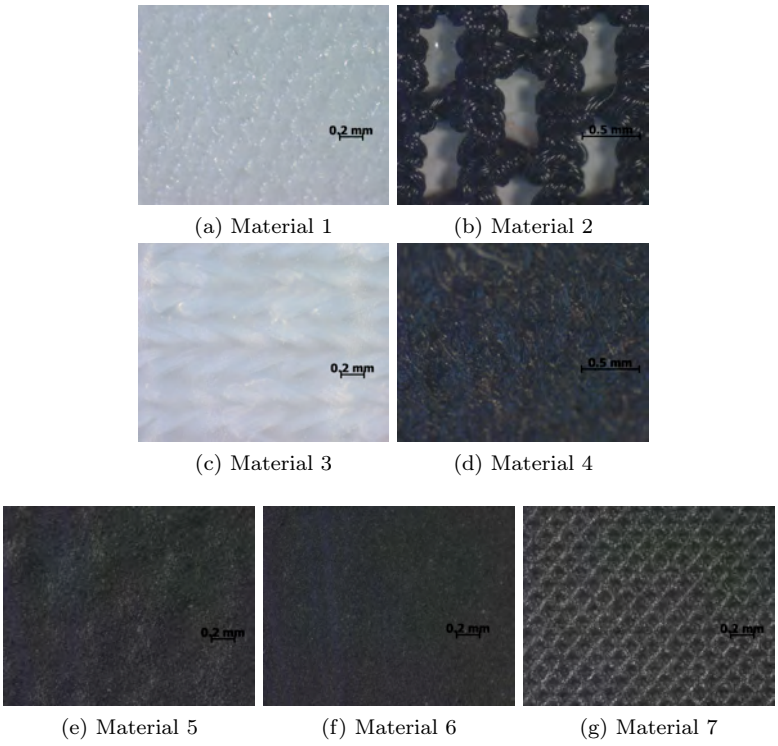

(a) Material 1 (b) Material 2

(c) Material 3 (d) Material 4

(e) Material 5 (f) Material 6 (g) Material 7

Figure 7.12: Micro-Surface (outer) of the Material Samples

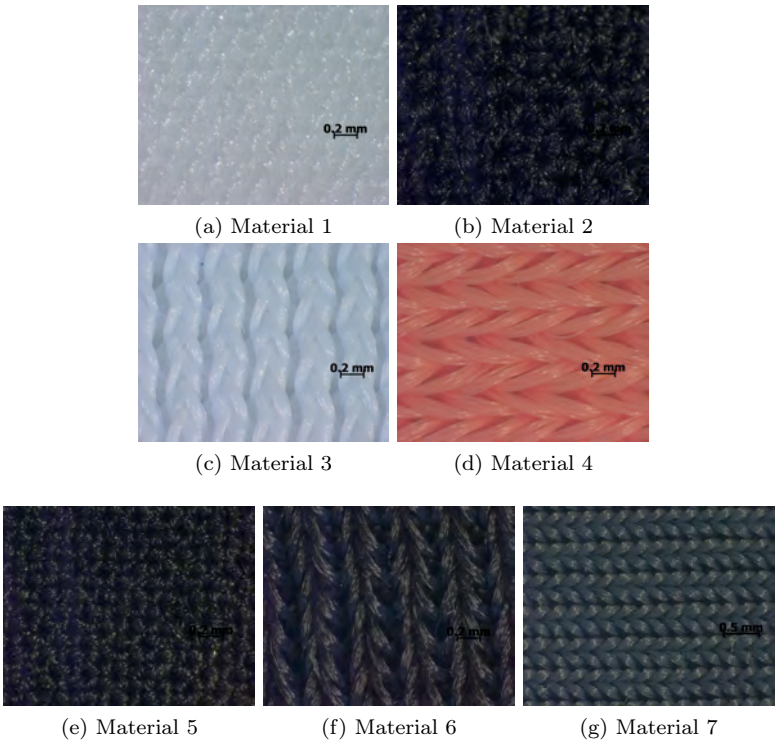

(a) Material 1 (b) Material 2

(c) Material 3 (d) Material 4

(e) Material 5 (f) Material 6 (g) Material 7

Figure 7.13: Micro-surface (inner) of the Material Samples

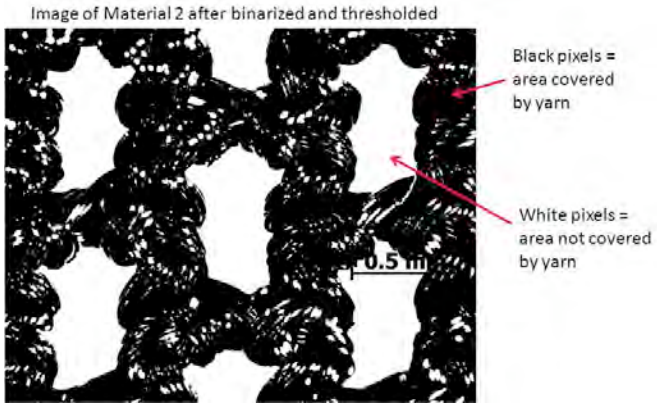

Figure 7.14: Calculating the Cover Factor using Image Processing

	Material	Coating	Area Mass (gm^{-2})
1	78% polyamide, 22% elastane, woven	Lightweight polyurethane membrane	187
2	78% polyamide, 22% elastane, woven	Polyurethane in 'honey-comb' texture	293
3	80% polyamide, 20% elastane, knitted	Dimpled polyurethane	213
4	80% polyamide, 20% elastane, knitted	Dimpled polyurethane with heavy all-over polyurethene induction	267
5	70% polyamide, 30% elastane, woven	Waterproof membrane	213
6	76% polyamide, 24% polyeurothane elastane, knitted	unknown coating	187
7	rubberised lycra with bonded seams, knitted	unknown coating	213

Table 7.10: Properties of the Material Samples

Material	# Black Pixels	# White Pixels	% Black Pixels	% White Pixels	Total # Pixels	Cover Factor	Yarn Colour in Image (Black or White)
1	726373	612627	54.25	45.75	1339000	0.46	White
2	888515	450485	66.36	33.64	1339000	0.66	Black
3	357050	981950	26.67	73.33	1339000	0.73	White
4	1171141	167859	87.46	12.54	1339000	0.87	Black
5	467845	871155	34.94	65.06	1339000	0.65	White
6	529708	809292	39.56	60.44	1339000	0.60	White
7	932651	406349	69.65	30.35	1339000	0.70	Black

Table 7.11: Calculated Cover Factor Values for all Material Samples

The thickness of each material sample was determined by placing each sample under the microscope at a magnification of 5X and measuring the height of the peaks and troughs, including the coating, as shown in Figure 7.15. The results are shown in Table 7.12, and clearly show that Material 5 is by far the thinnest (0.274mm), and Material 2 is the thickest (0.660mm); the thickness varied by only 0.386mm between samples. By placing the materials on the cylinders, the diameter of the cylinders would only increase by a minimum of 0.548mm and a maximum of 1.32mm. Figure 7.15 also clearly shows the difference in structure between the woven and knitted fabrics, and between the different coatings.

Material	Thickness ($\pm$0.005mm)
1	0.410mm
2	0.660mm
3	0.555mm
4	0.630mm
5	0.274mm
6	0.480mm
7	0.422mm

Table 7.12: Thickness of Material Samples

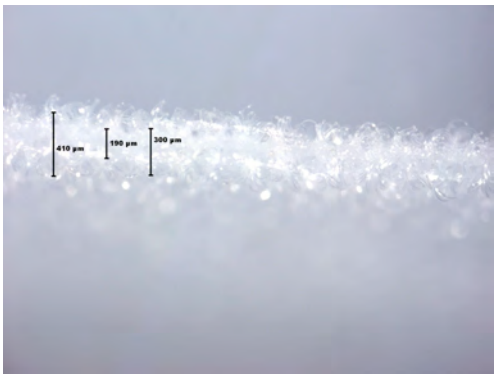

(a) Material 1

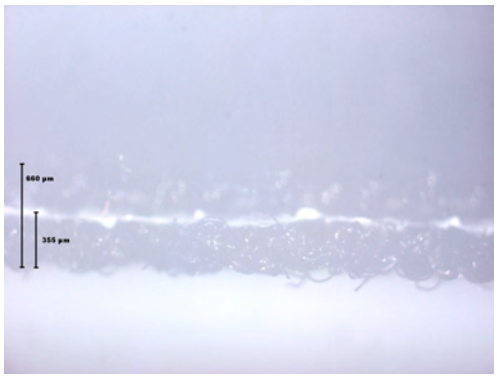

(b) Material 2

(c) Material 3

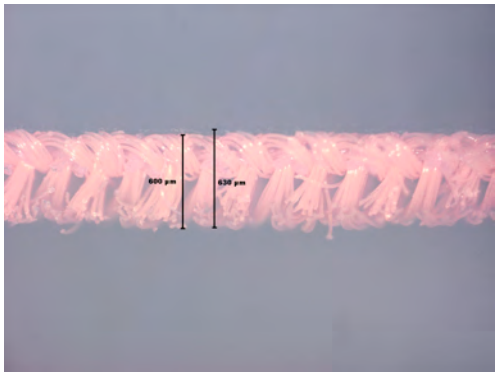

(d) Material 4

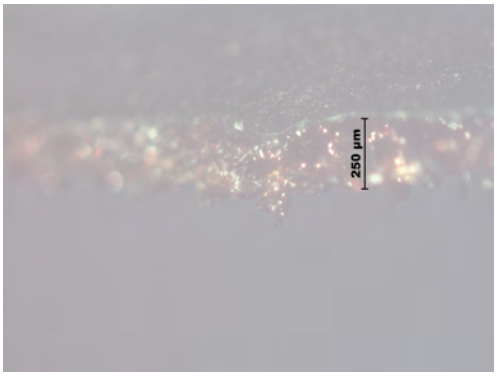

(e) Material 5

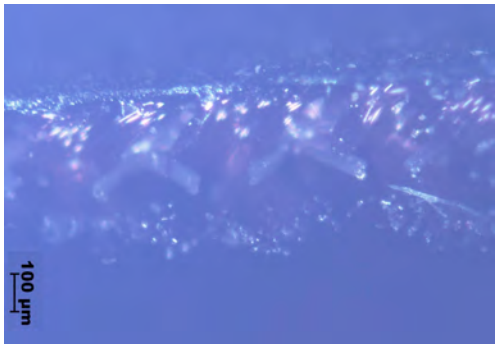

(f) Material 6

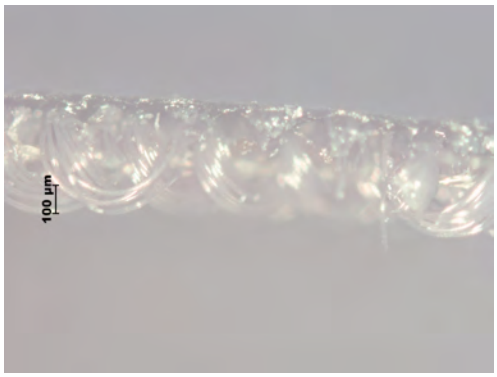

(g) Material 7

Figure 7.15: Thickness of Materials

The elastic modulus of the materials was determined by placing a 150mm by 25mm sample of each material in an Instron machine (MTS 858 Desktop load frame with 10 kN load cell) and applying load to a maximum displacement of 95mm at a test speed of 300±10mm/min. In order to determine whether the orientation of the weave had any effect on the elasticity of the materials, samples of each material in the warp, weft and bias orientations were cut to size. Each material sample was then clamped in the instron machine at a pressure of 15±2psi and stretched to maximum displacement or until failure. The clamped area of the material samples and the area where direct extension occurred can be seen in Figure 7.16. Each material sample was only stretched for one cycle, as during elite track cycling competitions athletes wear a new skinsuit when racing. Therefore it was deemed unneccesary to analyse the elastic properties of each material sample under cyclic loading, although it would be expected that there would be some loss in elastic modulus during repeat cycles. It was also expected that the materials would be strongest in the bias orientation, due to the no-slip condition.

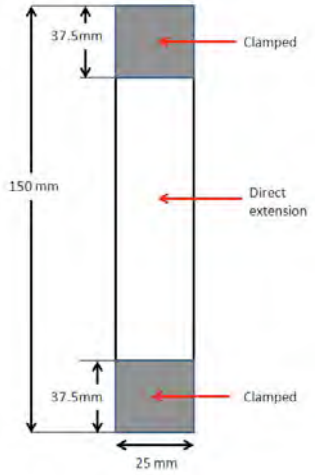

Figure 7.16: Clamped Area and Area where Direct Extension Occurred for each Material Sample

The force-displacement and stress-strain curves were generated for each sample, and the force at maximum displacement (95mm displacement, 1.26 strain) or at failure was determined for each material. The stress-strain curves are shown in Figure 7.17, and a bar chat of the force at maximum displacement or at failure for each sample shown in Figure 7.18.

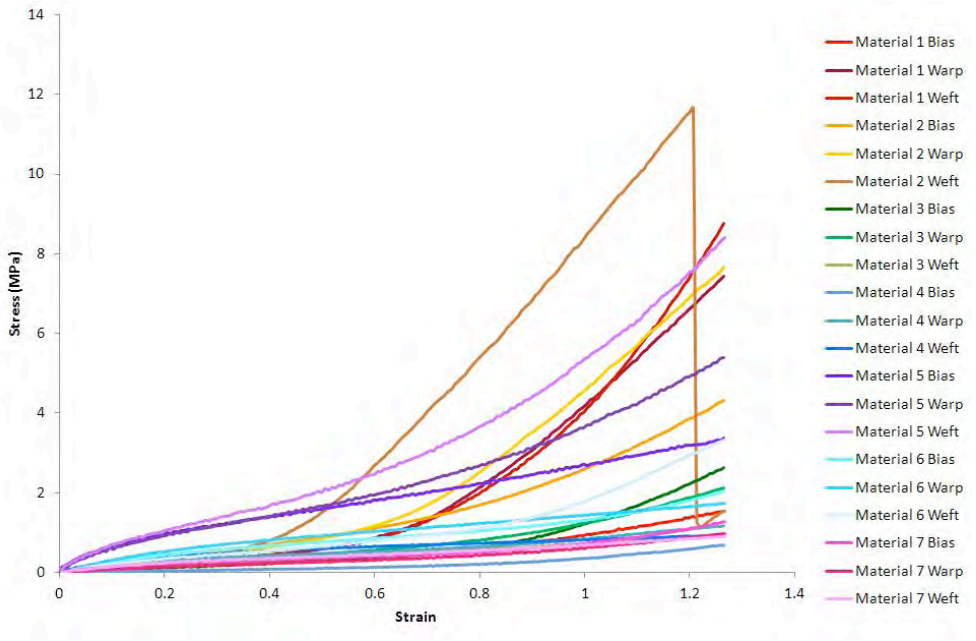

Figure 7.17: Stress-Strain Curve

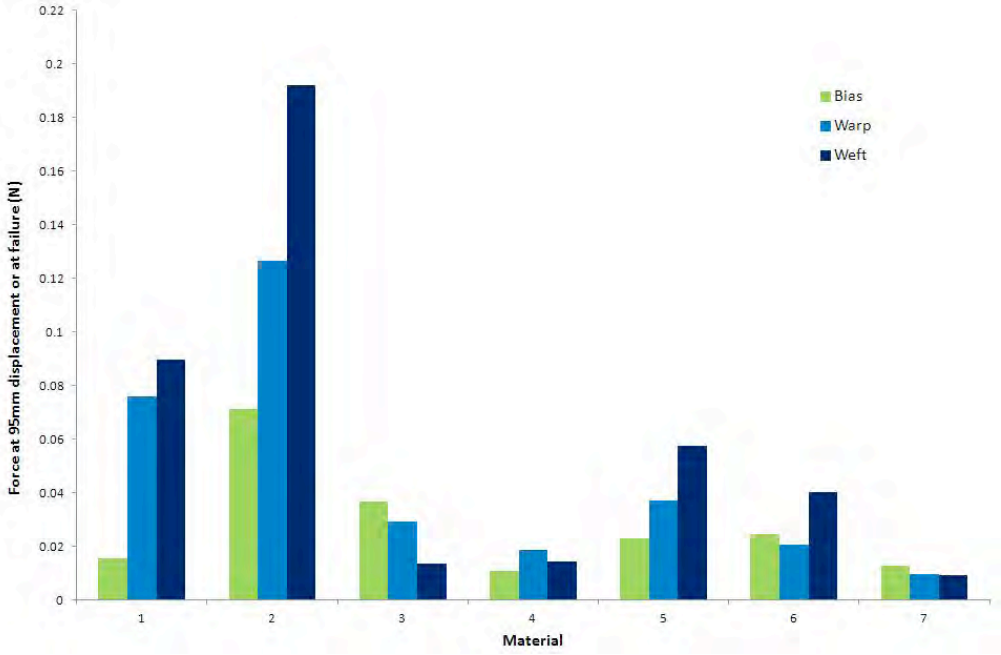

Figure 7.18: Force at Maximum Displacement (95mm) or Failure

The results for the elasticity of the materials show that the relationship between stress and strain is almost linear for most materials when stretched to maximum displacement. Only Material 2 in the weft orientation

failed, at a stress of 11.64MPa and strain of 1.19, which suggests that all other samples are strong and have good stretchability. All materials had a low stress up to 0.4 strain, with Material 5 showing a slightly higher stress up to 0.4 strain in all orientations compared to the other materials tested. At 0.4 strain Material 2 in the warp orientation showed a large increase in stress. Materials 4 and 7 appeared to have the lowest force at maximum deformation, suggesting these two materials were the most elastic out of all samples tested. The results show that all materials except for Material 2 in the weft orientation would be suitable for skinsuit material, as no permanent deformation was observed, although materials 4 and 7 provide a more gentle and linear stretching force. The results also show that the stress-strain curve did not differ significantly for most materials regardless of the orientation. This information is useful for the manufacturers of skinsuits, as they would not need to take into account the orientation of the material when cutting the patterns for a skinsuit made out of any of these materials, except perhaps for Material 2.

A calculation of the elastic modulus was performed for each material sample in all orientations to a strain of 0.6. This strain value was chosen as it represented the actual strain of a skinsuit on a swimmer's thigh [Searle, 2012], which was thought to be similar to the actual strain of a skinsuit on a cyclist. In order to calculate the elastic modulus a second order polynomial trend line was fitted to the stress strain curve for each material sample in each orientation up to a strain of 0.6, and the equation of the trend line differentiated. This differential is equivalent to the elastic modulus, which was calculated for a strain of 0.6. The stress-strain curves and polynomial trends for each material sample are shown in Figure 7.19, and the calculated elastic modulus for each sample in each orientation shown in Table 7.13.

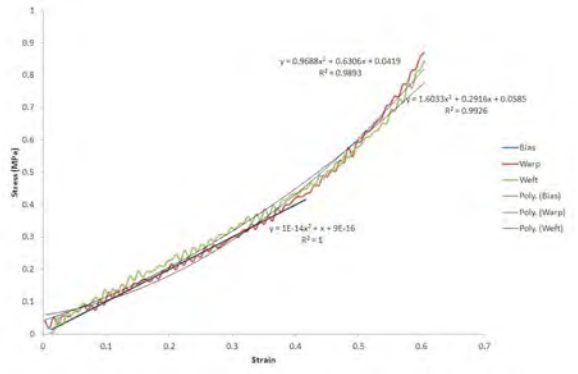

(a) Material 1

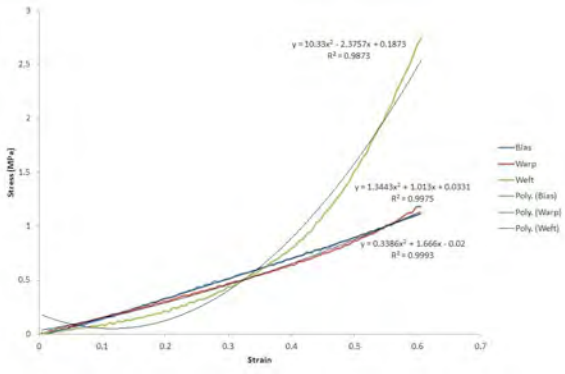

(b) Material 2

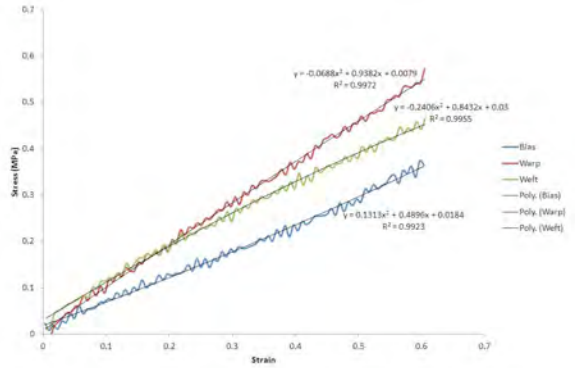

(c) Material 3

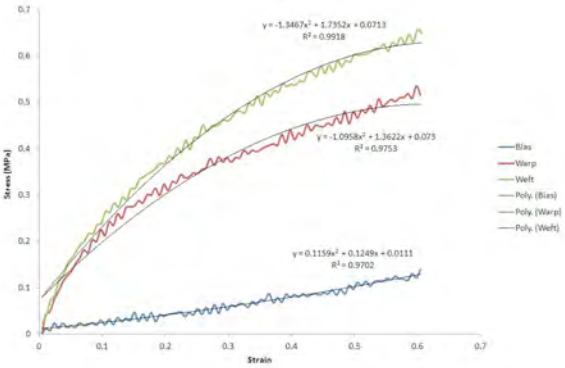

(d) Material 4

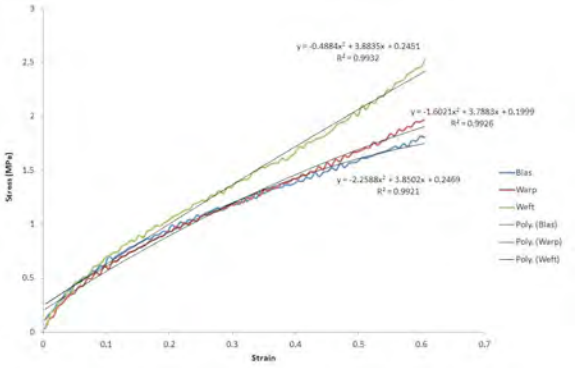

(e) Material 5

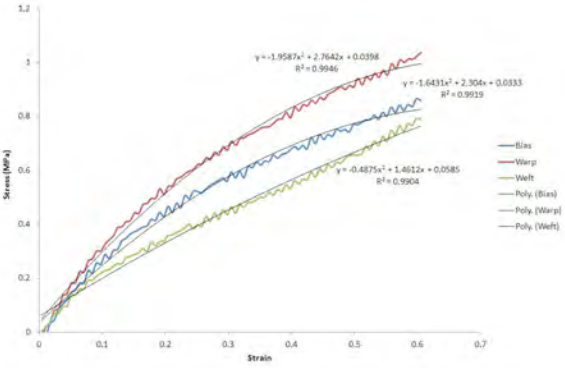

(f) Material 6

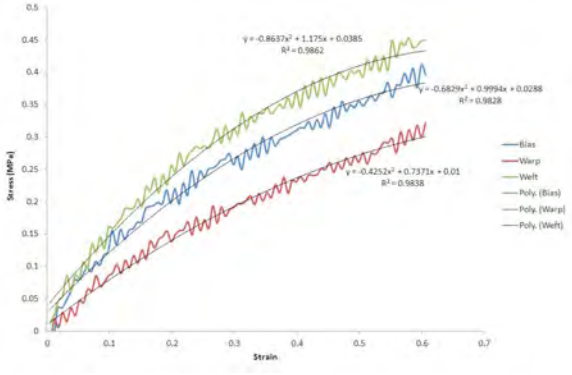

(g) Material 7

Figure 7.19: Stress-Strain Curves to 0.6 Strain and Polynomial Trend

Material	Orientation	Elastic Modulus at 0.6 strain (MPa)
Material 1	Bias	1.00
	Warp	1.79
	Weft	2.22
Material 2	Bias	2.07
	Warp	2.63
	Weft	10.02
Material 3	Bias	0.65
	Warp	0.86
	Weft	0.55
Material 4	Bias	0.26
	Warp	0.05
	Weft	0.12
Material 5	Bias	1.14
	Warp	1.87
	Weft	3.30
Material 6	Bias	0.33
	Warp	0.41
	Weft	0.88
Material 7	Bias	0.18
	Warp	0.23
	Weft	0.14

Table 7.13: Elastic Modulus of each Material Sample in each Orientation

The results in Table 7.13 show that the elastic modulus for Material 2 is significantly greater in the weft orientation compared to the bias and warp orientations (a 74-79% increase in elastic modulus). Materials 1 and 5 also showed a relatively large increase in elastic modulus in the weft orientation compared to the bias or warp orientations, but for all other materials the elastic modulus did not differ significantly with orientation. The orientation which resulted in the lowest elastic modulus differed between materials; the elastic modulus was lowest in the bias orientation for Materials 1, 2, 5 and 6, the warp orientation for Material 4, and the weft orientation for Materials 3 and 7. The results also show that Materail 7 had a relatively low elastic modulus in all orientations, which could have been due to the rubberised lycra material.

Although the results show that the stress-strain curves did not differ significantly between the orientations, except for Material 2, it is possible that these materials will have different aerodynamic properties depending on the strain. Therefore the aerodynamic drag of all the materials in the warp orientation at 0.2 and 0.6 strain was measured by placing sheaths on the 69.6mm diameter cylinder in the streamwise orientation with the simple, stitched seam underneath, and placing the cylinder in the high speed wind tunnel at wind speeds of 50kph, 60kph and 70kph. The drag of the supporting rods for the cylinder was subtracted from the measured drag so that only the drag of the cylinder was used to calculate the drag coefficient. The results are shown in Figure 7.20.

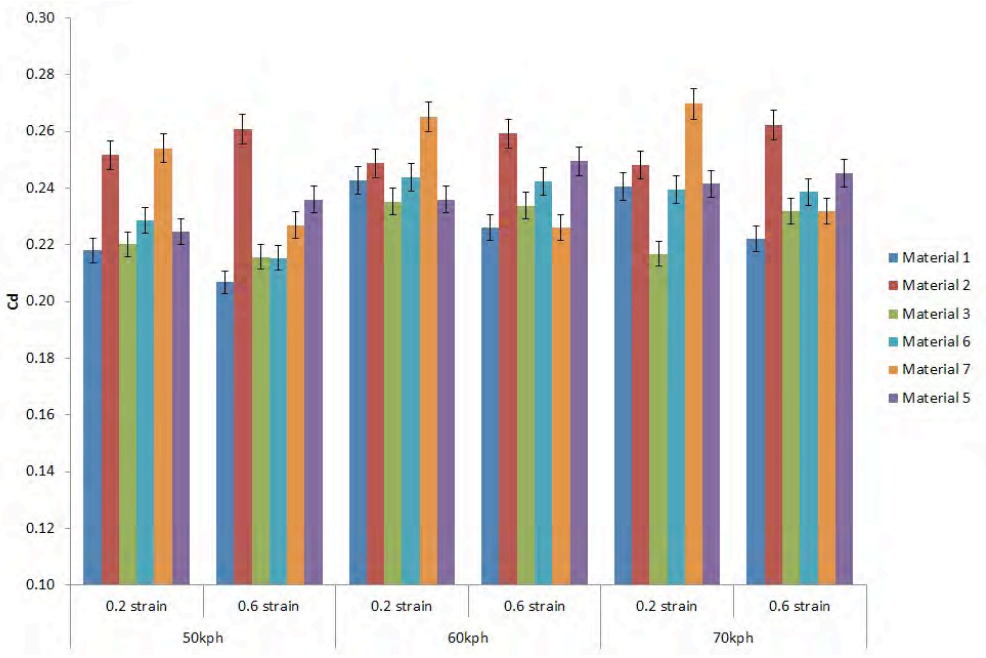

Figure 7.20: Drag coefficient for material samples at 0.2 and 0.6 strain on the 69.9mm diameter cylinder in the streamwise orientation

It appears that only Material 7 shows a significant decrease in drag coefficient with increase in strain, and that for all other materials there are no consistent trends between the drag coefficient at 0.2 and 0.6 strain outside the error bars. These results suggest that the degree to which the material is stretched when on an athlete in their racing position would only be important if Material 7 was used as the material to make the skinsuit.

Another factor which must be considered when analysing different materials for skinsuits is the surface roughness. The roughness of the material samples could not be analysed using the Talysurf 10 (Taylor Hobson Inc.) because some samples were too rough to be detected. Therefore the thickness of the peaks and troughs of the samples were estimated using a microscope with a magnification factor of 5X to provide a value for the depth, d, of the excrescences, as can be seen in Table Figure 7.21 and 7.14. In addition, the average length, L, and width, W, of the excrescences (average of 5 measurements at random locations) and the distance between the centres of excrescences, A, were estimated for each material, as shown in Figure 7.22 and Table 7.15. A roughness factor, k, and dimensionless roughness coefficient, r, could then be calculated using Equations 7.1 and 7.2 respectively to provide a roughness scale for the samples [Oggiano et al., 2006], where r is the dimensionless roughness coefficient, k is the roughness factor (mm), W is the width of the excrescences (mm), d is the depth of the excrescences (mm), and D is the diameter of the cylinder (m). The results for the roughness factor and roughness coefficient can be seen in Table 7.16. It was assumed that the height of the coating for the coated materials was equal to the maximum depth of the protrusions, and that the coated materials were smoother than the uncoated materials, because the length, width and distance between excrescences could not be measured for the coated samples. The rank of the material samples from rough to smooth can be seen in Table 7.17.

$$k = \sqrt{W.d} \tag{7.1}$$

$$r = \frac{k}{D} \tag{7.2}$$

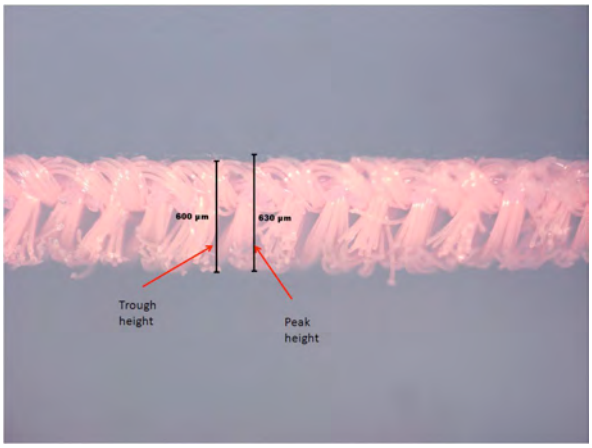

Figure 7.21: Depth of excrescences for Material 4

Material	Peak Height (mm)	Trough Height (mm)	Height of Peaks Above Troughs (Depth) (mm)	Rank of Materials Rough to Smooth
1	0.410mm	0.300mm	0.110mm	Material 2
2	0.660mm	0.355mm	0.305mm	Material 3
3	0.555mm	0.470mm	0.085mm	Material 1
4	0.630mm	0.600mm	0.030mm	Material 4
5	0.274mm	0.250mm	0.024mm	Material 7
6	0.480mm	0.415mm	0.065mm	Material 6
7	0.422mm	0.378mm	0.044mm	Material 5

Table 7.14: Height of Peaks and Troughs of the Material Samples

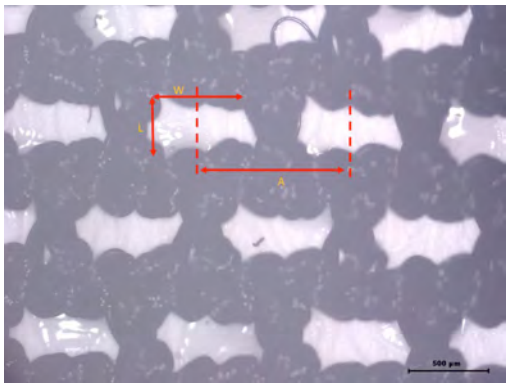

Figure 7.22: Calculating the length, L, and width, W, of excrescences and the distance, A, between them

Material	**Depth, d (μm)**	**Width, W (μm)**	**Length, L (μm)**	**Distance, A (μm)**	k **(μm)**
1	110	203	220	234	149
2	305	630	246	948	438
3	85	642	573	1066	85
4	30	N/A	N/A	N/A	N/A
5	24	N/A	N/A	N/A	N/A
6	68	N/A	N/A	N/A	N/A
7	26	51	51	67	36

Table 7.15: Parameters of Material Samples

Material	k	**r**		
	(mm)	**(D=56mm)**	**(D=69.6mm)**	**(D=111mm)**
1	0.149	$2.7\text{x}10^{-3}$	$2.1\text{x}10^{-3}$	$1.3\text{x}10^{-3}$
2	0.438	$7.8\text{x}10^{-3}$	$6.3\text{x}10^{-3}$	$3.9\text{x}10^{-3}$
3	0.085	$1.5\text{x}10^{-3}$	$1.2\text{x}10^{-3}$	$0.7\text{x}10^{-3}$
4	N/A	N/A	N/A	N/A
5	N/A	N/A	N/A	N/A
6	N/A	N/A	N/A	N/A
7	0.036	$0.7\text{x}10^{-3}$	$0.5\text{x}10^{-3}$	$0.3\text{x}10^{-3}$

Table 7.16: Roughness Factor and Roughness Coefficient of Material Samples

Rank	According to Peaks and Troughs	According to Roughness Factor
Roughest	2	2
|	3	3
|	1	1
|	4	7
|	7	
\\|/	6	
Smoothest	5	

Table 7.17: Rank of Materials: Rough to Smooth

These results show that Material 2 was the roughest sample tested, and Materials 5, 6 and 7 were the smoothest. The influence of surface roughness on circular cylinders in the spanwise orientation has been analysed by Hoerner [1965] who showed that the critical surface roughness is dependent on Reynolds number, and that the drag coefficient can be reduced between $5x10^4$<Re<$4x10^5$ by using varying degrees of surface roughness (Figure 7.23).

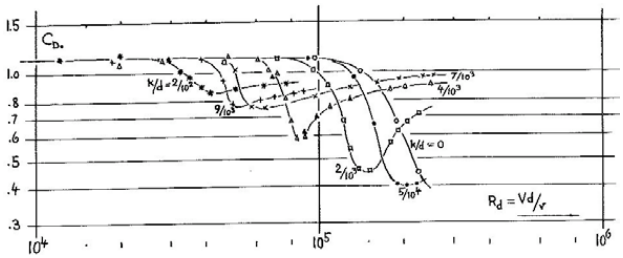

Figure 7.23: Effect of surface roughness on drag coefficient

Using the information from Figure 7.23 [Hoerner, 1965] it is possible to predict which material sample will have the lowest drag coefficient on each of the circular cylinders in the spanwise orientation. Firstly, the Reynolds number for the circular cylinders in the spanwise orientation between 50kph and 80kph must be calculated (Table 7.18):

Cylinder		Speed (kph)						
		49.5	**53.8**	**57.6**	**61**	**64.3**	**71.5**	**78.8**
Re ($x10^5$)	Small (Ø=0.056m)	0.51	0.55	0.59	0.63	0.66	0.73	0.81
	Medium (Ø=0.0696m)	0.63	0.69	0.74	0.78	0.82	0.91	1.00
	Large (Ø=0.111m)	1.01	1.09	1.17	1.24	1.31	1.45	1.60

Table 7.18: Reynolds Number for the Three Cylinders in the Spanwise Orientation

It is then possible to determine the roughness coefficient, k, that would result in the lowest drag coefficient for each cylinder at the relevant speeds. For example, the small cylinder, with a diameter of 0.056m, at 61kph has a Reynolds number of 0.63x10^5, which from Figure 7.23 shows that the lowest drag coefficient occurs at $\frac{k}{d} = \frac{2}{10^2} = 0.02$, so k=1.1mm. The calculated optimal roughness coefficients for all cylinders at all speeds are shown in Table 7.19:

Cylinder		**Speed (kph)**						
		49.5	**53.8**	**57.6**	**61**	**64.3**	**71.5**	**78.8**
k **(mm)**	Small (Ø=0.056m)	1.1	1.1	1.1	1.1	1.1	0.5	0.4
	Medium (Ø=0.0696m)	1.4	1.4	0.6	0.6	0.5	0.3	0.1
	Large (Ø=0.111m)	0.4	0.4	0.4	0.4	0.4	0.4	0.2

Table 7.19: Optimal Surface Roughness for Cylinders in the Spanwise Orientation according to Hoerner [1965]

Tables 7.18 and 7.19 show that according to Hoerner [1965] the material samples should have a roughness between k =0.1mm and 1.4mm, depending on the diameter of the cylinder and wind speed, in order to obtain the lowest possible drag coefficient. This would suggest that for wind speeds between 50kph and 80kph only Materials 1 and 2 are rough enough to cause the drag coefficient to drop when on the circular cylinders in the spanwise orientation. As the materials are stretched over the circular cylinders it would be expected that the roughess coefficient would be reduced slightly. However, the results for the aerodynamic drag when stretched (Figure 7.20) suggests that there is no significant change to the surface roughness for the degree to which the materials are stretched over the cylinders, as there was no significant gain or loss in drag coefficient for the rougher materials (Material 2).

7.5.2.3 Aerodynamic Drag of Material Samples

Once the thickness, elasticity, and roughness of all the material samples had been analysed it was possible to compare the aerodynamic drag of all the materials in both the streamwise and spanwise orientations. All material samples were stretched to 0.6 strain and cut in the bias orientation, as all material samples showed a relatively low elastic modulus in this orientation, and the material would remain in the bias orientation when on both the streamwise and spanwise cylinders.

Streamwise Orientation: seam underneath cylinder

The drag coefficient was calculated for each material sample when placed on each cylinder in the streamwise orientation, and the results plotted against the Reynolds number, as shown in Figure 7.24.

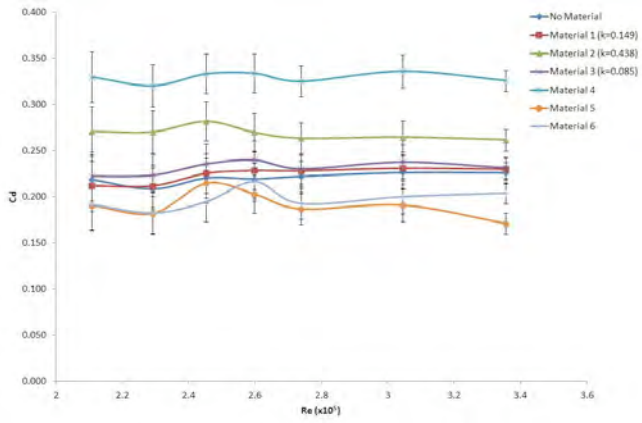

(a) Small Cylinder (56mm diameter)

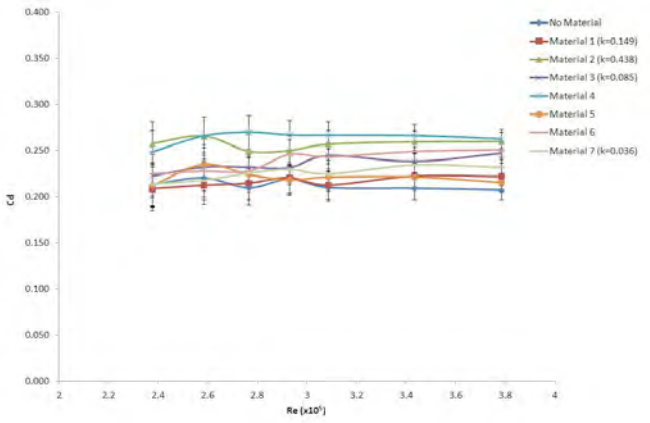

(b) Medium Cylinder (69.6mm diameter)

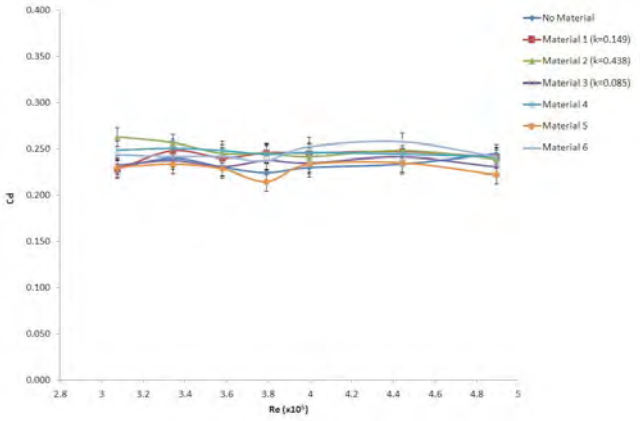

(c) Large Cylinder (110mm diameter cylinder)

Figure 7.24: Drag coefficient against Reynolds number for the circular cylinders in the streamwise orientation with the seam underneath

The results in Figure 7.24 show that there is virtually no difference in the drag coefficient for the different materials on the medium and large cylinders, but on the small cylinder Materials 5 and 6 appeared to have a lower drag coefficient than Materials 2 and 4 in particular. No material showed a significant drop in drag coefficient within the range of Reynolds numbers tested, which was as expected as there is no drag crisis at these Reynolds numbers for this particular geometry. It is possible that base drag, on which noise is superimposed, dominates all other effects on the cylinders in the streamwise orientation, which would explain the similar drag coefficient values between different material samples on all cylinders tested.

According to Hoerner [1965] the drag coefficient for circular cylinders in axial flow is dependent on the length to diameter ratio, L/D, and at L/D=0.5 a significant reduction in drag coefficient is seen, Figure 7.25. The length to diameter ratios for the small, medium and large cylinders are 2.68, 2.16 and 1.35 respectively, which is significantly higher than the length to diameter ratio for which a reduction in drag coefficient would be expected from Figure 7.25. The actual drag coefficient values for the small, medium and large cylinders however, are within the same range as the drag coefficient values reported by Hoerner [1965] for circular

cylinders in axial flow with similar length to diameter ratios (represented by the red markers on Figure 7.25).

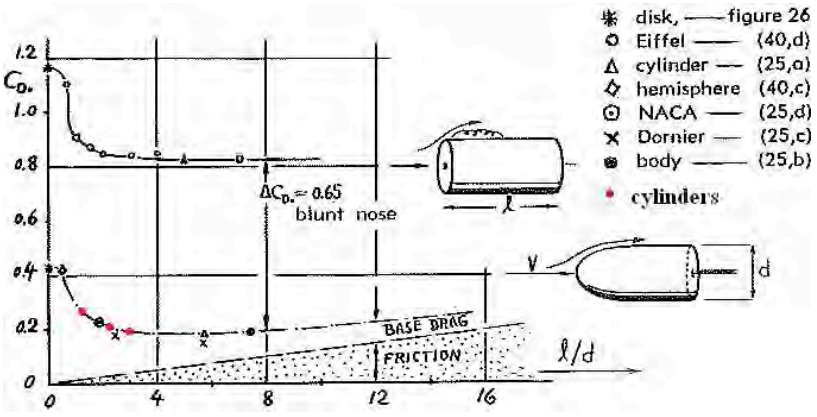

Figure 7.25: Comparison between drag coefficient results for cylinders and the results by Hoerner [1965]

A comparison of the Reynolds number of the streamwise parts of the body of a cyclist (forearm) to the Reynolds number of the cylinders in the streamwise orientation will enable the material with the lowest drag to be identified, as shown in Table 7.20. These results show that Material 5, one of the smoothest materials, appears to have a consistently low, although not necessarily always the lowest, drag coefficient for parts of the body in the streamwise orientation (forearms) at cycling speeds between 40kph and 70kph. Material 5 would therefore be the best choice of material to use for these parts of the body at speeds between 40 and 70kph. These results agree with Brownlie et al. [2009] who also found that smooth materials had a lower drag on streamwise parts of the body as they provided the least frictional drag.

Cycling Speed (kph)	**Re$_{cyclist}$ (x10^5)**	**Corresponding Cylinder**	**Material with the Lowest C$_d$**
40	2.7	Small 64kph	5 or 6
50	3.4	Medium 71kph	1, 5 or 7
60	4.1	Large 65kph	Any
70	4.7	Large 76kph	Any

Table 7.20: Optimal material for the forearm of a cyclist

Spanwise Orientation: seam behind cylinder

The drag coefficient was calculated for each material sample when placed on each cylinder in the spanwise orientation, and the results plotted against the Reynolds number (Figure 7.26).

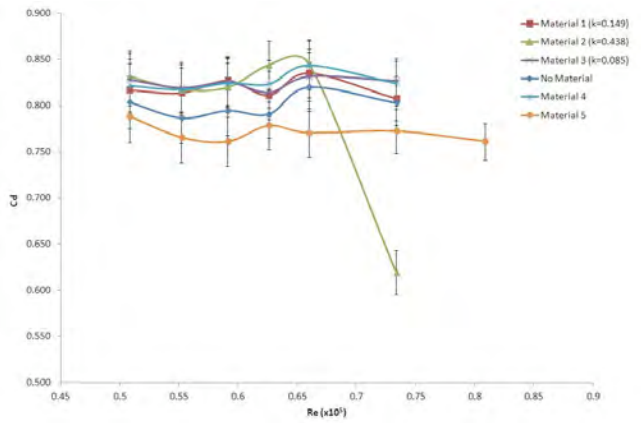

(a) Small Cylinder

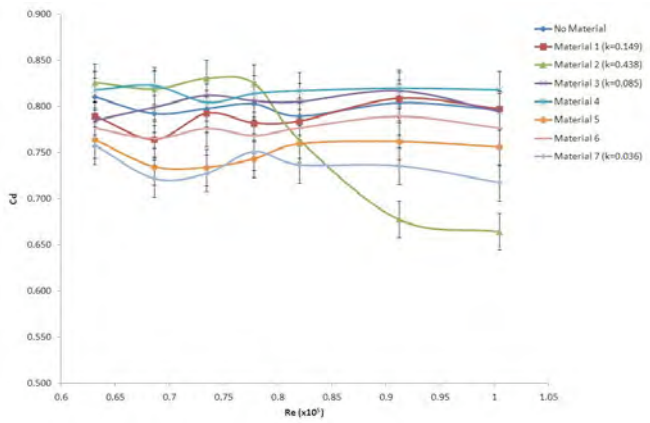

(b) Medium Cylinder

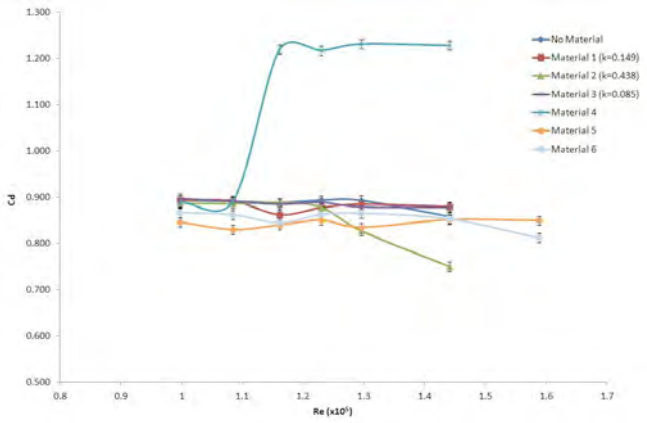

(c) Large Cylinder

Figure 7.26: Drag coefficient against Reynolds number for the circular cylinders in the spanwise orientation with the seam at the rear

The results in Figure 7.26 show that on the small cylinder Material 5 had the lowest drag coefficient at $Re \leq 0.65 \times 10^5$, but at $Re > 0.7 \times 10^5$ Material 2 showed a drop in drag coefficient and became the material with the lowest drag coefficient at higher Reynolds numbers on this cylinder. On the medium cylinder both Materials 5 and 7 had the lowest drag coefficient at $Re < 0.8 \times 10^5$, but at $Re > 0.9 \times 10^5$ Material 2 again showed a drop in drag coefficient and became the material with the lowest drag coefficient at higher Reynolds numbers. On the large cylinder Materials 5 and 6 had the lowest drag coefficient at $Re < 1.2 \times 10^5$, but again at higher Reynolds numbers ($Re > 1.35 \times 10^5$) Material 2 showed a drop in drag coefficient. The results show that the material with the lowest drag coefficient was dependent on the wind speed (and hence Reynolds number) and cylinder diameter; no material showed a consistently low drag coefficient on all cylinders at all Reynolds numbers tested.

All materials showed a slight decrease in drag coefficient at a specific Reynolds number, after which point the drag coefficient slowly increased as the Reynolds number increased further. In particular, Material 2 had a significant drop in drag coefficient at a Reynolds number of 0.65x10^5, 0.78x10^5 and 1.22x10^5 for the small,

medium and large cylinders respectively, which corresponds to the critical Reynolds number region for rough cylinders in axial flow ($6.4x10^4 < Re < 1.4x10^5$). This trend is typical for rough cylinders in axial flow, as was shown in Figure 7.23, where the reduction in drag coefficient and the Reynolds number at which this drop in drag coefficient takes place is dependent on the surface roughness and diameter of the cylinder, after which point the drag coefficient begins to increase again due to an increase in surface friction.

It was expected that only Materials 1 and 2 would be rough enough to cause the drag coefficient to drop when on the circular cylinders in the spanwise orientation, but the results in Figure 7.26 suggest that only Material 2 was actually rough enough to trip the boundary layer from laminar to turbulent flow. The reduction in drag ceofficient for Material 2 on the three cylinders in axial flow was slightly lower than the empircal reduction in drag coefficient for similar roughness coefficients to diameter ratios shown in Figure 7.23 [Hoerner, 1965]. This discrepancy is most likely due to the fact that the cylinders used for this study had rounded ends rather than blunt ends, and the materials also had a seam which may have affected the flow. As Material 2 failed in the weft orientation it would be unwise to make a skinsuit out of Material 2 cut in this orientation. However, cutting Material 2 in the bias orientation would be suitable and would also provide the lowest drag coefficient at higher Reynolds numbers. Material 4 showed an unexpected increase in drag coefficient with Reynolds number on the large cylinder, which could be due to delamination of the coating on Material 4 when it was stretched over the cylinder.

A comparison of the Reynolds number of the spanwise parts of the body of a cyclist (upper arms and thighs) to the Reynolds number of the cylinders in the spanwise orientation will enable the most aerodynamic material to be identified, as shown in Table 7.21 (where the seam is located at the rear of the cylinder for all cases). These results show that a smooth material (Material 5, 6 or 7) is optimal for the forearms, as the Reynolds number has not yet reached the point at which turbulence should be induced, but for the thighs at cycling speeds $\geq$50kph the roughness of Material 2 trips the flow from laminar to turbulent and reduces the drag coefficient. As most elite cyclists spend the majority of their race at speeds greater than 50kph it would recommended for the thighs to be made out of Material 2.

	Cycling Speed (kph)	**$Re_{cyclist}$ (x10^5)**	**Corresponding Cylinder Tested**	**Most Aerodynamic Material**
Upper Arm	40	0.66	Medium 49.5kph (Re=0.63x10^5)	5 or 7
	50	0.82	Medium 64.3kph (Re=0.82x10^5)	5 or 7
	60	0.99	Large 49.5kph (Re=1.00x10^5)	5 or 6
	70	1.15	Large 57.6kph (Re=1.15x10^5)	5 or 6
Thigh	40	1.17	Large 57.6kph (Re=1.15x10^5)	5 or 6
	50	1.47	Large 71.5kph (Re=1.44x10^5)	2
	60	1.76	Large 78.8kph (Re=1.59x10^5)	Not tested - 2?
	70	2.05	Large 102kph	Not tested - 2?

Table 7.21: Optimal material for the upper arms and thighs of a cyclist

Spanwise Orientation: comparison of seam placement

As previous studies have shown that trips are a successful method of reducing the drag coefficient as well as surface roughness (see Section 3.2.1.4) it was necessary to analyse the effect of the seam placement as well as material roughness on the drag coefficient. A comparison of seam placement was made by measuring the

drag of each material on the medium and large cylinders in the spanwise orientation and rotating the seam from 0° (stagnation point) to 180° (rear) in 30° increments. Plots of the drag coefficient against Reynolds number were made for each material to compare the seam placement, as shown in Figure 7.27.

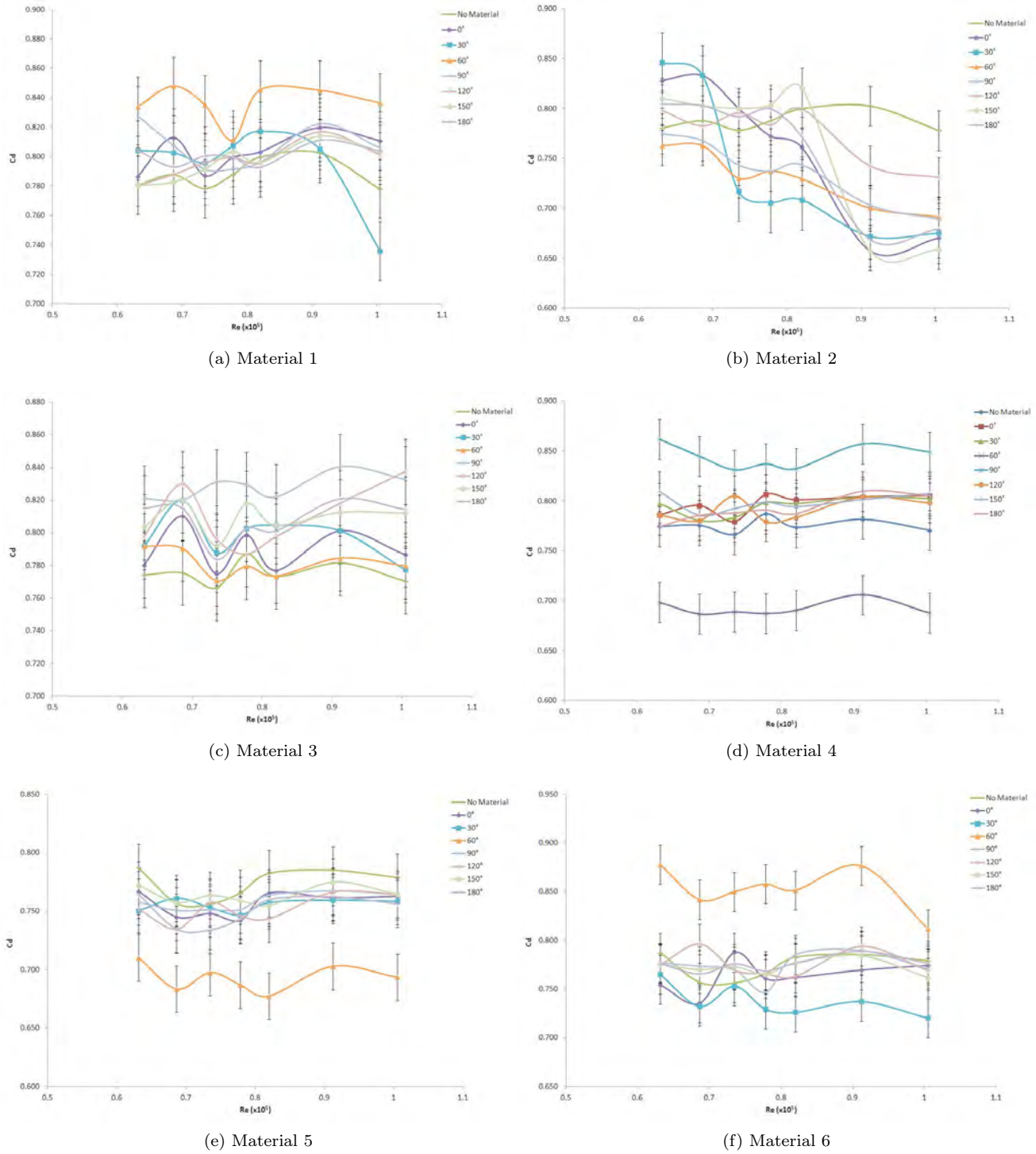

(a) Material 1

(b) Material 2

(c) Material 3

(d) Material 4

(e) Material 5

(f) Material 6

Figure 7.27: Comparison of seam placement for each material on the medium spanwise cylinder

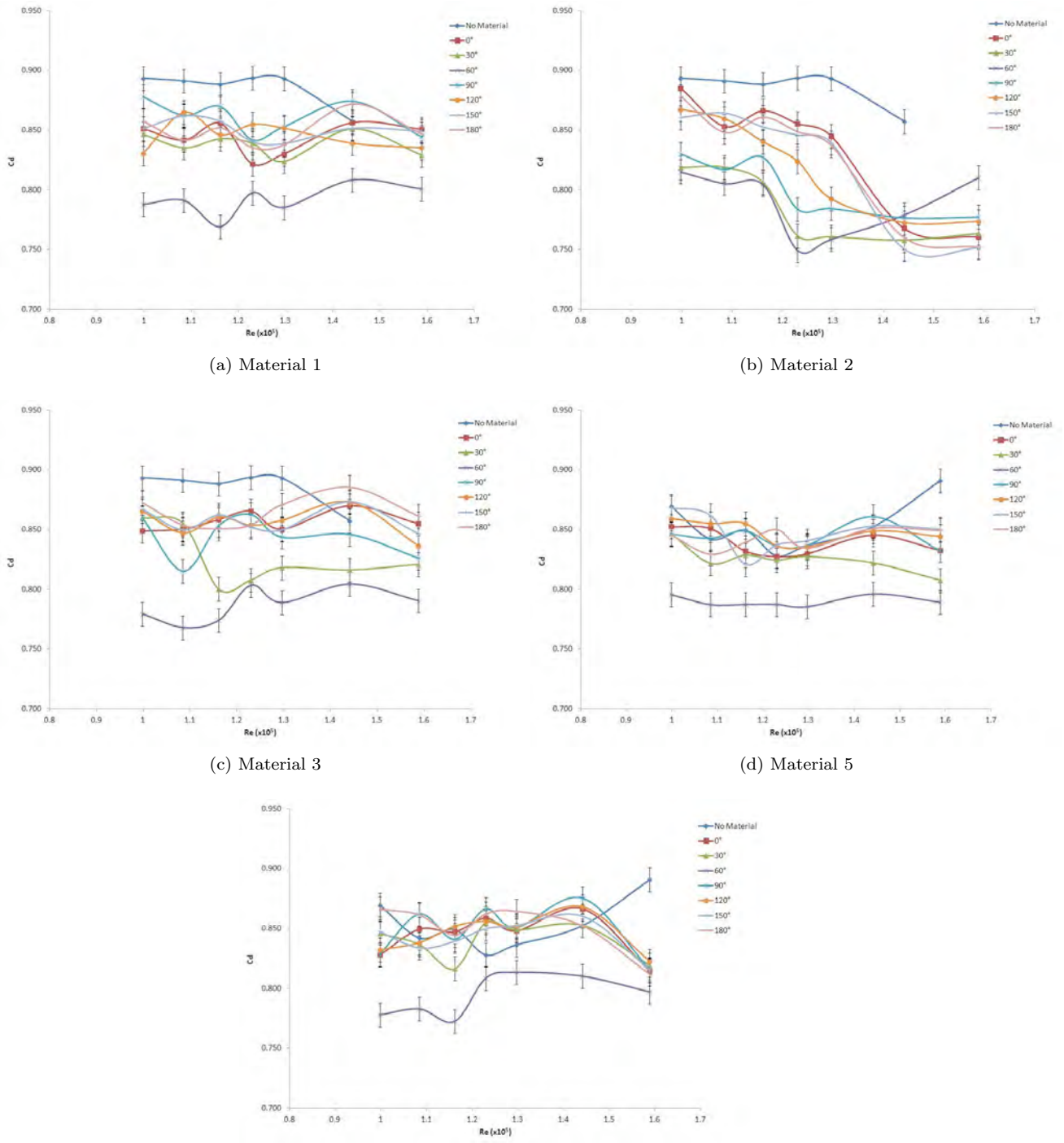

(a) Material 1

(b) Material 2

(c) Material 3

(d) Material 5

(e) Material 6

Figure 7.28: Comparison of seam placement for each material on the large spanwise cylinder*

* The coating of the sheath of Material 4 for the large cylinder began to peel away from the surface, so was not tested.

The results in Figures 7.27 and 7.28 show that the drag coefficient varies for each material depending on the Reynolds number and seam placement. Material 2 was the only material that showed a significant drop in drag coefficient, although this drop in drag coefficient occured at different Reynolds numbers depending on the placement of the seam. By placing the seam at 60° on the large cylinder the drag coefficient was reduced for all materials at all Reynolds numbers tested, with the exception of Material 2 which showed a drop in drag coefficient at a different Reynolds number depending on the seam placement. However, a different trend was seen on the medium cylinder where the drag coefficient was higher for Materials 1 and 6 with the seam at 60°, but significantly lower for Materials 4 and 5 with the seam at 60°. Again Material 2 showed a drop in drag coefficient at a different Reynolds number depending on the seam placement on the medium cylinder. These results highlight the importance of selecting the material and seam placement depending on the speed of the cyclist and the size of the upper arm and thigh. It should be noted that the seam was formed in the same way for all material samples, created by sewing a simple stitch to join the material when inside-out, and then turning the material sample the right-way so that the two un-joined ends were sitting on the inside of they cylinder, as shown in Figure 7.29.

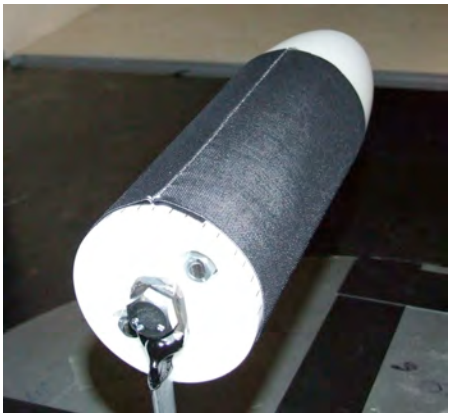

Figure 7.29: Simple, stitched seam

In order to identify the optimal material and seam placement for the body parts of a cyclist in the spanwise orientation it is necessary to compare the Reynolds number of the upper arm and thigh to the Reynolds number of the cylinders in the spanwise orientation, as shown in Figure 7.30 and Table 7.22. By analysing both the material and seam placement the best possible combination in terms of aerodynamic drag can be determined.

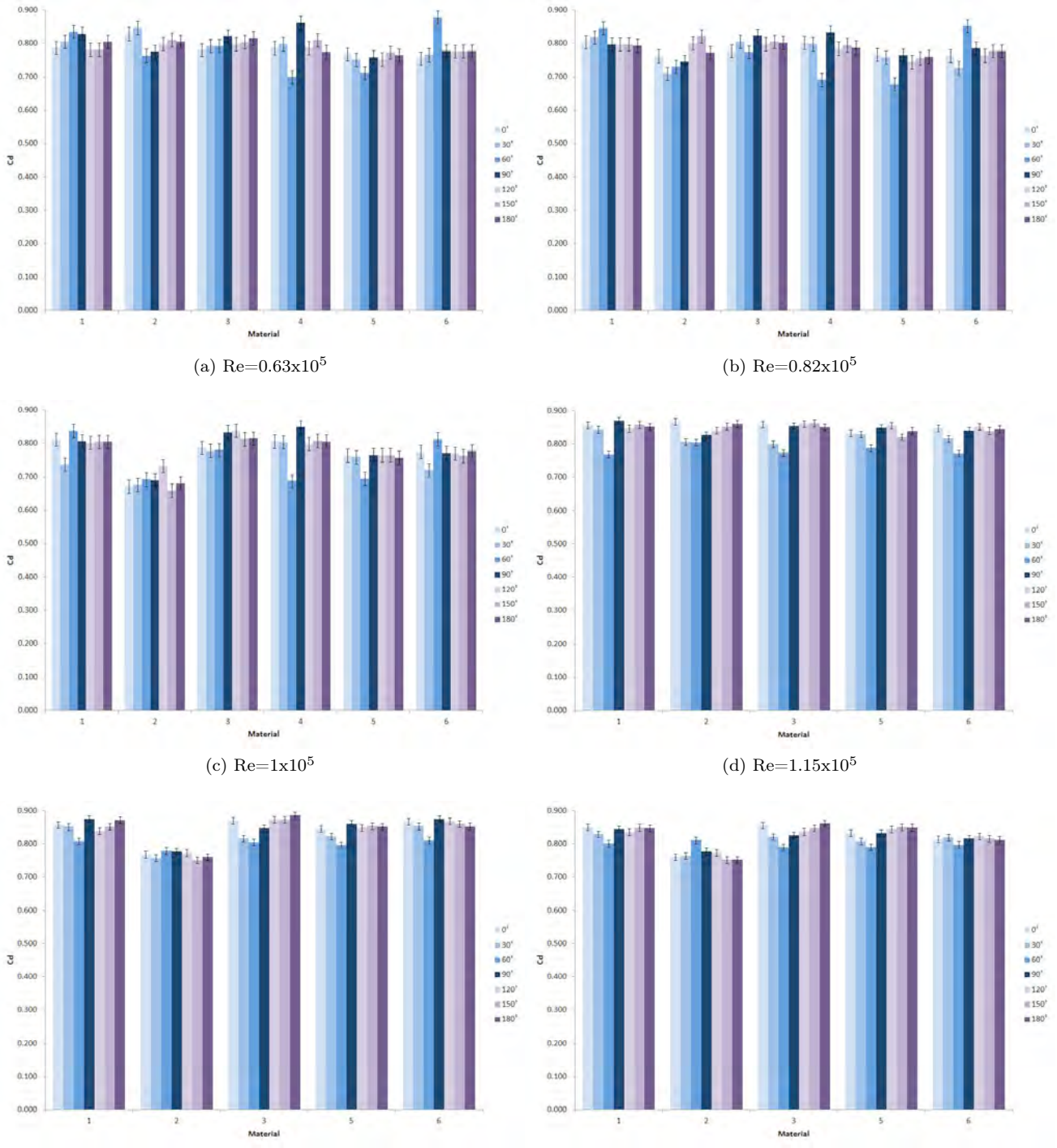

(a) Re=0.63x10^5

(b) Re=0.82x10^5

(c) Re=1x10^5

(d) Re=1.15x10^5

(e) Re=1.44x10^5

(f) Re=1.59x10^5

Figure 7.30: Comparison of material and seam placement for the Reynolds number of the upper arm and thigh of a cyclist

	Cycling Speed (kph)	$Re_{cyclist}$ (x10^5)	Corresponding Cylinder Tested	Most Aerodynamic Material
Upper Arm	40	0.66	Medium 49.5kph (Re=0.63x10^5)	4 or 5 seam 60°
	50	0.82	Medium 64.3kph (Re=0.82x10^5)	4 or 5 seam 60°, or 2 seam 30°
	60	0.99	Medium 78.8kph (Re=1.00x10^5)	2 seam any location except 120°, or 4 or 5 seam 60°
	70	1.15	Large 57.6kph (Re=1.15x10^5)	1, 3, 5 or 6 seam 60°
Thigh	40	1.17	Large 57.6kph (Re=1.15x10^5)	1, 3, 5 or 6 seam 60°
	50	1.47	Large 71.5kph (Re=1.44x10^5)	2 seam 0°, 30°, 150° or 180°
	60	1.76	Large 78.8kph (Re=1.59x10^5)	2 seam 0°, 30°, 150° or 180°
	70	2.05	Large 102kph	not tested (2 seam 0°, 30°, 150° or 180°?)

Table 7.22: Optimal material for the upper arm and thigh of a cyclist

The results in Table 7.22 show that the lowest drag coefficient does not necessarily occur with a smooth material, as was found when the seam location was not taken into account. The optimal material and seam placement when the location of the seam is considered is dependent on the cylinder size and wind speed. At lower Reynolds numbers ($Re \leq 0.63 \times 10^5$) a smoother material (Material 4 or 5) with the seam at 60° had the lowest drag coefficient. As the Reynolds number increased ($0.63 \times 10^5 < Re < 1.15 \times 10^5$), although smoother materials (Material 4 or 5) with the seam at 60° still had a low drag coefficient, rougher materials (Material 2) showed a drop in drag coefficient when the seam was is in a specific location, resulting in a similar value of drag coefficient to the smoother materials. At $Re = 1.15 \times 10^5$ all materials except for Material 2 (the roughest material) had a low drag coefficient when the seam was at 60°, but a further increase in Reynolds number ($Re > 1.15 \times 10^5$) resulted in the roughest material (Material 2) having the lowest drag coefficient at 0°, 30°, 150° or 180°. Therefore, these results highlight the importantance of determining the average speed of each individual cyclist before selecting the material and seam placement for a skinsuit design.

The primary objective for analysing materials and seam placement for cycling skinsuits was to develop a new skinsuit design for endurance track cyclists, whose cycling speed tends to be relatively constant at 53kph for female athletes and 56kph for male athletes. Considering the fact that the coating on Material 4 showed signs of delamination, it would be recommended to use Material 5 with the seam at 60° for the upper arms, and to use Material 2 with the seam at 0°, 30°, 150° or 180° for the thighs. The selection of the seam placement of Material 2 on the thighs could therefore be dependent on ease of manufacture of the skinsuit.

By comparing the roughness coefficient with the minimum drag coefficient for the materials on the cylinders in the spanwise orientation, Figure 7.31, it is clear to see that the aerodynamic drag can be reduced by manipulating both the surface roughness and seam placement. Figure 7.31 shows that an increase in surface roughness reduces the drag coefficient for when the seam is both at the rear of the cylinder and when in the most aerodynamic position. This suggests that surface roughness is more significant at reducing the aerodynamic drag than using a seam to trip the flow, but an analysis of both material roughness and seam placement will provide the best results.

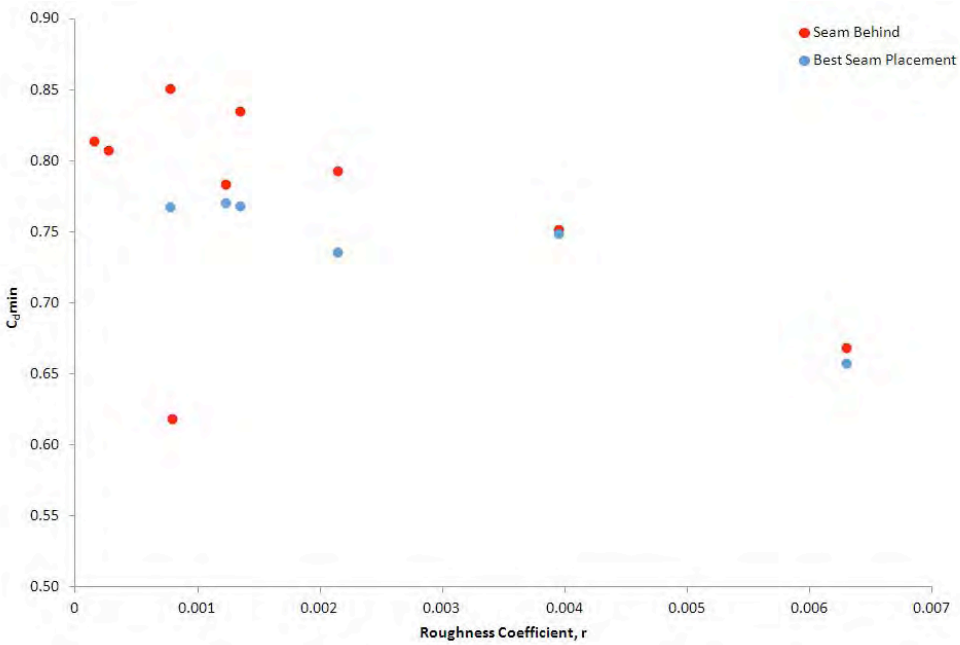

Figure 7.31: Relationship between the roughness coefficient on C$_d$*min*

The influence of the cylinder diameter on the aerodynamic properties of the cylinder can be determined by comparing the relationship between the diameter of the cylinders and the minimum value of drag coefficient, C_dmin, when the seam for each material was placed at the rear of the cylinder (180°) and in the location yielding the lowest drag. This relationship is shown in Figure 7.32, which highlights that in general an increase in diameter causes an increase in the minimum drag coefficient, with the exception of most materials on the small cylinder. It is possible that the ratio of the seam size relative to the cylinder diameter has some affect on the drag coefficient, which must also be taken into account, and this could be a possible explanation for the higher C_dmin values observed on the small cylinder compared to the medium cylinder.

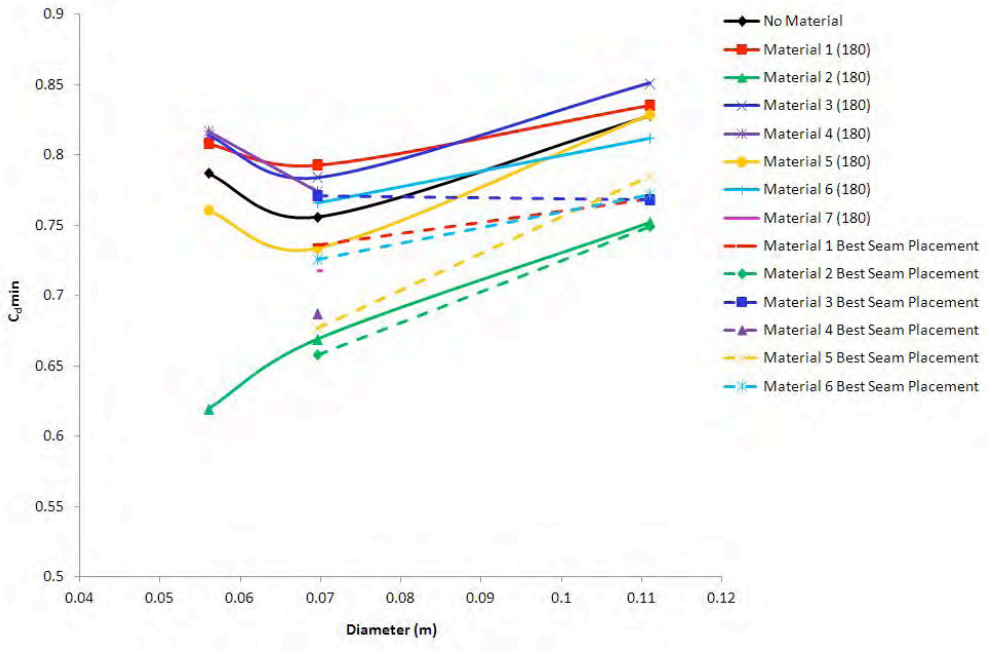

Figure 7.32: Relationship between C_dmin and the cylinder diameter

These results from these studies on material roughness, seam location and cylinder diameter have shown that the roughness of the fabric, the diameter of the cylinder, and also the location and size of the seam relative to the diameter of the cylinder all have an influence on the aerodynamic properties of the cylinder.

7.5.2.4 Most Significant Factor on Aerodynamic Drag

In order to determine the most significant factor on the drag coefficient for different parts of the body at racing speeds the greatest difference in drag coefficient was determined for each material factor at 50kph and 60kph, as shown in Tables 7.23 and 7.24 respectively. The results indicate that the type of material used has the most influence on the aerodynamic drag for parts of the body in the streamwise orientation, but in the spanwise orientation the seam placement or the material type both have a significant influence on drag compared to all other factors.

Factor	$\triangle C_d$ **Forearm** **Medium Cylinder 71kph** **Re=3.4x10^5**	$\triangle C_d$ **Upper Arm** **Medium Cylinder 64.3kph** **Re=0.82x10^5**	$\triangle C_d$ **Thigh** **Large Cylinder 71.5kph** **Re=1.5x10^5**
Roughness	0.038	0.056	0.093
Thickness	0.038	0.056	0.093
Material	0.045	0.059	0.125
Stretch	0.038	n/a	n/a
Seam placement	n/a	0.150	0.081
Knit vs weave	0.045	0.059	0.125
Maximum Difference in C$_d$	**0.045**	**0.150**	**0.125**
Most Significant Factor	**Material**	**Seam Placement**	**Material**

Table 7.23: Most significant factors for parts of the body for cycling at 50kph

Factor	$\triangle C_d$ **Forearm** **Large Cylinder 65kph** **Re=4.1x10^5**	$\triangle C_d$ **Upper Arm** **Medium Cylinder 78.8kph** **Re=0.99x10^5**	$\triangle C_d$ **Thigh** **Large Cylinder 78.8kph** **Re=1.76x10^5**
Roughness	0.008	0.076	0.097
Thickness	0.008	0.076	0.097
Material	0.019	0.134	0.109
Stretch	not tested on large cylinder	n/a	n/a
Seam placement	n/a	0.190	0.110
Knit vs weave	0.019	0.134	0.109
Maximum Difference in C$_d$	**0.019**	**0.190**	**0.110**
Most Significant Factor	**Material**	**Seam Placement**	**Seam Placement**

Table 7.24: Most significant factors for parts of the body for cycling at 60kph

7.5.2.5 Summary

The results from analysing material type, seam location, cycling speed, cylinder diameter and cylinder orientation have identified the best possible material and seam placement for different parts of the body for track cyclists, particularly for endurance athletes. The results have shown that for parts of the body in the streamwise orientation (forearms) a smooth material is the best in terms of aerodynamics at 50-60kph, which was Material 5 for this study. For parts of the body in the spanwise orientation (upper arms and thighs) the best material and seam placement in terms of aerodynamics was dependent on both the cycling speed and cylinder diameter. It was found that Material 5 with the seam at 60° would be the best combination for the upper arms at 50kph-60kph, and Material 2 with the seam at 0°, 30°, 150° or 180° would be the best combination for the thighs at 50-60kph. The results from the stress-strain analysis showed that Material 2 failed in the weft orientation, so it would be unwise to use this material in this orientation for a skinsuit. However, in the bias or warp orientations Material 2 did not fail up to maximum load (95mm) and would therefore be suitable as a skinsuit material. Material 5 did not fail to maximum load in any orientation and showed a relatively low elastic modulus, suggesting the orientation of the weave was not important for Material 5.

However, when in the bias orientation Material 5 showed more gentle and linear stretching force compared to the warp or weft orientations, which would be beneficial for cyclists when putting on the skinsuit. Material 2 showed a slight increase in drag coefficient with increase in strain, where as Material 5 showed a slight decrease in drag coefficient with strain at 50-70kph. This suggests that Material 2 should not be stretched above a strain of 0.2, where as Material 5 should be at a strain of 0.6 when the cyclist is in their racing position.

7.5.2.6 Prototype Testing

Once an analysis had been carried out on different materials and seam locations, a prototype skinsuit was made using the results from the circular cylinder tests. Although Material 2 was identified as a material that would provide a lower aerodynamic drag on the thighs, it was not possible to get hold of enough of this material within the required time frame, and the elastic modulus of this material was relatively high compared to the other material samples. Therefore a decision was made to use only Material 5 to create a prototype skinsuit, as this material had been identified as being the best in terms of aerodynamics for the forearms and upper arms, and was the second best in terms of aerodynamics for the thighs at speeds between 50 and 60kph. The results from the circular cylinder tests showed that for Material 5 the best seam placement in terms of aerodynamics on the upper arms and thighs was at 60°. Therefore the skinsuit pattern was designed so that the seams would lie in this location when the athlete was in their racing position. The seams for the forearms were designed to be underneath the forearms when the athlete was in their racing position, and all other seams were designed for ease of manufacture of the skinsuit. The prototypes did not include a chamois during this early stage of development.

The prototype was made to fit a specific athlete so that it was tight fitting, and was compared to the most aerodynamic, existing New Zealand skinsuit (Skinsuit 1 in Section 7.5.1, made from Material 7) to determine whether the aerodynamic drag had been reduced through the new skinsuit design and choice of material. The athlete for which the prototype skinsuit was made for tested both skinsuits in the boundary layer wind tunnel at 45kph, using their own equipment and adopting their current racing position, which was monitored from side on by projecting their shadow on to the white board. The athlete was pedalling at 90rpm for all tests. The drag was measured three times consecutively for each skinsuit, as well as once for removing and putting back on each skinsuit to determine the repeatability of putting the skinsuit back on in the same place. Images of both the prototype and best existing New Zealand skinsuit (Skinsuit 1) on the athlete can be seen in Figure 7.33 and the results for the measured aerodynamic drag are shown in Table 7.25.

(a) Prototype Skinsuit (Material 5) (b) Existing New Zealand Skinsuit (Material 7)

Figure 7.33: Prototype Skinsuit Testing

Test #	**Prototype Skinsuit (Material 5)**	**Existing NZ Skinsuit (Material 7)**
1	2.104 kg	2.108 kg
2	2.102 kg	2.110 kg
3	2.106 kg	2.111 kg
Average	***2.104 kg***	***2.110 kg***
Repeat once removed	2.109 kg	2.107 kg
Repeatability	0.005 kg (0.24%)	0.003 kg (0.14%)

Table 7.25: Drag Results of Prototype Skinsuit Testing

The results in Table 7.25 show that the difference in measured aerodynamic drag between the two skinsuits was only 0.006kg (0.28%), which is less than the 1% calculated repeatability of the cycle rig. These results suggest that although significant differences in drag were identified between Material 5 and Material 7 on the circular cylinder models, especially in the spanwise orientation, the gains were not nearly as great when transferred to a complete skinsuit. This could be due to the influence of the cycling equipment, the difference in seam type between the skinsuits, the moving legs of the athlete, and because the flow further downstream (towards the thighs) would be affected by the flow further upstream, which was not taken into account on the cylinder models. Nevertheless, the initial prototype skinsuit has shown the potential for skinsuit design, and to be able to create an initial prototype that has the same aerodynamic drag as the best existing New Zealand skinsuit, which can now only be improved on, is a significant first step. Further development of the prototype skinsuit would include getting hold of Material 2 to use on the thighs, looking into different types of seams to identify the significance of bonded or raised seams on different parts of the body, and to develop the design around the torso in a similar way to the circular cylinder body parts.

7.6 Shoe Covers

In order to determine the influence of shoe covers on the aerodynamics of cyclists, wind tunnel tests were carried out on an athlete in the boundary layer wind tunnel and also on a leg model in the high speed wind tunnel. It was believed that the difference in drag between different types of shoe covers would be small, and that greater differences would be seen on a leg model compared to an athlete due to the greater contribution of the shoe cover to the overall drag on the leg model.

7.6.1 Athlete Tests

A male, elite track cyclist was used as the subject for analysing the influence of shoe covers on the aerodynamic drag of a cyclist. Both stationary and pedalling tests were carried out, with the drag readings being accurate to ±1% (as calculated in Section 5.1.2.3). The cyclist used their own equipment and adopted their current racing position for all tests. The cyclist wore Sidi Hi-Tech bike shoes with Shimano SPD SL cleats and pedals, but no socks were worn as this represented actual race conditions. The athlete pedalled at 90rpm for all dynamic tests, and maintained the same foot position for all stationary tests with the right foot at 270° and the left foot at 90° from the TDC (a horizontal foot position). In order to ensure the athlete maintained the same position for each test the shadow of the athlete from side on was projected onto a white board and the shadow drawn around, and a camera was placed to the side of the athlete so that photos could be compared between tests. The frontal area of the athlete was calculated using the digitising method, and the ambient temperature and pressure recorded for each test. A comparison was made between three different shoe covers, as well as when no shoe cover was worn. Details of the shoe covers can be seen in Table 7.26 and Figure 7.34. The wind speed was set at 45kph and the aerodynamic drag measured. All tests were repeated and the average drag was recorded.

Shoe Cover	Description
Prototype 1	78%PES / 22% elastane, seam down front-middle, zip at rear, one hole for cleat, 250mm high
Prototype 2	78%PES / 22% elastane, seam around ankle, zip at rear, one hole for cleat, 250mm high
Champion Systems	80%PES / 20% elastane, seam down front-middle, zip at rear, two holes for cleat, 200mm high

Table 7.26: Shoe Covers

(a) Prototype 1

(b) Prototype 2

(c) Champion Systems

Figure 7.34: Shoe Covers used for Athlete Testing

The results of the measured aerodynamic drag for stationary and pedalling tests for all shoe covers and for the shoe without any cover are shown in Figure 7.35.

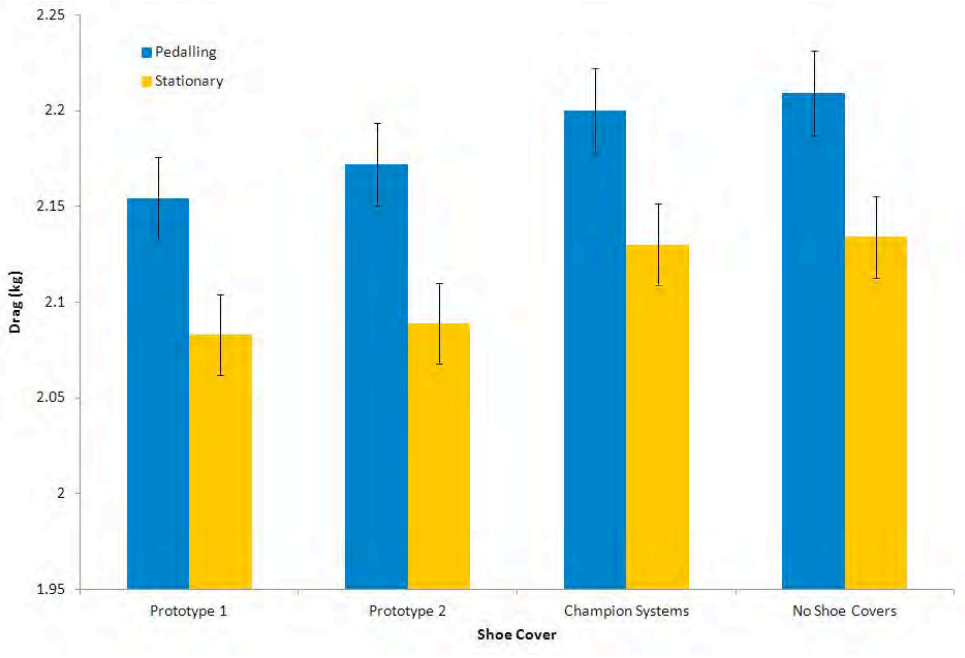

Figure 7.35: Drag results of shoe cover testing on an athlete

The results in Figure 7.35 show that a similar trend was observed for the stationary and pedalling tests, with a lower drag measured for all tests where a shoe cover was worn compared to no shoe cover. The Prototype 1 shoe cover had the lowest drag, with a 2.5% reduction in drag compared to no shoe cover for pedalling tests. Both the Prototype 1 and Prototype 2 shoe covers were higher on the leg than the Champion System shoe covers (250mm compared to 200mm in height) and the aerodynamic drag was lower for these shoe covers. This suggests that the material used for shoe covers has a lower skin friction or lower pressure drag than human skin, and that it is more beneficial to cover as much of the skin as possible in order to minimise the drag of a cyclist. It should be noted that the UCI states that shoe covers must not exceed the mid-distance between the ankle and the knee [Reid, 2012]. The Prototype 1 and Champion Systems shoe covers both had a seam down the front-middle of the shoe cover, but the effect of the seam on the drag did not appear to be as significant as the height of the shoe covers; the Prototype 1 shoe covers had the lowest drag and the Champion Systems shoe covers had the highest drag. However, a comparison between the Prototype 1 and Prototype 2 shoe covers suggests that it is more aerodynamic to have the seam down the front of the shoe cover than across the ankle, probably because the seam down the front runs with the airflow, where as the seam around the ankle runs across the flow; the seam position was the only difference between the Prototype 1 and Prototype 2 shoe covers, with the seam down the front on Prototype 1 and the seam across the ankle on Prototype 2 (Figure 7.36) and the Prototype 1 shoe covers had a lower drag.

(a) Prototype 1: Seam down the front

(b) Prototype 2: Seam across ankle

Figure 7.36: Seam Placement Comparison

7.6.2 Leg Model Tests

A prosthetic lower leg used for paralympic road cycling was used to measure the aerodynamic drag of different shoe covers and no shoe cover in the closed-section, high speed wind tunnel. The same shoe, cleat and pedal as used for the athlete tests (Sidi Hi-Tech shoe and Shimano SPD SL cleat and pedal) were used for the leg model tests, but no crank was used. The maximum extended distance of the pedal and cleat from the sole of the shoe was 37.5mm. Tests were also carried out with shoe covers on the leg model with the cleat and pedal removed to identify their influence on the aerodynamic drag. The lower leg was attached to a rod, which was passed through the wind tunnel floor and then connected to a load cell so that the aerodynamic drag could be measured. The leg was placed upside down in the wind tunnel, with the shoe towards the ceiling, so that the shoe covers could be taken off and put on easily without the need to dismantle the leg after each test. The set up is shown in Figure 7.37.

Figure 7.37: Set up of Lower Leg Model in the High Speed Wind Tunnel

The aerodynamic drag was measured for the leg and shoe without a shoe cover on, as well as for six different shoe covers, details of which are shown in Table 7.27 and Figure 7.38. The wind speed was varied from 50kph to 75kph to analyse the effect of speed on the aerodynamic drag of the shoe covers. Once all measurements had been recorded, the tests were repeated a further three times for one shoe cover, each time fitting and then removing the shoe cover, to identify the repeatabilty of taking the shoe covers on and off. The results were found to be repeatable to ±3%. The frontal areas of (a) the shoe, (b) shoe and shoe cover, (c) the shoe, cleat and pedal, and (d) the shoe, cleat, pedal and shoe cover, were all calculated using the digitising method. The error associated with calculating the frontal area was determined by using the digitizing method to calculate the frontal area of the shoe from the same image three times. The maximum difference in the frontal area calculation was $\pm 0.005 m^2$.

Shoe Cover	**Description**
Prototype 1	78% polyamid / 22% elastane, seam down front-middle, zip at rear, one hole for cleat 250mm high
Prototype 2	78% polyamid / 22% elastane, seam around ankle, zip at rear, one hole for cleat 250mm high
Champion Systems	80% polyamid / 20% elastane, seam down front-middle, zip at rear, two holes for cleat, 200mm high
Base	84% polyamid / 16% elastane, seam down front-middle, no zip, two holes for cleat, 180mm high
Nike	80% polyamid / 20% elastane, coated, seam down front-middle, zip at rear, two holes for cleat, 200mm high
Pearl Izumi	80% polyamid / 20% elastane, coated, seam down front-middle, zip at rear, one hole for cleat, 180mm high

Table 7.27: Description of Shoe Covers

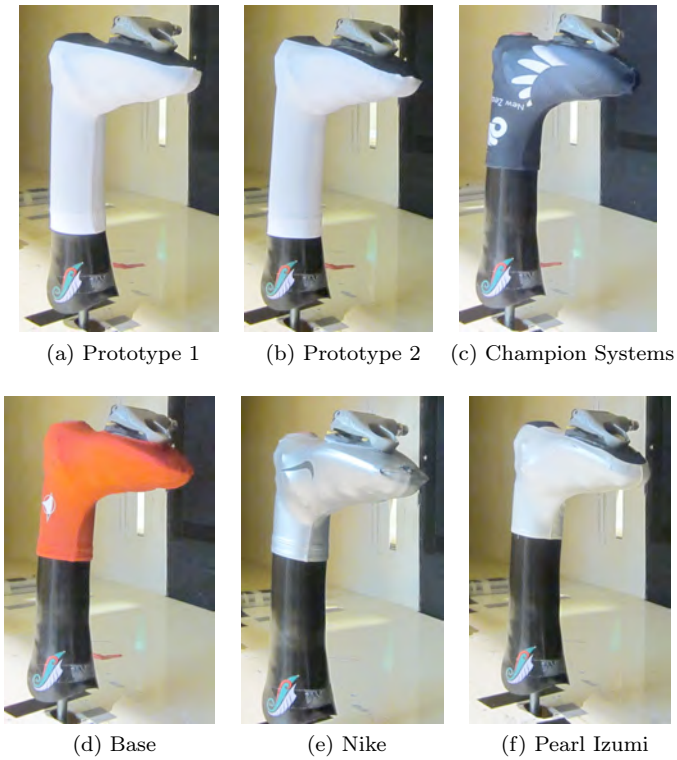

(a) Prototype 1 (b) Prototype 2 (c) Champion Systems

(d) Base (e) Nike (f) Pearl Izumi

Figure 7.38: Shoe Covers used for Leg Model Testing

The measured drag results for the leg model tests without and with the cleat and pedal are shown in Figures 7.39 and 7.40 respectively. The results show that there was a greater difference in drag between the shoe covers at faster wind speeds for tests both with and without the cleat and pedal. However, the trend between the most and least aerodynamic shoe cover differed between the results without the cleat and pedal compared to the results with the cleat and pedal. For example, the Base shoe cover was significantly less aerodynamic than all other shoe covers when there was no cleat or pedal, but when a cleat and pedal were attached to the shoe the Base shoe cover was more aerodynamic than the Prototype 2 and Champion Systems shoe covers. This suggests that the cleat and pedal influence the flow around the shoe and should therefore be present when analysing the aerodynamic drag of shoe covers in order to represent racing conditions more accurately. For this reason, only the results for the shoe covers with the cleat and pedal will be discussed further.

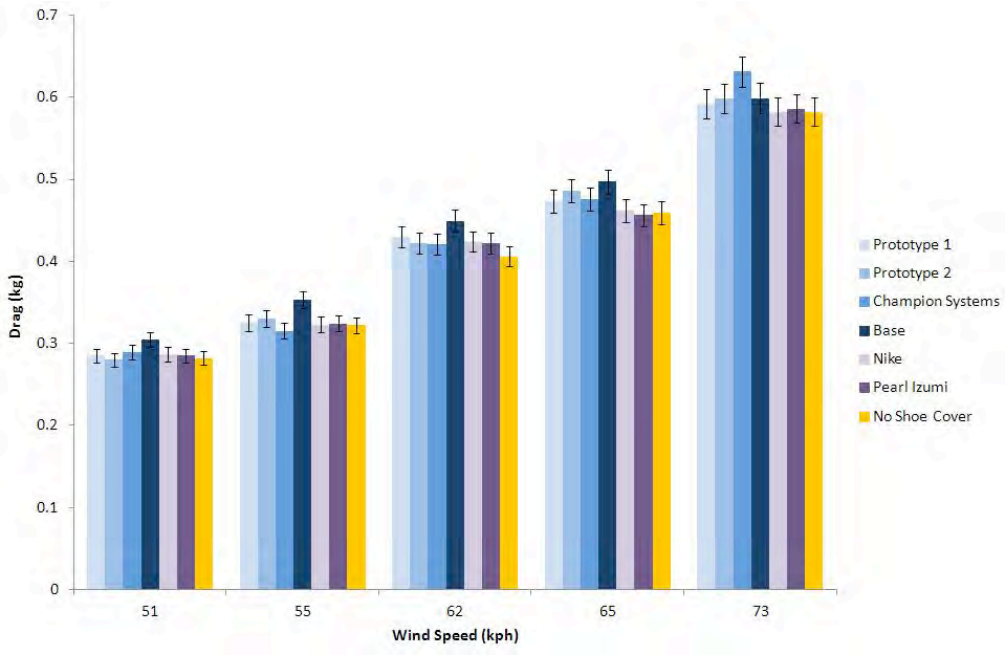

Figure 7.39: Drag Results without the Cleat and Pedal

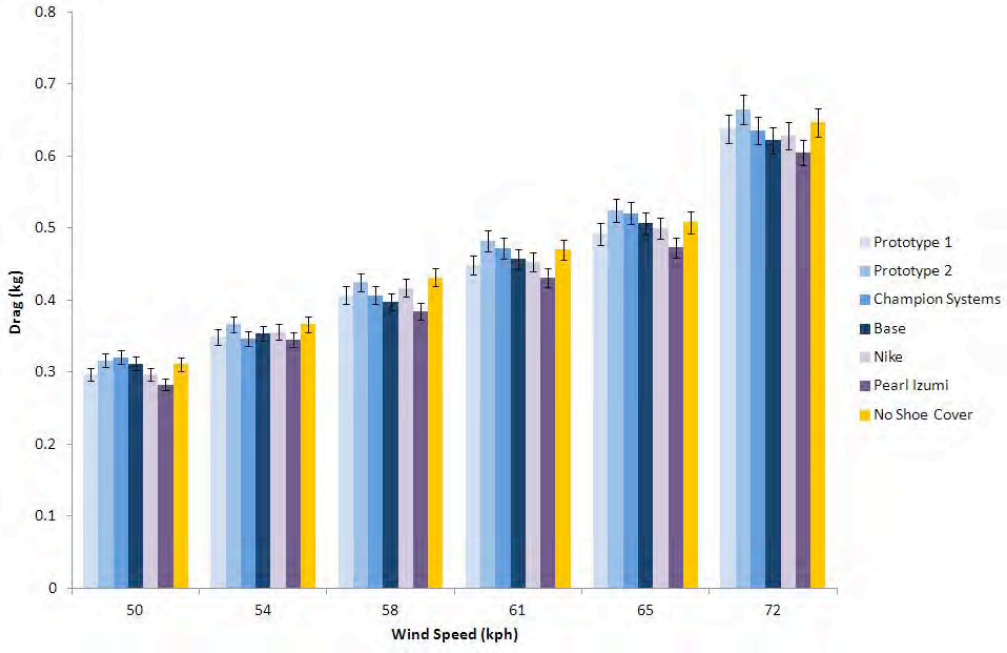

Figure 7.40: Drag Results with the Cleat and Pedal

For tests carried out with the cleat and pedal, the only significant difference identified was that the Pearl Izumi shoe covers appeared to have a slightly lower drag compared to no shoe cover at all speeds tested;

any other shoe cover showed a similar drag to no shoe cover at all speeds tested when a cleat and pedal were present. Unlike the results in Section 7.6.1 for athlete tests where the Prototype 1, Prototype 2 and Champion Systems shoe covers had a lower drag compared to no shoe cover, these shoe covers all had a similar or greater drag compared to no shoe cover when on the leg model. This suggests that the artificial leg has a lower drag compared to human skin.

The percentage reduction in drag for all shoe covers compared to no shoe cover for the tests on the leg model with the cleat and pedal are shown in Figure 7.41. The dotted lines represent the ±3% repeatability of the drag measurements, and a positive percentage relates to a reduction in drag and a negative percentage relates to a gain in drag. These results show that although some shoe covers did reduce the drag at certain speeds, only the Pearl Izumi shoe covers reduced the aerodynamic drag by more than the 3% repeatability at all speeds tested. The Champion Systems and Prototype 2 shoe covers appear to be the least aerodynamic, showing either a minimal reduction in drag or an increase in drag compared to no shoe covers.

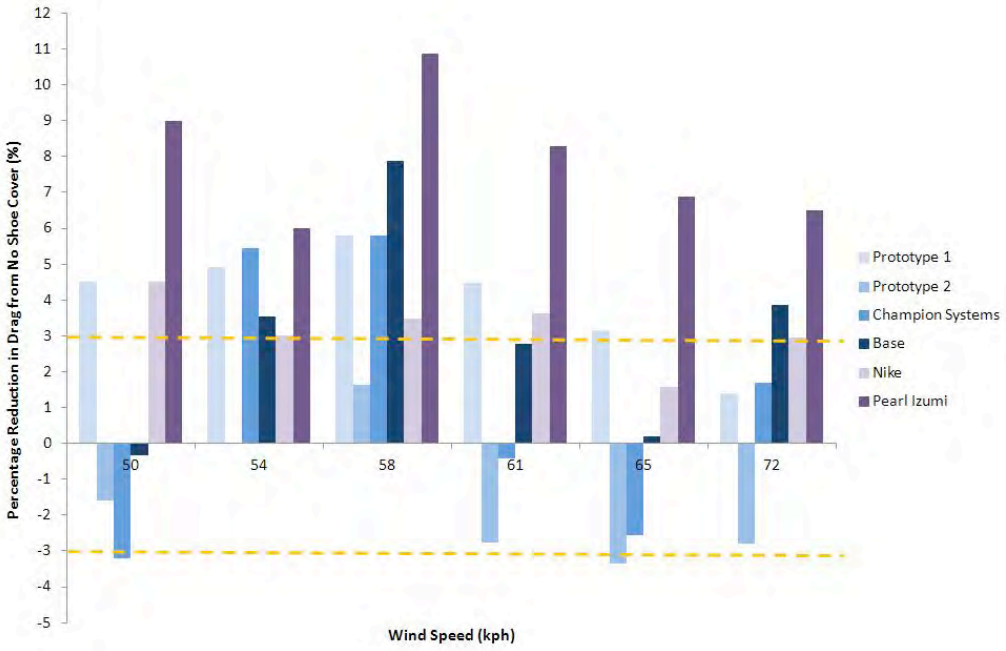

Figure 7.41: Percentage Reduction in Drag for all Shoe Covers Compared to No Shoe Cover

The presence of a zip at the rear of the shoe covers did not appear to affect the aerodynamic drag, as the aerodynamic drag of the Base shoe cover (no zip) was neither significantly lower nor higher than the other shoe covers, all of which had a zip down the back. If the zip had been placed directly in the flow rather than at the rear of the shoe cover, out of the flow, it is likely that an increase in drag would have been seen. The number of holes for the cleat did not appear to influence the drag results either, as the Prototype 1, Prototype 2 and Pearl Izumi shoe covers only had one hole compared to the other shoe covers which had two holes, but the aerodynamic drag was not significantly lower nor higher for these shoe covers within the range of speeds tested.

Unlike the athlete tests, the length of the shoe covers did not appear to have a significant influence on the drag on the leg model; the Pearl Izumi shoe covers were one of the shortest tested (180mm) but were more aerodynamic than the Prototype 1 and Prototype 2 shoe covers which were the longest (250mm). It is possible that the leg model had a lower skin friction drag than human skin, and was in fact more aerodynamic than some of the materials used for the shoe covers.

In terms of seam placement the results tend to suggest that it is more beneficial for shoe covers to have a seam down the front-middle rather than around the ankle, probably due to the fact that the seam would be in line with the flow when in this position; the Prototype 1 shoe cover successfully reduced the drag compared to no shoe cover (1.4% to 5.8% reduction in drag depending on the wind speed) where as the Prototype 2 shoe cover only showed a reduction in drag of 5.4% and 5.8% at 54kph and 58kph respectively, but at all other wind speeds tested the Prototype 2 shoe cover was no different from no shoe cover at all. These results are in agreement with the results from the athlete tests.

The fit of the shoe covers over the shoe also has a significant influence on the aerodynamic drag; the Pearl Izumi shoe cover had a very tight fit over the shoe, stretching the material so that it did not wrinkle and was pulled away from the shoe to create a more streamlined shape for the flow to pass over, particularly away from the straps to eliminate recesses. This shoe cover also had a very tight and neat fit around the front of the shoe (see Figure 7.38) with no wrinkles or dimples where the seams were joined, which would also help reduce the drag.

A comparison of the calculated frontal area for the shoe and shoe covers is shown in Table 7.28. These results show that the presence of a shoe cover increases the frontal area by only 0.004-0.005m^2 (within the inaccuracy of the frontal area calculation) but the presence of a pedal increases the frontal area by 0.009-0.01m^2 compared to just a shoe. The presence of a pedal and shoe cover increases the frontal area by 0.014m^2 compared to just a shoe, but the majority of this increase is due to the cleat and pedal. Although the presence of a shoe cover may increase the frontal area slightly, the results shown above indicate that the aerodynamic drag can actually be reduced by using a shoe cover, which implies that a reduction in the skin friction coefficient of the material of shoe covers compared to human skin outweighs the small increase in frontal area.

	Frontal Area (m^2) $\pm 0.005m^2$
Shoe	0.028
Shoe + Cover	0.032
Shoe + Pedal	0.037
Shoe + Pedal + Cover	0.042

Table 7.28: Calculated frontal area for the shoe and shoe covers

7.6.3 Comparison between Athlete Tests and Leg Model with the Cleat and Pedal

A comparison between the reduction in drag for shoe covers versus no shoe covers for a pedalling athlete and the leg model (with cleat and pedal) is shown in Table 7.29. A positive number represents a drag reduction and a negative number represents a drag increase. These results show that for similar cycling speeds, the

effect of wearing a shoe cover for a pedalling cyclist is significantly different from a stationary leg model, in terms of both actual values and trends. However, the Prototype 1 shoe cover did show a reduction in drag greater than the measurement accuracy on both the athlete and the leg model, although the reduction in drag was significantly less on the athlete. This is probably due to the greater contribution of the drag of the shoe cover on the leg model compared to on the athlete, the changing angle of orientation of the shin to the flow, and the unsteadiness of the foot position of an athlete compared to a stationary leg model.

Shoe Cover	**Reduction in Drag from No Shoe Cover (%)**	
	Pedalling Athlete (45kph/100rpm) ±1%	**Leg Model with Cleat and Pedal (50kph)** ±3%
Prototype 1	2.5	4.5
Prototype 2	1.7	-1.6
Champion Systems	0.4	-3.2

Table 7.29: Comparison between reduction in drag when wearing shoe covers for a pedalling athlete and leg model

As previously mentioned, the skin friction drag of the leg model may have been lower than human skin and even lower than some of the materials used to make the shoe covers. This would have resulted in an increase in drag for shoe covers made out of material with a higher skin friction on the leg model, where as all materials probably had a lower skin friction compared to human skin. The results on the leg model are still valid, but actual values would differ if the set up had involved a leg model made from material more closely related to human skin.

Using the definition of pedal/foot angles shown in Figure 7.42 [Gibertini et al., 2010], where ε_F is the pitch angle of the foot, ε_S is the pitch angle of the shank, and θ is the crankarm angle, the pitch angles for the leg model and athlete tests can be calculated and compared to results by Gibertini et al. [2010] for actual cyclist pitch angles determined from photographs taken during wind tunnel tests at the four different crankarm positions (0, $\frac{\pi}{2}$, π, and $\frac{3\pi}{2}$). This comparison is shown in Table 7.30.

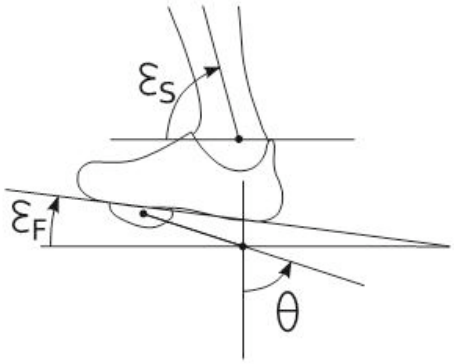

Figure 7.42: Definition of pedal/foot angles [Gibertini et al., 2010]

	θ	ε_F	ε_S	$\triangle\varepsilon = \varepsilon_S - \varepsilon_F$	Angle of foot to wind,α
Athlete Data [Gibertini et al., 2010]	0	-0.40	0.86	1.26	-0.4
	$\frac{\pi}{2}$	0.15	1.41	1.26	0.28
	π	-0.29	1.46	1.75	-0.29
	$\frac{3\pi}{2}$	-0.71	0.71	1.42	-0.84
Leg Model (left foot)	$\frac{\pi}{2}$	0.15	1.57	1.42	0.14
Athlete Test (left foot)	$\frac{3\pi}{2}$	-0.33	1.20	1.53	-0.34

Table 7.30: Comparison between pitch angles (rads) of the leg model to athlete data

Although the left foot for the athlete tests was at a crankarm angle of $\frac{3\pi}{2}$, the pitch angles of the foot, shank, and the angle between the foot and shank, as well as the angle of the foot to the wind, all differed from the results published by Gibertini et al. [2010] and from the leg model. These differences in pitch angles of the foot and shank on the leg model compared to the athlete tests, and the differences in the angle of the foot to the wind could explain the difference in drag results for the shoe cover tests. It should be noted that Gibertini et al. [2010] found that for a buckled shoe, similar to that used for the present athlete and leg model tests with a cleat and pedal attached, the presence of a shoe cover increased the drag by 0.002kg (3%) and increased the frontal area by 0.00064m^2 at a crankarm angle of $\frac{\pi}{2}$ and wind speed of 54kph. These results are within the same range as the present results, although Gibertini et al. [2010] do not provide details of the shoe cover used for their study, making it difficult to draw accurate comparisons.

Although differences have been identified between the drag results of shoe covers on an athlete compared to a leg model, these differences can be attributed to the angle of the foot and shank, and the surface roughness of the leg model compared to human skin. It is recommended that shoe covers are made from a material with a low skin friction, are tightly fitting with minimal wrinkles and seams aligned with the flow, and are as high on the leg as possible in order to minimise the aerodynamic drag. Although the results from the leg model do not show that higher shoe covers reduce the drag, the results from athlete testing do suggest that the material used to make shoe covers has a lower skin friction than human skin, and should therefore cover as much as the leg as possible. It would be useful to compare the effect of different shoes and pedals on the aerodynamic drag, both with and without shoe covers, as it has been suggested that the buckles on shoes similar to those used for the present testing increase the frontal area and aerodynamic drag of shoes [Gibertini et al., 2010], however, limited access to equipment and time meant this study was not possible.

Summary

The main aim of this chapter was to identify the most aerodynamic material and seam placement combination for a new skinsuit for the London 2012 Olympics, primarily for the endurance athletes. A successful method for comparing the aerodynamic drag of different material samples in both the streamwise and spanwise orientations was developed, which could also be used to determine the optimal seam placement for each material sample in the spanwise orientation at different speeds. The accuracy of this method was dependent on the cylinder diameter, wind speed, and cylinder orientation, and ranged from a minimum of 0.9% on the largest cylinder at the fastest wind speed when in the spanwise orientation, to a maximum of 11.6% on the smallest cylinder at the slowest wind speed in the streamwise orientation. This study showed that

the optimal material selection and seam placement was dependent on the orientation and diameter of the cylinders as well as the wind speed, the results of which could be related to different parts of the body of a cyclist. The surface roughness and seam placement appeared to have a greater impact on the aerodynamic drag compared to the thickness, stretch or weave of the material samples, and Material 2 appeared to be the only material rough enough to cause a significant decrease in the drag coefficient within the critical Reynolds number range. An analysis of the stress-strain relationship for the different material samples in the weft, warp and bias orientations showed that Material 2 failed in the weft orientation before maximum displacement. No other material failed, and Material 5 in the bias orientation showed a more gentle and linear stretching force, which would be beneficial when getting the skinsuit over the shoulders of a cyclist. The best choice of material for the forearms of a cyclist travelling at 50-60kph in terms of aerodynamics was found to be Material 5, the best material on the upper arms was found to be Material 5 with the seam at 60° from the point of stagnation, and the best material for the thighs was found to be Material 2 with the seam at 0°, 30°, 150° or 180° from the point of stagnation.

Once the best material and seam placement had been identified for the forearms, upper arms and thighs a prototype skinsuit was made, but only using Material 5 due to difficulties obtaining Material 2 (Material 5 was the second best material in terms of aerodynamics on the upper arms and thighs). Although significant differences were identified between materials on the circular cylinder models, these differences were not transferred to a complete skinsuit design to the same extent; using the results from the cylinder tests a prototype skinsuit was developed and compared to the best, existing New Zealand skinsuit, for which the aerodynamic drag results did not differ significantly. Nevertheless, for an initial prototype design it was promising to see that the same aerodynamic drag could be achieved using the results from the cylinder tests, from which point only improvements can be made. Further development on the type of seam used, and the use of zoned fabric may lead to an improvement in the prototype design, and a greater gain in athlete performance.

Although no indepth study was carried out on the aerodynamic drag of cycling equipment, some simple, initial tests showed that frame modifications contributed to only 0.3% of the total aerodynamic drag of a cyclist, pedal and strap combinations contributed to only 2.1% of the overall drag, and frame and wheel combinations contributed to only 3% of the overall drag. Previous research has shown that disc wheels have a lower drag than spoked wheels at zero yaw, but the improvements that can be made to bicycle frames and wheels is small compared to gains that can be made from modifications to athlete position. Although aero helmets have also been shown to have a lower drag than non-aero helmets at zero yaw, the high variability between athlete body shapes and sizes results in differences between the helmet with the lowest drag for individual riders.

A comparison of shoe covers used by elite, track cyclists was carried out on athletes and on a leg model, but differences in the actual drag results and in the trends was observed between these two methods, primarily due to the difference in skin friction drag of the artificial leg compared to human skin. Nevertheless, the results showed that shoe covers that are higher on the leg and that minimise wrinkles and recesses help to reduce the aerodynamic drag, and shoe covers where the seam was placed down the front-centre had a lower drag compared to similar shoe covers with the seam across the ankles. The influence of a zip at the rear of the shoe cover or the number of holes on the bottom of the shoe cover (for the cleat) did not appear to affect the aerodynamic drag. The typical degree of difference between different shoe covers on an athlete and between shoe covers and no shoe covers was found to be $\leq 2.5\%$.

Chapter 8

Optimal Athlete Position

Introduction

Although it has been suggested that a low, crouched position is the most aerodynamic cycling position [Kyle, 2003a, Burke and Pruitt, 2003, Broker, 2003] there is limited information on the actual optimal set up for a track cyclist that results in this aerodynamic position. This chapter aims to identify some of these factors, in particular the optimal handlebar width and height, hand position, and torso and shoulder angles, in order to provide a more quantitative analysis of the optimal position for a track cyclist compared to the general comparisons already described in the literature.

8.1 Handlebar Width and Height

An analysis of the effect of the width and height of the handlebar extensions was made by measuring the aerodynamic drag of seven elite male cyclists and seven elite female cyclists in their current, favoured racing position, and then independently adjusting the separation of the elbow pads and the height of the handlebars from their current favoured position. The degree to which the adjustments were made were dependent on the athlete, their current racing position, and the equipment used; not all handlebars had the same amount of adjustment to the pad separation and/or height. The handlebars were raised or lowered using spacers on the stem, and the elbow pads were placed wider apart or closer together using the adjustment slots on the pads. Each athlete was asked to pedal at a cadence of 100rpm, and all tests were carried out at a wind speed of 42kph and the drag results converted for an actual cycling speed of 60kph for the male cyclists and 50kph for the female cyclists using Equation 8.1. The athletes were told to maintain a position that they could comfortably ride in for each handlebar change, which may have also resulted in a change in head position in order to maintain their line of vision. The drag area was calculated for each athlete in each position using Equation 8.2, where D is the measured drag (N), ρ is the air density (kgm^3) and V is the velocity (ms^{-1}). The drag readings were accurate to $\pm 1\%$, the air density accurate to $\pm 0.4\%$, and the velocity accurate to $\pm 0.13\%$. This gives a drag area accuracy of $\pm 1.1\%$ $\left(\frac{\triangle C_d A}{C_d A} = \sqrt{(0.01)^2 + (0.004)^2 + (2 \times 0.013)^2}\right)$.

The results for drag area were plotted to identify the optimal handlebar position for each athlete. These results are shown in Figure 8.1 for the male athletes and Figure 8.2 for the female athletes.

$$Drag_{50/60kph} = \frac{50/60kph^2}{42kph^2} \times Drag_{42kph} \tag{8.1}$$

$$C_dA = \frac{D}{\frac{1}{2}\rho V^2} \tag{8.2}$$

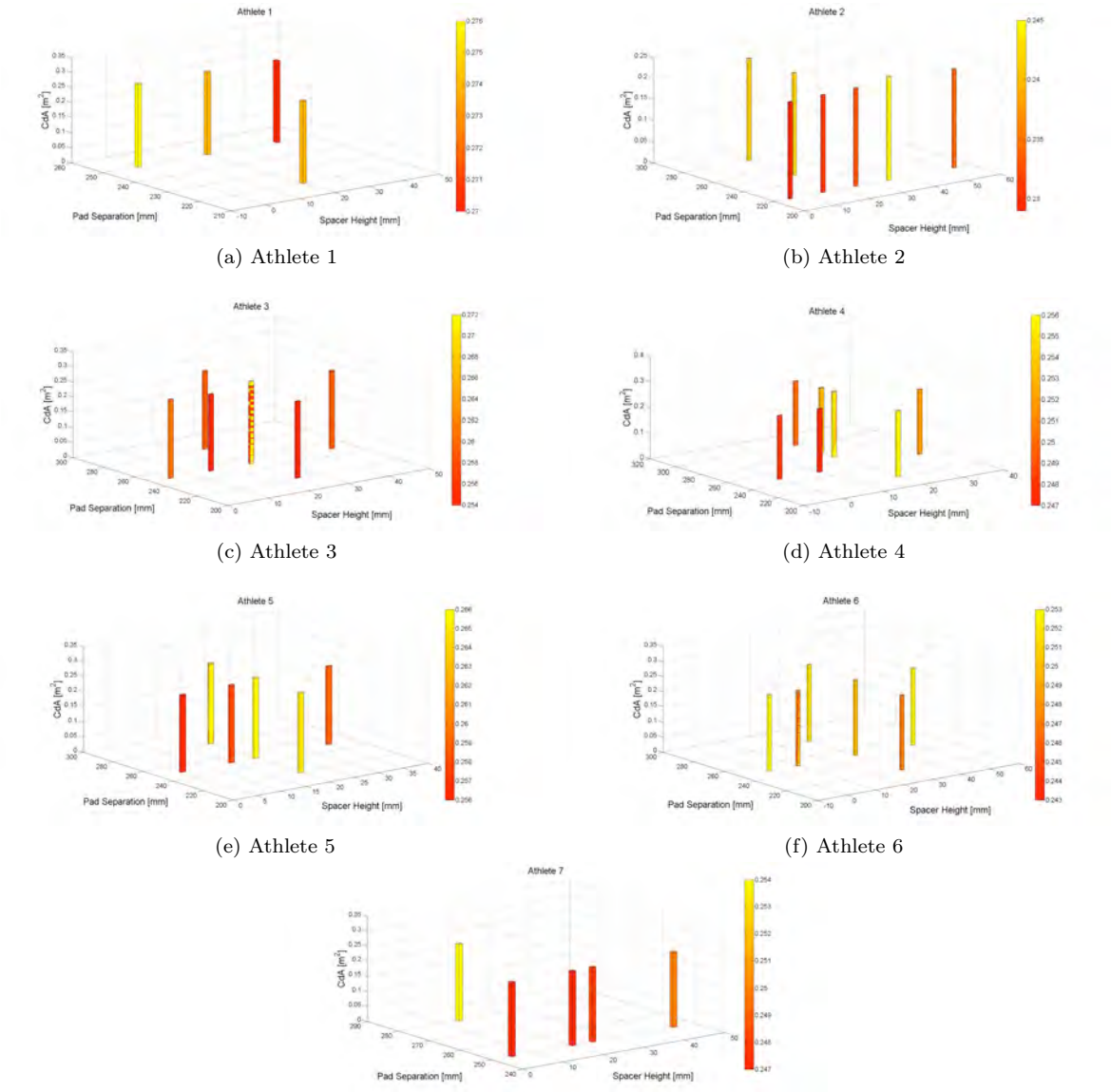

(a) Athlete 1

(b) Athlete 2

(c) Athlete 3

(d) Athlete 4

(e) Athlete 5

(f) Athlete 6

(g) Athlete 7

Figure 8.1: Optimal Handlebar Position for Male Athletes

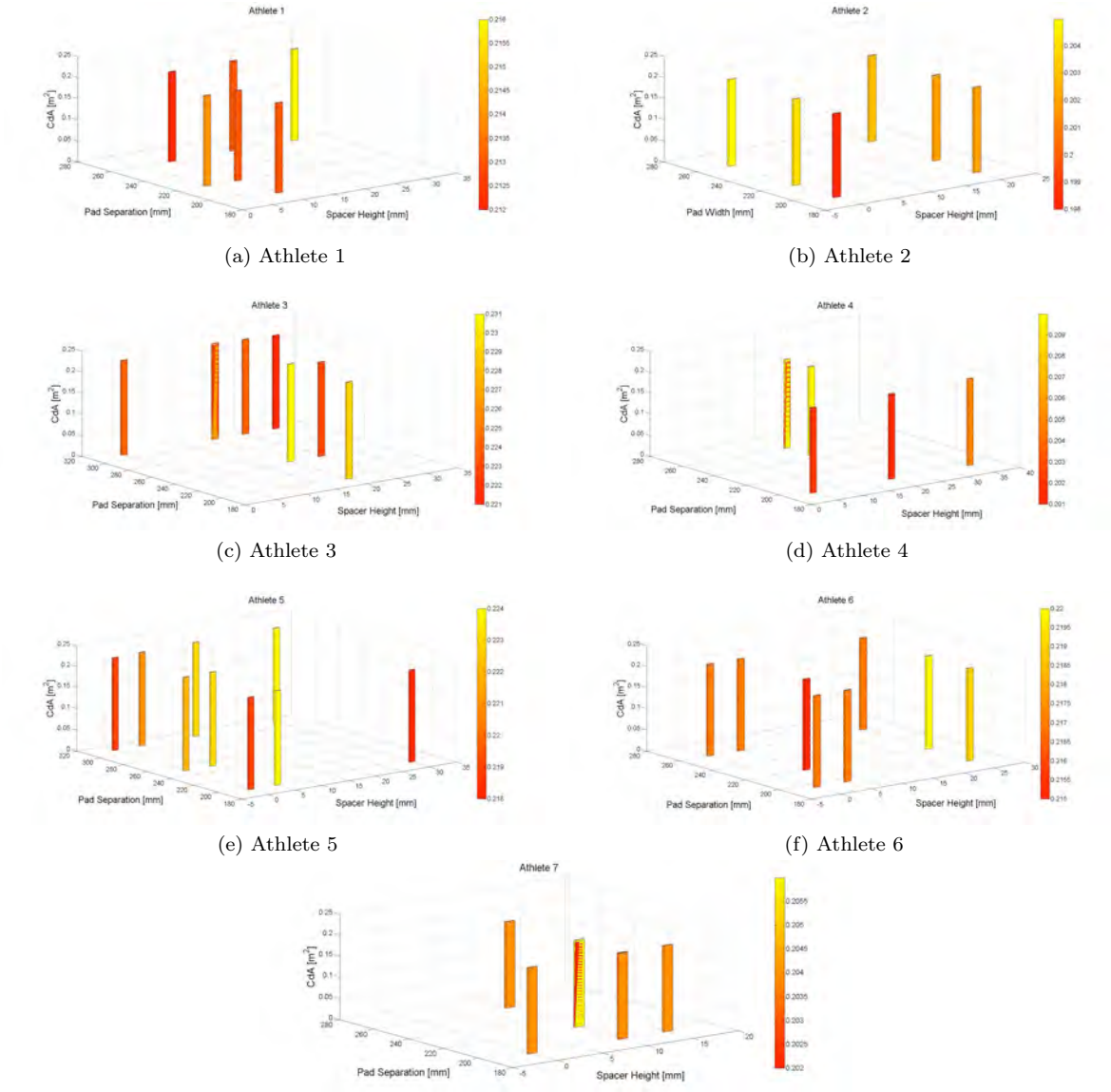

(a) Athlete 1

(b) Athlete 2

(c) Athlete 3

(d) Athlete 4

(e) Athlete 5

(f) Athlete 6

(g) Athlete 7

Figure 8.2: Optimal Handlebar Position for Female Athletes

The results in Figures 8.1 and 8.2 show that the optimal handlebar position varies between all athletes, and that there is no noticeable trend between the position with the lowest drag for all male or all female athletes. However, these results do show the influence of the handlebar separation and height individually on the drag, and that there is one specific handlebar position that produces the lowest drag area for each athlete. Tables 8.1 and 8.2 show a summary of the position with the lowest drag (best position) and highest drag (worst position) for each male and female athlete respectively, and also whether the greatest change in drag was from a change in bar height or pad separation. The handlebar separation was classified into narrow (<230mm for male athletes, <210mm for female athlete), mid (230-260mm for male athletes, 210-250 for female athletes) and wide (>260mm for male athletes, >250mm for female athletes) for each athlete in order to help identify

if there were any trends. The difference in classification between male and female athletes was due to the difference in handlebars used.

Male Athletes					
	Best Position		Worst Position		
Athlete	Spacer Height (mm)	Pad Width	Spacer Height (mm)	Pad Width	$\Delta drag_{max}$ due to
1	40	wide	0	wide	bar height
2	5	narrow	35	narrow	bar height
3	15	mid	25	mid	bar height
4	0-10	mid	20	narrow/mid	both
5	5	mid	20	mid	bar height
6	10	mid	0 or 50	mid/wide	bar height
7	5-25	narrow	15	wide	bar width

Table 8.1: Handlebar Position with the Lowest Drag for Male Athletes

Female Athletes					
	Best Position		Worst Position		
Athlete	Spacer Height (mm)	Pad Width	Spacer Height (mm)	Pad Width	$\Delta drag_{max}$ due to
1	10	wide	30	wide	bar height
2	0	narrow	0	wide	bar width
3	30	wide	20	mid	both
4	5-20	narrow	20	mid/wide	bar width
5	0 or 30	narrow or wide	5 or 25	narrow or wide	both
6	5	mid	25	mid	bar height
7	10	narrow	10	mid	bar width

Table 8.2: Handlebar Position with the Lowest Drag for Female Athletes

It was expected that the lowest drag would be seen for the lowest and narrowest handlebar setup, as this would relate to a low, crouched position which has been described as being the optimal cycling position in the literature. However, the results show that although a relatively low handlebar position (between 0-20mm spacer height) resulted in the lowest drag for most of the athletes tested (71%) the handlebar separation for which the lowest drag was identified varied signficantly between the athletes. In general, a low handlebar position results in a lower aerodynamic drag due to the reduction in frontal area as the athlete gets lower. However, for some athletes it is likely that a handlebar height that is too low causes the athlete to raise rather than lower their head, as they cannot maintain their line of vision. This could be a reason why the lowest handlebar height did not result in the lowest drag for all athletes. A handlebar height with spacers of 20mm or more appeared to result in the highest aerodynamic drag for just more than half of the athletes (57%) again indicating that a relatively low handlebar position is optimal in terms of aerodynamics. There is no clear indication of the optimal pad separation for the athletes used as subjects for this study; although each athlete had a pad separation that yielded a minimum drag, this separation varied between the athletes.

This variability between optimal pad separation is most likely due to the difference in body sizes of athletes, as well as the athlete's ability to maintain a low head position when the handlebars are narrow; athletes with wider shoulders may find it easier to maintain a low head position with wider handlebars, and handlebars that are too narrow for these athletes may in fact cause the athlete to raise their head and shoulders, causing an increase in frontal area. With narrow extensions a large proportion of the flow is directed around the body, but with wider extensions the flow passes over the handlebars, beneath the chest, between the legs, and across the seat tube towards the rear wheel [Broker, 2003]. This suggests it is better to have narrow extensions than wide extensions, but the results in Table 9.3 indicate that some athletes actually benefit from having slightly wider extensions. It is likely that the separation of the extensions should be set in proportion to the shoulder width in order to direct the flow around the body; for athletes with wide shoulders the extensions should be slightly wider than for athletes with narrow shoulders. In addition, narrow extensions may limit the lung expansion and steering control, and may also affect the athlete's ability to lower the head whilst maintaining their line of vision.

In order to determine whether or not there was a correlation between aerodynamic drag and head position, the distance from the highest point on the helmet to the top of the extensions was measured from side images taken during testing for each athlete in each position, as shown in Figure 8.3. The camera was placed in the same position for each test for each athlete, with no zoom, and the number of pixels determined for a known height of the bike stands in each image. This enabled the distance from the highest point on the helmet to the top of the handlebar extensions to be calculated from pixels to millimetres. The results were then plotted against percentage change in drag area from the reference position for each athlete, to determine whether an increase in head height resulted in a greater aerodynamic drag, as shown in Figure 8.4.

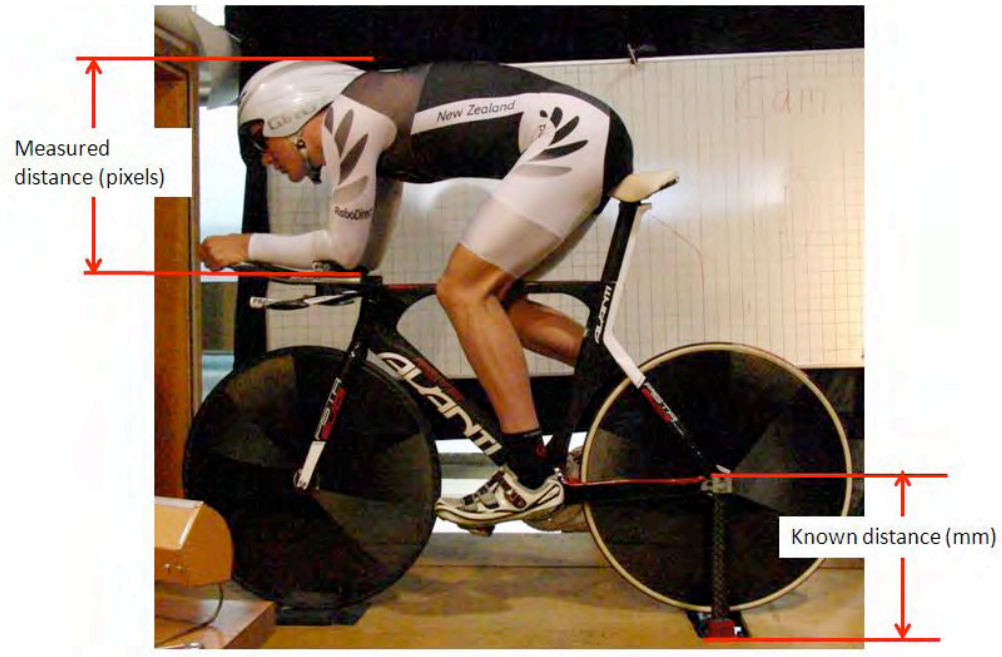

Figure 8.3: Measuring the distance between the highest point on the helmet to the top of the handlebar extensions from side images

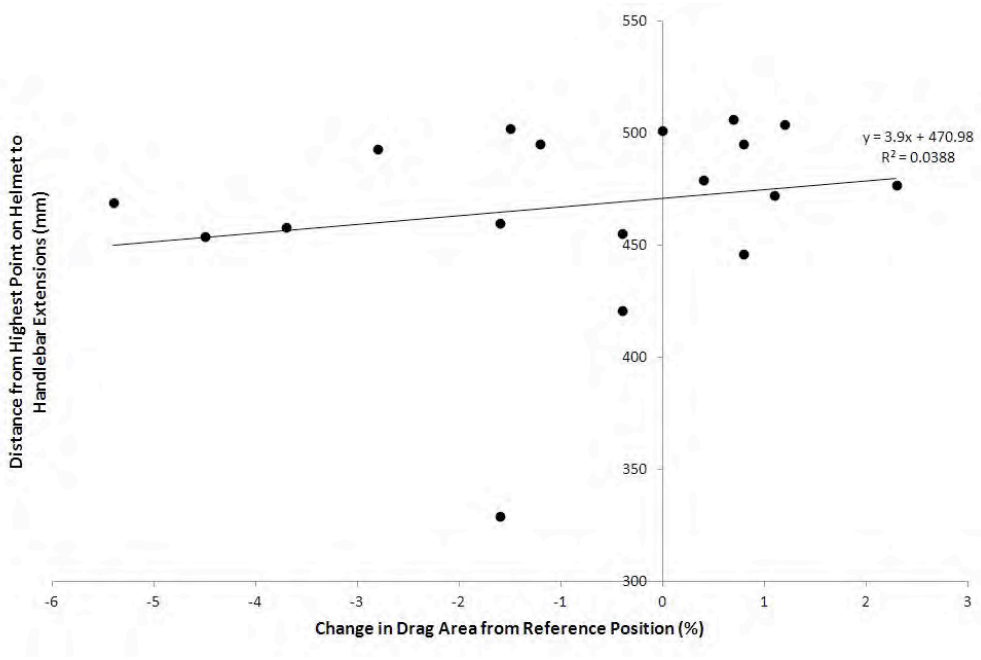

Figure 8.4: Relationship between drag area and head position

Figure 8.4 shows that there is no significant correlation between head position and drag area, i.e. head position alone is not a good indicator of drag. It is likely that athletes adopt a head position that is comfortable, and this will vary between athletes due to differences in body size and shape. The choice of head position in relation to handlebar position appears to be athlete specific, and may have been made in conjunction with other body position changes during their career. These other body position changes may mitigate the effect of head position on drag.

Although no correlation between aerodynamic drag and head position has been identified, by analysing both the pad height and separation independently it is possible to determine the optimal handlebar setting for each athlete. These results indicate that it is more important to optimise the handlebar height, after which the athlete can adopt a handlebar separation that is most comfortable and which allows them to maintain a lower head position whilst still being able to maintain their line of vision. As there is no universal, optimal handlebar setting due to differences in body sizes of athletes, it is important to assess each athlete individually in order to minimise their drag.

Table 8.3 shows the maximum percentage difference in drag from the reference position for each athlete when changing the height of the handlebars and separation of the elbow pads. These results again show the high variability between the optimal handlebar position for athletes, as well as the variability between actual gains and losses for athletes when making the same handlebar change. It is therefore important to recognise that although trends may be seen, for example that the handlebar height has a slightly greater impact on drag than the handlebar separation, the actual gains or losses made by individual athletes will vary. For future studies it would be useful to determine whether there is a trend between anthropometric characteristics, such as shoulder width, and the optimal handlebar position for cyclists.

Male Athletes					Female Athletes				
	Height		Separation			Height		Separation	
Athlete	Up	Down	Narrow	Wide	Athlete	Up	Down	Narrow	Wide
1	2.4	4.1	3.7	baseline	1	2.0	0.7	1.0	baseline
2	-3.4	-5.7	baseline	-2.5	2	baseline	1.2	0.1	0.7
3	0.4	-1.6	-1.2	0.8	3	-1.4	baseline	-1.9	baseline
4	2.0	0.4	1.2	-1.2	4	1.8	0.5	-4.2	baseline
5	1.2	0	-0.4	0	5	1.4	baseline	1.0	baseline
6	0	-4.1	0.4	2.4	6	baseline	-1.0	baseline	-1.0
7	-0.1	-0.9	baseline	1.8	7	0.1	baseline	0.9	baseline

Table 8.3: Maximum percentage difference in drag from reference position

8.2 Hand Position

The position of the hands and forearms when riding with aerobars has an important effect on the aerodynamic drag of cyclists, as this is the first point of contact for the flow of air around the athlete. However, competitive and elite track cyclists do not all adopt the same hand position when racing in similar events. It appears that riders tend to adopt a hand and forearm position depending on the type of aerobars used, and perhaps for individual reasons relating to comfort and stability. Baker et al. [2001] researched the relationship between power output and grip style, and Bressel and Cronin [2005] studied the relationship between the position of the hands on top and drops of handlebars and the pressure on the seat. However, there is limited information in the literature about hand positions which reduce the aerodynamic drag on aerobars without compromising power output or stability. The aim of this study was to determine those hand positions which reduce aerodynamic drag and increase or maintain power output, therefore resulting in a significant time saving for track cyclists.

Eight healthy, elite, New Zealand track cyclists (5 male and 3 female) between 20 and 26 years of age, were used as subjects for this study. All athletes used their own equipment, including track bike, handlebars, skinsuit and helmet, and adopted their own racing position on the bike apart from their hand position. The athletes were placed on the cycle rig in the boundary layer wind tunnel at the University of Canterbury and the wind speed set at 41kph. The athletes were asked to pedal at a cadence of 90rpm for each test, and were instructed to adopt each of the four different hand positions shown in Figure 8.5. The aerodynamic drag and power output were recorded for each athlete in all hand positions. For each athlete, the differences in drag and average power output between (a) the normal hand position, and the other three hand positions (b) thumbs inside, (c) fist grip, and (d) arrow grip, were determined and the drag values extrapolated to 56kph or 53kph for male or female athletes respectively using Equation 8.3. An estimation of the time to complete a 250m lap on an indoor velodrome, with zero wind and zero gradient, was determined using Equations 8.3, 8.4 and 8.5, assuming an average pedalling speed of 56kph for male athletes and 53kph for female athletes. The time gain for hand positions (b), (c) and (d) relative to the normal hand position (a) was then determined using Equations 8.6 and 8.7, where D_{wind} is the drag force measured at wind speed (N), D_{actual} is the drag at the average pedalling speed of the cyclist (N), V_{wind} is the velocity of the wind (m/s), V_{actual} is the average pedalling speed of the cyclist (m/s), C_dA is the product of drag coefficient and frontal area of the rider (m^2),

$C_dA_{baseline}$ is the product of drag coefficient and frontal area (m^2) in the normal hand position (a), ρ is the air density (kg/m^3), g is the acceleration due to gravity (m/s^2), T is the estimated finishing time (s), d is the event distance (m), and P is the power output of the cyclist measured at the torque transducer at wind speed (W). A positive value for the time gain represents a time saving, whereas a negative number represents a time loss.

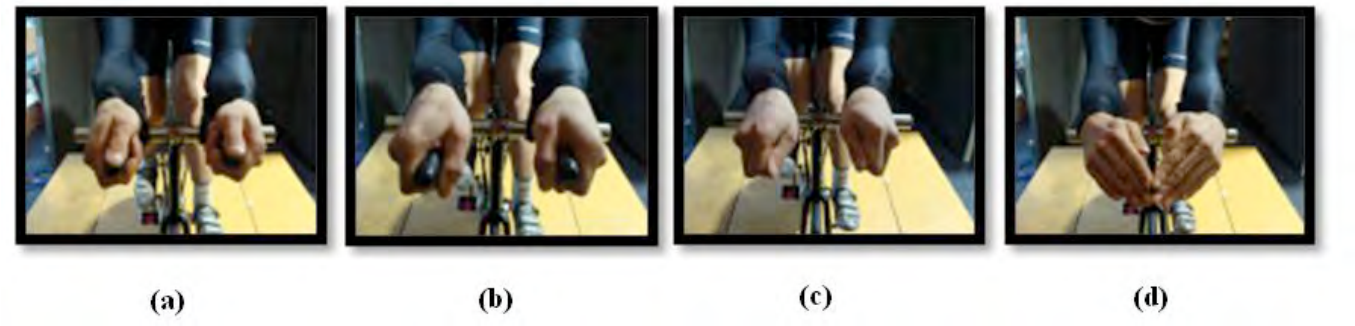

Figure 8.5: Hand positions (a) Normal (b) Thumbs inside (c) Fist grip (d) Arrow grip

$$D_{actual} = \frac{V_{actual}^2}{V_{wind}^2} \times D_{wind} \tag{8.3}$$

$$C_dA = \frac{D_{wind}}{\frac{1}{2}\rho V_{wind}^2} \tag{8.4}$$

$$T = \frac{d}{\sqrt[3]{\frac{P}{\frac{1}{2}\rho C_d A}}} \tag{8.5}$$

$$TimeGain(\%) = 1 - \left(\frac{C_dA}{C_dA_{baseline}}\right)^{\frac{1}{3}} \tag{8.6}$$

$$TimeGain(sec/min) = \% \times \frac{3600}{60} \tag{8.7}$$

Changes in position that resulted in increases or decreases in aerodynamic drag or power output were only considered relevant if the magnitude of the change was greater than 0.1N or 5W respectively. Smaller changes lie within the $\pm 1\%$ uncertainty of the drag and power measurement protocols and may mislead. The results for aerodynamic drag, power output and time gain for all athletes in all hand positions tested are shown in Table 8.4.

Hand Position (b) Thumbs Inside				Hand Position (c) Fist Grip				Hand Position (d) Arrow Grip			
Athlete	Time Gain (sec/min)	Drag (N)	Power (W)	Athlete	Time Gain (sec/min)	Drag (N)	Power (W)	Athlete	Time Gain (sec/min)	Drag (N)	Power (W)
7	1.14	-1.09	26	2	0.22	-0.186	-3	5	1.23	-1.17	3
2	0.25	-0.22	-2	3	0.16	-1.373	-23	2	0.79	-0.69	-15
6	0.09	-0.09	89	1	0.03	-0.029	-18	1	0.35	-0.34	-31
5	0.01	-0.01	-10					3	0.35	-0.30	-31
3	-0.01	0.01	-11								
1	-0.11	0.11	3								
8	-0.20	0.21	-149								
4	-0.68	0.65	99								

Table 8.4: Relationship between the time gain, drag and power output for changes in hand position from

Results in terms of aerodynamic drag

The fist grip (c) and arrow grip (d) hand positions both decreased the aerodynamic drag for all athletes compared to the normal hand position (a). Although the drag decreased significantly for athlete 7 when adopting the thumbs inside hand position (b), the drag increased for all other athletes in this position. The arrow hand position (d) was the most effective at reducing aerodynamic drag in general; the drag was reduced by 0.30-1.2N when athletes adopted the arrow grip hand position.

Results in terms of power output

Out of all the hand positions tested, only the thumbs inside hand position (b) resulted in an increase in power output, but for only three of the athletes involved. The same hand position also resulted in a reduction in power output for three other athletes, significantly so for athlete 8. Both the fist grip (c) and arrow grip (d) hand positions reduced the power output for all the athletes. The results show that a reduction in drag and corresponding increase in power was seen for only athletes 6 and 7, and this was when the thumbs inside hand position (b) was adopted.

Results in terms of time gain

A positive value for time gain represents time saved and a negative value represents time lost. The fist grip (c) and arrow grip (d) hand positions both resulted in a time saving for all athletes tested. The arrow grip hand position (d) resulted in the greatest time saving in general, of over 0.35sec/min for all athletes. The only noticable time loss was seen for the thumbs inside hand position (b), however, this same hand position also showed a significant time saving for athlete 7.

Relationship between drag, power and time gain

The greatest time saving (1.23 sec/min) was found when athlete 5 adopted an arrow hand position (d). This was also the same athlete with the same hand position (d) where the lowest reduction in drag was observed (-1.167N). Although there was no noticeable increase in power output for athlete 5 in this hand position, the power output did not decrease. The second greatest time saving (1.14 sec/min) was found when athlete 7 adopted the thumbs inside hand position (b). This was also the same athlete and hand position with the second lowest drag reduction (-1.09N). For this athlete with this hand position there was also an increase of 26W in power output. Similarly the athlete and hand position with the greatest time loss (-0.68sec/min) also

had the highest increase in aerodynamic drag (0.647N). However, this athlete showed an increase in power output by nearly 100W in this hand position (b). The results clearly show that for all hand positions (b), (c) and (d) there is a negative relationship between time gain and aerodynamic drag; the athlete with the greatest time saving is also the athlete with the greatest reduction in drag for all hand positions. However, the results do not show a distinct relationship between power output and time gain or drag; the power output increases or decreases depending on the athlete and hand position adopted.

A visual analysis of the flow around the hands and forearms for each position tested was carried out by applying cotton tufts, 30mm in length, to the hands and forearms of the skinsuit using ultra thin, clear, mylar tape. The flow pattern was captured for each hand position using a high speed video camera and then analysed. Images of the cotton tufts for each hand position can be seen in Figure 8.6.

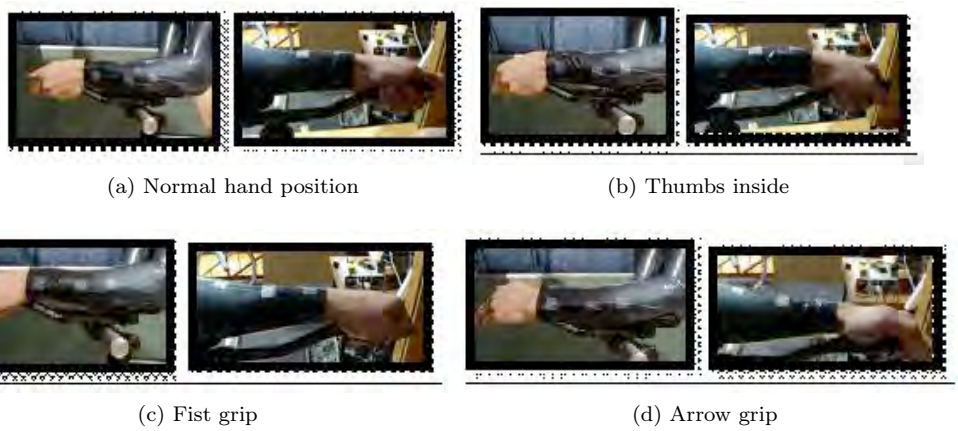

(a) Normal hand position (b) Thumbs inside

(c) Fist grip (d) Arrow grip

Figure 8.6: Video analysis of hand positions using cotton tufts

For the normal (a) thumbs inside (b) and fist grip (c) hand positions the cotton tufts showed a smooth, steady flow pattern around all areas of the hands and forearms except for the region behind the thumbs, where the tufts showed separated flow. However, when the athletes adopted the arrow grip hand position (d) the cotton tufts in the region behind the thumbs were completely inverted, suggesting smooth recirculation occurs. For all other areas of the hands and forearms in the arrow grip hand position (d) the flow remained laminar, similar to all other hand positions (a), (b) and (c).

This study has shown that there is a strong relationship between the hand position and time savings for a cyclist through reduction in aerodynamic drag; optimal time savings are achieved when drag is reduced and power is maximised. Aerodynamic drag can be reduced significantly by adopting an arrow style hand position when riding with aerobars. Although there was no clear relationship between power output and drag or time gain, power output was reduced by less than 30W with the arrow style hand position. When adopting an arrow style hand position, a region of smooth recirculation developed in the area behind the thumbs. This may be more favorable than a region of turbulent separation, which was seen for all other hand positions tested. Although an arrow style hand position does not compromise the power output of athletes, the effects of riding stability in this position needs further investigation before it can be concluded that this is a more beneficial position for athletes. Baker et al. [2001] showed that when riding in unstable conditions power is

used for changing the centre of mass rather than being applied directly to the cranks, which results in an overall reduction in power output. There is a possibility that riders can train in a new hand position in order to increase stability and power output for a hand position that has aerodynamic benefits. However, it can be concluded that athletes should focus on minimising their aerodynamic drag together with maximising their power output in order to gain the most benefit in terms of time savings.

8.3 Torso and Shoulder Angle

The significance of body position on aerodynamic drag has been widely known for a number of years. Although many studies have concluded that a low, crouched position where the frontal area is reduced also reduces the aerodynamic drag, there is limited literature on the optimal angles of the hip, torso and shoulder for a track cyclist. Oggiano et al. [2008] found that drag was more sensitive to handlebar position than seat position. Therefore the aim of this study was to determine the optimal position of a pursuit cyclist in terms of aerodynamic drag and power output through changes in the elbow, shoulder and torso angles, as these are the only angles affected by changes in handlebar position. The knee and hip angles are therefore kept constant, due to a constant seat position for each athlete. The UCI state that the forearms must be horizontal, the tip of the saddle behind the bottom bracket (BBB) must be 5cm maximum, and the distance from the bottom bracket to the end of the handlebars must be no more than 75cm [Regulations, 2009, version 1.02.11]. These contraints limit the adjustability of the handlebars and saddle, which in turn affects the range of elbow, shoulder and torso angles. As the elbow angle is a function of the torso and shoulder angles, due to the constraint that the forearms must be horizontal, it is only possible to analyse the effect of changes in torso and shoulder angles (together with changes in elbow angle) on the aerodynamic drag and power output through adjustments made to the handlebars.

The angles which define the position of a cyclist are shown in Figure 8.7, where the knee angle, α, is the angle between the thigh and the lower leg, the hip angle, β, is the angle between the thigh and the horizontal, the torso angle, γ, is the angle between the torso and the horizontal, the shoulder angle, δ, is the angle between the torso and upper arm, and the elbow angle, ε, is the angle between the upper arm and forearm.

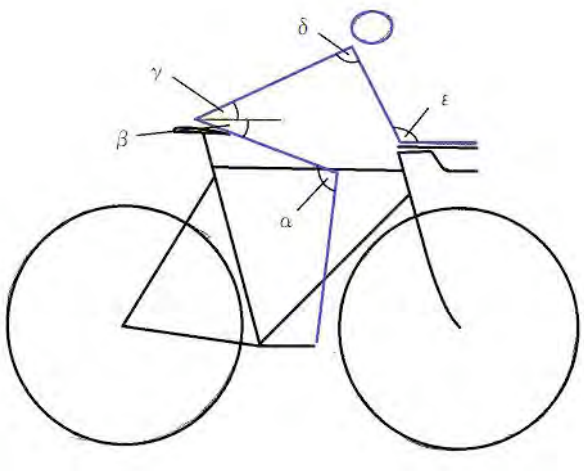

Figure 8.7: Definition of angles of a cyclist

In order to change the shoulder angle, a circle with the centre located at the shoulder point and which passed through the elbow joint was drawn, as shown in Figure 8.8a. The torso angle will remain the same for all points at which the elbow joint crosses this circle. In order to change the torso angle, a circle with the centre located at the hip point and which passed through the elbow joint was drawn, as shown in Figure 8.8b. The shoulder angle will remain the same for all points at which the elbow joint crosses this circle. These relationships are fixed because it is not possible to change the length of the upper body or forearms of a cyclist.

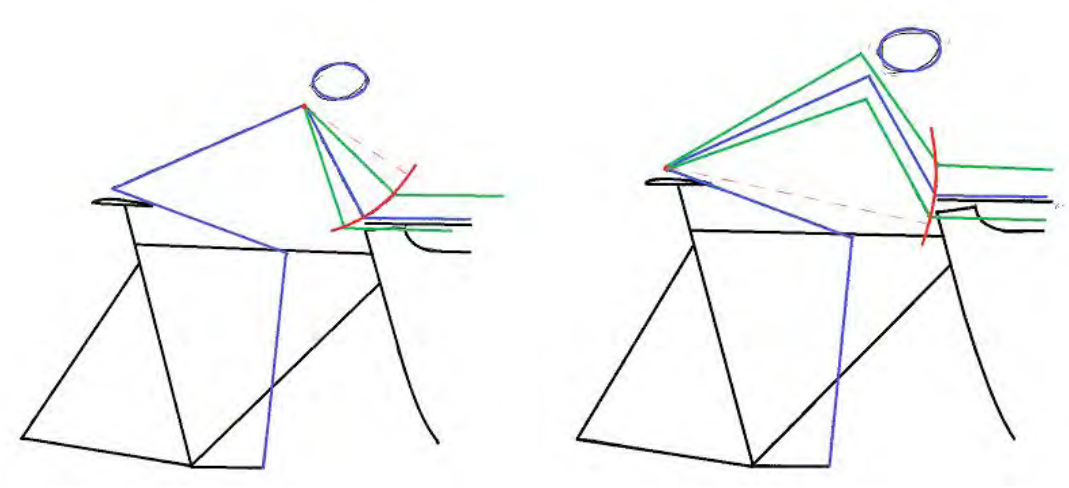

(a) Shoulder angles (b) Torso angles

Figure 8.8: Changes in shoulder and torso angles

The effect of torso and shoulder angles on the aerodynamic drag and power output was analysed by using a modified handlebar setup, shown in Figure 8.9, consisting of an aluminium cylindrical rod of diameter 31.8mm and length 400mm, with Profile Design T1+ aerobars attached. Three athletes were used as subjects for this study, each with their own equipment, except for the handlebar setup which was connected to each bike using an Oval R710 adjustable stem of length 110mm, with 1mm spacers between the frame and stem for adjustment. This setup allowed a complete range of torso and shoulder angles to be tested for the three athletes. The shape of the handlebar extensions only allowed one wrist angle, which did not change throughout the testing. The wind speed was set at 40kph ($\pm 0.03 kph$) for all tests. All tests were static (no pedalling) with the cranks in the horizontal orientation, although each athlete was told to pedal first to ensure their position would be equivalent to how they would ride on a track. Details of each athlete can be seen in Table 8.5.

Figure 8.9: Modified handlebar setup

	Athlete		
	1	**2**	**3**
Height (m)	173	178	177
Weight (kg)	65	74	76
BMI	21.7	23.4	25
Age (years)	16	27	45
Event	Road and track 3-4km	Road criterium 30-100km, track endurance 15-50km	Road cycling, time trial 25-40km
Years in Discipline	2.5	9	20

Table 8.5: Athlete Details

White adhesive tape was placed on the athlete's elbow, shoulder, hip, and wrist joints for identification of the different angles. To locate the placement of the adhesive tape, the rider was asked to sit in their reference position and flex and extend each joint. The adhesive tape was placed at the point which moved the least. An additional marker was placed on the head tube of the bike to monitor adjustments of the handlebar. A laser with a horizontal and vertical beam was used to ensure the handlebars were horizontal at this point. Each rider was asked to adopt their current racing position, and changes to the shoulder and torso angles were made from this reference position. For each position, a side and rear photo was taken to record the starting position and for measurement of the frontal area using a calibration stick with a 0.5m marked length. In addition, a shadow of the rider's position from the side was projected on to a white board so that each position was controlled during testing, and so that the angle of the helmet to the horizontal remained the same for each athlete. The distance between the handlebar extensions, the position of the hands on the extensions, and the location of the elbow pads were measured using the laser and a ruler for each test to ensure these did not change and that the handlebars were always pointing forwards and were not tapered. An example of the test setup can be seen in Figure 8.10.

Figure 8.10: Test setup

The side photos were imported into a CAD programme (Catia) and calibrated. Lines were then drawn to connect the adjacent joint markers to display the current angles, as shown in Figure 8.11. To calculate the necessary adjustment for the next testing position a sketch with changeable angles was drawn, which displayed the distances to the previous elbow position. This method allowed not only the angles to be measured, but also the necessary adjustments to the handlebar to be determined in order to obtain specific shoulder and torso angles.

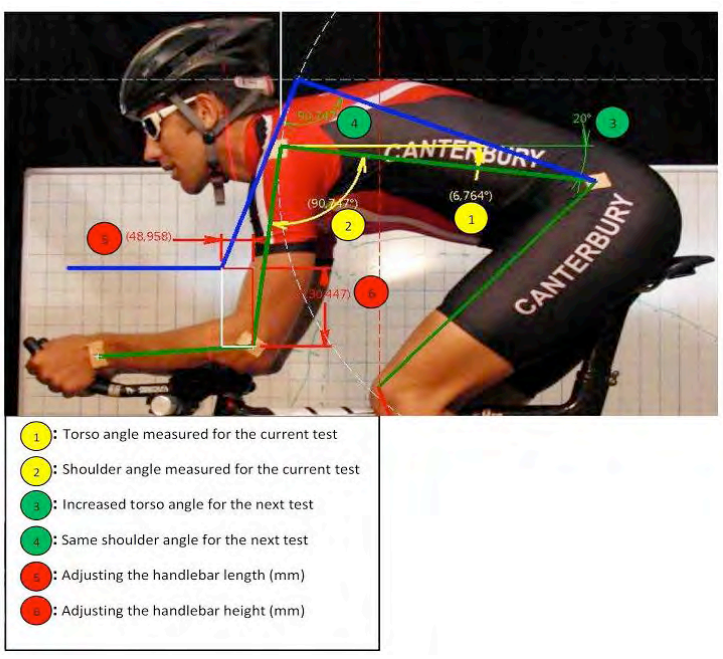

Figure 8.11: Side photo imported into Catia to determine the changes in shoulder and torso angles

Each test was repeated, and the ambient air temperature and pressure was recorded before each test. The reference position of each athlete was also repeated at the very end to verify the results. An SRM Power Meter was fixed to each bike and the power data was collected without the wind while each rider pedalled at a cadence comfortable for themselves for 30 seconds. Although the riders were not able to hold the exact cadence for 30 seconds, a linear relationship could be assumed between power and cadence to determine the average power output at an average cadence. The wind trainer resistance could be adjusted in five increments and the same resistance was used for all riders. By calculating the power required by each rider to overcome the measured drag in each position (Equation 8.8) assuming their gearing would allow them to achieve this velocity at the cadence they used in the wind tunnel tests, the surplus power was determined by subtracting this value from the power output measured by the SRM in each position (Equation 8.9), where C_{rr} is the coefficient of rolling resistance (0.002 for track cycling [Wilson, 2004]), g is the acceleration due to gravity (m/s^2) and m is the total mass of the rider and bike (kg). The optimal position in terms of power output is therefore the position which results in the greatest surplus power. Surplus power is the power available for acceleration, gradient climbing etc.

$$P_d = \frac{1}{2}\rho C_d A V^3 + C_{rr} V \tag{8.8}$$

$$P_{surplus} = P_{measured} - P_d \tag{8.9}$$

The drag area, $C_d A$, and drag coefficient, C_d, were calculated using Equations 8.10 and 8.11 respectively, where D is the measured drag force (N), ρ is the air density (kg/m^3), V is the wind speed (m/s) and A is the calculated frontal area of the rider and bike (m^2).

$$C_d A = \frac{2D}{\rho V^2} \tag{8.10}$$

$$C_d = \frac{C_d A}{A} \tag{8.11}$$

Finally the relationship between the drag area and torso angle, and between the drag area to body mass ratio and torso angle was determined, for comparison to the results published by Garcia-Lopez et al. [2008].

Plots of the drag area against shoulder and torso angles were created to determine the optimal position in terms of aerodynamic drag, where the lowest drag area is the optimum. These plots can be seen in Figure 8.12 for each athlete tested. Table 8.6 shows the average drift between the recorded drag at the beginning and end of each test for each athlete, the maximum difference in drag between tests in the same position for each athlete, and the greatest difference in drag between the best and worst position out of those tested for each athlete.

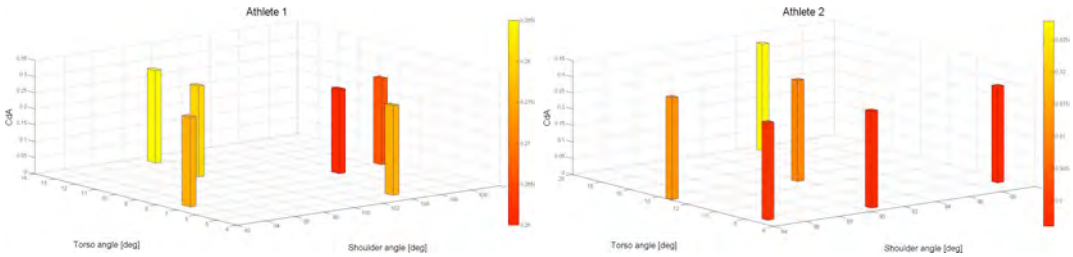

(a) Athlete 1

(b) Athlete 2

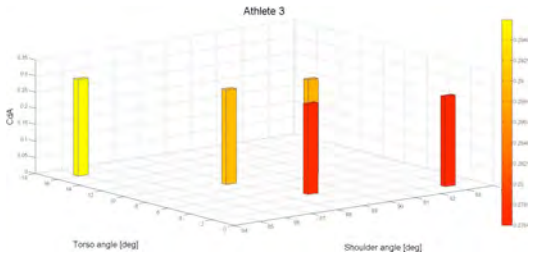

(c) Athlete 3

Figure 8.12: Drag area results

	Average Drift (g)	**Max Difference in Drag for Same Position (g)**	**Difference between highest and lowest drag in different positions (g)**
Athlete 1	6.1	20	200
Athlete 2	14.7	52	270
Athlete 3	6.0	40	180

Table 8.6: Drift and drag results for each athlete

Plots of the calculated surplus power against shoulder and torso angles were created to determine the optimal position in terms of power output, where the highest surplus power is the optimum. Note that the power output was taken at a cadence which was comfortable for each athlete. The results are shown in Figure 8.13.

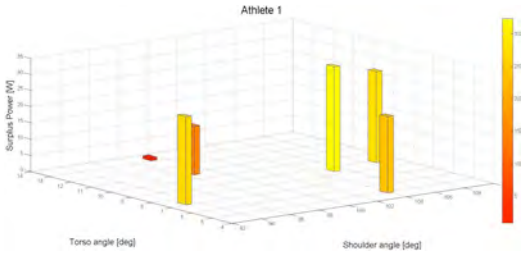

(a) Athlete 1 (Cadence 110rpm, Speed 12m/s)

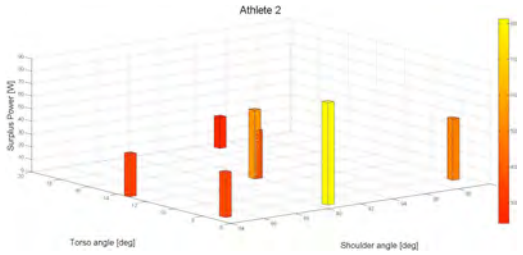

(b) Athlete 2 (Cadence 90rpm, speed 10m/s)

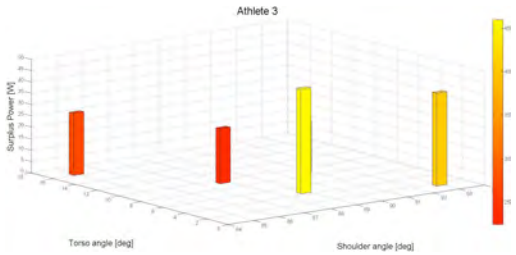

(c) Athlete 3 (Cadence 82rpm, speed 10m/s)

Figure 8.13: Results for Surplus Power

A summary of the torso and shoulder angles at which the minimum drag area and drag coefficient, and maximum power output and surplus power was found for each athlete are shown in Tables 8.7 and 8.8.

	Torso Angle (°) ±1°					
	Min Angle Tested	**Max Angle Tested**	C_dA_{min}	C_{dmin}	**Max P**$_{out}$	**Max P**$_{surplus}$
Athlete 1	5.0	13.3	8.6	8.6	7.3	8.6
Athlete 2	6.8	19.3	6.8	7.4	6.8	6.8
Athlete 3	1.6	16.2	1.6	9.0	4.5	4.5

Table 8.7: Torso angle (degrees) at which the minimum drag area and drag coefficient, and maximum power output and surplus power was found for each athlete

	Shoulder Angle (°) ±3°					
	Min Angle Tested	**Max Angle Tested**	C_dA_{min}	C_{dmin}	**Max P**$_{out}$	**Max P**$_{surplus}$
Athlete 1	93.3	108.6	105.3	105.3	93.3	105.3
Athlete 2	84.3	99.3	90.7	84.9	90.7	90.7
Athlete 3	85.0	92.9	92.9	90.8	88.9	88.9

Table 8.8: Shoulder angle (degrees) at which the minimum drag area and drag coefficient, and maximum power output and surplus power was found for each athlete

For athlete 1, the minimum drag area (C_dA=0.260) occurred at a torso angle of 8.6 ° and shoulder angle of 105.3 °. However, the greatest power output (329.04W) occurred at a torso angle of 6.8 ° and shoulder

angle of 93.3°. The greatest surplus power (32.39W) and lowest drag coefficient (C_d=0.837) were found to be at the same position as the minimum drag area (torso angle of 8.6° and shoulder angle of 105.3°). The greatest difference between the highest and lowest drag for different positions was 200g (9.6%).

For athlete 2, the minimum drag area (C_dA=0.296) occurred at a torso angle of 6.8° and shoulder angle of 90.7°. This was also the position at which the highest power output (248.21W) and greatest surplus power (55.46W) occurred. However, the minimum drag coefficient (C_d=0.864) was at a torso angle of 7.4° and shoulder angle of 84.9°. The greatest difference between the highest and lowest drag was 300g (12.4%).

For athlete 3 the minimum drag area (C_dA=0.276) occurred at a torso angle of 1.6° and shoulder angle of 92.93°. However, the maximum power output (227.3W) and greatest surplus power (42.42W) occurred at a torso angle of 4.5° and shoulder angle of 88.87°. The minimum drag coefficient (C_d=0.803) occurred at a torso angle of 8.97° and a shoulder angle of 90.79°. The greatest difference between the highest and lowest drag was 180g (7.6%).

The results show that the optimal torso and shoulder angle varies between athletes, most likely due to differences in body size and shape. The drag area was mainly influenced by changes in the torso angle, and the power output was mainly influenced by changes in the shoulder angle. Although Savelberg et al. [2003] suggested trunk angle influences power output as well as aerodynamic drag, these results suggest that trunk angle primarily affects the drag area of a cyclist. Maximum surplus power was more closely related to drag than power output, which highlights the importance of minimising aerodynamic drag for improvements in high performance cycling.

The minimum drag area was found to be at a low torso angle and high shoulder angle. This position would reduce the frontal area of the athlete and result in a more streamlined body shape. The minimum drag area was also the same position at which the minimum frontal area was found for all riders. However, the optimum torso angle was not necessarily the lowest possible torso angle, varying from 1.6 to 8.6 degrees depending on the rider. The maximum power output was found to be at a low shoulder angle and a middle torso angle, with the optimum shoulder angle varying between 88 to 93 degrees depending on the rider. This suggests that the shoulder angle has a greater influence on the power output than the torso angle, and highlights the importance of individual testing in order to determine the optimal position for a particular athlete. The maximum surplus power, which accounts for both aerodynamic drag and power output, was found to be at a low torso angle (between 4.5 and 8.6 degrees) and middle shoulder angle (between 88.87 and 105.3 degrees). This was the same position that resulted in the lowest drag area for 2 of the athletes.

It should be noted that the reference position was not the position that resulted in the maximum power output for any of the athletes tested. This suggests that training in a position may not necessarily lead to an increase in power output, and therefore in order to determine the optimum position of an athlete both power and drag must be accounted for.

Although significant gains in drag were seen for all athletes through changes in position, the actual percentage gain varied between the athletes due to individual differences; athlete 1 showed a gain of 9.6%, athlete 2 showed a gain of 12.4% and athlete 3 showed a gain of 7.6%. Again, this highlights the importance of individual testing in order to determine the optimal position in terms of aerodynamics.

The minimum drag area and minimum drag area to body mass ratio were plotted for each athlete to determine if there was a relationship between the two. The results, Figure 8.14, show that the minimum drag area did

not coincide with the minimum drag area to body mass ratio, which is in agreement with the study by Garcia-Lopez et al. [2008] and suggests that body mass is not a significant factor in terms of drag reduction.

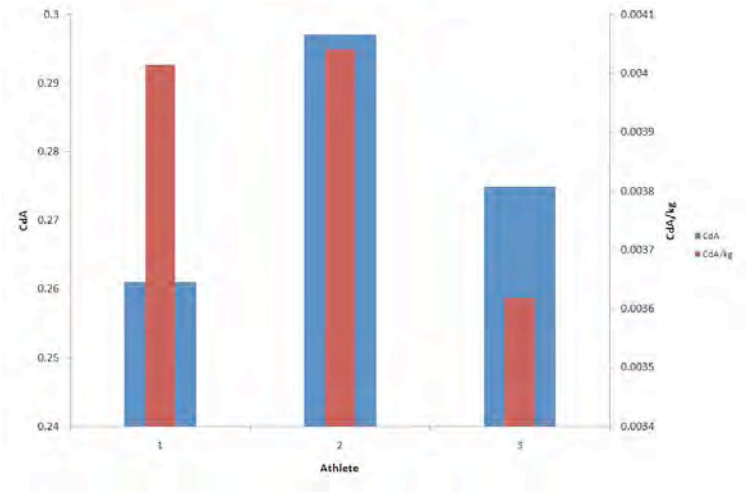

Figure 8.14: Relationship between the minimum drag area and drag area to body mass ratio for each athlete

Plots of drag area with change in torso angle, and drag area to body mass ratio with change in torso angle were also generated to determine if there was any significant correlation. The results, shown in Figures 8.15 and 8.16 respectively, indicate that there was a significant correlation between torso angle and drag area (r=0.6604) and a significant correlation between torso angle and drag area to body mass ratio (r=0.5973), which is also in agreement with the results published by Garcia-Lopez et al. [2008]. These results suggest that a low torso angle reduces the drag area for riders of different all body masses tested, but that body mass is not a significant factor in terms of drag reduction.

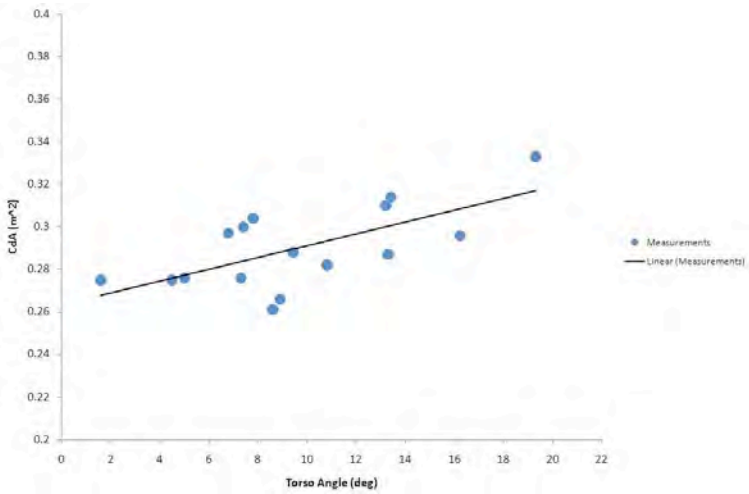

Figure 8.15: Drag area as a function of torso angle

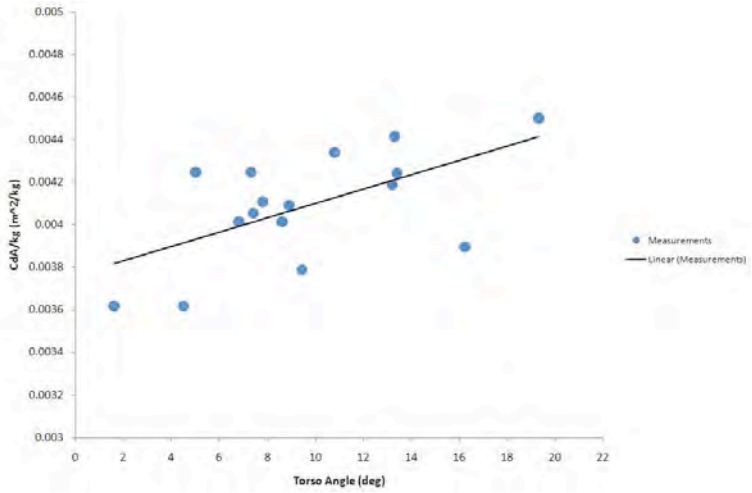

Figure 8.16: Drag area to body mass ratio as a function of torso angle

It should be noted that drag was measured at a single speed. During a race the speed will vary, as will the Reynolds number and drag coefficient. The cyclists' Reynolds number, taking the length scale as 1m, is of order one million, and the drag coefficient is not expected to vary much as the boundary layer over much of the cyclist will be fully turbulent. However the drag contribution of individual elements exposed to the undisturbed wind, such as the helmet, arms and front wheel, may vary to a greater degree. Future studies should attempt to match the resistance applied to the wheels to the drag and rolling resistance experienced at the speed simulated, and considering the gearing, ensure the cadence is appropriate to this speed. Higher speeds should also be tested.

Summary

The aim of this chapter was to provide a more quantitative analysis of the optimal athlete position, in particular for the handlebar width and height, hand position, and torso and shoulder angles. It has been shown that the optimal position for an athlete is very individual, due to differences in body size and shape, although some trends do exists even though actual percentage gains and losses differ between athletes. The height of the handlebars showed to have a slightly greater influence on the aerodynamic drag than the handlebar height, with a low handlebar height ($<$20mm spacing under the stem) resulting in a lower drag for the majority of athletes tested. A strong relationship was identified between hand position and time saving, with an arrow style hand position reducing the drag without compromising the power output. However, the stability of an arrow style hand position was questioned, suggesting that a further study was needed to identify if athletes could train in this position and hold it for the duration of a race without feeling unstable. In terms of the torso and shoulder angle, the minimum drag area was identified at a low torso angle, but not necessarily the lowest angle tested, and a high shoulder angle. The maximum power output was identified at a mid torso angle and low shoulder angle, suggesting that the shoulder angle has a greater influence on the power output and the torso angle has a greater influence on the drag. The concept of surplus power was used to identify the optimal torso and shoulder angle in terms of both drag and power output, and the results

showed that the maximum surplus power for the athletes tested was at a low torso angle (4.5° to 8.6°) and mid shoulder angle (88.9° to 105.3°). The actual percentage gain varied between athletes, again highlighting the importance of individual testing to identify the exact set up that results in the lowest drag and highest power output for each athlete. For future studies it would be beneficial to identify whether any trends exist between anthropometric data and the optimal position of individual athletes in terms of handlebar position and torso and shoulder angles.

Chapter 9

Overall Gains and Losses

Introduction

The experimental results for all positional and equipment changes described in Chapters 7 and 8 were combined so that the potential gains to be had from optimising equipment and/or position could be ranked. As not all tests included pedalling athletes as subjects, a comparison was made between stationary and pedalling tests for the same changes in position and equipment (using the same athletes) to determine whether there was a significant difference between the percentage gains or losses in drag for changes made using pedalling athletes compared to stationary athletes. Two athletes compared stationary and pedalling tests for changes made to athlete position, one athlete compared stationary and pedalling tests for different skinsuits, and one athlete compared stationary and pedalling tests for different shoe covers. The wind tunnel was set at 42kph for all tests and the results can be seen in Table 9.1.

Athlete	Test	Drag Static (kg)	% Difference from Baseline	Drag Pedalling (kg)	% Difference from Baseline	% Difference Pedalling vs Stationary
	Baseline	1.831	-	2.012	-	-
	Bars down 10mm	1.974	7.2	2.155	6.6	-0.6
1	Longer extensions	1.957	6.4	2.135	5.8	-0.7
	Wider bars	2.054	10.9	2.262	11.1	0.2
	Narrower bars	2.034	10.0	2.254	10.7	0.8
	Baseline	2.001	-	2.055	-	-
	Bars lower	1.942	-3.0	1.978	-3.9	-0.9
2	Extensions 20mm higher	1.981	-1.0	2.022	-1.6	-0.6
	Bars 10mm lower	1.952	-2.5	2.001	-2.7	-0.2
	Helmet change	1.986	-0.8	2.037	-0.9	-0.1
	Skinsuit 1	1.972	-	2.102	-	-
3	Skinsuit 2	1.988	0.8	2.106	0.2	-0.6
	Skinsuit 3	2.030	2.9	2.153	2.4	-0.5
	Skinsuit 4	1.965	-0.4	2.079	-1.1	-0.8
	No Shoe Covers	2.134		2.209		
4	Prototype 1	2.083	-2.4	2.154	-2.6	-0.1
	Prototype 2	2.089	-2.2	2.172	-1.7	0.5
	Champion Systems	2.130	-0.2	2.200	-0.4	-0.2

Table 9.1: Comparison between pedalling and stationary tests for the same changes in position and equipment

The results from Table 9.1 show that the difference in the percentage gains and losses between pedalling tests compared to stationary tests was $<\pm 1\%$, which is the same as the uncertainty of the cycle rig. Therefore it can be assumed that the percentage gains and losses for stationary tests are the same as for pedalling tests, and so all experimental results for changes in position and equipment described in Chapters 7 and 8, whether stationary or pedalling, will be included in the overall ranking of potential gains to be had from optimising equipment and/or position. The only experimental results that will be omitted are those where no athlete was used for testing (shoe covers on a leg model and material testing for skinsuits).

In addition to the detailed wind tunnel tests described in Chapters 7 and 8, a number of individual and multiple changes in position and equipment were carried out on elite athletes in the wind tunnel with the overall aim of identifying the optimal set up for individual track cyclists. All athletes were pedalling at approximately 90rpm for each change made, and the wind tunnel speed was set at 42kph. Individual changes in position included changes to the bar height, bar width, bar length, seat height, seat lateral position, helmet tip position, degree of tapering to the bars, and lowering the head into a more crouched position. Multiple changes in position were made by combining one or more of the individual changes mentioned. Equipment changes included testing different skinsuits, different helmets, taping helmet holes, comparing shoe covers to no shoe covers, and tucking long hair into the helmet or in a bun to eliminate the hair from the oncoming flow. All changes were made from the reference position of each athlete, and the difference in drag recorded. Not every athlete compared all changes in position and/or equipment due to differences in equipment, reference position, and time constraints. Also, as the position of the seat is related to the athlete's leg length, a change in seat height was only considered worthwhile if the athlete believed that they could produce the same or greater power output. No athlete believed that they could produce the same or greater power with a lower seat, so therefore this change in position was not carried out.

In order to determine the impact of each change on the aerodynamic drag, the greatest difference in drag from the reference position (gain or loss) was recorded for each change for each athlete. The reference position was chosen to be the current racing position for each individual athlete, including their own bike, wheels, helmet and skinsuit. Although the actual setup varied between athletes, most athletes adopted a relatively low, aero position using handlebar extensions and wearing an aero helmet. The average impact of each change on the aerodynamic drag could then be calculated. For this analysis the degree to which changes were made, for example the actual angle of the helmet tip to the horizontal or the actual degree of tapering of the bars, was not important, as the aim was to determine the impact of each change on the drag and not to compare the actual position or equipment used between athletes. The average impact on drag was separated into individual, multiple, and equipment changes because it cannot be assumed that gains and losses are additive; the flow field around an athlete is not a linear superposition of component flow fields. The approximate time saving for each change in position and/or equipment was then calculated using the mathematical model and the data for one of the male athletes used to validate the model (Athlete 11) described in Chaper 4; percentage changes in drag area, C_dA, made on other athletes were applied to the drag area of Athlete 11 in the model. Any trends between changes in position and/or equipment with gender, competitive level, or between road and track cyclists were identified by categorising the data and generating plots to compare the average change in drag from the reference position for each category. This chapter aims to identify the most significant factors in terms of aerodynamic drag, to help athletes and coaches quickly identify those areas where performance gains can be made and to quantify these gains in terms of an approximate time saving.

9.1 Calculation of Time Saving

The mathematical model described in Chapter 4 was used to calculate the finishing time for each change in position and/or equipment using the data for one of the athletes used to validate the model (Athlete 11). A summary of the data for Athlete 11 can be seen in Table 9.2.

Data for Athlete 11 (male, elite, track cyclist)	
Measured $\text{Drag}_{windtunnel}$ (at 42kph) (N)	29.07
Temperature (°C)	28
Pressure (mbar)	1021
Relative Humidity (%)	60
Air density (kg/m^3)	1.1806
Average velocity (kph)	55
Height (m)	1.85
Weight (kg)	75
Seat height (m)	1.2
Drag area, C_dA (m^2)	0.195
Gear Ratio	3.8
Drive chain efficiency (%)	98
Frame Mass (kg)	8
Wheel Mass (kg)	1.255
Wheel Radius (m)	0.3315
Bearing Radius (m)	0.012
Tyre Coefficient of Rolling Resistance (C_{rr})	0.002
Bearing Coefficient of Rolling Resistance (C_{rr})	0.002
Increase in Rolling Resistance in Bends (scrubbing) (%)	28
Increase in Rolling Resistance in Straights (scrubbing) (%)	4
Percentage Weight on Rear Wheel (%)	60
Track Grade Angle (rad)	0
Track Banking Angle in Straights (rad)	0.733
Track Banking Angle in Bends (rad)	0.22
Track Radius of Curvature in Bends (m)	26.101
Track Radius of Curvature in Straights (m)	1x10^{21}
Race distance (m)	4000
Actual finishing time (s)	265.023
Predicted finishing time (s)	268.370

Table 9.2: Data for Athlete 11 used to calculate the approximate time saving for each change in position and/or equipment

For each change made to the position or equipment the change in drag area, C_dA, from the reference position was calculated from the measured drag results using Equation 9.1, where $\triangle D$ is the change in measured drag from there reference position (N), ρ is the air density (kgm^{-3}) and V is the wind speed (ms^{-1}). This enabled a new drag area to be inserted into the mathematical model, while all other inputs remained the same, in order to calculate the time difference between each change and the reference position for a 4000m Individual Pursuit event.

$$\triangle C_dA = \frac{\triangle D}{\frac{1}{2}\rho V^2} \tag{9.1}$$

9.2 Rank of Changes in Terms of Impact on Drag

The maximum change in drag from the reference position (increase or decrease) for each variable tested (e.g. stem height) for each athlete was averaged and these results were then ranked in terms of impact, i.e. from

highest to lowest gains or losses. These results for individual, multiple, and equipment changes can be seen in Tables 9.3, 9.4 and 9.5 respectively. The time savings for each individual change in position, multiple change in position, and equipment change for a 4000m IP athlete are shown in Tables 9.6, 9.7 and 9.8 respectively. Change in drag means the difference in drag force from the reference position (N). A more detailed description of each change can be seen in Appendix E.

Change	Maximum percentage change in drag (+ or -) from the reference position for each, individual athlete (1 to 25)*																									Av. Δ drag (%)
	1	2	3	4	5	6	7	8	9	10	11	12	13	14	15	16	17	18	19	20	21	22	23	24	25	
Head low/crouch		3.8	0.7			5.1	3.7	0.7		4.2			6.5	2.2			2.3			4.4			2.6		5.4	3.5
Helmet tip up	4.1	2.3						2.4	1.9																	2.7
Extensions shortened					1.7					3.2																2.5
Hand change			0.5	3.3	0.4		1.6	3.5	3.0		4.1		0.9					2.1					1.6			2.1
Tip down	4.3			2.5		2.4	2.1		1.9		0.5	1.4					1.1		2.0							2.0
Stem down	0.5	0.4	0.7	2.8	1.3		2.3				1.0		1.6		3.9		4.1			5.7				0.5	1.2	2.0
Seat back								1.8																		1.8
Hair tucked in										2.5	1.0															1.8
Seat forwards								1.7																		1.7
Extensions wider	0.6	1.2			0.2		1.4			1.2	1.0	5.4	0.8				2.4			2.5					0.7	1.6
Stem up		2.0	2.0	1.9		0.1			1.4	2.0	1.9	1.4	0.4	1.2	0.8				1.2	3.4	1.2			1.8		1.5
Tapered bars		0.3		2.6	1.7	1.6	1.3	2.4			3.0	0.4	0.2													1.5
Extensions narrower		1.2	1	5.4		0.9	0.1		1.0			1.9	1.2	0.4					0.4					4.2	0.1	1.5
Extensions lengthened		1.3	1.2									1.7	1.6													1.5
Raise seat						0.1	1.3	1.5																		1.0

Table 9.3: Rank of Gains or Losses in Drag for each Individual Change in Position per athlete
*These are the maximum changes in drag (increase or decrease) from the reference position for each athlete for each variable tested.

Change	Maximum change in drag (%) from reference position for each athlete																							Av Δ drag (%)
	1	2	3	4	5	6	7	8	9	10	11	12	13	14	15	16	17	18	19	20	21	22	23	
Extension height and length	9.6	11.1	7.6																					**9.4**
Helmet tip up & stem down	4.6																							**4.6**
Stem down & hand change				6.1											1.8									**4.0**
Extensions forward & head low		5.1	3.5									0.7	6.2											**3.9**
Extension height and width with head low		2.4											4.6						4.8					**3.9**
Stem down & head low													2.2				4.7							**3.5**
Extensions wider & head low		4.1																	1.0					**2.6**
Extensions forward & narrow		1.0																		3.4				**2.2**
Seat raised & stem down						1.7																		**1.7**
Extension height and width								0.5					1.9								3.8	0.6		**1.7**
Bars tapered & hand change							2.7	0.5			1.6													**1.6**
Extensions forward & hand change			2.3										0.9											**1.6**

Table 9.4: Rank of Gains or Losses in Drag for each Multiple Change in Position per Athlete

Change	Maximum change in drag (%) from reference position for each athlete																									Av Δ drag (%)
	1	2	3	4	5	6	7	8	9	10	11	12	13	14	15	16	17	18	19	20	21	22	23	24	25	
Different skinsuit			2.3					4.5							7.6	2.0	8.0	8.9	7.6	7.7	7.7					6.3
Different frame & wheels*	3.0																									3.0
Different helmet					3.7				3.2					1.8	3.3	2.8					6.2	1.2		1.2		2.9
Same wheels different frame*	2.8																									2.8
Same frame different wheels*	2.5																									2.5
Visor vs no visor		2.2			1.8				3.0	0.2	4.7	2.8	1.7	3.4	2.4					0.2			2.7	1.5		2.2
Pedal/strap combination														2.1												2.1
Shoe covers vs no shoe covers	2.4	1.5																1.7		1.7					1.8	1.8
Same pedal different strap														1.8												1.8
Gloves vs no gloves														1.3												1.3
Helmet holes taped vs untaped										1.0													0.7			0.9
Same strap different pedal														0.3												0.3
Modified seat tube shape	0.3																									0.3
Modified fork shape	0.2																									0.2
Modified Stem shape	0.1																									0.1

Table 9.5: Rank of Gains or Losses in Drag for each Equipment Change per Athlete

* Wheels were disc wheels.

Change	Average Δ Drag (%).	Δ CdA	Δ Time
Tucked head/crouch/head low	3.5	0.0068	2.940
Helmet tip up	2.7	0.0053	2.520
Extensions shortened	2.5	0.0049	2.105
Hand change	2.1	0.0041	1.690
Tip down	2.0	0.0039	1.690
Stem down	2.0	0.0039	1.690
Seat back	1.8	0.0035	1.690
Hair tucked in	1.8	0.0035	1.690
Seat forwards	1.7	0.0033	1.690
Extensions wider	1.6	0.0031	1.270
Stem up	1.5	0.0029	1.270
Tapered bars	1.5	0.0029	1.270
Extensions narrower	1.5	0.0029	1.690
Extensions lengthened	1.5	0.0029	1.270
Raise seat	1.0	0.0020	0.850

Table 9.6: Calculated Time Savings for Each Individual Change in Position from the Reference Position

Change	Average Δ Drag (%).	Δ CdA	Δ Time
Extension height and length	9.4	0.0183	8.180
Helmet tip up & stem down	4.6	0.0090	4.170
Stem down & hand change	4.0	0.0078	3.350
Extensions forward & head low	3.9	0.0076	3.350
Extension height and width with head low	3.9	0.0076	3.350
Stem down & head low	3.5	0.0068	2.940
Extensions wider & head low	2.6	0.0051	2.105
Extensions forward & narrow	2.2	0.0043	2.105
Seat raised & stem down	1.7	0.0033	1.690
Extension height and width	1.7	0.0033	1.690
Bars tapered & hand change	1.6	0.0031	1.270
Extensions forward & hand change	1.6	0.0031	1.270

Table 9.7: Calculated time savings for Multiple Changes in Position from the Reference Position

Change	Average Δ Drag (%).	Δ CdA	Δ Time
Different skinsuit	6.3	0.0123	5.370
Different frame & wheels	3.0	0.0059	2.520
Different helmet	2.9	0.0057	2.520
Same wheels different frame	2.8	0.0055	2.520
Same frame different wheels	2.5	0.0049	2.105
Visor vs no visor	2.2	0.0043	2.105
Pedal/strap combination	2.1	0.0035	1.690
Shoe covers vs no shoe covers	1.8	0.0035	1.690
Same pedal different strap	1.8	0.0035	1.690
Gloves vs no gloves	1.3	0.0031	1.270
Helmet holes taped/untaped	0.9	0.0018	0.850
Same strap different pedal	0.3	0.0006	0.425
Modified seat tube shape	0.3	0.0006	0.425
Modified fork shape	0.2	0.0004	0.000
Modified Stem shape	0.1	0.0002	0.000

Table 9.8: Calculated time savings for Equipment Changes

The individual change in position that had the greatest impact on drag came from adopting a crouch position, where the head was lowered into the shoulders while ensuring the cyclists continue to look forwards and maintain their line of vision, with an average of a 3.5% change in drag from the reference position and a time saving of 2.94s over 4000m. The multiple change in position that had the greatest impact on drag came from changing the extension height and length, with an average of a 9.4% change in drag from the reference position and a time saving of 8.18s over 4000m. The equipment change that had the greatest impact on drag was a change in skinsuit, with an average of a 6.3% change in drag from the reference position and a time saving of 5.37s over 4000m. By adopting a crouch position athletes are able to reduce their frontal area significantly, and previous published results have shown that there is a strong correlation between frontal area and aerodynamic drag [Defraeye et al., 2010]. A change to the height and length of the extensions has an influence on the torso and shoulder angle of a cyclist, and by lengthening the extensions and lowering the handlebars it is possible to bring the torso closer to the horizontal, which has also been shown to help reduce the aerodynamic drag significantly [Kyle, 2003a] and reduce the frontal area. A change in skinsuit can affect both skin friction drag and pressure drag through the use of a different material, seam placement, and fit (number of wrinkles). By strategically placing material and seams on different parts of the body it is possible to induce turbulence and delay separation, which consequently reduces the drag. Minimising the number of wrinkles and ensuring the skinsuit is a tight fit will also help reduce the drag, and the results in this study have shown how great an impact a skinsuit can have in terms of athlete performance.

The results from this study show that in general, multiple changes result in a greater gain or loss in drag compared to individual changes, probably because multiple changes in position reduce the frontal area more than individual changes in position. However, that the gains and losses are not additive; a combination of the individual changes which result in the greatest difference from the reference position will not necessarily result in the greatest difference for multiple changes, nor will the total gain or loss be an addition of the individual gains or losses. For example individual changes made by moving the stem down and lowering head resulted in an average change in drag from the reference position of 2.0% and 3.5% respectively, but when combined as a multiple change in position the average change in drag from the reference position was 5.5%.

A change in skinsuit had a significantly greater impact on the aerodynamic drag compared to all other changes made to the equipment, and a change to the shape of the bike frame had no significant impact on the drag (<0.3%). This low change in drag for the bike frame is likely to be due to the fact that all bikes used in this study were already optimised in terms of aerodynamics with an aerodynamic frame; a comparison between a non-aerodynamic and aerodynamic frame would likely lead to a greater change in drag. In general, changes in position had a greater impact on drag compared to changes in equipment, which is in agreement with previous studies that state that athlete position is the most influential factor on aerodynamic drag when cycling on the flat at speeds greater than 13kph [Kyle, 2003a]. However, certain changes made to the equipment also had a significant impact on the drag, which should not be ignored in order to maximise athlete performance. Specifically, by changing both the bike frame and wheels, or changing the type of helmet used, a difference in drag of 3% and 2.9% from the reference position respectively was observed. This equates to a time saving of 2.52s over 4000m. A relatively large impact on drag was also found by changing either the frame (2.8%) or the wheels (2.5%) individually. A change in the frame includes a change in the type of handlebars used, which in turn affects the position of the forearms and hands, and alters the frontal area and direction of the flow over the rest of the body. According to Lukes et al. [2005] the handlebars can influence the overall drag by 3%, which is a similar result to the 2.8% average difference in drag for a change in bike frame. These results highlight the importance of selecting the best possible equipment for each rider, in particular the handlebars, so that the aerodynamic drag is reduced as much as possible.

The best type of helmet used depends on the shape of the athelte's body and the way in which the helmet sits on the athlete's head. The aim is to get the helmet to sit so that the curvature of the streamlines are lower and separation is delayed. Due to the big differences in body shapes and head sizes, the optimal helmet for each athlete in terms of aerodynamics is likely to be different. However, a change in helmet did show a significant impact on the drag of 2.9%, highlighting the importance of selecting the best possible helmet for each, individual athlete. It is hypothesised that the influence of a helmet visor on aerodynamic drag depends on the type of helmet used, the shape of the athlete's face, the length of the athlete's neck and width of their shoulders. Ideally, the profile of the helmet and visor should smooth the flow around the face, so that the rest of the flow over the body is as streamlined as possible. The impact of wearing a visor on the aerodynamic drag was also relatively significant (2.2% change in drag) but not as significant as a change in helmet. The influence of the helmet holes on the aerodynamic drag was only compared for two athletes (one helmet each) and although the results showed a slight increase in drag when the holes were taped compared to untaped, a more detailed study would be needed to determine whether helmet holes in general do have a significant effect on the drag of a cyclist, or whether the effect of taping the helmet holes is dependent on the type of helmet, and/or the size, shape and location of the holes themselves.

A summary of the range of change in drag values for each individual change in position, multiple change in position, and equipment change for all athletes is shown in Tables 9.9, 9.10 and 9.11 respectively. These results show that there is a significant range of the actual impact on the aerodynamic drag between athletes for nearly all changes where more than one athlete was tested. Exceptions include lengthening the extensions, wearing shoe covers, and taping the helmet holes, where the range of the change in drag values between athletes was only 0.5%, 0.9% and 0.3% respectively; for all other changes in position and equipment the change in drag ranged from 1% to 6.9%. This highlights that although trends may be seen, the actual gain or loss in drag from the reference position can vary significantly between athletes and not all athletes will obtain the same benefit from making the same changes. This is probably due to differences in body shape and size, athlete experience at holding a specific position, how easy athletes find it to adopt a new position, and

how aerodynamic an athlete's reference position is already; if an athlete already has a relatively aerodynamic reference position then they are less likely to see big reductions in drag from changes in position.

Change	Average Δ drag (%)	Lower Δ drag (%)	Upper Δ drag (%)	Range	Number of Athletes Tested
Tucked head/crouch/head low	3.5	0.7	6.5	5.8	12
Helmet tip up	2.7	1.9	4.1	2.2	4
Extensions shortened	2.5	1.7	3.2	1.5	2
Hand change	2.1	0.4	4.1	3.7	10
Stem down	2.0	0.4	5.7	5.3	13
Tip down	2.0	0.5	4.3	3.8	9
Hair tucked in	1.8	1.0	2.5	1.5	2
Seat back	1.8	1.8	1.8	0.0	1
Seat forwards	1.7	1.7	1.7	0.0	1
Extensions wider	1.6	0.2	5.4	5.2	11
Extensions narrower	1.5	0.1	5.4	5.3	12
Stem up	1.5	0.1	3.4	3.3	15
Tapered bars	1.5	0.2	3.0	2.8	9
Extensions lengthened	1.5	1.2	1.7	0.5	4
Raise seat	1.0	0.1	1.5	1.4	3

Table 9.9: Range of drag values for individual changes in position

Change	Average Δ drag (%)	Lower Δ drag (%)	Upper Δ drag (%)	Range	Number of Athletes Tested
Extension height and length	9.4	7.6	11.1	3.5	3
Helmet tip up & stem down	4.6	4.6	4.6	0.0	1
Stem down & hand change	4.0	1.8	6.1	4.3	2
Extensions forward & head low	3.9	0.7	6.2	5.5	4
Extension height and width, head low	3.9	2.4	4.8	2.4	3
Stem down & head low	3.5	2.2	4.7	2.5	2
Extensions wider & head low	2.6	1.0	4.1	3.1	2
Extensions forward & narrow	2.2	1.0	3.4	2.4	2
Extension height and width	1.7	0.5	3.8	3.3	4
Seat raised & stem down	1.7	1.7	1.7	0.0	1
Bars tapered & hand change	1.6	0.5	2.7	2.2	3
Extensions forward & hand change	1.6	0.9	2.3	1.4	2

Table 9.10: Range of drag values for multiple changes in position

Change	Average Δ drag (%)	Lower Δ drag (%)	Upper Δ drag (%)	Range	Number of Athletes Tested
Different skinsuit	6.3	2.0	8.9	6.9	9
Different frame & wheels	3.0	3.0	3.0	0.0	1
Different helmet	2.9	1.2	6.2	5.0	8
Same wheels different frame	2.8	2.8	2.8	0.0	1
Same frame different wheels	2.5	2.5	2.5	0.0	1
Visor vs no visor	2.2	0.2	4.7	4.5	12
Pedal/strap combination	2.1	2.1	2.1	0.0	1
Shoe covers vs no shoe covers	1.8	1.5	2.4	0.9	5
Same pedal different strap	1.8	1.8	1.8	0.0	1
Gloves vs no gloves	1.3	1.3	1.3	0.0	1
Helmet holes taped vs untaped	0.9	0.7	1.0	0.3	2
Same strap different pedal	0.3	0.3	0.3	0.0	1
Modified seat tube shape	0.3	0.3	0.3	0.0	1
Modified fork shape	0.2	0.2	0.2	0.0	1
Modified Stem shape	0.1	0.1	0.1	0.0	1

Table 9.11: Range of drag values for equipment changes

The athletes used for this study were a combination of elite, competitive, male, female, adult and junior riders. Therefore, the reference position of the elite, adult riders may have been more aerodynamic than the reference position of the competitive, junior riders. In this case, the change in drag from the reference position of the elite, adult riders is likely to be less than that of the competitive, junior riders. This may explain some of the low change in drag values in this study when it would be expected that the change in position and/or equipment would result in a significant gain or loss. Also the UCI rules limit the degree to which changes can be made, especially to the extension length and seat height. If the reference position of one athlete is already at this limit, the number of changes that could be made to improve their position would be minimal, and the overall aim of wind tunnel testing is to reduce, not increase, the drag. Although all riders selected were at least at a competitive level (not recreational riders) there would still have been some variability in riding experience. This would affect the athlete's ability of adopting a new position and holding this position for the length of the test. Each rider used their own equipment for the testing, which would have differed between athletes. The type of equipment used will have an effect on the degree of changes that can take place; some athletes may have only been able to adjust their handlebars or stem by a small degree compared to other athletes, limiting the range of testing. The hand and forearm position will depend on the type of extensions used, as well as how stable and comfortable the rider feels. The type of helmet used and shape of the body of the rider, in particular how flat or curved the back is, will affect the head position at which the rider can reduce their drag the most. The gains or losses from either wearing or not wearing a visor will also depend on the type of helmet used and the shape of the athlete's face; the more streamlined the leading elements the lower the aerodynamic drag.

Although a wide range of change in drag values was seen between athletes, and although there may appear to be a number of influences on the extent to which changes can be made for different athletes, being able to identify where significant changes can be made regardless of body size and shape or equipment used is beneficial to athletes and coaches in order to prioritise areas for spending time and money. Therefore changes in position and/or equipment where more than 1 athlete was involved and where the lowest change in drag

from the reference position was greater than 1% was considered to have a significant effect on the performance of all athletes. These changes are highlighted in Table 9.12. It should be noted that these changes indicate significant losses as well as gains in drag, as the aim of this study was to determine those changes that had a significant impact on drag, and not to identify the change that resulted in the lowest drag.

	Change	Average) Δ drag (%)	Lower Δ drag (%)	Upper Δ drag (%)	Range	Number of Athletes Tested
Individual	Helmet tip up	2.7	1.9	4.1	2.2	4
	Extensions shortened	2.5	1.7	3.2	1.5	2
	Hair tucked in	1.8	1.0	2.5	1.5	2
	Extensions lengthened	1.5	1.2	1.7	0.5	4
Multiple	Extension height and length	9.4	7.6	11.1	3.5	3
	Stem down & hand change	4.0	1.8	6.1	4.3	2
	Extension height and width, head low	3.9	2.4	4.8	2.4	3
	Stem down & head low	3.5	2.2	4.7	2.5	2
	Extensions wider & head low	2.6	1.0	4.1	3.1	2
	Extensions forward & narrow	2.2	1.0	3.4	2.4	2
Equipment	Different skinsuit	6.3	2.0	8.9	6.9	9
	Different helmet	2.9	1.2	6.2	5.0	8
	Shoe covers vs no shoe covers	1.8	1.5	2.4	0.9	5

Table 9.12: Changes in position and equipment considered to be significant on the performance of all athletes

The results in Table 9.12 show that there are a number of individual, multiple, and equipment changes that can be made that are likely to have a significant impact on the drag of all cyclists. Particular changes include those that result in getting the head and body low to reduce the frontal area, and ensuring the helmet tip is in the right position. In addition, the type of skinsuit and helmet worn, and wearing shoe covers also affected the drag significantly for all athletes tested. Athletes and coaches should therefore concentrate on optimising these factors first through wind tunnel testing, as these changes are likely to result in the greatest gains in terms of drag, time and speed for all athletes involved. These results however, do not identify the best overall position for athletes in general, due to high variability between the size and shape of the body, experience, equipment used by each athlete, and the ability of the athlete to adopt and hold a different position from their reference position.

In order to see if there was a certain position which resulted in the lowest aerodynamic drag for a large proportion of the athletes tested in the wind tunnel, regardless of body size and shape, a summary of the best overall position for each athlete was created, as shown in Table 9.13. Table 9.14 shows a tally of those changes which contribued to the position with the lowest drag for all the athletes.

Athlete	Best Position	$C_dA_{WindTunnel}$
1	Stem down, helmet tip up	0.237
2	Extensions lengthened, head low crouch	0.232
3	Stem down 5mm	0.211
4	Stem down, hand change	0.258
5	Hand change	0.240
6	Seat up & extensions down	0.257
7	Tucked head/crouch	0.242
8	Head low	0.248
9	Hand change	0.275
10	Head low	0.244
11	Stem down 6mm	0.262
12	Extensions lengthened 1cm	0.280
13	Stem down, extensions wider, crouch	0.247
14	*Equipment*	-
15	Stem down 15mm	0.287
16	*Equipment*	-
17	Helmet tip down	0.236
18	Hand change	0.251
19	*Equipment*	-
20	Stem down	0.229
21	Stem up 20mm	0.268
22	*Equipment*	-
23	Head down	0.258
24	Stem 20mm higher and narrow extensions	0.201
25	Stem down and narrow extensions	0.198

Table 9.13: Best position for each athlete

Change	Number of athletes who used this change to obtain the most aerodynamic position	Total number of athletes who tested this position
Stem down	8	13
Head/helmet low or crouch	6	12
Hand change	4	10
Extensions narrower	2	12
Extensions lengthened	2	4
Stem up	2	15
Seat up	1	3
Extensions wider	1	11
Helmet tip down	1	9
Helmet tip up	1	4

Table 9.14: Number of athletes who used each change to obtain the lowest possible aerodynamic drag

Table 9.14 shows that by lowering the head and/or helmet, and moving the stem down were the most common changes for obtaining the lowest aerodynamic drag, where more than half of the athletes who tested those changes found a reduction in drag. Moving the stem down and lowering the head/helmet reduces the frontal

area of the athlete and helps to obtain a more horizontal torso and streamlined position. These results agree with the literature, which suggests that a horizontal torso, chin down, low position, and tucked head are the most effective ways of reducing the aerodynamic drag because these changes reduce the frontal area of the rider [Broker, 2003, Burke and Pruitt, 2003, Garcia-Lopez et al., 2008, Kyle, 2003a, Oggiano et al., 2008, Zdravkovich et al., 1996]. These results also show that it is important to lower both the head and helmet, and not just the helmet tip in order to obtain the most aerodynamic position. Interestingly, making a hand change was also a beneficial way of obtaining a low aerodynamic drag. The hands are the first point of contact of the airflow, so these results suggest that by adopting a certain hand position the athlete can actually direct the flow around the rest of the body so that it is more streamlined.

The results in Tables 9.12 and 9.14 indicate that the handlebar position, in particular the bar height, and getting the head low are the two most significant factors that affect the aerodynamic drag of a cyclist, and that by getting low to reduce the frontal area leads to a significant reduction in drag, and therefore an increase in cycling speed and athlete performance.

9.3 Significant Trends

In order to identify any trends between changes in position and/or equipment with gender, competitive level, or between road and track cyclists the data was sorted into male and female categories, elite and competitive categories, and then track and road cyclists, and the average change in drag from the reference position determined for each. Table 9.15 shows a summary of the biometric data for all the athletes used in this study. As there were only three junior riders used for testing, a valid comparison between adults and junior riders could not be made. Plots were created to compare the average change in drag for different changes in position and equipment for male and female athletes, elite and competitive riders, and road and track cyclists, as shown in Figures 9.1, 9.2 and 9.3 respectively.

Athlete	Gender	Competitive Level	Road/Track	Adult/Junior
1	Male	Competitive	Road	Adult
2	Male	Elite	Track	Adult
3	Female	Elite	Track	Adult
4	Male	Competitive	Track	Adult
5	Female	Elite	Road	Adult
6	Female	Competitive	Track	Junior
7	Male	Competitive	Track	Junior
8	Male	Competitive	Track	Junior
9	Female	Elite	Track	Adult
10	Male	Elite	Track	Adult
11	Female	Elite	Track	Adult
12	Female	Elite	Track	Adult
13	Male	Elite	Track	Adult
14	Male	Elite	Track	Adult
15	Male	Elite	Track	Adult
16	Male	Competitive	Road	Adult
17	Male	Elite	Track	Adult
18	Male	Competitive	Road	Adult
19	Male	Elite	Track	Adult
20	Male	Elite	Road	Adult
21	Male	Competitive	Track	Adult
22	Male	Competitive	Road	Adult
23	Male	Elite	Track	Adult
24	Female	Elite	Track	Adult
25	Female	Elite	Track	Adult

Table 9.15: Biometric data for all athletes used as subjects for testing

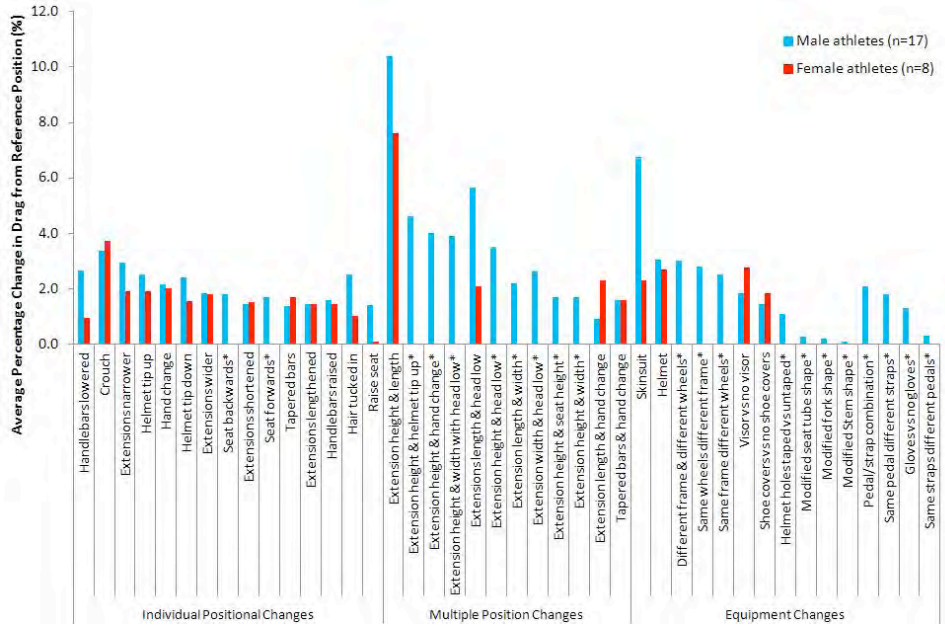

Figure 9.1: Comparison of average change in drag for male and female athletes
* No females tested these changes
** No males tested these changes

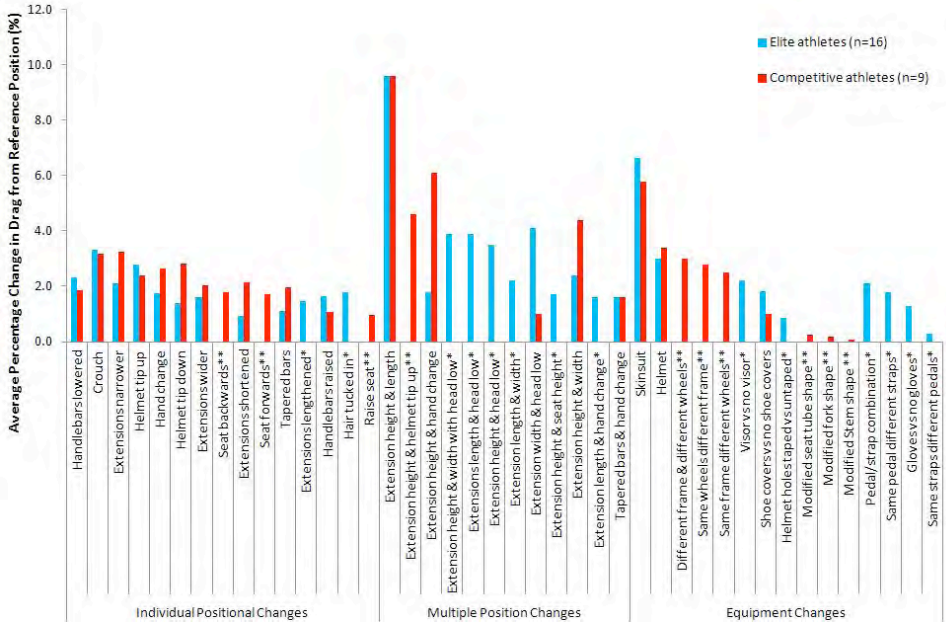

Figure 9.2: Comparison of average change in drag for elite and competitive athletes
* No competitive riders tested these changes
** No elite riders tested these changes

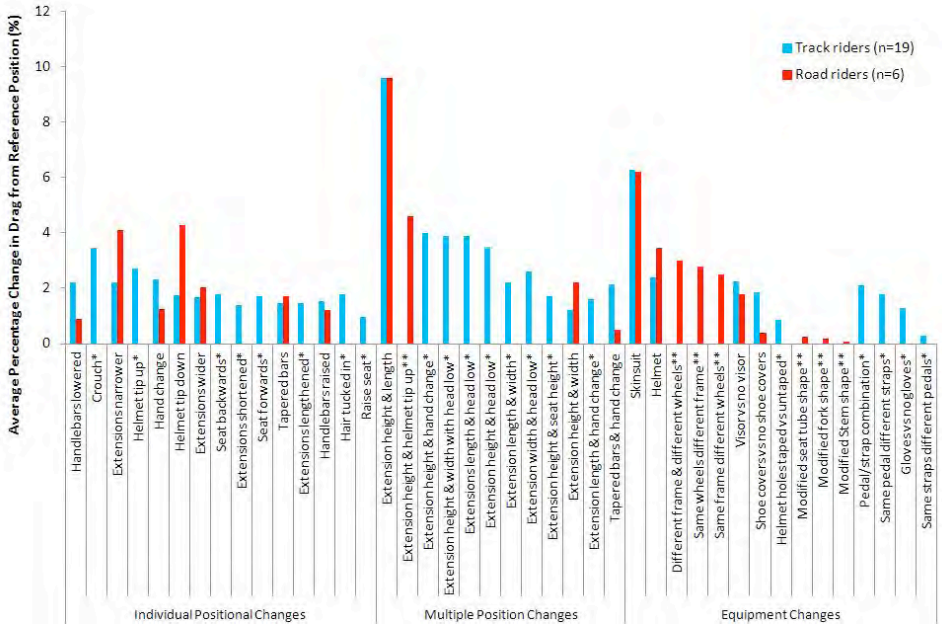

Figure 9.3: Comparison of average change in drag for road and track cyclists
* No road riders tested these changes
** No track riders tested these changes

The impact of changes in position and equipment on the drag was similar for both male and female athletes, with changes to the extension length and height (multiple change) having the greatest impact on drag for both categories. A slightly greater impact on drag was seen for male athletes with changes made to the extension length and lowering the head, raising the seat, and for a change in skinsuit, but there is no obvious explanation for this. It is possible these differences solely arise from differences in the body shape of male athletes compared to female athletes.

The impact of changes in position and equipment on the drag was mostly similar for elite and competitive athletes, although changes to the extension width and lowering the head had a slightly greater impact on drag for elite athletes, and changes to the handlebar height and width had a slightly greater impact on drag for competitive athletes. It is possible that elite athletes already adopt a reference position that they believe to be aerodynamic, with a relatively horizontal torso and narrow forearms. Although no big gains may be seen when changing the handlebar height and width for these athletes, by actually widening the forearms so that they can lower their head without losing their line of vision may actually reduce their drag significantly. On the contrary, competitive athletes are less likely to have an aerodynamic reference position, so these athletes will see bigger gains from trying to adopt a more horizontal torso position by making changes to the handlebar height and width. Again, changes made to the extension length and height (multiple change) and to the skinsuit had the greatest impact on both elite and competitive athletes.

The impact of changes in position and equipment on the drag was similar for both road and track cyclists, with changes to the extension length and height (multiple change) and to the skinsuit having the greatest impact on drag for both categories. The only significant difference was seen for lowering the helmet tip, where a greater impact on drag was seen for road riders. It is unclear why this difference occurred between

road and track riders, but it could be due to a more aerodynamic reference position of the helmet tip for track riders compared to road riders. The results from this study show that changes made to the extension length and height, and changing the skinsuit have the most significant impact on aerodynamic drag for all athletes regardless of gender, competitive level, and field.

The results from this study have shown that significant changes in drag from the reference position can be found through changes in position and/or equipment. However, in order to identify which changes are likely to be the most successful at reducing drag and which are most likely to increase drag, the maximum change in drag for each variable for each athlete (shown in Tables 9.3, 9.4 and 9.5) were sorted into gains and losses, and then the total percentage increase and total percentage decrease in drag for all the athletes for each variable was calculated, as shown in Figure 9.4 and Tables 9.16, 9.17, and 9.18 for individual changes in position, multiple changes in position, and equipment changes, respectively.

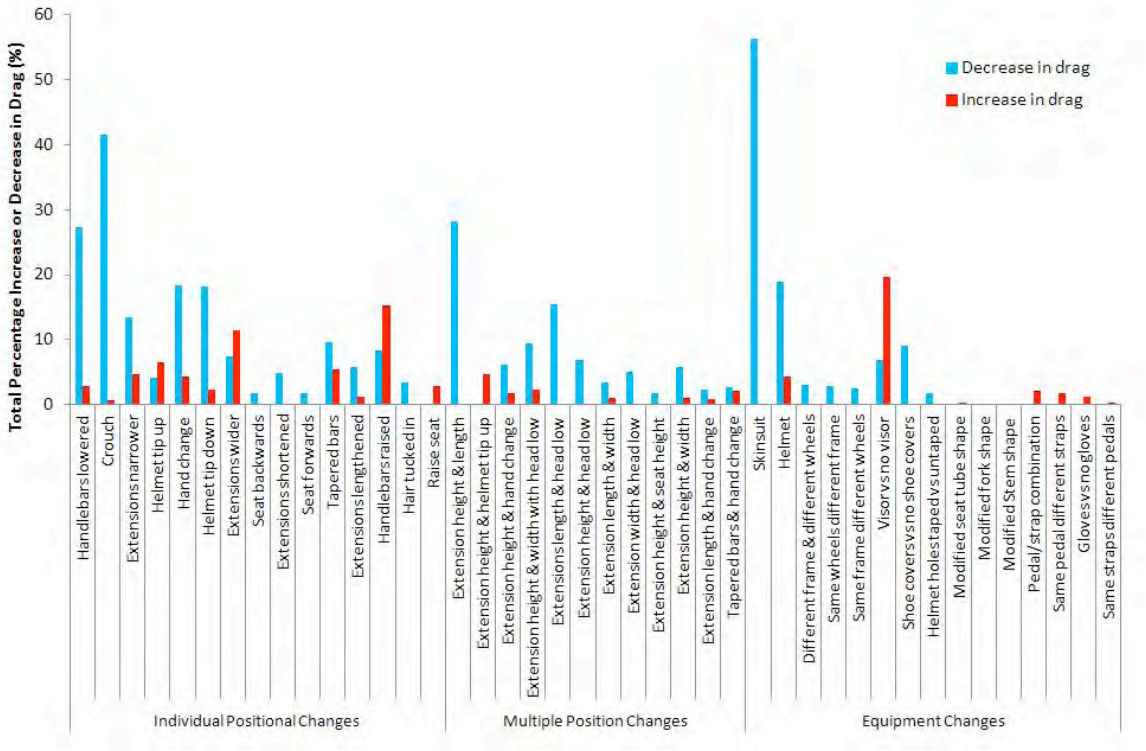

Figure 9.4: Total percentage increase and decrease in drag for all athletes

	Maximum Increase (+) or Decrease (-) in Drag from Reference Position for Each Athlete Individual Athlete (1 to 25)																								Total Increase	Total Decrease
Change	**1**	**2**	**3**	**4**	**5**	**6**	**7**	**8**	**9**	**10**	**11**	**12**	**13**	**14**	**15**	**16**	**17**	**18**	**19**	**20**	**21**	**22**	**23**	**24**	**25**	**in Drag (%)**	**in Drag (%)**
Head low/crouch		-3.8	-0.7			-5.1	-3.7	+0.7		-4.2			-6.5	-2.2			-2.3			-4.4			-2.6		-5.4	0.7	41.6
Helmet tip up	-4.1	+2.3						-2.4	+1.9																	4.2	6.5
Extensions shortened					-1.7					-3.2																-	4.9
Hand change			-0.5	-3.3	-0.4		-1.6	+3.5	-3.0		-4.1		+0.9					-2.1					-1.6			4.4	16.6
Tip down	-4.3			-2.5		2.4	-2.1		-1.9		-0.5	-1.4					-1.1		-2.0							2.4	15.8
Stem down	-0.5	+0.4	+0.7	-2.8	-1.3		-2.3				-1.0		-1.6		-3.9		-4.1			-5.7				+0.5	-1.2	1.6	24.4
Seat back								-1.8																		-	1.8
Hair tucked in										-2.5	-1.0															-	3.5
Seat forwards								-1.7																		-	1.7
Extensions wider	+0.6	-1.2			+0.2		+1.4			-1.2	-1.0	+5.4	+0.8				+2.4			-2.5					+0.7	11.5	5.9
Stem up		+2.0	+2.0	-1.9		+0.1			-1.4	+2.0	+1.9	+1.4	+0.4	+1.2	-0.8				+1.2	-3.4	+1.2			+1.8		14.0	7.5
Tapered bars		-0.3		-2.6	-1.7	-1.6	1.3	2.4			-3.0	0.4	0.2													4.3	9.2
Extensions narrower		+1.2	+1.0	-5.4		+0.9	+0.1		+1.0			+1.9	-1.2	-0.4					-0.4					-4.2	+0.1	6.2	11.6
Extensions lengthened		-1.3	+1.2									-1.7	-1.6													1.2	4.6
Raise seat						-0.1	+1.3	+1.5																		2.8	0.1

Table 9.16: Increases and Decreases in Drag from the Reference Position for each Athlete for Individual Changes in Position

	Maximum Increase (+) or Decrease (-) in Drag from Reference Position for Each Athlete																									Total Increase	Total Decrease
Change	**1**	**2**	**3**	**4**	**5**	**6**	**7**	**8**	**9**	**10**	**11**	**12**	**13**	**14**	**15**	**16**	**17**	**18**	**19**	**20**	**21**	**22**	**23**	**24**	**25**	**in Drag (%)**	**in Drag (%)**
Extension height and length	-9.6	-11.1	-7.6																							-	28.3
Helmet tip up & stem down	+4.6																									4.6	-
Stem down & hand change				-6.1											+1.8											1.8	6.1
Extensions forward & head low		-5.1	-3.5									-0.7	-6.2													-	15.5
Extension height and width with head low		+2.4											-4.6						-4.8							2.4	9.4
Stem down & head low													2.2				+4.7									-	6.9
Extensions wider & head low		-4.1																	-1.0							-	5.1
Extensions forward & narrow		-1.0																		+3.4						3.4	1.0
Seat raised & stem down						-1.7																				-	1.7
Extension height and width								+0.5					-1.9								-3.8	+0.6				1.1	5.7
Bars tapered & hand change							-2.7	+0.5			+1.6															2.1	2.7
Extensions forward & hand change			-2.3										+0.9													0.9	2.3

Table 9.17: Increases and Decreases in Drag from the Reference Position for each Athlete for Multiple Changes in Position

	Maximum Increase (+) or Decrease (-) in Drag from Reference Position for Each Athlete																								Total Increase	Total Decrease
Change	**1**	**2**	**3**	**4**	**5**	**6**	**7**	**8**	**9**	**10**	**11**	**12**	**13**	**14**	**15**	**16**	**17**	**18**	**19**	**20**	**21**	**22**	**23**	**24**	**25**	**in Drag (%)**	**in Drag (%)**
Different skinsuit			-2.3					-4.5							-7.6	-2.0	-8.0	-8.9	-7.6	-7.7	-7.7					-	56.3
Different frame & wheels*	-3.0																									-	3.0
Different helmet					-3.7				+3.2					-1.8	-3.3	-2.8					-6.2	-1.2		+1.2		4.4	19.0
Same wheels different frame*	-2.8																									-	2.8
Same frame different wheels*	-2.5																									-	2.5
Visor vs no visor		-2.2			-1.8				+3.0	-0.2	+4.7	+2.8	+1.7	+3.4	+2.4					+0.2			-2.7	+1.5		19.7	6.9
Pedal/strap combination														-2.1												-	2.1
Shoe covers vs no shoe covers	-2.4	-1.5																-1.7		-1.7					-1.8	-	9.1
Same pedal different strap														-1.8												-	1.8
Gloves vs no gloves														-1.3												-	1.3
Helmet holes taped vs untaped										+1.0													+0.7			1.7	-
Same strap different pedal														-0.3												-	0.3
Modified seat tube shape	+0.3																									0.3	-
Modified fork shape	-0.2																									-	0.2
Modified Stem shape	+0.1																									0.1	-

Table 9.18: Increases and Decreases in Drag from the Reference Position for each Athlete for Equipment Changes
*All wheels were disc wheels.

The results in Figure 9.4 show that the majority of changes in position and equipment made during this study reduced the aerodynamic drag, although this is not surprising as the overall aim of wind tunnel testing of athletes is to optimise their position and reduce the drag. However, certain changes resulted in a significant increase in drag, namely wearing a visor, raising the handlebar height, and widening the extensions. By raising the handlebars and widening the extensions the frontal area will increase, and the trend between frontal area and drag has already been identified as being significant. It is unclear why the addition of a visor has shown to increase the drag, but a poor fit of the visor on the helmet and around the face of the athlete may be possible reasons for this increase. A further analysis of different helmet and visor combinations on a number of athletes would be needed in order to validate this hypothesis. For changes to equipment, an increase in drag was seen when modifications were made to the seat tube and stem, which suggests that the design of the competitive bike frame is already very aerodynamic. The greatest overall reductions in drag were seen for a change in skinsuit, a change to the height and length of the extensions, and by adopting a crouch position. These changes in position help reduce the frontal area, and the material and seam placement of one of the skinsuits used for testing is likely to have been specifically designed to induce turbulence, delay separation and reduce the skin friction drag in comparison to a standard, road skinsuit.

Another noticeable result from this study is the reduction in drag for all athletes when wearing shoe covers compared to not wearing shoe covers. Although the influence of the actual shoe on the aerodynamic drag was not tested in this study, all athletes wore their own shoes, which differed in shape, size and design. As the presence of a shoe cover reduced the drag for all athletes tested, this implies that the design of the shoe itself is not as important in terms of athlete performance as ensuring the athlete wears a shoe cover that eliminates seams, buckles and recesses from the oncoming flow.

The changes made to athlete position and to equipment can be ranked in order of their impact on aerodynamic drag using the results described in this chapter, as shown in Table 9.19. These results show that multiple changes in position have the most impact on aerodynamic drag, and therefore coaches should ensure that athletes are in the most aerodynamic position as possible, specifically concentrating on lowering the stem and head position to reduce the frontal area, before making changes to equipment in order to maximise athlete performance.

Rank	**Change**	**Average change in drag from reference position (%)**
1	Multiple change in position	9.4
2	Skinsuit	6.3
3	Individual change in position	3.5
4	Frame and wheel combination	3.0
5	Helmet type	2.9
6	Visor vs no visor	2.2
7	Pedal/strap combination	2.1
8	Shoe Covers	1.8
9	Gloves vs no gloves	1.3

Table 9.19: Rank of factors in order of most influential on aerodynamic drag

Summary

This chapter has provided an insight into the overall gains and losses from changes in position and/or equipment, and attempted to rank these gains and losses in terms of their impact on the aerodynamic drag of a cyclist. The results have shown that the greatest reductions in drag came from obtaining a crouched position, wearing a different skinsuit, and changing the extension height and length, but there was a wide range between the smallest and greatest difference in drag from the reference position between athletes, mainly due to differences in body size and shape, riding experience, and reference position from which the changes were made. However, certain changes in position and equipment resulted in having a significant impact on the drag of all athletes tested (>1% gain or loss). Changes to the position of a cyclist affect the frontal area and the flow over the rest of the body, which has shown to have a strong influence on the aerodynamic drag. By bringing the handlebars down and lowering the head the aerodynamic drag was reduced for the majority of athletes, although actual percentage gains and the actual optimal set up varied between athletes. In general, multiple changes in position resulted in a greater impact on drag compared to individual changes, but changes were not additive. The reduction in drag by wearing shoe covers for all athletes tested, regardless of shoe, pedal or cleat used, suggests that the design of the shoe itself is not as important as ensuring athletes wear a shoe cover that eliminates seams, buckles and recesses from the oncoming flow. The results suggested that elite riders were already in a fairly aerodynamic reference position, so smaller gains were identified for some changes in position than were expected. Nevertheless this chapter has shown that changes to position and equipment can be ranked in order of their influence on the aerodynamic drag, which can assist athletes and coaches with identifying those areas to focus on in order to maximise the speed of a cyclist and improve athlete performance.

Chapter 10

Conclusions

Introduction

A summary of the work and final conclusions are provided in this chapter. The original aims and objectives are referred back to, and at the end of this chapter possible future research in this area is discussed.

10.1 Summary of Research

The aim of this research was to identify ways in which the velocity of a track cyclist could be maximised, and which factors had the greatest impact on the performance of all athletes involved by gaining a greater understanding of the aerodynamics of cycling and the flow around a cyclist. As elite races are often won by milliseconds, even small gains are significant and can result in a difference between an Olympic medal and no medal.

10.1.1 Objective 1: Appropriate Test Methods

The primary objective of this thesis was to develop appropriate test methods using the wind tunnel to measure the aerodynamic drag and drag area of a cyclist, in order to make comparisons between changes in position and/or equipment.

This aim was achieved by developing a cycle rig with a fixed and floating platform and a 50kg load cell to measure the drag for pedalling cyclists in the boundary layer wind tunnel at a wind speed of up to 46kph. The frontal area of the cyclist was measured using the digitising method, and a white board was used to project the shadow of the cyclist from side, which proved to be a successful method for monitoring athlete position during tests. The uncertainty of the force balance ($\pm 2.5\%$), wind speed ($\pm 0.13\%$), air density ($\pm 0.4\%$) and frontal area ($\pm 2.5\%$) all propagate to the calculation of the drag coefficient, resulting in a total error for the drag coefficient of $\pm 2.6\%$. The boundary layer of the cycle rig was calculated to increase from 45mm to 70mm, but all changes to position and/or equipment were made above the boundary layer and within the core flow, so any effects of the boundary layer on the aerodynamic drag could be ignored.

The simple model of a cyclist consisting of cylindrical arms, thighs and calves enabled an analysis to be carried out on the drag of material samples for the development of a new skinsuit for track cycling. Three, circular cylinders with rounded heads at the leading edge and diameters similar to the forearm, upper arm and thigh of a cyclist were manufactured, and the aerodynamic drag measured for different material samples in the spanwise and streamwise orientations at 50kph to 80kph. The influence of the seam placement on the drag was also measured for the spanwise cylinders. The accuracy of the material tests was dependent on the speed, orientation and diameter of the cylinders; the smallest inaccuracy of 0.9% was for the large cylinder in the spanwise orientation at the highest speed, but the largest inaccuracy of 13% was for the small cylinder in the streamwise orientation at the lowest speed. However, the actual error of the drag readings was only $\pm$0.002kg. The results from the comparison of different material samples and seam placement on the circular cylinders in different orientations lead to the development of a prototype skinsuit, which was then compared to the best existing New Zealand skinsuit by using a pedalling athlete on the cycle rig in the wind tunnel. Although the overall aerodynamic drag was similar for these two skinsuits, the results were promising for an initial prototype.

10.1.2 Objective 2: Mathematical Model

The secondary objective of this thesis was to generate a mathematical model for track cycling that could be used to predict the velocity profile and finishing time for pursuit athletes, as well as to identify the optimal pacing strategy for pursuit cyclists.

This objective was achieved by using first principles to analyse the forces acting on a cyclist, leading to the formation of equations for the power demand and power supply of cycling. The demand side equations included the power to overcome drag, tyre and bearing rolling resistance, and weight, and the supply side equations included the power produced by the athlete taken from actual SRM power data collected during a specific race. It was assumed that any surplus power lead to acceleration of the system. This mathematical model included the effect of leaning in the bends, something that most previous models had excluded. The calculation was performed in Microsoft Excel, firstly by calculating the initial acceleration and then using this result to determine the change in velocity over a specific timestep. The change in velocity was then used to calculate the initial velocity for the next timestep, as well as the distance of the centre of mass and wheels over that timestep. This process was continued until the final distance was reached, at which point the finishing time could be identified. This method also allowed the velocity profile to be determined, which clearly indicated the difference between the speed of the centre of mass of a cyclist in the bends compared to the straights. The model was validated using SRM power data for eleven, pursuit, track cyclists, and the average accuracy of the model was shown to be 0.31s (0.16%). The greatest difference between the actual SRM data and the mathematical model was found to occur during the first lap, where the model would underpredict the lap time. This was probably due to the increased drag area during the standing start in reality, which was not accounted for in the model. The model also underpredicted the velocity profile in both the bends and straights by approximately 0.2ms^{-1}, but nevertheless the model clearly proved to be able to predict the finishing time of IP athletes to a high degree of accuracy.

The model was successfully used to predict the difference in finishing times and velocity profiles for changes made to the athlete, bike, and environmental conditions, the results of which indicated that the drag area, C_dA, and the air density had the greatest influence on the finishing time. The model was also used to compare the finishing times for different pacing strategies whilst maintaining the same overall work done.

The results suggested that an all-out strategy for 12s followed by an even or variable power output resulted in the fastest finishing time for a male, IP athlete (height of 1.85m, weight of 75kg, drag area of 0.195m^2, and coefficient of rolling resistance of 0.002) completing 4000m with a fixed stock of energy whose efficiency is not a function of power output or speed. An all-out and even or all-out and variable strategy resulted in a significantly faster finishing time than any other pacing strategy simulated for the 4000m IP, and length of time spent in the initial acceleration phase appeared to have a significant effect on the predicted finishing time.

10.1.3 Objective 3: Most Significant Factors on Athlete Performance

The final objective of this thesis was to compare changes made in the wind tunnel to athlete position and equipment to identify those factors with the greatest impact on drag, to provide a rank of importance, and to identify the most significant ways in which the drag can be reduced.

This objective was achieved by using elite and competitive cyclists to compare changes in equipment, attire and position in the wind tunnel, and measuring the change in drag from the reference position for all changes made. The reference position was chosen as the starting point from which changes were made because all athletes use different equipment and adopt different reference positions when riding to begin with, and this was agreed to be the most repeatable method to gain relative data for all athletes. By limiting the athletes to being at competitive or elite level, it was assumed that their reference position would already be fairly aerodynamic and the results could therefore be comparable; recreational riders are likely to have a less aerodynamic reference position, from which great gains would be seen by just changing to a position which is similar to the reference position of an elite rider.

The changes made included frame and wheel combinations, modifications to the frame, different types of helmets, helmets with and without a visor, pedal and strap combinations, gloves and no gloves, different skinsuits, hand position, handlebar width and height, athlete torso and shoulder angle, and some general changes such as crouching, helmet tip position, seat position, and tucking the hair into the helmet or in a bun. The impact on drag was determined for each change made to the position and equipment, which included both gains and losses from the reference position of each athlete. The average difference in drag for each change was determined, which allowed the results to be ranked in order of greatest to least impact on the overall drag of a cyclist. The mathematical model was also used to provide an estimate of time savings or time gains for each change in position and equipment for a pursuit cyclist.

It was found that multiple positional changes had a greater impact on drag compared to individual postional changes, but changes were not additive, and a change in skinsuit had the greatest impact on drag out of all equipment changes. A low handlebar position and a crouched or low head position resulted in a lower drag for most athletes, but it was not always the case that the lowest position was the best. Most positional changes were athlete dependent; not all athletes experienced the same gain or loss in drag for the same positional change due to differences in body size and shape, riding experience, and reference position from which the changes were made. However, the results did indicate that some changes in position had an impact of $\pm 1\%$ in drag for all athletes tested, which was considered to be a significant change for all track cyclists. A comparison of different shoe covers concluded that the aerodynamic drag can be reduced by wearing shoe covers regardless of shoe, strap, pedal and cleat, which indicates that the design of the shoe itself may not be as important as ensuring athletes wear a shoe cover. Although smaller gains in drag were seen for elite

riders in general, probably due to their more aerodynamic reference position compared to competitive riders, the method of ranking changes from an athlete's reference position showed to be a useful way to highlight where significant gains or losses can be made to the majority of athletes, which is beneficial to both coaches and athletes when deciding where to focus time, effort and money.

10.2 Conclusions

- Wind tunnel testing is an accurate method for measuring the aerodynamic drag of a cyclist, and can be used successfully to compare changes in position and/or equipment;
- Mathematical models for track cycling should incorporate a factor for leaning in the bends in order to account for the difference in velocity of the centre of mass in the bends compared to the straights. By generating supply and demand equations using first principles, an accurate model for track cycling can be produced;
- Assuming a fixed work output of 128.3kJ, an all-out strategy for 12s followed by even or variable power output (with a higher power in the bends compared to the straights) resulted in the fastest finishing time for a male, IP athlete (height of 1.85m, weight of 75kg, drag area of 0.195m^2, and coefficient of rolling resistance of 0.002) completing 4000m with a fixed stock of energy whose efficiency is not a function of power output or speed. The time spent in the initial acceleration phase also had a significant influence on the finishing time;
- The drag area and air density have the greatest impact on the finishing time for pursuit cyclists;
- Multiple changes in athlete position have the greatest impact on the aerodynamic drag of a cyclist, but the actual gains and losses seen by individual athletes will differ due to differences in body size and shape, riding experience, and reference position from which changes were made;
- A low handlebar position and low head position reduces the frontal area of a cyclist, reducing the overall drag by an average of 2% and 3.5% respectively. However, the lowest position is not necessarily the most aerodynamic position for all athletes;
- Changes to the skinsuit have the greatest impact on drag out of all equipment changes (an average change in drag of 6.3%), primarily due to the choice of material and seam placement, but the optimal material and seam placement is dependent on the diameter and orientation of the cylindrical limbs, as well as the cycling speed.
- Time savings of as much as 8 seconds over 4000m can be achieved through changes in position, and as much as 5 seconds over 4000m achieved through changes to the skinsuit (+/- 2%);
- In order to maximise the velocity of a cyclist athletes and coaches should concentrate on optimising athlete position, primarily by lowering the handlebars and bringing the head into a more crouched position, followed by optimising equipment, in particular the skinsuit. However, individual testing is needed in order to identify the optimal position for each athlete, due to the wide variablility between athlete body shapes and sizes, riding experience, and available equipment.

10.3 Future Work

This study has highlighted the benefits of using wind tunnel tests to help reduce the aerodynamic drag of cyclists through changes in position and equipment. At present there is limited research on the aerodynamics of drafting cyclists using wind tunnel tests, especially for track cyclists. Although it is well known that drafting cyclists do not need to produce as much power as leading cyclists in order to maintain the same speed, it is unclear of the true effects of spacing between athletes, the optimal order of team pursuit cyclists, the optimal position of each team pursuit rider, or the optimal changeover path. The effect of body size and shape on leading and drafting cyclists is not well understood, and these factors may have a significant effect on the performance of a team pursuit. A mathematical model of a team pursuit would also be a useful tool to identify the best order of team pursuit cyclists and how the position and spacing of each athlete affects the performance of the whole team. Although a few mathematical models do exist for drafting riders, these models use only average power and velocity data for the entire team and it is not possible to analyse the effects of individual athletes on team performance.

In terms of optimal pacing strategy, it would be beneficial to generate different scenarios for two different athletes adopting the same pacing strategy, as well as for different combinations of pacing strategies to identify the outcome when two athletes compete against each other. A better understanding and preferably a quantitative model of the effects of fatigue and athlete psychology on the total work output of the rider is necessary in order to model different pacing strategies for conditions where the energy supplied by the athlete is not necessarily fixed, as it may be the case that athlete efficiency is a function of power output or speed.

This thesis has concentrated on pursuit events for track cycling, but the principles of aerodynamics used for this study are applicable to all other cycling events as well as to other sports. Track cycling however, does exclude the effects of yaw angle, as it is assumed that there is no external wind present on an indoor velodrome. For road cycling the effects of wind cannot be ignored.

A further study on the optimal position and type of aero helmet used for track cycling for different athletes would be very beneficial, in particular to understand the effect of vent location, size and shape on the aerodynamic drag. This thesis did not include a specific study on helmets, but only explored the difference in drag for riders comparing different types of helmets. It would be useful to understand if there is a specific helmet tip location that results in a low drag for all athletes wearing any type of helmet, or whether the position of the helmet tip is dependent on the type of helmet as well as the size and shape of the athlete.

The effect of training was not part of this thesis, but experimental studies showed that certain positions, in particular the arrow style hand position, caused riders to feel unstable. Therefore it would be beneficial to analyse the effect of training on power output and stability of elite cyclists to determine whether athletes are able to train in a specific position in order to maximise their power output whilst minimising their drag. The experimental results for the optimal torso and shoulder angle for track cyclists indicated that maximum power and minimum drag occurred at different torso and shoulder angles, and that the shoulder angle had a greater influence on the power output of cyclists whereas the torso angle had a greater influence on the aerodyanmic drag. However, if athletes are able to train in a position that results in a lower drag in order to maximise their power output, then it would not matter that their power output would initially be low in this position.

As a closing remark, the significance of aerodynamics in gaining a competitive advantage in cycling is clear,

and it is worth investing time and money in research and technology to find new ways to reduce the aerodynamic drag and maximise the speed of a cyclist.

Bibliography

C. R. Abbiss and P. B. Laursen. Describing and understanding pacing strategies during athletic competition. *Sports Medicine*, 38(3):239, 2008.

E. Achenbach. Influence of surface roughness on the cross-flow around a circular cylinder. *Journal of Fluid Mechanics*, 46(2):321–335, 1971.

E. Achenbach. Experiments on the flow past spheres at very high reynolds numbers. *Journal of Fluid Mechanics*, 54:565–575, 1972.

F. Alam, R. Brooy, A. Subic, and S. Watkins. Aerodynamics of cricket ball-an effect of seams (p70). *The Engineering of Sport 7*, pages 345–352, 2008a.

F. Alam, A. Subic, A. Akbarzadeh, M. Estivalet, and P. Brisson. Aerodynamics of bicycle helmets. *The Engineering of Sport 7*, pages 337–344, 2008b.

Bicycle Apparel. http://bicycleapparel.com/fabric.html, 2012.

G. Atkinson, R. Davison, A. Jeukendrup, and L. Passfield. Science and cycling: current knowledge and future directions for research. *Journal of Sports Sciences*, 21(9):767–787, 2003.

G. Atkinson, O. Peacock, and L. Passfield. Variable versus constant power strategies during cycling time-trials: Prediction of time savings using an up-to-date mathematical model. *Journal of Sports Sciences*, 25 (9):1001–1009, 2007.

A.D. Auteuil, G.L. Larose, and S.J. Zan. Relevance of similitude parameters for drag reduction in sport aerodynamics. *The Engineering of Sport 8*, 2(2):2393–2398, 2010.

J. Baker, J. Gal, B. Davies, D. Bailey, and R. Morgan. Power output of legs during high intensity cycle ergometry: influence of hand grip. *Journal of Science and Medicine in Sport*, 4(1):10–18, 2001.

C. Barelle, V. Chabroux, and D. Favier. Modeling of the time trial cyclist projected frontal area incorporating anthropometric, postural and helmet characteristics. *Sports Engineering*, pages 1–8, 2010.

D. R. Bassett Jr, C. R. Kyle, L. Passfield, J. P. Broker, and E. R. Burke. Comparing cycling world hour records, 1967-1996: modeling with empirical data. *Medicine and Science in Sports and Exercise*, 31(11): 1665, 1999.

B. S. Baum and L. Li. Lower extremity muscle activities during cycling are influenced by load and frequency. *Journal of Electromyography and Kinesiology*, 13(2):181–190, 2003.

P. W. Bearman and J. K. Harvey. Control of circular cylinder flow by the use of dimples. *AIAA journal*, 31 (10):1753–1756, 1993.

N. Belluye and M. Cid. Approche biomécanique du cyclisme moderne, données de la littérature: Biomechanics approach to modern cycling, literature data's. *Science and Sports*, 16(2):71–87, 2001.

K. B. Blair and S. Sidelko. Aerodynamic performance of cycling time trial helmets (p76). *The Engineering of Sport 7*, pages 371–377, 2008.

E. Bressel and J. Cronin. Bicycle seat interface pressure: reliability, validity, and influence of hand position and workload. *Journal of biomechanics*, 38(6):1325–1331, 2005.

J. P. Broker. *Cycling Power: Road and Mountain*, chapter 6, pages 147–174. Human Kinetics, 2 edition, 2003.

J. P. Broker, C. R. Kyle, and E. R. Burke. Racing cyclist power requirements in the 4000-m individual and team pursuits. *Medicine and Science in Sports and Exercise*, 31(11):1677, 1999.

L. Brownlie, C. Kyle, J. Carbo, N. Demarest, E. Harber, R. MacDonald, and M. Nordstrom. Streamlining the time trial apparel of cyclists: the nike swift spin project. *Sports Technology*, 2, 2009.

L. Brownlie, P. Ostafichuk, E. Tews, H. Muller, E. Briggs, and K. Franks. The wind averaged aerodynamic drag of competitive cycling time trial helmets. *8th Conference of the International Sports Engineering Association*, 2(1):2419–2424, 2010.

L. W. Brownlie, I. Gartshore, A. Chapman, and E. W. Banister. The aerodynamics of cycling apparel. *Cycling Science*, 3(3-4):44–50, 1991.

E.R. Burke and A.L. Pruitt. *Body Positioning for Cycling*, chapter 3, pages 69–92. Human Kinetics, 2 edition, 2003.

R. B. Candau, F. Grappe, M. MÉNard, B. Barbier, G. Y. Millet, M. D. Hoffman, A. R. Belli, and J. D. Rouillon. Simplified deceleration method for assessment of resistive forces in cycling. *Medicine and Science in Sports and Exercise*, 31(10):1441, 1999.

V. Chabroux, M. N. Mba, P. Sainton, and D. Favier. Wake characteristics of time trial helmets using piv-3c technique. In *15th International Symposium to Laser Techniques to Fluid Mechanics*, 2010.

S. S. Chaudhari, R. S. Chitnis, and R. Ramkrishnan. Waterproof breathable active sports wear fabrics. *Man-made Textiles in India*, 5:166–171, 2004.

J Choi, WP Jeon, and H Choi. Mechanism of drag reduction by dimples on a sphere. *Physics of Fluids*, 18 (4), 2006.

H. Chowdhury, F. Alam, and A. Subic. Aerodynamic performance evaluation of sports textile. *The Engineering of Sport 8*, 2(2):2517–2522, 2010.

K. R. Cooper, E. Mercker, and J. Wiedemann. *Improved blockage corrections for bluff bodies in closed and open wind tunnels*, pages 1627–1634. Balkema, Rotterdam, 1999.

N. P. Craig and K. I. Norton. Characteristics of track cycling. *Sports Medicine*, 31(7):457, 2001.

N. P. Craig, K. I. Norton, P. C. Bourdon, S. M. Woolford, T. Stanef, B. Squires, T. S. Olds, R. A. J. Conyers, and C. B. V. Walsh. Aerobic and anaerobic indices contributing to track endurance cycling performance. *European Journal of Applied Physiology*, 67(1):150–158, 1993.

R. S. Davis. Equation for the determination of the density of moist air(1981/91). *Metrologia*, 29(1):67–70, 1992.

J. J. De Koning, M. F. Bobbert, and C. Foster. Determination of optimal pacing strategy in track cycling with an energy flow model. *Journal of Science and Medicine in Sport*, 2(3):266–277, 1999.

P. Debraux, W. Bertucci, A. V. Manolova, S. Rogier, and A. Lodini. New method to estimate the cycling frontal area. *International journal of sports medicine*, 2009.

T. Defraeye, B. Blocken, E. Koninckx, P. Hespel, and J. Carmeliet. Aerodynamic study of different cyclist positions: Cfd analysis and full-scale wind-tunnel tests. *Journal of biomechanics*, 43(7):1262–1268, 2010.

T. Defraeye, B. Blocken, E. Koninckx, P. Hespel, and J. Carmeliet. Computational fluid dynamics analysis of drag and convective heat transfer of individual body segments for different cyclist positions. *Journal of biomechanics*, 44(1):1695–1701, 2011.

P. E. Di Prampero. The concept of critical velocity: a brief analysis. *European journal of applied physiology and occupational physiology*, 80(2):162–164, 1999.

P. E. Di Prampero. Cycling on earth, in space, on the moon. *European Journal of Applied Physiology*, 82 (5):345–360, 2000.

P. E. Di Prampero, G. Cortili, P. Mognoni, and F. Saibene. Equation of motion of a cyclist. *Journal of Applied Physiology*, 47(1):201, 1979.

R. Drillis, R. Contini, and M. Bluestein. Body segment parameters: A survey of measurement techniques. *In Selected articles from artificial limbs*, Huntington, NY: Rovert E. Krieger Publishing Co. Inc.:329–351, 1964.

A. G. Edwards and W. C. Byrnes. Aerodynamic characteristics as determinants of the drafting effect in cycling. *Medicine and Science in Sports and Exercise*, 39(1):170, 2007.

Eschler. http://www.eschler.com/english/ecs/ecs.html, 2012.

E. W. Faria, D. L. Parker, and I. E. Faria. The science of cycling: Factors affecting performance-part 2. *Sports Medicine*, 35(4):313, 2005.

C. Foster, J. J. De Koning, F. Hettinga, J. Lampen, K. L. La Clair, C. Dodge, M. Bobbert, and J. P. Porcari. Pattern of energy expenditure during simulated competition. *Medicine and Science in Sports and Exercise*, 35(5):826, 2003.

J. Garcia-Lopez, J. A. Rodriguez-Marroyo, C. E. Juneau, J. Peleteiro, A. C. Martinez, and J. G. Villa. Reference values and improvement of aerodynamic drag in professional cyclists. *J Sports Sci*, 1:10, 2008.

A.S. Gardner, P. Barratt, A. Wylie, C. White, D. Locke, M. Hughes, and J. Martin. Relative rider size does not influence drag reductions during velodrome cycling: 948: May 29. *Medicine and Science in Sport and Exercise*, 41(5):129, 2009.

G. Gibertini, G. Campanardi, D. Grassi, and C. Macchi. Aerodynamics of biker position. In *BBAA VI International Colloquium on: Bluff Bodies Aerodynamics and Applications*, 2008. Proceedings of the BBAA VI International Colloquium on: Bluff Bodies Aerodynamics and Applications.

G. Gibertini, D. Grassi, C. Macchi, and G. De Bortoli. Cycling shoe aerodynamics. *Sports Engineering*, 12 (3):155–161, 2010.

M.N. Godo, D. Corson, and S.M. Legensky. An aerodynamic study of bicycle wheel performance using cfd. *American Institute of Aeronautics and Astronautics*, 47th AIAA Aerospace Sciences Meeting(1):1–18, 2009.

C. González-Haro, P. A. Galilea Ballarini, M. Soria, F. Drobnic, and J. F. Escanero. Comparison of nine theoretical models for estimating the mechanical power output in cycling. *British Journal of Sports Medicine*, 41:506–509, 2007.

F. Grappe, R. Candau, A. Belli, and J. D. Rouillon. Aerodynamic drag in field cycling with special reference to the obree s position. *Ergonomics*, 40(12):1299–1311, 1997.

D. Greenwell, N. Wood, E. Bridge, and R. Addy. Aerodynamic characteristics of low-drag bicycle wheels. *Aeronautical Journal*, 99(983):109–120, 1995.

G. D. E. Groot, A. Sargeant, and J. O. S. Geysel. Air friction and rolling resistance during cycling. *Medicine and Science in Sports and Exercise*, 27(7):1090, 1995.

S.J Haake, S.R Goodwill, and M.J Carre. A new measure of roughness for defining the aerodynamics of sports balls. *Proceedings of the Institution of Mechanical Engineers Part C - Journal of Mechanical Engineering Science*, 221(7):789–806, 2007.

J. Hamill and E.C. Hardin. Special topics in biomechanics. *In Foundations of Exercise Science, Ed. Kaman, G.*, 1st Ed.(Lippincott Williams and Wilkins):187, 2001.

F. J. Hettinga, Josj De Koning, F. T. Broersen, P. Van Geffen, and C. Foster. Pacing strategy and the occurrence of fatigue in 4000-m cycling time trials. *Medicine and Science in Sports and Exercise*, 38(8): 1484, 2006.

S.F. Hoerner. *Fluid-Dynamic Drag*. 1965.

M. Hopkins, F. Principe, and K. Kelleher. Beyond materials: Du pont's aerodynamic bicycle wheel. *Advanced Materials: the Challenge for the Next Decade*, 1(170):947–959, 1990.

A.F Huber II and T.J Mueller. The effect of trip wire roughtness on the performance of the wortmann fx 63-137 aurfoil at low reynolds numbers. *Experiments in Fluids*, 5:263–272, 1987.

K Hyun Paul and S Kwang. The criterion of separation of incompressible laminar boundary layer flow over an axially symmetric body. *Journal of the Franklin Institute*, 325(4):419–433, 1988.

A Iniguez-de-la Torre and J Iniguez. Aerodynamics of a cycling team in a time trial: does the cyclist at the front benefit? *European Journal of Physics*, pages 1365–1369, 2009.

K Jensen, L Johansen, and NH Secher. Influence of body mass on maximal oxygen uptake: effect of sample size. *European Journal of Applied Physiology*, 84:201–205, 2001.

S Jeon, J Choi, WP Jeon, H Choi, and J Park. Active control of flow over a sphere for drag reduction at subcritical reynolds number. *Journal of Fluid Mechanics*, 517:113–129, 2004.

M. Jermy, J. Moore, and M. Bloomfield. Translational and rotational aerodynamic drag of composite construction bicycle wheels. *Proceedings of the Institution of Mechanical Engineers, Part P: Journal of Sports Engineering and Technology*, 222(2):91–102, 2008.

A. E. Jeukendrup and J. Martin. Improving cycling performance: how should we spend our time and money. *Sports Medicine*, 31(7):559, 2001.

A. E. Jeukendrup, N. P. Craig, and J. A. Hawley. The bioenergetics of world class cycling. *Journal of Science and Medicine in Sport*, 3(4):414–433, 2000.

G. H. Kuper and E. Sterken. Do skin suits affect the average skating speed? *Sports Technology*, 1, 2008.

C. R. Kyle and D. R. Bassett Jr. *The Cycling World Hour Record*, chapter 7, pages 175–196. Human Kinetics, 2 edition, 2003b.

C. R. Kyle and M. D. Weaver. Aerodynamics of human-powered vehicles. *Proceedings of the Institution of Mechanical Engineers, Part A: Journal of Power and Energy*, 218(3):141–154, 2004.

C.R. Kyle. *Selecting Cycling Equipment*, chapter 1, pages 1–48. Human Kinetics, 2 edition, 2003a.

J.C Lin. Review of research on low-profile vortex generators to control boundary-layer separation. *Progress in Aerospace Sciences*, 38:389–420, 2002.

R Lukes, M Carre, and S Haake. *Track Cycling: An Analytical Model*, volume 1, pages 115–120. Springer, 2006.

R. A. Lukes, S. B. Chin, and S. J. Haake. The understanding and development of cycling aerodynamics. *Sports Engineering*, 8(2):59–74, 2005.

J. C. Martin and N. A. T. Brown. Joint-specific power production and fatigue during maximal cycling. *Journal of biomechanics*, 42(4):474–479, 2009.

J. C. Martin, D. L. Milliken, J. E. Cobb, K. L. McFadden, and A. R. Coggan. Validation of a mathematical model for road cycling power. *Journal of Applied Biomechanics*, 14:276–291, 1998.

J. C. Martin, A. S. Gardner, M. Barras, and D. T. Martin. Modeling sprint cycling using field-derived parameters and forward integration. *Medicine and Science in Sports and Exercise*, 38(3):592, 2006.

J. C. Martin, C. J. Davidson, and E. R. Pardyjak. Understanding sprint-cycling performance: the integration of muscle power, resistance, and modeling. *International journal of sports physiology and performance*, 2 (1):5, 2007.

B. D. McLean and A. W. Parker. An anthropometric analysis of elite australian track cyclists. *Journal of Sports Science*, 7:247–255, 1989.

K. de Vey Mestdagh. Personal perspective: in search of an optimum cycling posture. *Journal of Applied Ergonomics*, 29(5):325–334, 1998.

J.J. Miau, H.W. Tsai, Y.J. Lin, J.K. Tu, C.H. Fang, and M.C. Chen. Experiment on smooth, circular cylinders in cross-flow in the critical reynolds number regime. *Exp Fluids*, 51:949–967, 2011.

R. R. Neptune, C. P. McGowan, and J. M. Fiandt. The influence of muscle physiology and advanced technology on sports performance. *Annual Review of Biomedical Engineering*, 11:81–107, 2009.

L. Oggiano and L. Sætran. A low deag skinsuit for ski-cross competitions. *The Engineering of Sport 8*, 2(2): 2387–2392, 2010.

L. Oggiano, L. Sætran, S. Løset, and R. Winther. Reducing the athletes aerodynamical resistance. *Journal of Computational and Applied Mechanics*, 5(2):1–8, 2006.

L. Oggiano, S. Leirdal, L. Sætran, and G. Ettema. Aerodynamic optimization and energy saving of cycling postures for international elite level cyclists (p114). *The Engineering of Sport 7*, pages 597–604, 2008.

L. Oggiano, O. Troynikov, I. Konopov, A. Subic, and F. Alam. Aerodynamic behaviour of single sport jersey fabrics with different roughness and cover factors. *Sports Engineering*, 12(1):1–12, 2009.

T Olds. The mathematics of breaking away and chasing in cycling. *European journal of applied physiology and occupational physiology*, 77(6):492–497, 1998.

T. Olds. Modelling human locomotion. *Sports Med*, 31(7):497–509, 2001.

T. Olds and S. Olive. Methodological considerations in the determination of projected frontal area in cyclists. *Journal of sports sciences*, 17(4):335–345, 1999.

T. S. Olds, K. I. Norton, and N. P. Craig. Mathematical model of cycling performance. *Journal of Applied Physiology*, 75(2):730–737, 1993.

T. S. Olds, K. I. Norton, E. L. Lowe, S. Olive, F. Reay, and S. Ly. Modeling road-cycling performance. *Journal of Applied Physiology*, 78(4):1596, 1995.

J.C. Owen and P.W Bearman. Passive control of viv with drag reduction. *Journal of Fluids and Structures*, 15:597–605, 2001.

Craig Palmer. Bikenz personal communication, 2009.

R. C. Pankhurst and D. W. Holder. *Wind-tunnel technique: an account of experimental methods in low-and high-speed wind tunnels*. Sir Isaac Pitman and Sons Ltd, 1952.

D. R. Pendergast, J. C. Mollendorf, R. Cuviello, and A. C. Termin. Application of theoretical principles to swimsuit drag reduction. *Sports Engineering*, 9(2):65–76, 2006.

Kathryn Phillips. Bikenz personal communication, 2011.

PropellerGuard. www.propellersafety.com/propeller-guard-reduced-drag/, 2011.

C. C. Raasch, F. E. Zajac, B. Ma, and W. S. Levine. Muscle coordination of maximum-speed pedaling. *Journal of biomechanics*, 30(6):595–602, 1997.

UCI Cycling Regulations. www.uci.ch,, 2009.

Andy Reid. Bikenz personal communication, 2012.

S.K Roberts and M.I Yaras. Boundary-layer transition affected by surface roughness and free-stream turbulence. *Journal of Fluids Engineering*, 127:449–457, 2005.

S.K Roberts and M.I Yaras. Effects of surface-roughness geometry on separation-bubble transition. *Journal of Turbomachinery*, 128:349–356, 2006.

N.R Rodriguez, N.M DiMarco, and S Langley. Nutrition and athletic performance. *Med Sci Sports Exerc*, 41(3):709–731, 2009.

Roymech. www.roymech.co.uk, 2011.

David Salazar. A2 wind tunnel charlotte personal communication, 2011.

Hhcm Savelberg, I. G. L. Van de Port, and P. J. B. Willems. Body configuration in cycling affects muscle recruitment and movement pattern. *JAB*, 19:4, 2003.

H Schlichting. *Boundary layer theory*. McGraw-Hill Series in Mechanical Engineering, 7th edition, 1979.

Helen Searle. University of canterbury personal communication, 2012.

L. Seatran and L. Oggiano. Skin suit aerodynamics in speed skating. *Sport Aerodynamics: CISM Courses and Lectures*, 506, 2008.

R. C. H. So, J. K. F. Ng, and G. Y. F. Ng. Muscle recruitment pattern in cycling: a review. *Physical Therapy in Sport*, 6(2):89–96, 2005.

D.P. Swain. A model for optimizing cycling performance by varying power on hills and in wind. *Medicine and Science in Sports and Exercise*, 29(8):1104, 1997.

J. Sznitman, F. Kritter, and T. Rosgen. Flow visualization of bicycle helmets for optimal ventilation design. *Summer Heat Transfer Conference. San Francisco*, 1(1):HT2005–72751, 2005.

M. Tapias, M. Rallo, J. Escofet, I. Algaba, and A. Riva. Objective measure of woven fabric's cover factor by image processing. *Textile Research Journal*, 80(1):35–44, 2010.

G. S. Tew and A. T. Sayers. Aerodynamics of yawed racing cycle wheels. *Journal of Wind Engineering and Industrial Aerodynamics*, 82(1-3):209–222, 1999.

B. E. Thompson, W. A. Friess, and K. N. Knapp. Aerodynamics of speed skiers. *Sports Engineering*, 4(2): 103–112, 2001.

D Too and G.E Landwer. The biomechanics of force and power production in human powered vehicles. *Human Power*, 55:3–6, 2004.

M Torres. Technical soaring. *The Soaring Society of America*, 1999.

Weather Underground. www.wunderground.com, 2009.

S. G. J. van Ingen and P. R. Cavanagh. Power equations in endurance sports. *Journal of biomechanics*, 23 (9):865, 1990.

F.M. White. *Viscous Fluid Flow*. McGraw-Hill, Inc., 2nd edition, 1991.

R.L. Wilber. *Altitude Training in Preparation for Competition at Sea Level*, chapter 8, pages 197–240. Human Kinetics, 2 edition, 2003.

D.G. Wilson. *Bicycling Science*. The MIT Press, London, 3 edition, 2004.

Y. Yamagishi and M. Oki. Effect of groove shape on flow characteristics around a circular cylinder with grooves. *Journal of Visualization*, 7(3):209–216, 2004.

M. Zdravkovich, M. Ashcroft, S. Chisholm, and N. Hicks. Effect of cyclist's posture and vicinity of another cyclist on aerodynamic drag. *The Engineering of Sport 6*, 1(1):21–28, 1996.

C Çengel and JM Cimbala. *Fluid mechanics, fundamentals and applications*. McGraw-Hill, 2006.

Appendix A

UCI Rules and Regulations

All equipment used on the track for world events must be approved by the UCI and must comply with the specifications described in the Approval Protocols [Regulations, 2009]. These rules and regulations ensure all athletes compete on an equal level, but they also limit the options for changes to position and equipment.

Frames and Forks

A bicycle is defined as a vehicle which has two wheels of the same diameter: the front wheel steerable and the rear wheel driven through a system comprising of chains and pedals (Rule 1.3.006). The bike must be available to all participants, and therefore must be marketed or for sale by the manufacturer. The bike must comply with all safety regulations and allow the rider to adopt the necessary position without difficulty or risk. The bike must weigh a minimum of 6.8kg, excluding any additional accessories, such as an SRM Power Meter. The minimum and maximum measurements for which the bike must comply with are shown in Figure A.1 and Table A.1.

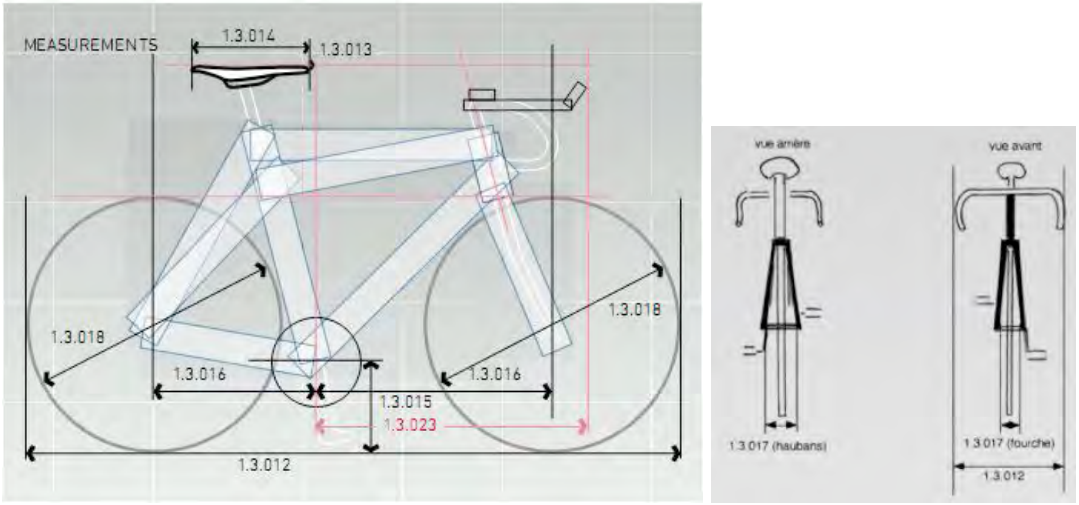

Figure A.1: Bike Measurements

	Measurement	Minimum	Maximum
1.3.012	Bike overall dimensions	-	185cm in length and 50cm in width
1.3.013	Distance between the centre of the bottom bracket axle and tip of the saddle		5cm
1.3.014	Saddle length	24cm	30cm
1.3.015	Distance between bottom bracket spindle and ground	24cm	30cm
1.3.016	Distance between vertical passing through bottom bracket spindle and front wheel spindle	54cm	65cm
1.3.016	Distance between vertical passing through bottom bracket spindle and rear wheel spindle	35cm	50cm
1.3.017	Distance between internal extremities of front forks	-	10.5cm
1.3.017	Distance between internal extremities of rear triangle	-	13.5cm
1.3.018	Wheel diameter including tyres (for non mass start races)	55cm	70cm
1.3.023	Distance between bottom bracket spindle and end of extensions*	-	75cm

Table A.1: Bike Measurements

*+5cm tolerance

The frame must be built around a main triangle and constucted from straight or tapered tubular elements. The cross section of the tubular elements may be round, oval, flattened, teardrop shaped or otherwise, so that the form of each element encloses a straight line, and they must be connected in a specific way [Regulations, 2009, 1.3.020c]. The stem, handlebar, handlebar extension, and seat post elements must be a maximum height of 8cm and minimum thickness of 2.5cm, as shown in Figure A.2, and must conform to a 3:1 ratio. Moving parts, pedals, front/rear derailleur mechanisms, wheel brake mechanisms and the saddle are exempt from this rule. The pedal crank is also exempt from this rule, but its transverse dimension is restricted to 8cm. The minimum thickness may be reduced to 1cm for the chain stays and the seat stays. The minimum thickness of the front fork must be 1cm, and these may be straight or curved. For track competitions, the elements of the frame may be solid or tubular, assembled or cast in a single piece in any form. These elements must fit within the triangular form template.

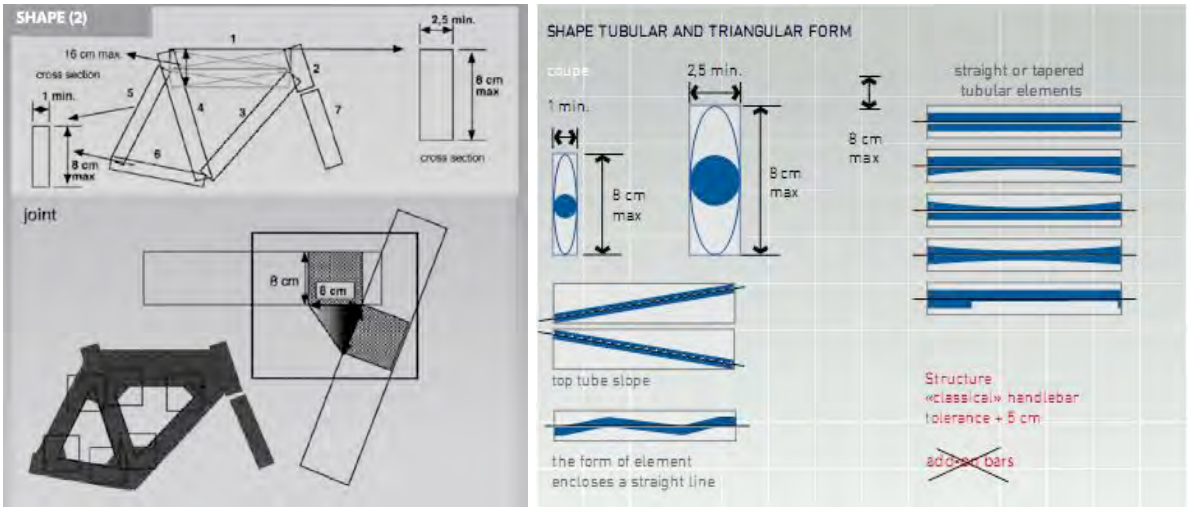

Figure A.2: Shape of frame elements

It is prohibited to have any device to decrease air resistance or artificially accelerate propulsion, such as protective screening, windscreens, or fuselage form fairing. A fuselage form shall be tolerated provided that the ratio between the length, L, and diameter, D, does not exceed 3 (see Figure A.3). Therefore the shape of the frame elements may similar to a tear drop, provided the length to diameter ratio is less than 3. Fairings are also prohibited, and it should be possible to pass a rigid card, such as a credit card, between the fixed structure and moving part.

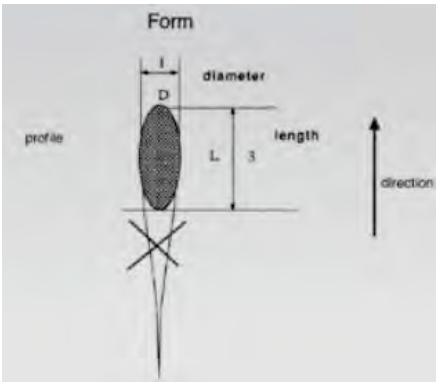

Figure A.3: Length to diameter ratio

Only traditional handlebars are permitted for track races, with the exception of the IP, TP, and 500m TT, where the bike may be fitted with a handlebar extension upon which the forearm or elbow rests. The rider's forearms must be in a horizontal plane and the extension designed so that the rider can adopt and maintain a regulatory position for the entire duration of the event. The profile of the extensions must also conform to the 3:1 ratio, and the extensions must be fixed so that changes in length or angle are not possible during the race. The extensions only permit extension in the horizontal plane, and must be fitted with hand grips. The hand grips may be horizontal, inclined or vertical, as shown in Figure A.4, but must be recognisable and only be used for hand contact. Extensions that are raised or arc-shaped are not permitted. Riders must have at least one hand on the handlebars at all times.

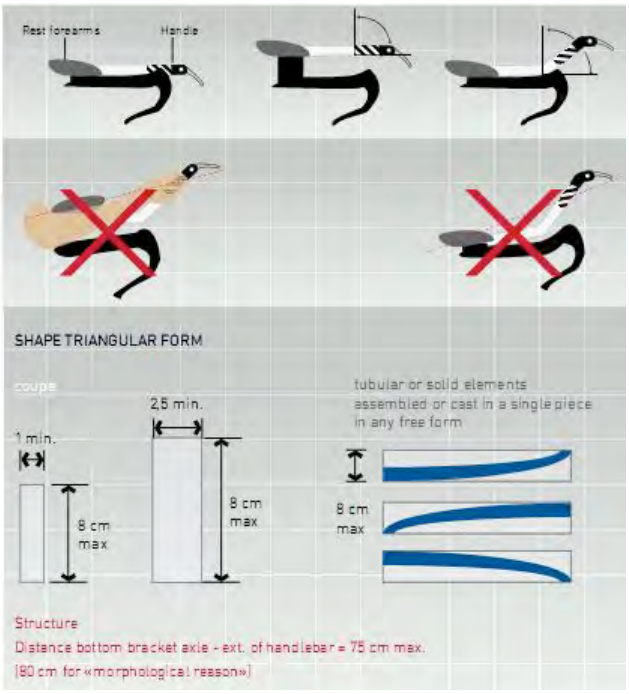

Figure A.4: Handlebar extensions

Rider Position

The rider position for the pursuit races is defined by two measurements: (1) the position of the tip of the saddle behind the bottom bracket (-5cm minimum), and (2) the advanced position using the extensions (+75cm maximum). Riders who consider that they cannot respect these regulations due to morphological reasons may request for an exemption from the regulations. This request only applies to either the saddle position or the advanced handlebar position, not both.

Apparel

The rules state that when competing, athletes must wear a jersey with sleeves and shorts, possibly in the form of a skinsuit, where the shorts must come above the knee and sleeveless jerseys are not allowed. In addition, one must be able to distiguish between riders in the same team wearing the same clothing. For the IP, TP, 500m TT and 1km TT events the rider must wear one race number, but for all other events the rider must wear two race numbers.

Appendix B

Existing Mathematical Models for Cycling

DiPrampero et al. (1979)

$P = (0.045MV) + (0.041BSA\frac{P_B}{T}V^3)$

where P is the power output (W), M is the mass of the cyclist (kg), V is the velocity of the system (m/s), P_B is the barometric pressure (Torr), T is the temperature (K), BSA is the body surface area (m^2) $\left[(BSA = 0.007184BM^{0.425}Ht^{0.725}),\right]$, BM is the mass of the cyclist (kg), Ht is the height of the cyclist (m).

Bassett Jr et al. (1999)

$P = K(0.00953M_tV + 0.00775V^2 + K_1(A_f)0.007551V^3)$

where K is a factor which allows for adjustment for track roughness or other external conditions, K_1 is an aerodynamic factor which incorporates a correction for altitude, rider position, bicycle type, components, clothing, helmets etc. (but not wind because the model is used for track cycling in a velodrome where the effect of wind is unpredictable), V is the cycling speed (ms^{-1}), and A_f is the frontal area of the system (m^2) ($A_f = 0.0293H^{0.725}M^{0.425} + 0.0604$).

Candau et al. (1999)

$P = C_R \cdot M \cdot g \cdot (\frac{D_R}{T_R}) + \frac{\rho}{2} \cdot AC_d \cdot (\frac{D_R}{T_R})^3$

where P is the mechanical power output (W), C_R is the coefficient of rolling resistance (0.00563), M is the mass of the bike and rider (kg), g is the acceleration due to gravity ($9.81ms^{-1}$), D_R is the race distance (m), T_R is the race time (s), ρ is the air density (1.22 kgm^{-3} at sea level), and AC_d is the effective frontal area ($0.333m^2$).

Lukes et al. (2006)

$ma = (\eta \frac{P_r}{V}) - (C_d A \frac{1}{2} \rho V^2) - ((m \frac{V^2}{r_m} cos\alpha + mgsin\alpha)\mu_R C_s)$

where m is the total mass of the system (kg), a is the acceleration (ms^{-2}), η is the efficiency factor, P_r is the rider's power, V is the bike velocity (ms^{-1}), C_d is the drag coefficient, A is the frontal area of the system (m^2), ρ is the air density (kgm^{-3}), r_m is the radius of curvature of the centre of mass (m), g is the acceleration due to gravity (ms^{-2}),α is the tipping angle relative to the horizontal (°), μ_R is the coefficient of rolling resistance, and C_s is the scrubbing correction coefficient.

Martin et al. (1998)

$P_{TOT} = \frac{[V_a^2 V_G \frac{1}{2} \rho (C_d A + F_W) + V_G C_{RR} m_T g + V_G (91 + 8.7 V_G) 10^{-3} + V_G m_T g G_R + \frac{1}{2}(m_T + \frac{I}{r^2}) \frac{(V_{Gf}^2 - V_{Gi}^2)}{(t_i - t_f)}]}{E_c}$

where E_c is the chain efficiency factor (97.698%), V_a is the air velocity (ms^{-1}), V_G is the ground velocity of the bike and rider (ms^{-1}), C_d is the drag coefficient, A is the frontal area of the system (m^2), C_{RR} is the coefficient of rolling resistance, m_T is the total mass of the bike and rider (kg), g is the acceleration due to gravity (ms^{-2}), G_R is the grade (rise/run), I is the moment of inertia of the 2 wheels ($0.14 kgm^2$), t_i is the initial time (s) and t_f is the final time (s), and V_{Gi} is the initial ground velocity (ms^{-1}) and V_{Gf} is the final ground velcity (ms^{-1}).

Martin et al. (2006)

$Power = (C_d A \times (\frac{1}{2} \rho V_a^2 V_G) + \mu \times (V_g F_N) + \frac{\triangle PE}{\Delta t} + \frac{\Delta KE}{\triangle t}) E$

where C_d is the drag coefficient, A is the frontal area of the rider, bike and wheel spokes, μ is the global coefficient of friction (including Crr and bearing friction), E is the efficiency of the drive system (assumed to be 97.7%), PE is potential energy, KE is kinetic energy, ρ is the air density, and F_N is the normal force excerted by the bike on the rolling surface (essentially the weight of the bike and rider). $C_d A$ and μ are found by regression analysis.

Olds et al. (1993)

$E_{TOT} = E_{Rr} + E_{Ra} + E_G + E_{acc}$

where E_{TOT} is the total energy (J), E_{Rr} is the energy required to overcome rolling resistance (J), E_{Ra} is the energy required to overcome air resistance (J), E_G is the energy required to ride on a grade (J), and E_{acc} is the energy required for acceleration (J).

$E_{Rr} = C_{Rr} cos(arctanS)(M + Mb)d$

where $C_{Rr} = constant$ (coefficient of rolling resistance = 0.0457), S is the slope (%), M is the mass of the cyclist (kg), Mb is the mass of the bike (kg), and d is the race distance (m).

$E_{Ra} = 0.19 \cdot CF_\rho \cdot CF_A \cdot (V_{ss} + V_w)^2 \cdot (d - d_{acc})$

where CF_ρ is the correction factor for air density, CF_A is the correction factor for body surface area, V_{ss} is the steady state bike speed (m/s), V_w is the head wind speed (m/s), d_{acc} is the distance required to achieve the final V_{ss} (m).

$CF_\rho = \frac{(P_B \cdot 288)}{(755 \cdot T)}$

$CF_A = \frac{BSA}{1.77}$

$BSA = M^{0.425} Ht^{0.725} \cdot 0.007184$

where P_B is the barametric pressure (mmHg), T is the ambient temperature (K), BSA is the body surface area (m^2), M is the mass of the cyclist (kg), and Ht is the height of the cyclist (m).

$E_G = (M + M_b) \cdot g \cdot sin(arctanS) \cdot d$

$E_{acc} = 0.5 \cdot (M + M_b) \cdot V_{ss}^2 + 0.19 \cdot CF\rho \cdot CF_A \cdot (V_w^2 + (V_{ss} + V_w)^2) \cdot (\frac{d_{acc}}{2})$

Olds et al. (1995)

$Demand = E_{Rr} + E_{air} + E_{grade} + E_{KE}$

where Demand is the energy demand of cycling (J), E_{Rr} is the energy required to overcome rolling resistance (J), E_{air} is the energy required to overcome air resistance (J), E_{grade} is the energy to move system vertically (J), E_{KE} is the energy required to impart kinetic energy to the system (J).

$E_{Rr} = d \cdot \mu_R \cdot cos(arctanS) \cdot CF_{grav} \cdot 9.80665 \cdot (M + M_b)$

$\mu_R = \frac{(a + \frac{b}{P})}{Diam} \cdot CF_{surface}$

$CF_{grav} = (\frac{6.378}{(6.378 + (\frac{Alt}{1000}))})^2$

$E_{grade} = d \cdot (M + M_b) \cdot CF_{grav} \cdot 9.80665 \cdot sin(arctanS)$

where d is the race distance (m), μ_R is the coefficient of rolling resistance, S is the slope (%), CF_{grav} is the factor correcting the acceleration due to gravity for altitute, M is the nude mass of the rider (kg), M_b is the mass of the bike and accessories, including clothing (kg), a=-0.00051, b=9.73744, P is the tyre pressure (psi), Diam is the diameter of the wheels (inches), $CF_{surface}$ is the factor correcting μ_R for road surface (asphalt = 1, concrete = 0.87), and Alt is the altitude above sea level (m).

$E_{air} = 0.5 \cdot CF_D \cdot C_d \cdot A_p \cdot \rho \cdot CF_{xwind} \cdot V_{ss} \cdot (t + 3k^{(-t/k)} - 1.5k^{(-2t/k)} + (\frac{k}{3})^{(-3t/k)} - \frac{11k}{6}) + KE_{ang}$

$CF_D = 1 - 0.3835 + 1.25 \cdot Spacing^2$

$A_p = 0.4147 \cdot (\frac{A_b}{1.771}) + 0.1159$

$A_b = Ht^{0.725 \cdot} M^{0.425} \cdot 0.007184$

$\rho = 1.225 \cdot (\frac{P_B}{260}) \cdot (\frac{288.15}{T}) \cdot CF_{humidity}$

$CF_{humidity} = (\frac{P_{O2} \cdot 32 + P_{N2} \cdot 28 + P_{H2O} \cdot 18}{0.2093 \cdot 32 \cdot P_B \cdot + 0.7904 \cdot 28 \cdot P_B})$

$P_{H2O} = 15.573^{(0.0606 \cdot (T - 291))} \cdot (\frac{RH}{100})$

$P_{O2} = 0.2093 \cdot (P_B - P_{H2O})$

$P_{N2} = 0.7904 \cdot (P_B - P_{H2O})$

$$CF_{xwind} = \sqrt{(V_{ss}^2 + V_w^2 + 2 \cdot V_{ss} \cdot V_w cos X_{wind}) \cdot (V_{ss} + \frac{V_w cos X_{wind}}{V_{ss}^2})}$$

where CF_{draft} is the factor correcting E_{air} for drafting, C_d is the drag coefficient of the system (0.592), A_p is the projected frontal area of the system (m^2) ($A_p = 0.3176 \cdot 0.007184 \cdot BM^{0.425} \cdot Ht^{0.725} - 0.1478$ where BM is the mass of the cyclist (kg) and Ht is the height of the cyclist (m)), ρ is the air density ($kg.m^{-3}$), CF_{Xwind} is the factor correcting air resistance for cross winds, Spacing is the distance between cyclist and pack/paceling/vehicle (m), A_b is the body surface area (m^2), Ht is the height of the cyclist (cm), P_B is the barometric pressure (mmHg), T is the ambient temperature (K), $CF_{humidity}$ is the factor correcting air density for humidity, P_{H2O} is the partial pressure of water vapour (Torr), RH is the relative humidity (%), P_{O2} is the partial pressure of oxygen (Torr), P_{N2} is the partial pressure of nitrogen (Torr), V_{ss} is the steady state bike speed (ms^{-1}), V_w is the wind speed (ms^{-1}), X_{wind} is the angle of the wind relative to direction of travel of system (rad), t is the time (s), k is the time constant for acceleration (10) (s), and KE_{ang} is the angular kinetic energy.

$$E_{KE} = 0.5 \cdot (M + M_b) \cdot (V_{ss} \cdot (1 - exp^{(-t/k)}))^2 + KE_{ang}$$

where KE_{ang}= hip joint + knee joint + ankle joint + cranks/pedal + pedal + cluster + wheels + chainwheels

Hip joint $= 0.3536 \cdot M \cdot (0.39 \cdot \frac{Ht}{170.18} \cdot 0.785 \cdot \frac{cad}{60}$

Knee joint $= 0.1286 \cdot M \cdot (0.27 \cdot \frac{Ht}{170.18} \cdot 1.309 \cdot \frac{cad}{60}$

Ankle joint $= 0.0276 \cdot M \cdot (0.18 \cdot \frac{Ht}{170.18} \cdot 0.349 \cdot \frac{cad}{60}$

Cranks/pedal $= 1.2 \cdot 0.14 \cdot cad \cdot \frac{\pi}{30}$

Pedals $= 0.45 \cdot 0.03 \cdot cad \cdot \frac{\pi}{30}$

Cluster $= 0.46 \cdot 0.02 \cdot V_{ss} \times \frac{(1^{-(-t/k)})}{(Diam \cdot 0.0127)}$

Wheels $= 3.16 \cdot 0.23 \cdot V_{ss} \times \frac{(1^{-(-t/k)})}{(Diam \cdot 0.0127)}$

Chainwheels $= 0.25 \cdot 0.08 \cdot cad \cdot \frac{\pi}{30}$

where cad is the cadence (rpm)

Appendix C

Details of Simulated Pacing Strategies

Strategy	**Equation Parabolic All-out Phase**	**Equation Linear Phase**	**P_{bends} (W)**	**$P_{straights}$ (W)**
All-out 10s & variable higher bends	$P = -17.76t^2 + 177.6t + 600$		507.5	407.5
All-out 12s & variable higher bends	$P = -12.33t^2 + 148t + 600$		504	404
All-out 14s & variable higher bends	$P = -9.0612t^2 + 126.86t + 600$		501	401
All-out 16s & variable higher bends	$P = -6.9375t^2 + 111t + 600$		497	397
All-out 18s & variable higher bends	$P = -5.48t^2 + 98.67t + 600$		493	393
All-out 10s & variable higher straights	$P = -17.76t^2 + 177.6t + 600$		438	538
All-out 12s & variable higher straights	$P = -12.33t^2 + 148t + 600$		435	535
All-out 14s & variable higher straights	$P = -9.0612t^2 + 126.86t + 600$		431.5	531.5
All-out 16s & variable higher straights	$P = -6.9375t^2 + 111t + 600$		427.5	527.5
All-out 18s & variable higher straights	$P = -5.48t^2 + 98.67t + 600$		424	524
All-out 10s even	$P = -17.76t^2 + 177.6t + 600$		473 even	
All-out 12s even	$P = -12.33t^2 + 148t + 600$		470 even	
All-out 14s even	$P = -9.0612t^2 + 126.86t + 600$		466 even	
All-out 16s even	$P = -6.9375t^2 + 111t + 600$		452.5 even	
All-out 18s even	$P = -5.48t^2 + 98.67t + 600$		458.5 even	
Variable higher bends			515	415
Variable higher straights			449.5	549.5
All-out 10s linear decline	$P = -17.76t^2 + 177.6t + 600$	$P = -0.93t - 600$	363 end	
All-out 12s linear decline	$P = -12.33t^2 + 148t + 600$	$P = -0.945t - 601$	360 end	
All-out 14s linear decline	$P = -9.0612t^2 + 126.86t + 600$	$P = -0.96t - 602$	358 end	
All-out 16s linear decline	$P = -6.9375t^2 + 111t + 600$	$P = -0.986t - 603$	354 end	
All-out 18s linear decline	$P = -5.48t^2 + 98.67t + 600$	$P = -t - 604$	353 end	
Even			482.5 even	
Positive	113% (527W) 101% (471W) 100% (466W)			
Negative		$P = 0.458t - 1137$	466 even	695 end
U-shaped	$P = 0.00006d^2 - 0.233d + 631$	135.5% (631W) 85.5% (398W) 135.5% (631W)		
J-shaped	$P = 0.00002d^2 - 0.46d + 466$	100% (466W) 95% (443W) 135% (629W)		
Reverse J-shaped	$P = 0.00003d^2 - 0.141d + 607$	130.3% (607W) 90.3% (421W) 100.3% (467W)		

Table C.1: Details of Simulated Pacing Strategies

Appendix D

Wind Tunnel Testing Procedure

Images of LabVIEW displays

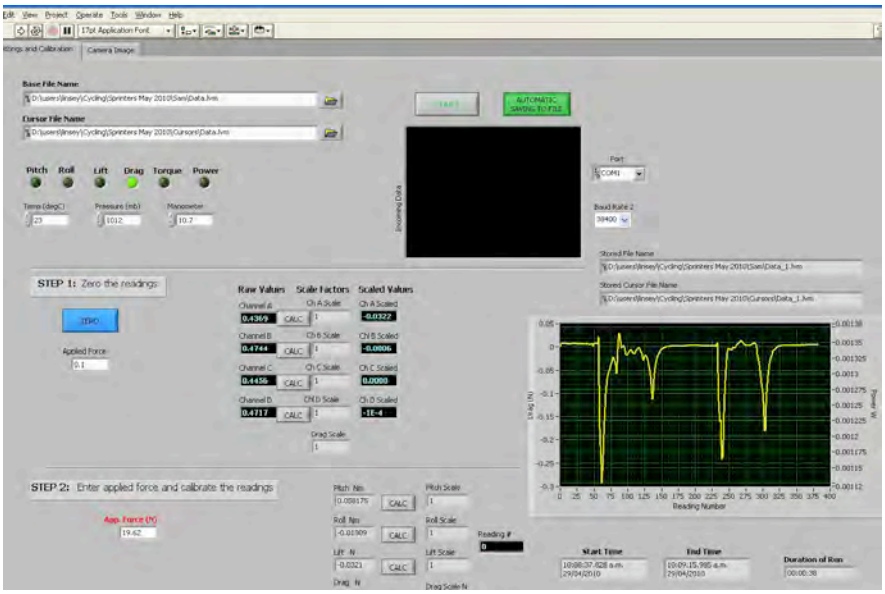

Figure D.1: LabVIEW front panel display

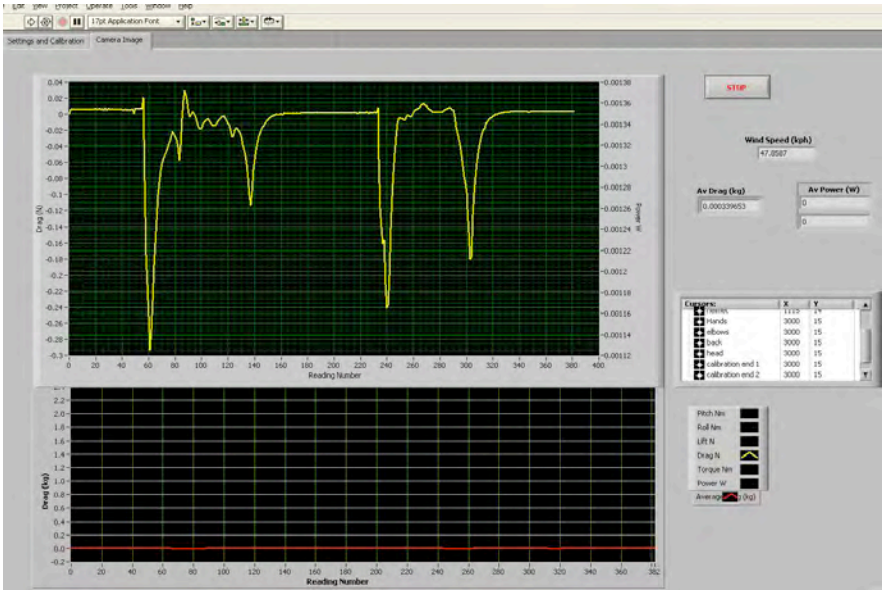

Figure D.2: LabVIEW graph of data collection

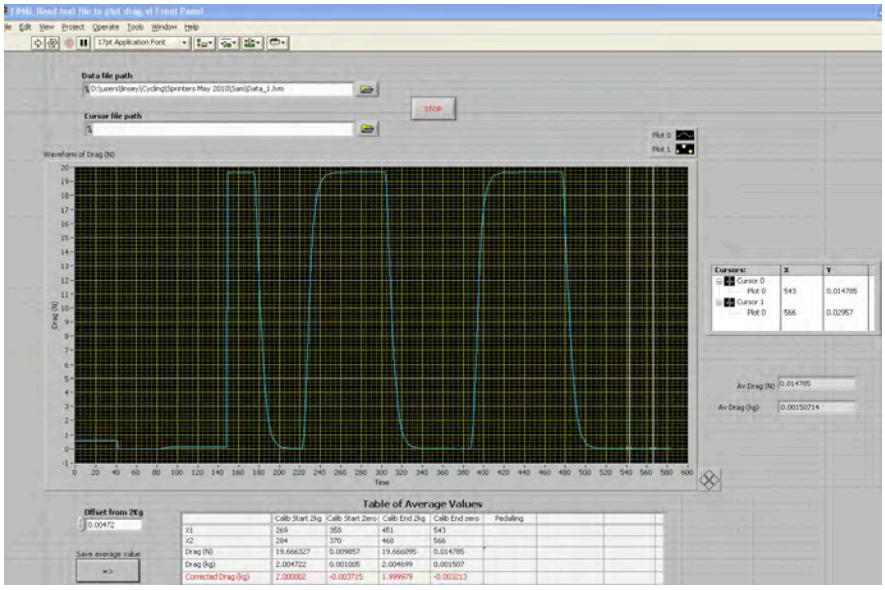

Figure D.3: LabVIEW display for analysing data

Description of Testing Procedure

1. The floating platform is locked to prevent movement while the bike is placed in position on the rig and the athlete gets on to the bike.

2. The atmospheric temperature and pressure are recorded.
3. A camera is placed to the side of the athlete and behind the athlete to video athlete position during each test and to take still images.
4. After ensuring the rider is in their correct racing position, an outline of the rider is drawn on a white board placed to the side of the athlete.
5. The system is calibrated by loading and unloading the 2kg weight using a syringe system.
6. The wind is turned on.
7. Once the wind is up to speed the athlete begins pedalling at a comfortable cadence for 30 seconds and the data recorded. At the same time the cameras are turned on to take video and still images, and the athlete position with respect to the white board monitored.
8. After 30 seconds the athlete stops pedalling but remains in their racing position. It is possible for the athlete to pedal for longer than 30 seconds in order to gather data for a number of position changes during the same test if this is desired. Labels can be made in the software to identify changes in position during the same test.
9. Once the wind has stopped completely the system is calibrated again by loading and unloading the 2kg weight using the syringe system, and the overall drift calculated by subtracting the initial calibration value from the final calibration value.
10. The platform is then locked again so the athlete can get off the bike, and the data then reloaded into another LabVIEW programme for analysis.
11. Moveable cursors on a graphical display of the drag data allow the average drag to be calculated for each test. For tests where the athlete has changed position during the run, the average drag for each position can be determined in the same way, by selecting the corresponding regions on the graph with the moveable cursors.
12. The data is imported into the Microsoft Excel spreadsheet shown in Figure D.4 to calculate the time gains for different changes in position.

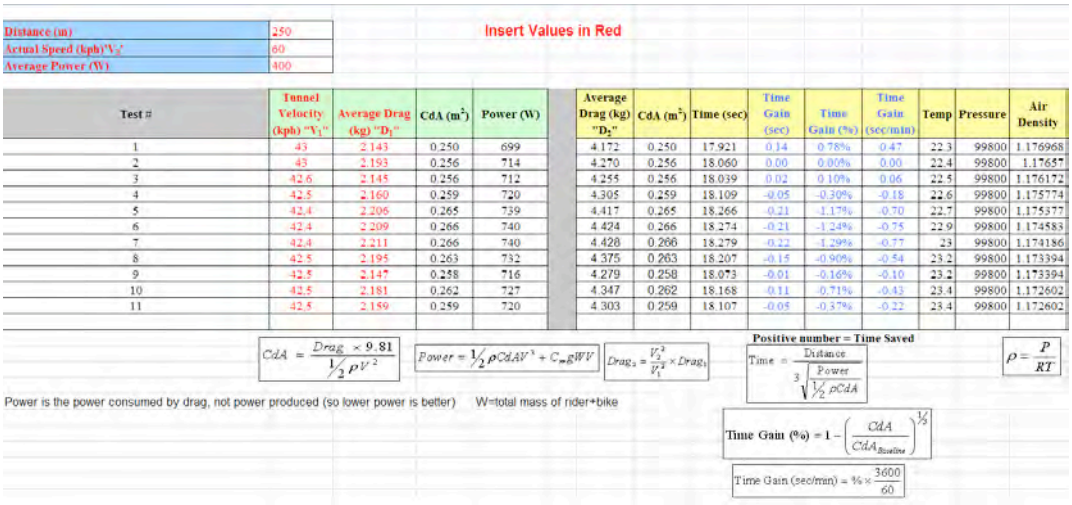

Distance (m)	250
Actual Speed (kph) "V_2"	60
Average Power (W)	400

Insert Values in Red

Test #	Tunnel Velocity (kph) "V_1"	Average Drag (kg) "D_1"	CdA (m^2)	Power (W)	Average Drag (kg) "D_2"	CdA (m^2)	Time (sec)	Time Gain (sec)	Time Gain (%)	Time Gain (sec/min)	Temp	Pressure	Air Density
1	43	2.143	0.250	699	4.172	0.250	17.921	0.14	0.78%	0.47	22.3	99800	1.176968
2	43	2.193	0.256	714	4.270	0.256	18.060	0.00	0.00%	0.00	22.4	99800	1.17657
3	42.6	2.145	0.256	712	4.255	0.256	18.039	0.02	0.10%	0.06	22.5	99800	1.176172
4	42.5	2.160	0.259	720	4.305	0.259	18.109	-0.05	-0.30%	-0.18	22.6	99800	1.175774
5	42.4	2.206	0.265	739	4.417	0.265	18.266	-0.21	-1.17%	-0.70	22.7	99800	1.175377
6	42.4	2.209	0.266	740	4.424	0.266	18.274	-0.21	-1.24%	-0.75	22.9	99800	1.174583
7	42.4	2.211	0.266	740	4.428	0.266	18.279	-0.22	-1.29%	-0.77	23	99800	1.174186
8	42.5	2.195	0.263	732	4.375	0.263	18.207	-0.15	-0.90%	-0.54	23.2	99800	1.173394
9	42.5	2.147	0.258	716	4.279	0.258	18.073	-0.01	-0.16%	-0.10	23.2	99800	1.173394
10	42.5	2.181	0.262	727	4.347	0.262	18.168	-0.11	-0.71%	-0.43	23.4	99800	1.172602
11	42.5	2.189	0.259	720	4.303	0.259	18.107	-0.05	-0.37%	-0.22	23.4	99800	1.172602

$$CdA = \frac{Drag \times 9.81}{\frac{1}{2}\rho V^2}$$

$$Power = \frac{1}{2}\rho CdAV^3 + C_{rr}gWV$$

$$Drag_2 = \frac{V_2^2}{V_1^2} \times Drag_1$$

Positive number = Time Saved

$$Time = \frac{Distance}{3\sqrt{\frac{Power}{\frac{1}{2}\rho CdA}}}$$

$$\rho = \frac{P}{RT}$$

Power is the power consumed by drag, not power produced (so lower power is better) W=total mass of rider+bike

$$\text{Time Gain (\%)} = 1 - \left(\frac{CdA}{CdA_{Baseline}}\right)^{\frac{1}{3}}$$

$$\text{Time Gain (sec/min)} = \%\times\frac{3600}{60}$$

Figure D.4: Calculation of Time Gain for Wind Tunnel Tests

13. The images taken from the rear of the rider during each test can be used to calculate the frontal area of the rider in that position using the digitising method.

Appendix E

Changes for Overall Gains

Changes in Position

- Tucked head/crouch/head low - moving the head down, tucking the head in, but ensuring the cyclists continue to look forwards.
- Helmet tip up - lifting the tip of the helmet only, but ensuring the athletes can still look forwards.
- Extensions shortened - bringing the extensions closer to the body, but keeping them parallel.
- Hand change - changing the position of the hands on the extensions.
- Tip down - lowering the tip of the helmet so it is lower than the reference position, but not necessarily touching the back of the rider.
- Stem down - moving the stem down to lower the front of the body.
- Seat backwards - moving the seat backwards, but maintaining the same height (this will also alter the leg extension of the rider).
- Hair tucked in - only for athletes with hair long enough to tie into a bun or secure under the helmet.
- Seat forwards - moving the seat forwards, but maintaining the same height (this will also alter the leg extension of the rider).
- Extensions wider - keeping the extensions parallel, but moving them wider.
- Stem up - raising the stem to lift the handlebars.
- Tapered bars - maintaining the same hand position, but moving the elbows out by either widening the elbow pads or tilting the extensions.
- Extensions narrower - maintaining parallel extensions, but bringing them closer together.
- Extensions lengthened - moving the extensions further away from the body to lengthen the athlete.
- Raise seat - making the seat higher without changing the fore-aft position of the seat (this will also alter the leg extension).

Equipment Changes

- Different skinsuit - comparison between road and track, competitive and recreational skinsuits.
- Different frame and wheels - all wheels were disc wheels, but the frames were a combination of road and track racing frames.
- Different helmet - comparison between different racing helmets, including aero helmets and non-aero helmets.
- Same frame, different wheels - changing the front and rear wheels (all disc wheels).
- No visor vs visor - removing the visor from the helmet.
- Pedal/strap combination - changing the type of pedals and straps used in sprint cycling.
- Shoe covers vs no shoe covers - covering the shoes and ankle socks with a shoe cover.
- Same pedal different strap - changing the type of strap used in sprint cycling, but with the same pedal as the reference position.
- Gloves vs no gloves - wearing different types of gloves while holding the same hand position on drop bars (cowhorn bars).
- Helmet holes taped vs untaped - taping over the vents of the helmet with electrical tape.
- Same strap different pedal - changing the type of pedal used in sprint cycling, but with the same strap as the reference position.
- Modified seat tube - changing the shape of the seat tube by using polestyrene covered in electrical tape to try and make a more streamlined shape.
- Modified fork shape - changing the shape of the front forks by using polestyrene covered in electrical tape to try and make a more streamlined shape.
- Modified stem shape - changing the shape of the stem by using polestyrene covered in electrical tape to try and make a more streamlined shape.